Antenna Modeling Notes

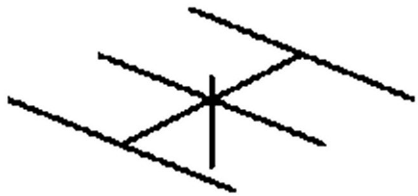

Volume 4

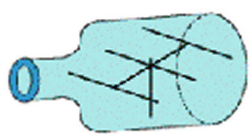

L. B. Cebik, W4RNL

Antenna Modeling Notes

Volume 4

L. B. Cebik, W4RNL

Published by
antenneX Online Magazine
http://www.antennex.com/
POB 271229
Corpus Christi, Texas 78427-1229 USA

ISBN: 1-877992-78-X

Table of Contents

Dedication

This volume of studies of antenna modeling is dedicated to the memory of Jean, who was my wife, my friend, my supporter, and my colleague. Her patience, understanding, and assistance gave me the confidence to retire early from academic life to undertake full-time the continuing development of my personal web site at the URL, http://www.cebik.com. The site is devoted to providing, as best I can, information of use to radio amateurs and others--both beginning and experienced--on various antenna and related topics. This volume grew out of that work--and hence, shows Jean's help at every step.

Preface

This collection of antenna modeling notes continues the compilation of the series that I began in 1998 in *antenneX*. It contains numbers 76 through 100 of the long-running series that continues even today. The time has come to collect these columns into a more convenient form for the reader. There is just too much material for a single volume, so I have broken the collection into four 25-column units. I have reviewed the text and graphics for each column to ensure as much accuracy as I can muster. I have also reviewed the sample models used in each column. That process permitted me to add something to these volumes that is not available in *antenneX* or at my own web site. The Appendix to each of these volumes contains a collection of antenna modeling files in three formats: .NEC (ASCII), .EZ (EZNEC), and .NWP (NEC-Win Plus). However, not every model appears in every format. Some models require elements of the command set not included in entry-level programs such as EZNEC or NEC-Win Plus. Others require NEC-4. I have revised the text to include a file name for the applicable model in the Appendix. Therefore, should you wish to do so, you will be able to read a column in front of your computer and to test for yourself the ideas involved.

This volume begins with a series of items devoted to showing how we may use modeling software to develop reasonable expectations from antennas. The multi-column series includes fundamental antennas in both horizontal and vertical orientations.

The columns also continue our exploration of various NEC commands. This volume includes notes on the GR and GA geometry structure commands. We shall also look at the spirals that are possible within the NEC-4 version of the GH command. Among the control commands, you will find notes on near field commands, including NE and NH, which are common to both NEC-2 and NEC-4, and on LE and LH, which appear only in NEC-4. Specific to NEC-2 is the EK command that expands the current calculation algorithm in that core for use when the segment-length to wire-radius ratio is low. Also included are a few notes on the NT or network commands; the goal is only a basic familiarity with its use. We shall also explore ways to develop models as an integrated set of commands rather than as a simple string of them. Although this series does not usually deal with the surface-patch commands, we shall encounter one special use for the SM command and how it compares with a more complex wire-grid structure.

Along the way, we shall explore some basic NEC calculations, including electric fields at a distance. We shall also learn how to supplement NEC calculations by using its output data to arrive at circular gain. Finally, we shall explore the relationship between the EX command and the PT command for special receiving-mode models. The NEC-2 and NEC-4 manuals provide fundamental collections of sample models designed to illustrate in the most compact way possible as many NEC features as possible. These models appear only in print form. In this volume, we shall examine the models, and the model collection will include them in .NEC format.

The adequacy of our models is, as it should be, a continuing challenge. Therefore, we shall revisit the convergence test with particular reference to its use with NEC. In addition, we shall take a look at some of the correctives that we use to work around some of the core's limitations. However, finding limitations and faults is not our goal. Rather, the goal is to make effective use of the program. Toward that end, we shall look at a techniques that will let us in NEC-2 handle insulated wires in a way that is comparable to the IS command in NEC-4. We shall also examine the various ground calculation systems that appear in NEC (and MININEC) software.

Although the list of topics seems to grow more advanced and complete, the appearance is an illusion. The command set is far too large for full coverage even in 4 volumes. As well, good antenna simulations depend as much on the ingenuity of modelers as they do on simply knowing how to apply various commands. Hence, the list of techniques by which to improve our models may well be endless. Mastering antenna modeling software has a further: the use of the software to educate ourselves on the capabilities of various types of antennas. If we add this dimension of the use of NEC and MININEC to further mastery of the command structures and additional modeling techniques, then we may fairly predict that the series is far from its final episode.

76. Developing Antenna Expectations Using Modeling Software 1A: Horizontal Wires in the Lower to Medium HF Range

Preamble

On numerous occasions, I have suggested that antenna-modeling software (using either NEC or MININEC) is a good self-instruction tool for learning to have proper expectations of many types of antennas. In this and the next few columns, I shall illustrate how you can accomplish this goal. Each column will focus on a basic antenna type and develop a set of modeling exercises for exploring the basic properties of that type of antenna. Most of the exercises will be simple and in no way challenge either your software or your modeling ingenuity. However, the lack of challenge does not make the exercises any less important if you have not already been through them (or any number of variations on them).

Modeling software continues to grow easier to obtain for the individual who is relatively new to antennas, that is, who has not done systematic studies in basic antenna properties. I have discovered over the years that this group of folks includes many old-time as well as new radio amateurs, short-wave listeners, and others. This group of individuals is my target for these exercises. Modeling itself will not tell you exactly why–in terms derived from Maxwell's laws and supplemental research and engineering findings–antennas act as they do. Still, easily accessed modeling programs will help you develop a reasonable and extensive set of correct expectations from the types of antennas that you may encounter.

For the most part, our notes will by aimed at the antenna under discussion. I shall assume that you have mastered the basic operation of your software program. As well, I shall assume that you are familiar with the basic terminology that such programs use, although I shall include a few brief reminders as we go along. However, each basic type of antenna has many variables attached to it, each of which deserves exploration. So I shall remain focused on the modeling application rather than on the programs themselves.

The Center-Fed Horizontal Wire at Low to Medium High Frequencies

Let's begin by thinking about a particular type of antenna and the number of variables that attach to it. Our subject is the center-fed wire antenna, commonly used at lower to medium high frequencies (HF). Here is a list of basic variables that we shall explore.

A. The antenna environment (free space or over ground)
B. The length
    1. Resonant vs. non-resonant lengths
    2. Physical length vs. electrical length
        a. Changing the physical length
        b. Changing the frequency of operation
C. Wire diameter
    1. Effect on the feedpoint impedance
    2. Length required for resonance
D. Height above ground
    1. Effect on the feedpoint impedance with a constant length
    2. Length required for feedpoint resonance
E. Ground quality
F. Wire conductivity
G. Operating (SWR) bandwidth vs. wire (element) diameter

In each case, I have paired up common variables encountered in basic antenna work, and the method of pairing means that we shall overlook some potential combinations. Nevertheless, with this beginning, you may go on to pair other sets of variables and explore more of the territory on your own.

Antenna modeling software has many forms and implementations, despite the fact that NEC-2 and MININEC are the most common calculating cores. Therefore, I shall not present models so much as describe them. However, applicable models accompany this volume. The models are all simple, so you may create your own model within the set-up of the software that you have. You will encounter minor differences between the results that you obtain from your model and the sample results that I shall show. Nevertheless, you will be able easily to see the same trends in the results, and that is the most important factor in developing correct expectations of an antenna. For this initial exercise set, the models will be super-simple, consisting of a single horizontal wire. We shall specify all lengths in terms of both feet and meters. Wire diameters will use AWG gauge numbers, along with their diameters in inches and millimeters. Heights above ground will be listed in wavelengths, feet, and meters. Except where I shall try to focus your attention on some special aspect of a unit of measure, pick the one most comfortable for you. With so many variables attached to the horizontal center-fed wire, we need to move from these preliminaries to the actual work involved.

A. The Antenna Environment (Free Space or Over Ground)

Let's begin by setting our software for free space (or "no ground"). We shall create a 1/2-λ resonant dipole for 3.6 MHz. The wire will be AWG #12 (0.0808" or 2.052 mm). We shall set the conductivity of the wire for copper, using either a pre-set value in the program of a user-inserted conductivity of about 5.8E7 S/m (or a resistivity of 1.7E-8 Ω/m). We may specify a source (feedpoint) voltage of 1.0 at 0-degrees phase angle at the center of the 11-segment NEC wire (10 or 12 segments in MININEC). To set up the wire, as shown in **Fig. 76-1**, we shall run it from -Y to +Y, leaving both the X values and the Z values at zero. On my version of NEC-4, the Y-coordinates were -66.55 and +66.55 feet (+/-20.284 m). See model 76-1.

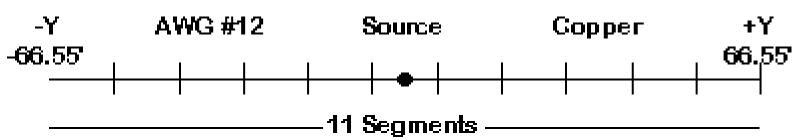

Fig. 76-1 **Setting Up the First Center-Fed Wire**

The first step is to learn why I used the length indicated. If I look at the source impedance, it reads 73.73 - j0.27 Ω. Since we want resonance, we need to define the term. For our purposes, we can set resonance as any source impedance where the reactance (or imaginary term) is less than +/-1.0. This limit is much tighter than you would need in a practical antenna and much looser than we can obtain by juggling the length value. However, it is just about right for determining trends in the source (feedpoint) impedance. Depending on your program, you may have to adjust the values of +/-Y to obtain resonance within the limits indicated, and your remaining impedance values may drift a bit from the result listed.

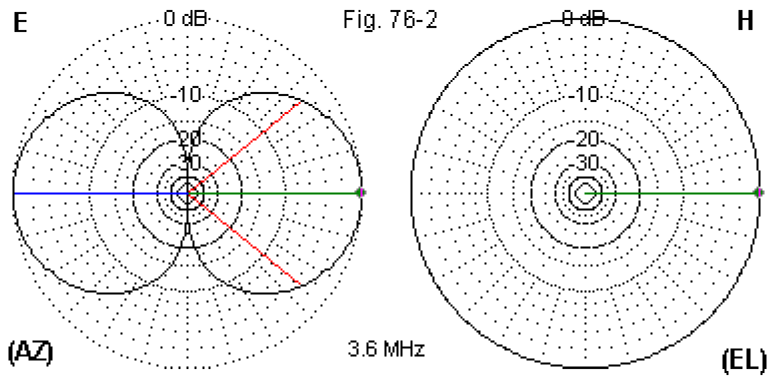

E-Plane (Azimuth) and H-Plane (Elevation) Patterns
Resonant Center-Fed Wire in Free Space

Having established a resonant center-fed wire at 3.6 MHz in free space, let's examine the patterns. Modeling programs use the terms "azimuth" and "elevation" for all patterns. However, the terms strictly apply only when we have a ground surface against which to measure an elevation angle. In free space, for a horizontal wire, the azimuth pattern corresponds to the E-plane pattern, and the elevation pattern corresponds to the H-plane pattern. Both appear in **Fig. 76-2**. The E-plane pattern is the figure-8 that we see in texts, while the H-plane pattern is a perfect circle. For reference, we can record the maximum free-space gain as 2.03 dBi (where your program my show a smidgen more or less, and where we remember that we are using copper wire, not a perfect conductor). We shall explore this value further on when we take up different values of wire conductivity.

Now let's make a few changes and re-run the model. First, we shall insert in each of the Z boxes a value of 1 λ (273.214' or 83.276 m). Next, we shall specify the use of a real ground. If using NEC, specify the Sommerfeld or "high accuracy" ground. Set the values for this ground at "good" (sometimes called "average"), that is, with a conductivity of 0.005 S/m and a permittivity (relative dielectric constant) or 13. Now set the pattern for elevation. See model 76-2.

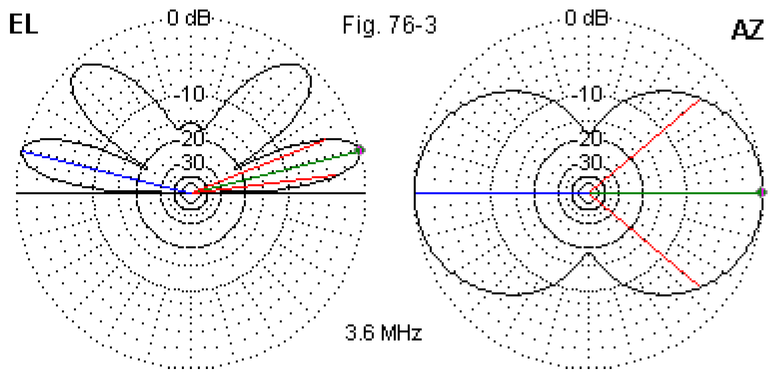

Elevation and Azimuth Patterns
Resonant Center-Fed Wire 1 WL Above Good Ground

Run the model and check the source impedance. See **Fig. 76-3**. You should discover that the antenna is no longer strictly resonant, with an impedance of 71.34 - j6.42 Ω. It is merely near-resonant. Next, check the elevation pattern at an azimuth bearing of 0 degrees. It is no longer circular, but shows the effects of ground reflection. Hence, the pattern breaks into elevation lobes and nulls. Since the lowest lobe is the one of main interest, we can record its elevation angle (14 degrees) and its strength, 7.85 dBi. (We shall take a closer look at that elevation angle a bit further onward.) Now check the azimuth pattern at the elevation angle of maximum radiation–the Take-Off (TO) angle. The pattern is no longer a tightly pinched figure-8, but more of a peanut. Ground reflections not only increase the azimuth gain at the TO angle, they also reduce the side nulls relative to a free-space pattern.

B. The Length: 1. Resonant vs. Non-Resonant Lengths

Let's use the 3.6-MHz wire antenna model that is 1 λ above good or average ground as our starting point. First, we should make it resonant within the limits we have set for that term. With the Y-values at +/-66.8' (20.361 m), we can obtain resonance. See model 76-3. Next, let's see what happens as we change the wire in 1' (0.3048 m) increments, going up two notches and then down two notches. Hence, our total antenna length will change by 2' (.6096 m) for each change. Within the limits of program differences, your table of results should resemble the one that follows.

Changing Antenna Length

Length +/-feet	Length +/-meters	Source Impedance R +/- jX Ohms	Gain at 14-deg. Elevation dBi
64.8	19.751	66.29 - j51.74	7.82
65.8	20.056	69.13 - j25.89	7.83
66.8	20.361	72.09 - j 0.07	7.85
67.8	20.665	75.16 + j25.74	7.86
68.8	20.970	78.35 + j51.56	7.87

Each 2' of antenna length change is about a 0.007-λ change–not a lot, but noticeable. Despite that fact that the total change in length from the shortest to the longest wire is 8' (2.438 m), the antenna gain has changed by only 0.005 dB–a truly insignificant amount. This explains why, for antennas using antenna tuners, we do not need lengths to be precise. Only when the exact source impedance is of some importance do we need to concern ourselves with precision pruning.

Our example presumes that some precision is useful, as shown by the changing values of the source impedance. But the table of values also has more to tell us. First, note the change in reactance. Allowing for the fact that we had j0.07 Ω reactance at the so-called resonant point, we can see that the reactance curve would be very nearly equal each side of resonance over the small span that we have covered. The very slightly higher change below the resonant length is due to the fact that each 1' (0.3048 m) of change below the resonant length is a slightly higher percentage of length reduction relative to the preceding length than each increment is a percentage of length increase above the resonant length.

The resistive portion of the source impedance tells a different story. The resistance increases more rapidly above the resonant length than below it. As the resistance decreases, it has only a small range to cover. However, as we increase the length toward 1 λ, the range over which the resistance may climb is monumental, suggesting that even for our small changes, we should expect more change per increment. Both the resistance and reactances changes–and their differences above and below the resonant antenna length–do not amount to anything noticeable for a broadband antenna like a center-fed wire. For other antenna types with more rapid changes in source impedance with element length changes, we often clearly see non-symmetrical changes in the impedance curves. When we see reversals in the non-symmetry, we have a good occasion to examine the antenna in order to understand why.

B. The Length: 2. Physical Length vs. Electrical Length

Let's now see what happens to the performance parameters when we increase the electrical length of our center-fed wire. We have sometimes referred to our wire as a dipole. This term is shorthand for a more complete but very unwieldy label: a resonant (or near-resonant) 1/2-λ center-fed dipole. The question of resonance, of course, refers to the feedpoint impedance and to what degree it is contained wholly in the resistive component, with no reactance. The antenna is about 1/2-λ long. A wavelength at 3.6 MHz is 273.214' (83.276 m) long, so a true half wavelength will be 136.607' (41.638 m). Our actual wire length was 133.6' (40.721 m) for the version that is resonant at 1 λ above average ground. We know that the physical length is less than the electrical length, which is–by the standard of resonance–almost exactly 1/2-λ. The physical length is 97.80% of the electrical length. See model 76-3.

We shall look again at the amount of shortening later, but for now we need only note that the difference results from what some call "end-effect." The surface at the end of the wire adds electrical length to the wire without adding any further physical length.

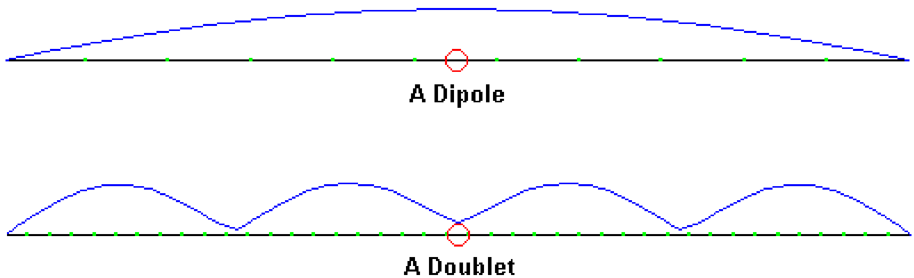

A Dipole vs. a Non-Dipole

Fig. 76-4

Since we feed the antenna at its precise center, it is center-fed. We call the antenna a dipole because there are exactly two transitions from maximum current (at the wire center) to minimum current (at the wire ends). When we change the length of the wire so that there are more than two such transitions, we technically no longer have a dipole. Center-fed antennas used on frequencies where they are no longer have only two transitions go under an unofficial but useful label: doublets. See **Fig. 76-4** for the contrast between a dipole and a doublet. A wire antenna becomes a doublet even if some frequencies at which we use it might qualify for the dipole label.

a. Changing the physical length

Now here is the exercise–or at least the first of two. Let's exactly double the length of the antenna. Then let's triple it. Finally, let's quadruple the original length. We shall retain the frequency and the height above ground. We need only be certain that the feedpoint remains in the exact center and that we have enough segments for the new length. To preserve the segment length, let's increase the NEC segments from 11 to 21 to 31 and finally to 41. MININEC segmentation, using even numbers, calls simply for multipliers of 2, 3, and 4. See models 76-4 through 76-6.

We shall record the source impedance for each step. When it comes to looking at patterns and finding maximum gain, we shall have to go back and forth between elevation and azimuth pattern to find the azimuth heading as well as the elevation angle of maximum radiation. If we do the job correctly, we shall end up with a table like the one that follows. Note that the lengths shown are for my resonant model. Apply the multipliers to the length of your own resonant dipole when 1 λ above ground. All wires remain AWG #12 copper.

Performance of Wire Antennas 1 Wavelength Above Average/Good Ground

Length wl*	Length feet	Length meters	Az hdg degrees	TO angle degrees	Gain dBi	Source Impedance R +/- jX Ohms
0.5	133.6	40.72	0	14	7.85	72.09 - j 0.07
1.0	267.2	81.44	0	14	9.62	6629 + j 1367
1.5	400.8	122.16	49	14	8.56	105.0 - j 69.08
2.0	534.4	162.88	34	14	9.15	4488 + j 1324

* Since we are multiplying times the physical length, the lengths in wavelengths are approximate.

Without looking at the patterns themselves, the table already tells us something important about them. For antennas in the range of 1/2-λ to 1-λ, the pattern is bi-directional, with the strongest (only) lobes broadside to the wire. However, as we further increase the length, the strongest lobe is at an angle relative to the broadside heading. How much depends on the wire length.

Fig. 76-5 shows the patterns for the three new wire lengths. A 1-λ wire acquires its gain mostly from narrowing the beamwidth. We still have a 2-lobe pattern. Let's skip to the pattern for the 2-λ antenna. Now we have 4 lobes, each quartering (but not exactly) to the broadside heading. Radiation broadside to the wire is negligible. This pattern gives you an intuition of what happens if we extend the wire to 3 λ: 6 lobes. You can check this for yourself and find that you are correct. In fact, with wire close to a any multiple of a full wavelength, the number of lobes will be double the element length in wavelengths.

However, let's move back to the case where the wire is 1.5-λ long. We find 6 azimuth lobes. Lobes do not suddenly appear and disappear as we increase a wire's length. They grow and shrink. At a length of 1.5 λ, the pair of lobes for a 1-λ wire are shrinking and the ones for a 2-λ antenna are growing. Hence we see all six lobes. (A 3.5-λ antenna would have the 6 lobes for 3 λ and the 8 for 4 λ, for a total of 14 lobes.) As we increase the number of lobes, the beamwidth for each one tends to become narrower.

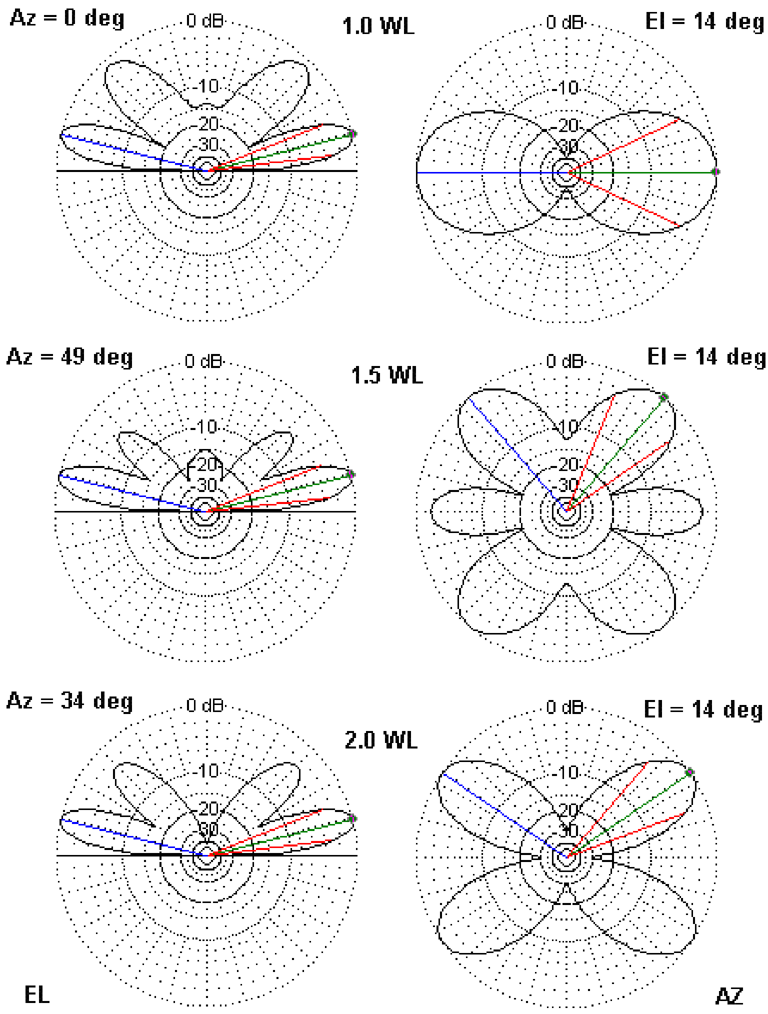

Elevation and Azimuth Patterns of Center-Fed Wire
When 1.0-WL, 1.5-WL, and 2.0 WL Long and
1 WL Above Good Ground

Fig. 76-5

Since the 1.5-λ wire has more lobes that either the 1-λ or the 2-λ wire, but only the same amount of power, we would expect the power in the strongest lobe to be somewhat less than for either of the other cases. If we look in the gain column, we can see the fulfillment of our expectation. The differential is not especially operationally significant, but it is noticeable.

Now let's turn to the feedpoint impedance column. The impedances for the lengths close to a multiple of a full wavelength are high, while those close to an odd multiple of a half-wavelength are low. But in all three cases, the antenna plays shorter than resonance. (As we approach but do not reach resonance for a multiple of a full wavelength, the inductive reactance indicates the antenna's shortness. As a side exercise, try to play with the length of the 1-λ antenna to achieve resonance as defined for our exploration. The range is extremely narrow, as the reactance changes from a very high value of inductive reactance to a very high value of capacitive reactance just past the resonant point.) The reason for the antenna being short is, again, the end effect. By simply multiplying our physical length, we effectively added in an end effect for each new length. However, the wire itself has only one set of ends. Hence, it needs to be longer than shown for true resonance.

Special note: although we changed the length of the wire radically, we did not change its height above ground. Therefore, the TO angle remained constant throughout the exercise. Increasing the length of a single wire does not lower (or raise) the elevation angle of maximum radiation.

b. Changing the frequency of operation

We can perform the same exercise in a second way. Instead of doubling the length of the antenna, we may instead simply double the frequency. If we use the 2, 3, and 4 multipliers, we obtain frequencies of 7.2, 10.8, and 14.4 MHz. If we perform the experiment in this manner, we shall have to change the physical height of the antenna each time so that it is exactly 1 ë up for each new frequency. As we did in the first experiment, we shall increase the number of segments for each trial to the same value used the first time (11, 21, 31, and 41 for the NEC model).

If we perform the trials in the manner just described, our new table will look like the one that follows.

Performance of Wire Antennas 1 Wavelength Above Average/Good Ground

Frequency MHz	Length wl*	Az hdg degrees	TO angle degrees	Gain dBi	Source Impedance R +/- jX Ohms
3.6	0.5	0	14	7.85	72.09 - j 0.07
7.2	1.0	0	14	9.49	5886 + j 703.2
10.8	1.5	49	14	8.45	103.5 - j 56.48
14.4	2.0	34	14	9.02	3644 + j 528.7

* Since we are multiplying frequency relative to the physical length, the lengths in wavelengths are approximate.

Some things did not change at all. The TO angle remained the same, because it is a function of the wire's height above ground as measured in wavelengths. The patterns that we produced are virtually identical to those from the previous exercise, and **Fig. 76-5** remains a proper portrayal of both the elevation and azimuth patterns.

We can notice a few changes in the table. For example, the impedance values appear to be a bit closer to resonance for each of the steps above the original frequency, relative to the values for doubling the wire length. The wire diameter is the source of this phenomenon. As we multiplied our frequency, we also divided the wavelength so that it became a smaller quantity. However, we kept our AWG #12 copper wire. Hence, relative to a wavelength, the wire became fatter with each multiplication. For straight-wire elements, the fatter the wire, the shorter the required physical length for resonance. Even though the frequency-multiplied versions of the antenna are the same relative physical lengths as in the first trials, they are electrically longer due to element fattening.

The second change to notice is the set of gain values. They are lower than in the earlier table. Wire size cannot be the culprit, since we would expect a fatter wire to have slightly lower losses than a thinner one. In fact, the radiation efficiency of the 14.14 version of the antenna appears as 98.83% in the NEC output file, whereas the efficiency of the 2.0-λ 3.6-MHz model shows as 97.70%. So we cannot even blame skin effect, which increases with frequency.

The source of the lower gain in the models that multiply frequency is actually the ground. Although we did not change any of the ground constants, losses due to the ground increase with frequency (as well as with proximity to it). Once more, even though the differentials make no operational difference that anyone could detect, they are numerically visible and give us indications of the influence of various factors on the actual gain of a given antenna.

C. Wire Diameter: 1. Effect on the Feedpoint Impedance

We noted in passing that changing the diameter of a wire had an effect upon its resonant length. We can get a small handhold on this phenomena in two ways, and we shall sample them both. This is a good exercise to perform with a wire in free space to minimize the number of possible variables at work. So let's return to our resonant 3.6-MHz center-fed wire that was +/-66.5 feet (20.284 m) long in **Fig. 76-1**. (Of course, you should begin with whatever length turned out to be resonant in free space within your own software.) The AWG #12 copper wire will be our center-point for the chart. Let's sample AWG wire sizes from #4 through #20 in steps of 4 gauges. We shall preserve the wire length and see what happens to the source impedance. See model 76-7.

Changing Wire Diameter: Effect Upon Source Impedance

AWG #	Diameter Inches	Diameter mm	Source Impedance R +/- jX Ohms
4	0.2043	5.189	73.22 + j 3.57
8	0.1285	3.264	73.34 + j 1.53
12	0.0808	2.052	73.73 - j 0.27
16	0.0508	1.290	74.53 - j 1.73
20	0.0320	0.813	75.99 - j 2.64

Over the 6.38:1 diameter range in our set of trials, we find a small but definite progression of impedance values. As we increase the copper wire diameter, the resistance component of the source impedance goes down. The reactive component becomes less capacitive and more inductive, indicating that the diameter increase is also increasing the electrical length for the same physical length of wire.

C. Wire Diameter: 2. Length Required for Resonance

We may alter the trial by aiming toward the wire length that will yield a resonant 3.6-MHz antenna. If we do the job, the results will look similar to those in the following table.

Changing Wire Diameter: Effect Upon Resonant Wire Length

AWG #	Diameter Inches	Diameter mm	Resonant Length Feet	Resonant Length Meters	Source Impedance R +/- jX Ohms
4	0.2043	5.189	132.80	40.477	72.76 + j 0.05
8	0.1285	3.264	133.00	40.538	73.19 + j 0.29
12	0.0808	2.052	133.10	40.569	73.73 - j 0.27
16	0.0508	1.290	133.20	40.599	74.69 - j 0.36
20	0.0320	0.813	133.30	40.630	76.31 + j 0.23

Between the largest conductor and the smallest, we find about 0.5' (0.153 m) difference in length. The trend is perfectly visible, but the effect on a practical 80-meter antenna in terms of selecting #12 or #14 wire is negligible. The change in the resistive (resonant) impedance is also quite visible as it changes by nearly 4 Ω. Once more, the change is more visible than significant for practical antenna building. Still, we need to be aware of small systematic changes as well as large ones.

The changes are a guide to the likely consequences of using fatter wires. We may simulate widely space wire pairs (with either open or closed ends) and of cages of wires used by some lower HF antenna designers to simulate truly fat elements and to obtain a wider operating bandwidth. However, the concept of operating bandwidth is farther down the list of properties that we wish to examine in our systematic survey of properties.

In fact, we have run out of space for this episode. So we shall have to reserve the remaining exercises for the next one.

77. Developing Antenna Expectations Using Modeling Software
1B: Horizontal Wires in the Lower to Medium HF Range

In the first half of our exploration of the modeled characteristics of horizontal wire antennas, we examined a number of basic properties. Starting with the differences that we encounter when placing the antenna in free space or over a specified ground, we moved on to look at the effects of selecting a resonant or non-resonant wire length. We continued our investigation of length by extending the wire's electrical length in two ways: by multiplying the initial length while staying at the initial frequency (3.6 MHz) and by multiplying the frequency while retaining the initial length. Finally, we examined differences made by changing the wire diameter from its initial AWG #12 value to a range from AWG #4 through AWG #20. We saw the difference that wire size made in the source impedance of a constant length antenna and also the difference in resonant antenna length as we changed the wire size.

In each case, we focused upon two features of the properties. First, we wanted to see what trends developed–and, if possibly, why. Second, we made note of those trends that might make a significant operating difference, separating them from those that were numerically interesting but not operationally significant.

In this continuation of the investigation, we should complete our preliminary study. As you may recall, we set up a list of modeling tasks.

A. The antenna environment (free space or over ground)
B. The length
   1. Resonant vs. non-resonant lengths
   2. Physical length vs. electrical length
      a. Changing the physical length
      b. Changing the frequency of operation
C. Wire diameter
   1. Effect on the feedpoint impedance
   2. Length required for resonance
D. Height above ground
   1. Effect on the feedpoint impedance with a constant length
   2. Length required for feedpoint resonance
E. Ground quality
F. Wire conductivity

G. Operating (SWR) bandwidth vs. wire (element) diameter

Having completed items A through C, we may move on to items D through G. As was true in the first half of our work, each modeling task is quite simple, although most involve several repetitions, each time making a small specified change in the model. As well, we shall begin with a resonant AWG #12 copper wire center-fed dipole 1 λ above good ground (conductivity 0.005 S/m, permittivity 13). **Fig. 77-1** outlines the model. In most cases, we shall retain the minimal but adequate segmentation, using 11 segments for the half-wavelength antenna in NEC models and 10 or 12 segments in MININEC models.

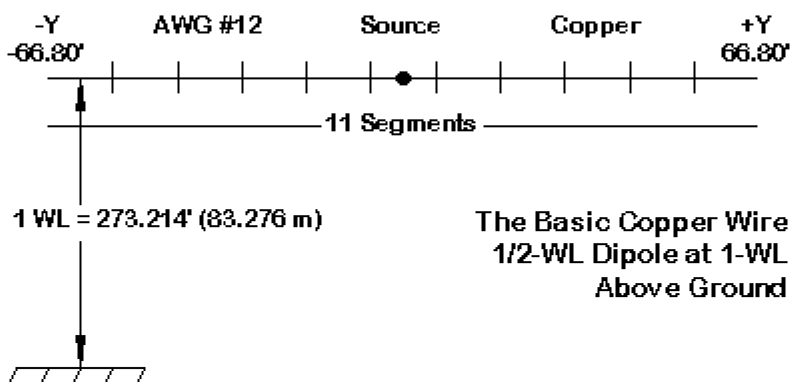

Fig. 77-1

Perhaps the only term for which we need a reminder is the idea of resonance. For our exercises, we shall treat an antenna as resonant if the source reactance is less than +/-j1 Ω. As always, slight differences between programs may make slight differences in the actual numbers you find in your program reports. This situation applies not only to the differences between NEC and MININEC programs, but also to different implementations of each calculating core. However, the trends that we discover should not change.

D. Height Above Ground: 1. Effect on the Feedpoint Impedance with a Constant Length

A number of erroneous generalizations pervade introductory literature on center-fed dipole antennas. We saw from our look at the effects of wire diameter on resonant length that the simplified cutting formulas that inhabit handbooks are very imprecise. In addition, I often hear that, as we reduce the height of a dipole toward ground, the impedance goes down. Now we have a way to find out. Let's begin with our older free-space resonant dipole and run it up and down a ladder of height. That dipole was 133.1' (40.57 m) long and reported a source impedance of 73.73 - j0.27 Ω. See model 77-1.

To see what happens to the source impedance at various heights, let's check it every 0.1-ë from 0.25-λ up to 1.25-λ. We shall start at a 1/4-λ height because MININEC programs are generally inaccurate in reporting both the gain and the source impedance for antennas with a horizontal radiation component when they are 0.2-λ or lower. If we perform the exercise, we shall obtain a table like the one that follows. Of course, we are retaining our 3.6-MHz test frequency.

The data form a complex pattern that may be clearer in graphical form. **Fig. 77-2** shows the changes in both resistance and reactance, with reference to left and right scales, respectively. Note the both the resistance and the reactance cover two complete cycles of peaks and nulls within the 1-λ span of antenna heights. The height of peaks and the depth of nulls diminish as we increase height, but the cycle continues indefinitely as we further increase height (until we reach a height at which succeeding differences are too small to detect or calculate).

Dipole Source Impedance Changes with Height Changes

Height WL	Feet	Meters	Source Impedance R +/- jX Ohms
0.25	68.30	20.82	87.61 + j 17.01
0.35	95.63	29.15	90.40 - j 4.69
0.45	122.95	37.47	75.47 - j 14.13
0.55	150.28	45.80	63.36 - j 5.76
0.65	177.59	54.13	66.26 + j 6.55
0.75	204.91	62.46	77.23 + j 7.86
0.85	232.23	70.78	81.55 - j 0.87
0.95	259.55	79.11	75.50 - j 7.08
1.05	286.88	87.44	68.38 - j 3.85
1.15	314.20	95.77	69.07 + j 3.34
1.25	341.52	104.09	75.54 + j 4.44

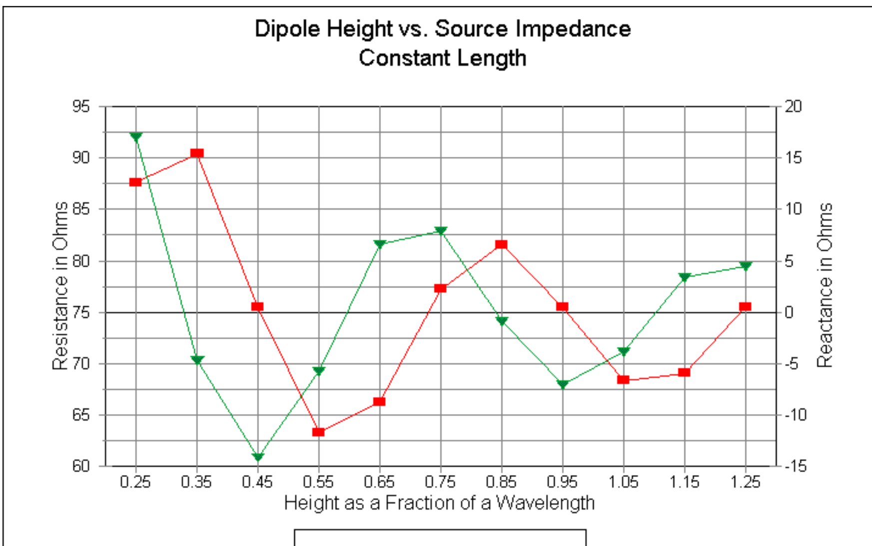

Fig. 77-2

More interestingly, the peaks and nulls for resistance do not occur at the same heights as corresponding peaks and nulls of reactance–where we may temporarily define a peak reactance as the maximum inductive value and a reactive null as the maximum capacitive value. Resistive peaks and nulls occur about 1/8 λ higher than their closest reactive counterparts. Moreover, the amount of change is actually greater than most folks expect from a simple wire antenna.

D. Height Above Ground: 2. Length Required for Feedpoint Resonance

There is a second way to examine these changes. Let's reformulate our question into this one: what is the resonant length of a wire dipole of the same composition for each height on the list? To this question, we may add, what is the corresponding resonant source impedance? We may start with our free space model and place it over good ground at the various heights. Then we may juggle the length until we achieve resonance. Finally, we may record the resulting wire length and the resonant feedpoint impedance to obtain a table like the following one.

Dipole Resonant Wire Lengths with Height Changes

Height			Resonant Length		Source Impedance
WL	Feet	Meters	Feet	Meters	R +/- jX Ohms
0.25	68.30	20.82	131.84	40.18	85.27 + j 0.15
0.35	95.63	29.15	133.46	40.68	91.09 - j 0.05
0.45	122.95	37.47	134.22	40.91	77.24 + j 0.13
0.55	150.28	45.80	133.54	40.70	63.94 - j 0.07
0.65	177.59	54.13	132.60	40.42	65.56 - j 0.06
0.75	204.91	62.46	132.50	40.39	76.25 - j 0.07
0.85	232.23	70.78	133.18	40.59	81.69 + j 0.17
0.95	259.55	79.11	133.64	40.73	76.36 - j 0.12
1.05	286.88	87.44	133.40	40.66	68.81 + j 0.03
1.15	314.20	95.77	132.84	40.49	68.70 - j 0.08
1.25	341.52	104.09	132.72	40.45	74.93 - j 0.16

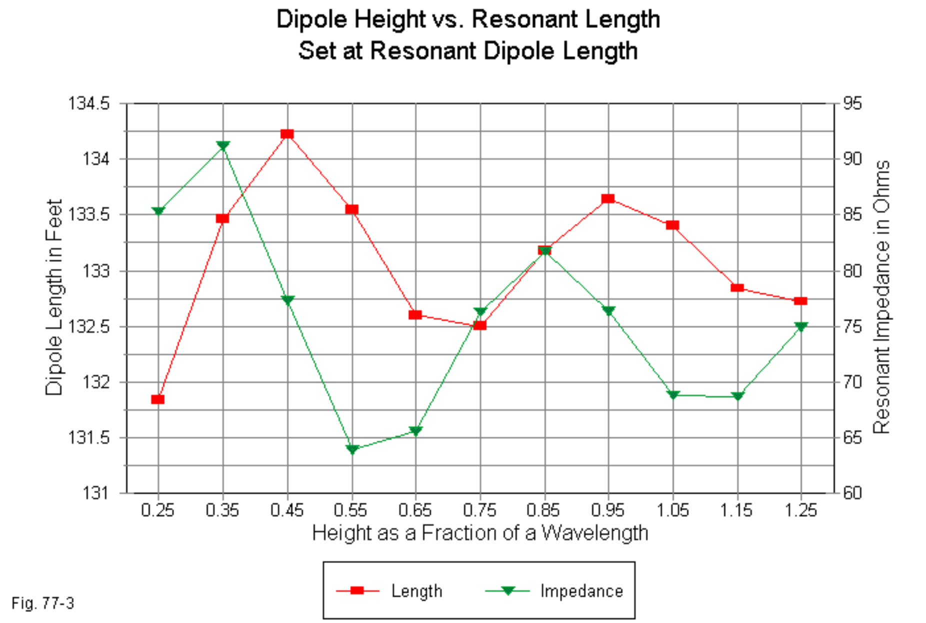

Fig. 77-3

Over the span of heights in the table, the range of resonant lengths varies by over 2' (0.6 m). As well, the resonant source impedance ranges from 64 to 91 Ω, a span of 27 Ω. The length reaches its maximums at greater heights than the maximums of source impedance. **Fig. 77-3** shows the relationship clearly. Note that, like the numbers in **Fig. 77-2**, the required resonant length for our wire undergoes two complete maximum-minimum cycles for each wavelength change of height.

The cycles that we have witnessed are not unique to simple dipoles. You will find similar phenomena in parasitic arrays based on the horizontal dipole, although with smaller excursions of resistance and reactance. Should you wish to pursue this aspect of horizontal antenna behavior further, examine the maximum gain values for each height. You will discover gain peaks at about 0.625-λ and 1.125-λ heights, with minimums near the 0.375-λ and 0.875-λ marks. Like the other dipole properties, both peaks and nulls are about 1/2-λ apart from the next peak or null. However, with respect to gain, there is another property to consider: the elevation pattern shape. Track the gain of the dipole at high elevation angles for both maximum and minimum gain values as you change antenna heights.

Since the gain and pattern shapes are applicable to our first table of values, using a constant antenna length, you may fairly conclude that the differences throughout the exercise are functions of the antenna's interaction with the ground. Even though that ground remained a constant in terms of its conductivity and permittivity, the antenna's height above it changed, resulting in altered patterns of ground reflections at a distance to add to or subtract from the direct radiation. As well, ground reflections in the immediate vicinity of the antenna resulted in variations in the source impedance as we changed heights. We saw the effects on resonant wire length and source impedance grow smaller with increasing height. We might well conclude that the effects will continue to diminish with further height increases until differences from step-to-step become too small to call for notice.

E. Ground Quality

Since the basic source of the changes that occur with dipole performance as we vary the height of the antenna above ground are a function of the antenna's interaction with the ground, a new question arises. Will the performance of a dipole change (or change significantly) as we alter the characteristics of the ground beneath it? Of course, modeling software provides the means for reaching an answer. See model 77-2.

Although there is no absolutely systematic reason for doing so, sampling of the effects of ground conditions on antennas typically uses four traditional categories of soil: very poor, poor, good, and very good. In fact, these categories perform quite well in providing a fair sampling of ground effects. Taken from FCC charts that date to the 1930s, we may define each ground quality level in terms of the associated conductivity and permittivity (relative dielectric constant).

Some Useful Soil Types

Soil Type	Conductivity S/m	Permittivity (Dielectric Constant)
Very Poor	0.001	5
Poor	0.002	13
Good	0.005	13
Very Good	0.0303	20

To create some trials, let's begin with our resonant dipole over good ground at a height of 1 λ at 3.6 MHz. Then we need only change the ground constants to obtain the simple table that follows.

Changes of Dipole Performance with Ground Quality: 1-WL Height

Soil Type	Gain	TO Angle	Source Impedance
	dBi	degrees	R +/- jX Ohms
Very Poor	7.45	14	72.35 + j 2.20
Poor	7.66	14	72.60 + j 0.76
Good	7.85	14	72.09 - j 0.07
Very Good	8.03	14	72.28 - j 1.72

Between the worst and best of the soil types listed, we find only a 0.6-dB difference in maximum gain. As well, the TO angle does not change at all. The resistive portion of the source impedance changes by well under 1 Ω, and the reactance varies by less than 4 Ω. All in all, the trial suggests that for a horizontal wire antenna, the ground quality will make little difference to the antenna performance.

MININEC users, of course, may track the far field gain values and TO angles. However, since MININEC reports the source impedance as if the antenna were over perfect ground, it cannot track the changes in the source impedance with changes in ground quality. For the present test, those changes are not significant to operation of the antenna.

However, the changes that we saw result from an antenna height of 1 λ above ground. Suppose that we simply drop the antenna height to a half-wavelength, that is, a height of 136.61' (41.64 m). Without readjusting the antenna length, let's repeat the trials we just performed to see what happens.

Changes of Dipole Performance with Ground Quality: 1/2-WL Height

Soil Type	Gain dBi	TO Angle degrees	Source Impedance R +/- jX Ohms
Very Poor	7.02	26	69.58 - j 0.82
Poor	7.38	27	69.77 - j 3.69
Good	7.74	28	68.58 - j 5.20
Very Good	8.11	29	68.61 - j 8.48

Elevation Patterns for AWG #12 Copper Wire Dipole
1/2-Wavelength Above Various Ground Qualities

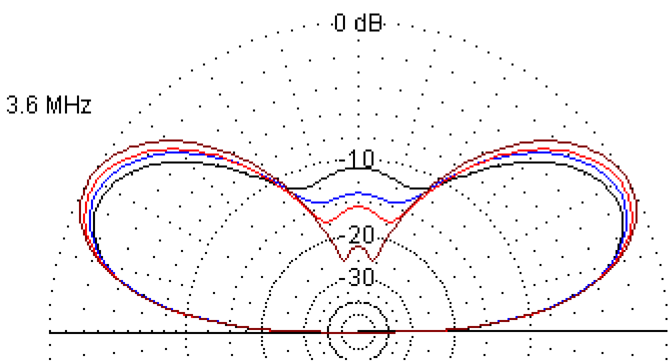

Ground Quality Traces:
Brown = Very Good
Red = Good
Blue = Poor
Black = Very Poor

Frequency: 3.6 MHz

Fig. 77-4

Immediately we see that the gain differential between the worst and best soils has grown to about 1.1 dB. This level of difference is sufficient to show up in overlays of the elevation patterns for the antenna above the 4 different soil types, as shown in **Fig. 77-4**. As well, the TO angle is no longer constant, but actually increases with improved soil quality. Although the range of resistance change in the source impedance remains about 1 Ω, the reactance change has increased.

The overall changes remain small, but the closer we bring the antenna to the ground, the greater the effect of soil quality upon the performance figures. You may wish to examine the antenna using other heights than the 2 that we have sampled. As well, you may wish to check performance at various heights using the ground constants for salt water (5 S/m, 81).

F. Wire Conductivity

The range of materials that we employ as antenna element materials ranges from silver-coated conductors to stainless steel. All of the materials are conductors, but with various levels of conductivity. Most implementations of NEC and MININEC permit the user to specify the material in order to account for losses that result from the fact that no conductor is perfect (since super-conductive wires for lower HF use are not available).

In fact, the most general procedure for the modeler is to introduce a value for conductivity. The program then calculates the losses incurred by each segment assigned that value and adjusts the results accordingly. Losses, of course, reduce far-field gain and near-field strength. As well, since these losses are resistive, they tend to increase the resistive portion of the source impedance slightly. Since the losses also have a very small but calculable effect on the resonant length of a wire element, the reactance will also show a small change from one level of conductivity to another. A few programs, such as EZNEC, call for the entry of values of resistivity, the inverse of conductivity. The following table lists the values of conductivity and resistivity that we shall use. However, different sources provide different numbers–usually only slightly different–so these numbers are not absolute by any means. However, they provide enough diversity for our purposes.

Some Values of Conductivity and Resistivity for Representative Conductors

Material	Conductivity S/m	Resistivity Ohms/m
Perfect	----	----
Silver	6.289E7	1.590E-8
Copper	5.747E7	1.740E-8
6061-T6 Aluminum	2.500E7	4.000E-8
Brass	1.563E7	4.099E-8
Zinc	1.667E7	6.000E-8
Phosphor Bronze	9.091E6	1.100E-8
Tin	8.772E6	1.140E-7
Type 302 Stainless Steel	1.389E6	7.200E-7

The values that we introduce are bulk values, which are adjusted relative to the wire surface area and skin effect into actual values per unit length. Hence, the effects of wire conductivity will vary with the surface area of the wire (as well as the frequency of use). To better see the effects of using different wire materials for antenna elements, we should not simply sample our AWG #12 wire (diameter 0.0808" or 2.05 mm). Instead let's use a range of material diameters. At the bottom end, we may sample AWG #20 wire (diameter 0.032" or 0.81 mm). The ratio of #12 to #20 wire is about 2.5:1. At the opposite end of the scale, let's specify a conductor 1" (25.4 mm) in diameter, about 12.4 times fatter than the #12 wire.

We shall use our #12 dipole at 1-λ above ground as the test vehicle. Because the source impedance will change so little, we shall be interested only in the maximum gain of the antenna. Since the maximum gain of a dipole does not change much as we move a little off the resonant frequency, we may perform the tests casually, retaining the initial dipole length throughout. The trends and degrees of performance change per change in material will not be altered by the procedure. However, you may refine the procedure to whatever degree you find most informative. The results of our runs appear in the following table.

Changes in Maximum Dipole Gain with Changes in Wire Conductivity

Material	Maximum Gain for Each Wire Diameter		
	AWG #20	AWG #12	1"
Perfect	7.94	7.94	7.95
Silver	7.70	7.85	7.94
Copper	7.60	7.85	7.94
6061-T6 Aluminum	7.56	7.79	7.94
Brass	7.55	7.79	7.94
Zinc	7.47	7.76	7.93
Phosphor Bronze	7.29	7.69	7.93
Tin	7.28	7.69	7.93
Type 302 Stainless Steel	6.22	7.29	7.90

The results have much to tell us. We expected the maximum gain to decrease with the increasingly poor conductivity of the materials as we move down our list of samples. For AWG #20 wire, the expectation seems to follow a nearly ideal pattern. The conductivity value for silver is nearly 3.8 times that for stainless steel, and there is a 1.5-dB net difference in gain. However, as we move up to AWG #12 wire, the difference between silver and stainless drops to just over 0.5 dB. With a 1" conductor, the difference is a mere 0.04 dB.

For each frequency, there is a diameter of element such that any larger diameter fails to improve the gain. In effect, the surface area of the conductor per unit length is sufficiently large that the conductor approaches the status of a perfect conductor. For our test frequency of 3.6 MHz, that diameter is in the vicinity of 1" (25.4 mm). Since there is no existing standard of just how well an element must perform to be accorded the “near-perfect” status, you will have to determine your own standard, most likely based on whatever design or analysis task you are performing.

The required diameter for near-perfection compresses the gain level of dipoles ranging from silver to stainless steel into a tight group without significant gain differential from the lowest to highest values. In part, the required diameter is a function of its ratio to the wavelength at the frequency of use. Although a 1" diameter stainless steel element for a 3.6-MHz dipole is impractical, much smaller diameters of “near-perfect” stainless steel conductors become feasible at VHF and UHF frequencies with insignificant loss relative to the more usual element material, aluminum. Where durability under extreme conditions may be necessary, antennas in this range often use stainless steel.

G. Operating (SWR) Bandwidth vs. Wire (Element) Diameter

The concept of "operating bandwidth" begins with the question of over what frequency range a given antenna will perform to specification. The specifications may include any of the operating parameters that we have come to associate with antenna use: gain, front-to-back ratio (if relevant), beamwidth, pattern "purity" (as defined for a given task), and source impedance. In some cases, source impedance is not a significant concern, as in the use of a doublet over a wide frequency range with an antenna-tuning unit to effect a match to the equipment involved. However, in many circles, operating bandwidth and 2:1-SWR bandwidth have come to be nearly synonymous.

Dipoles are a good case in point. Our AWG #12 copper dipole at a height of 1 λ shows the following properties at 3.5, 3.6, and 3.7 MHz.

Operating Properties of an AWG #12 Copper Dipole

Property	Frequency in MHz		
	3.5	3.6	3.7
Maximum Gain dBi	7.67	7.85	7.99
TO Angle degrees	14	14	14
Horizontal Beamwidth degrees	80.2	79.6	79.0
Pattern purity	fig-8	fig-8	fig-8
Source Impedance (R+/-jX Ohms)	68.80-j48.85	72.09-j0.07	75.86+j49.19
72-Ohm SWR	2.376	1.002	2.397

Only 1 set of numbers suggests any limitation to the operating bandwidth of the antenna: the 72-Ω SWR, as derived from the source impedance across the 3.5- to 3.7-MHz passband.

For other type of antennas, any of the operating properties may stray from specifications and hence defeat the use of an antenna for a given application over the desired passband. Mono-band quads very often have a wider SWR bandwidth than they do a front-to-back bandwidth, perhaps defined as a ratio of 20 dB or better. Other antenna may change pattern shape to undesirable forms. Some UHF long-boom Yagis suppress forward sidelobes by 20 dB or more only over a narrow bandwidth, even though the forward gain and SWR bandwidths are much wider.

With these cautions in mind, we may look at the SWR bandwidth of our dipole. We shall use the same set of dipoles that we employed for the conductivity studies, although we shall bring each to resonance at 3.6 MHz. The following table sets up the 3 copper dipoles for our exercise. For convenience, we may set the reference value for our SWR curves at 72 Ω.

3 Dipoles Used for SWR Bandwidth Exercises

Material	AWG #20	AWG #12	1"
Length feet (meters)	133.76 (40.77)	133.60 (40.72)	132.54 (40.40)
3.6-MHz Source Impedance (R +/- jX Ohms)	74.58 - j 0.06	72.09 - j 0.07	70.58 - j 0.02

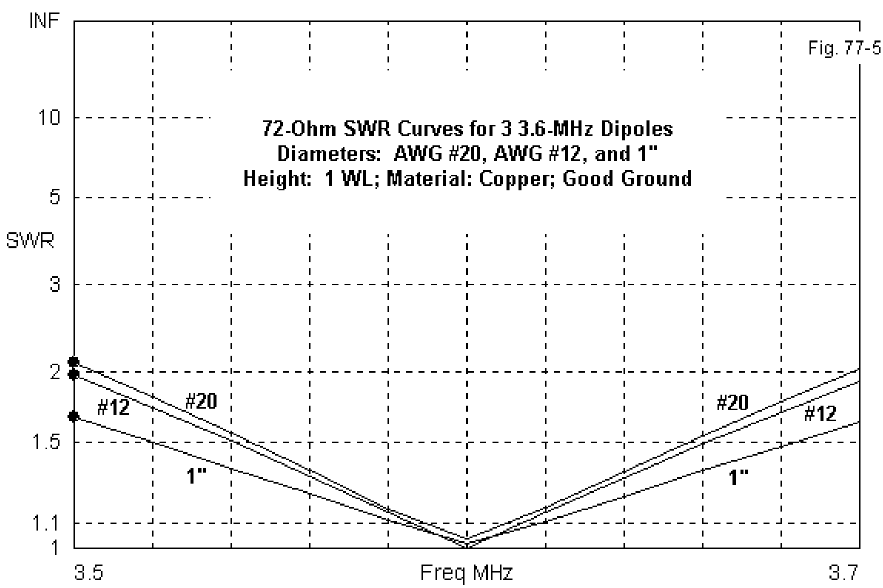

Fig. 77-5 presents the three 72-Ω SWR curves together. The curves show clearly the relationship of element diameter to the SWR bandwidth of a simple center-fed antenna. The 1" diameter version has a significantly wider bandwidth in terms of an SWR value below 2:1 than either of the wire dipoles. The #20 version has the worst of the 3 SWR bandwidths.

However, 1" elements are difficult to erect and maintain at 3.6 MHz, given their length in excess of 133' (40 m). Therefore, wire antenna users in the lower HF region often simulate larger elements with pairs (or cages) of wires. For example, we can simulate the large element with a pair of AWG #12 wires spread apart by about 12" (0.30 m). **Fig. 77-6** shows some of the modeling techniques used to capture this antenna. See model 77-3.

Fig. 77-6

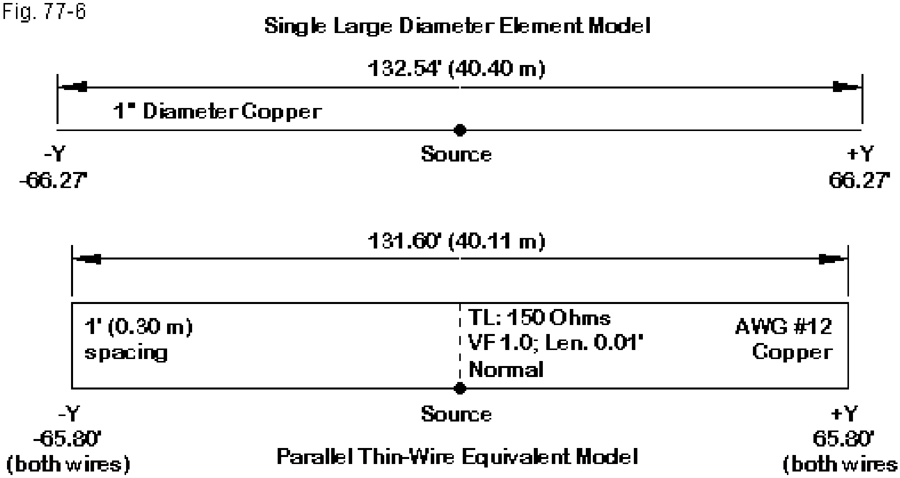

For the model, run both long wires in the same direction, a move necessary to use the feeding technique. Use enough segments so that the end wires (1 segment each) are about the same length as the segments in the long wires. Be sure to use the same number of segments in both long wires, since the close spacing requires good segment-junction alignment for maximum accuracy.

Place a source at the center of one of the long wires. From the source segment, run a TL-type transmission line to the center of the other wire. Specify a negligible length, for example 0.01' (3 mm). Assign the transmission line a characteristic impedance (Zo) of about twice the value expected at the source. In this case, a dipole would generally have an impedance between 70 and 75 Ω, so a Zo of 150 Ω will do. Let the velocity factor be 1.0, if applicable to your software. Unfortunately, this technique does limit the model to NEC-based software, since implementations of MININEC do not have a TL facility.

NEC gives the transmission line its assigned length, regardless of the physical distance between the terminal points. The effect of the minuscule TL length is to electrically join the source segment and its counterpart on the other wire as if the two were in a tapering junction. However, it saves the complexities involved in physically modeling the taper and often produces more accurate results, since it does not press NEC limits for angular junctions. The following small table gives the results of the modeling in comparison to the 1" dipole previously modeled.

A Comparison of a 1" Copper Dipole vs. Paired AWG #12 Copper Wires at 3.6 MHz

Property	Antenna	1" Element	2xAWG #12
Length feet (meters)		132.54 (40.40)	131.60 (40.11)
Maximum Gain dBi		7.93	7.91
TO Angle degrees		14	14
Horizontal Beamwidth degrees		79.8	79.8
Pattern purity		fig-8	fig-8
Source Impedance (R+/-jX Ohms)		70.58-j 0.02	71.18-j 0.41
72-Ohm SWR		1.020	1.013

The two antennas are virtually identical in performance. The paired AWG #12 wires do not quite reach the gain of the 1" element because their combined surface areas are still shy of what the single fat element achieves. However, the paired-wire dipole is more likely to be supportable in practice.

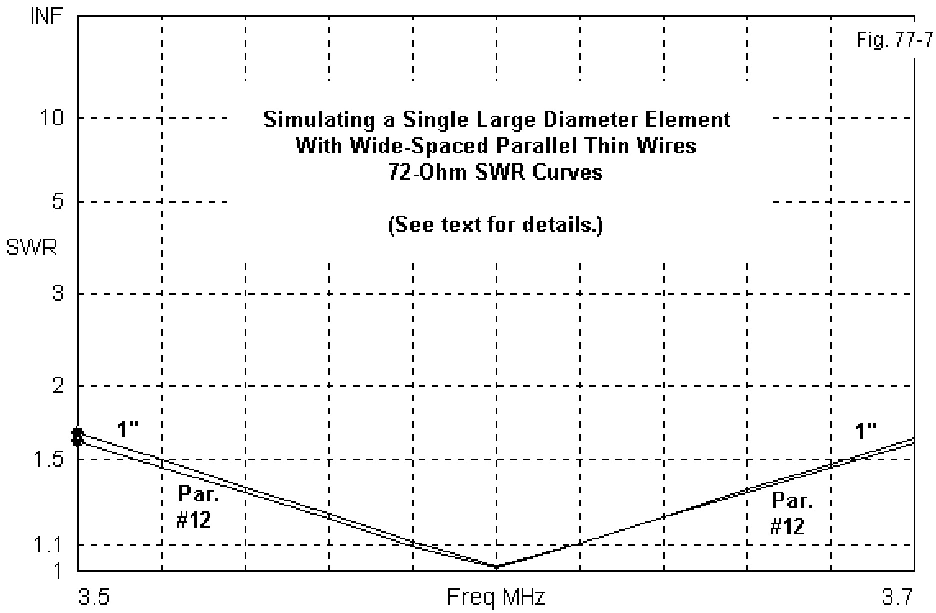

Fig. 77-7 combines the 72-Ω SWR curves for both antennas from 3.5 to 3.7 MHz. Actually, the dual-wire version has a slightly wider SWR bandwidth, suggesting that a wire separation of about 10" (0.25 m) would have achieved the initial goal.

Conclusion

We have covered a wide swath of properties associated with lower-HF wire horizontal dipoles and doublets, all of which are accessible via judicious modeling. Nevertheless, we have only scratched the surface. Many exercises remain for you to invent and develop to further refine your expectations from horizontal elements and antenna based upon them. You can replace assumptions, presumptions, and mythology with data derived from systematically modeling every aspect of the performance of basic antennas. From that data emerge more nearly correct expectations of the antennas that you design, build, or analyze.

78. Developing Antenna Expectations Using Modeling Software 2A: Vertical Dipoles

The second basic antenna type that we should systematically investigate through our modeling software is the vertical dipole. We shall look at the vertical monopole in the next column, but for now, the familiar dipole–turned on end–will be our subject. Although the exact parameters that we shall look at will differ in part from those we explored with the horizontal wire, we shall follow a similar procedure. The antenna properties that will interest us fall into the following categories.

A. Model convergence
B. Element diameter
C. Element material
D. Height above ground
E. Element length
F. Ground quality

As we have done before, we shall define resonance as a source impedance whose reactance is less than +/-j1 Ω.

A. Model Convergence

We may begin with a free-space model. Because we shall be working with the antenna–when we place it over ground–in wholly positive numbers that indicate its length, we may construct our free-space model in the same manner. **Fig. 78-1** shows the general outlines of the model. See model 78-1.

The figure does not indicate a specific length, because we shall soon look at several element diameters. However, to begin the process, let's consider the number of segments we need to use in the model. We shall begin by specifying a 1" (25.4-mm) element made from copper. (We shall look at alternative materials shortly.) Although the exact resonant free-space length may vary slightly depending upon the program used, we should also note that it may vary slightly with the number of segments used in the model–at least until the models converge. The table that follows **Fig. 78-1** shows the lengths and source impedance reports for the use of 11, 21, and 31 segments in a NEC-4 model. All models in this exercise will use 7.15 MHz as the test frequency.

Fig. 78-1

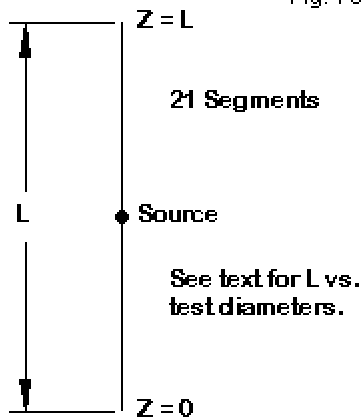

The Basic Free-Space
Vertical Dipole

Vertical Dipole Model Convergence

No. of	Resonant Length		Free-Space	Source Impedance
Segments	Feet	Meters	Gain dBi	R +/- jX Ohms
11	66.10	20.147	2.12	71.96 - j 0.08
21	66.06	20.135	2.13	71.95 - j 0.09
31	66.05	20.132	2.13	71.99 + j 0.02

Convergence is fairly simple, but worth looking at anyway. The 21-segment model is sufficiently converged with models using more segments to suffice for our purposes. Although the degree of convergence demanded is greater than would be operationally necessary under any conditions, it serves to indicate how model reports may vary slightly among otherwise identical models using different levels of segmentation.

I based my judgment of convergence upon the gain and the relative constancy of the resonant length. The impedance shows variations in resistance that are consistent with the different resonant points between the last two models. Because the second version shows a reactance slightly more negative than the first, we expect the resistance also to be slightly lower. In contrast, the reactance of the 31-segment model is (in relative terms) considerably higher than for either preceding model, and we expect the resistance to by a bit higher. Had I used 1 more decimal in the length determination, we could have easily brought the reactance to a level comparable to the 11- and 21-segment models. All such further maneuvering would likely have been of little value, since we shall simply adopt the 21-segment standard for all vertical dipole in these notes. However, we shall note in passing that the more complex the geometry of any antenna, the more important it becomes to go through the convergence process early on during the modeling task to ensure the greatest reliability possible for our results.

There is no need to show free-space E-plane and H-plane patterns for the vertical dipole, since they are the same as those shown for the free-space horizontal dipole. Relative to modeling software, there is a slight change of labels. For a horizontal wire, the E-plane pattern corresponds to the software designation of the azimuth pattern, while the H-plane pattern occurs on what the software calls the elevation pattern. However, we must reverse the software labels–and software place to look–for the patterns. For a vertical dipole, the E-plane pattern shows up when we request the elevation (or theta) pattern, while the H-plane pattern emerges when we call for the azimuth (or phi) pattern.

B. Element Diameter

While we are in free space, we may also confirm our expectations regarding changes in element length as we change the diameter of our vertical dipole element. Verticals for 40 meters come in many versions–some using tower structures and others using stepped-diameter tubing. Some even use wires suspended beneath tree limbs or other supports. For our checks, we may confine our sample to just a few sizes, perhaps 1" (25.4 mm), 0.5" (12.7 mm), and AWG #12 wire (0.0808" or 2.05 mm). For the test, we shall stay at 7.15 MHz and use 21 segments per element. Your results should resemble the ones in the following table. See models 78-1, 78-2, and 78-3.

Varying Vertical Dipole Diameter

El. Dia.	Resonant Length			Free-Space	Source Impedance
" (mm)	Feet	Meters	WL	Gain dBi	R +/- jX Ohms
1" (25.4 mm)	66.06'	20.135 m	0.480 wl	2.13	71.95 - j 0.09
0.5" (12.7 mm)	66.37'	20.230 m	0.482 wl	2.12	72.11 - j 0.05
AWG #12	66.88'	20.385 m	0.486 wl	2.07	73.18 - j 0.04

Consistent with our experience derived from looking at horizontal wires, the fatter the element, the shorter the resonant length. As well, fatter wires have slightly lower resistance values, since their losses are less than for thin wires. The effects are almost negligible for the move from a 1" to a 0.5" element. However, the differences are much more noticeable with the move from either of those two elements down to the thin #12 element.

The table lists the element length in 3 forms, adding the wavelength-measure to our normal lengths in feet and in meters. The underlying reason is that we shall be performing some essential tests of the vertical dipole in height increments measured in fractions of a wavelength. Knowing the antenna length as a fraction of a wavelength will let you easily calculate how far the bottom of the antenna is above the ground.

C. Element Material

Before moving our vertical dipole out of free space, let's examine the effects of selecting different materials for the element. Performing the exercise in free space will accustom you to seeing the differences in a different context than the one used for the horizontal dipole (which was 1 λ above good ground). We may also shrink the table of materials to give us a few widely separated materials from the longer list. (Modify models 78-1, 78-2, and 78-3.)

Some Values of Conductivity and Resistivity for Representative Conductors

Material	Conductivity S/m	Resistivity Ohms/m
Perfect	----	----
Copper	5.747E7	1.740E-8
6061-T6 Aluminum	2.500E7	4.000E-8
Tin	8.772E6	1.140E-7
Type 302 Stainless Steel	1.389E6	7.200E-7

If we look at both the free-space gain and the source impedance, we can tabulate the values. However, in examining the following table, remember that the resonant length of each vertical dipole came from the copper model.

Changes in Dipole Performance with Changes in Wire Conductivity

Material	Maximum Gain for Each Wire Diameter Source Impedance (R +/- jX Ohms) AWG #12	0.5"	1"
Perfect	2.14 71.97 - j 1.11	2.14 71.91 - j 0.22	2.13 71.85 - j 0.85
Copper	2.07 73.18 - j 0.04	2.12 72.11 - j 0.05	2.13 71.95 - j 0.09
6061-T6 Aluminum	2.03 73.81 + j 0.52	2.12 72.21 + j 0.04	2.13 72.00 - j 0.05
Tin	1.96 75.12 + j 1.63	2.11 72.41 + j 0.22	2.12 72.10 + j 0.04
Type 302 Stainless Steel	1.69 80.26 + j 5.73	2.06 73.19 + j 0.88	2.10 72.48 + j 0.36

The table shows us everything that we should have expected. The thinner the element, the greater is the loss in gain (from a perfect or lossless conductor) due to the lower conductivity value. With a 1" element, the losses through stainless steel are insignificant. However, the losses of an AWG #12 stainless steel wire become significant.

We may also notice a pattern to the impedance values in the table. First, the greater the material losses, the higher will be the source resistance. Second, as we increase the level of material losses, we also may notice a move to positive values of reactance, which would translate into a very slightly shorter resonant length for each element diameter. These effects are also related to the element diameter.

The final item for notice in the table is the gain of the dipole, even when using a perfect conductor. Both the AWG #12 and the 0.5" diameter dipoles show a gain of 2.14 dBi, but the 1" element shows a gain of 2.13 dBi. Because of the very small difference, it is easy to pass off the difference as a simple function of mathematical processing procedures for the core used. Indeed, in some programs, all 3 gains may be the same and in others, the 1" and 1/2" elements may show the same value.

However, the difference is real, even if not operationally significant. Dipole gain is also a function of the wire length. We saw with horizontal dipoles that if we lengthened a dipole beyond resonance, we encountered a slight increase in gain–and shrinking the dipole below resonance yielded a slightly lesser gain. Now compare the resonant lengths of the three vertical dipoles in free space. The 1" dipole is more than a quarter-foot shorter than the AWG #12 version, just about enough to make numerically visible the dependency of a dipole's gain on the dipole's length.

Perhaps a more important lesson emerges from the exercises. The gain of a wire element is not a function of its being resonant or non-resonant. Resonance is handy for numerous purposes, such as matching an antenna directly to a coaxial cable or–as in these exercises–for establishing a certain order of equivalence among models or for seeing clearly the effects of certain changes that we can make in the antenna or its operating environment. But the property of antenna gain is independent of the source impedance.

D. Height above Ground

For our remaining trials, we shall place the 1" (25.4-mm) vertical dipole over good ground (with changes in ground quality coming a bit later). We shall not change the length from its free-space resonant value (66.06' or 20.135 m). However, we shall be placing the antenna at different heights above ground, as shown in **Fig. 78-2**.

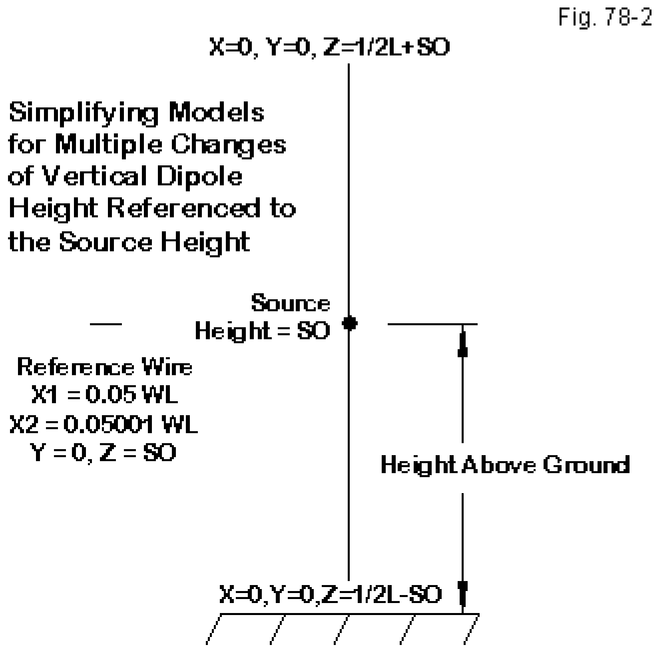

To effect the height changes, we need only add or subtract the required amount from both ends of the dipole. The key point in the height designations will be the source position, which is the center of the dipole. To ascertain that the source position is exactly where we need it, we can employ a second wire. The wire should be short–perhaps 0.001-λ long–and very thin–about AWG #20 or thinner. The wire position is at least 5' (1.52 m) away from the test antenna, but even with the source height. This wire is at right angles to the vertical dipole and too small to affect any of the performance report data from the main model. However, by changing the height of both the short wire and the vertical dipole together, we obtain a confirmation that the dipole center is precisely where we want it.

We shall move the vertical dipole from a source or center height of 0.25-λ above the ground to 1.25-λ above the ground. Because not all software can move a model in terms of wavelengths, the following table provides the 7.15-MHz source-point heights for the trials. For reference, 1 λ at 7.15 MHz is 137.56' or 41.93 m.

Trial Source-Point Heights

Height in	Wavelengths	Feet	Meters
	0.25	34.39	10.48
	0.35	48.15	14.68
	0.45	61.90	18.87
	0.55	75.66	23.06
	0.65	89.42	27.25
	0.75	103.17	31.45
	0.85	116.93	35.64
	0.95	130.69	39.83
	1.05	144.44	44.03
	1.15	158.20	48.22
	1.25	171.95	52.41

The lowest height is sufficient to place the bottom of the dipole less than a half-meter (1.36') above ground, since each side of the dipole is about 0.24-λ long. Since the azimuth pattern of the vertical dipole will be a circle, we may confine our interest in patterns to elevation. We shall record the maximum gain, the TO angle, and the source impedance of the antenna at each new source-point height. Results should resemble the following NEC-4 table. Use model 78-4, changing the height as needed.

Vertical Dipole Trial Performance Data

Height WL	Gain dBi	TO angle degrees	Source Impedance R +/- jX Ohms
0.25	-.11	18	98.16 + j 5.20
0.35	0.32	15	73.52 - j 7.43
0.45	0.30	14	68.44 - j 1.80
0.55	0.67	46	70.32 + j 1.72
0.65	1.97	41	72.82 + j 1.33
0.75	2.72	36	73.13 - j 0.39
0.85	3.20	32	72.00 - j 1.03
0.95	3.45	29	71.26 - j 0.36
1.05	3.52	26	71.57 + j 0.36
1.15	3.48	23	72.21 + j 0.31
1.25	3.43	21	72.34 - j 0.20

Let's begin with the source impedance data, since it is perhaps the simplest. **Fig. 3** shows the data in graphical form. Once we elevate a vertical dipole's center above about 0.4-λ, the impedance curves smooth out. In fact, for any height above about 0.4-λ, it would make no operational sense to adjust the length of the dipole to effect a more precise resonance. Only when the center of the dipole is lower than about 0.4-λ does the impedance show significant change, and the difference from resonance (within +/- j1 Ω) remains small. Contrast this impedance behavior with the behavior of a horizontal dipole at comparable heights, as noted in the preceding episode of this series.

Much more interesting is the gain and TO angle information in the table. If we examine only the gain column, we see a steady rise in gain until we reach 1.05 λ above ground. However, if we combine the gain and TO data, we discover a much more varied situation. Between the 0.45- and 0.55-λ level, the TO angle jumps from 14 degrees to 46 degrees. Since very little in antenna work shows a sudden large change, there must be an explanation to account for the change in the numbers, one that shows an evolution to the elevation pattern of the vertical dipole as we increase its height.

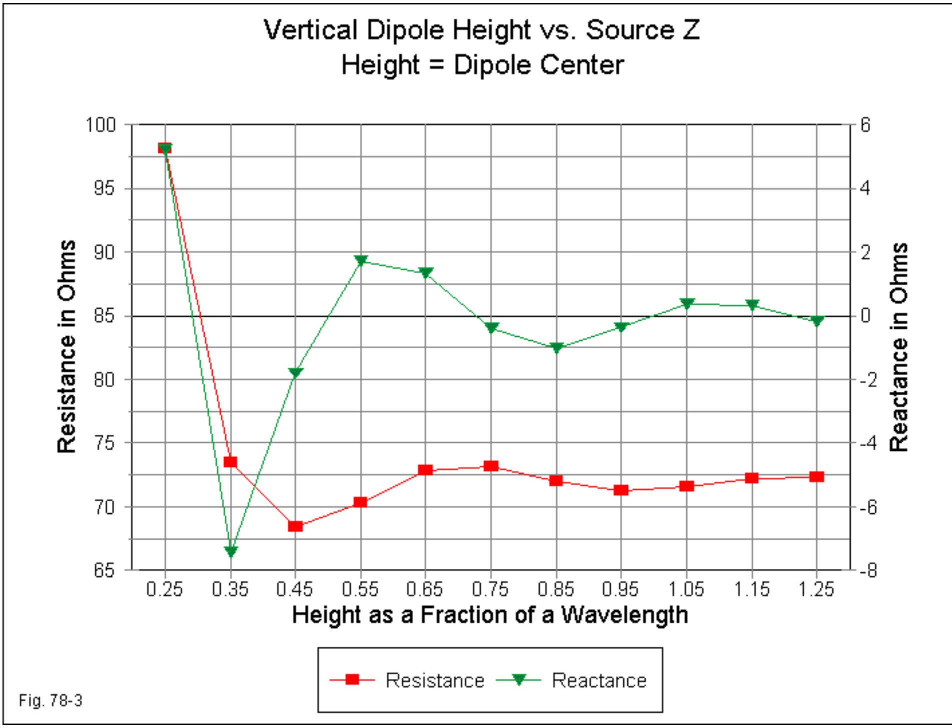

Fig. 78-4 samples the elevation pattern at various interesting heights, and you may fill in the missing heights with your own software. Only at 0.25-λ does the vertical dipole elevation pattern show a single lobe. At 0.35-λ, a second lobe emerges, initially as a bulge that is just recognizable as a second lobe. However, by 0.45-λ, the lobe has grown to serious proportions. We may pause here to note that this type of pattern evolution is common to many, if not most, vertically polarized antennas, not just to the vertical dipole. Many of the users of such antennas have two goals for the installation: to emphasize the low angle radiation (and reception), and to eliminate as much interference as possible arriving at high angles from shorter distances.

Hence, they prefer patterns like those at the two lower levels over the pattern for 0.45-λ, despite the lower gain level. The exact wire height required for a given vertically polarized array may differ somewhat from the one required for a vertical dipole. Hence, each vertical array needs careful planning (and modeling) to assure that it is at a height within the range of desirable heights.

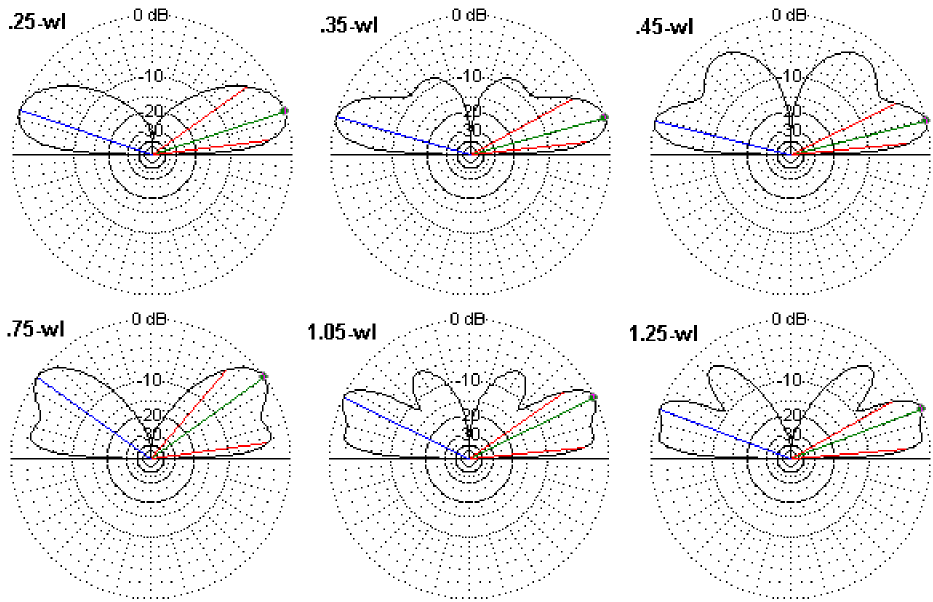

Representative Elevation Patterns as the Center of the Vertical Dipole Rises to the Heights Indicated

Fig. 78-4

If we extrapolate from the 0.45-λ level, we can imagine the secondary lobe continuing to grow until it becomes the lobe with maximum gain. **Fig. 78-4** skips to the 0.75-λ level to illustrate a second elevation pattern phenomenon: the merging of elevation lobes. As the elevation angle of the secondary lobe decreases, its vertical beamwidth does not narrow appreciably. Nor does the beamwidth of the lowest lobe decrease either in angle or beamwidth by any large amount. (Again, contrast this lobe behavior with lobe behavior for the horizontal dipole in the preceding episode.) The result is a merging of lobes into a “butterfly wing” appearance, which reaches its peak for 2 lobes at about 0.75 λ for our vertical dipole.

Above 0.75-λ, we see the emergence of a 3rd lobe, already well developed in the 1.05-λ pattern. This height, relative to our trial heights, shows the maximum gain for the second lobe. By 1.25 λ above ground, the 3rd lobe is large enough to reduce the gain in the second lobe by a small amount. However, we should note one more phenomenon. The lower two lobes are merging almost into one. The differential in gain between the two lobes is very small. At 10 degrees above ground, the gain is 2.61 dBi, well above the gain levels with the antenna closer to ground. Of course, elevating a vertical dipole to a center height of 1.25 λ is not practical at 40 meters. However, much higher center heights are common at VHF, where a vertical dipole gives a good account of itself in omni-directional point-to-point communications.

Let’s return to heights closer to the ground. We saw two interesting items in the table below the 0.55-λ mark. First was the sudden transition of maximum gain from the lower lobe to the upper lobe, a transition we now know to be a gradual transition in lobe development. Second, was the fact that at a height of 0.45-λ, the gain was lower than at 0.35-λ. Whenever we encounter such phenomena, we should take a more detailed look at the region. The following table gives the results every 0.05-λ from 0.25-λ to 0.50-λ above ground.

Vertical Dipole Trial Performance Data at Low Heights

Height WL	Gain dBi	TO angle degrees	Source Impedance R +/- jX Ohms
0.25	-.11	18	98.16 + j 5.20
0.30	0.12	17	81.52 - j 7.39
0.35	0.32	15	73.52 - j 7.43
0.40	0.35	14	69.62 - j 4.78
0.45	0.30	14	68.44 - j 1.80
0.50	0.22	13	68.98 + j 0.50

The source impedance information follows the curves shown in **Fig. 78-3**. Let's focus on the gain and TO angle data and graph it. See **Fig. 78-5**. The gain peaks at a height of 0.4-λ. Although the TO angle continues to descend slowly above that level, the gain decreases.

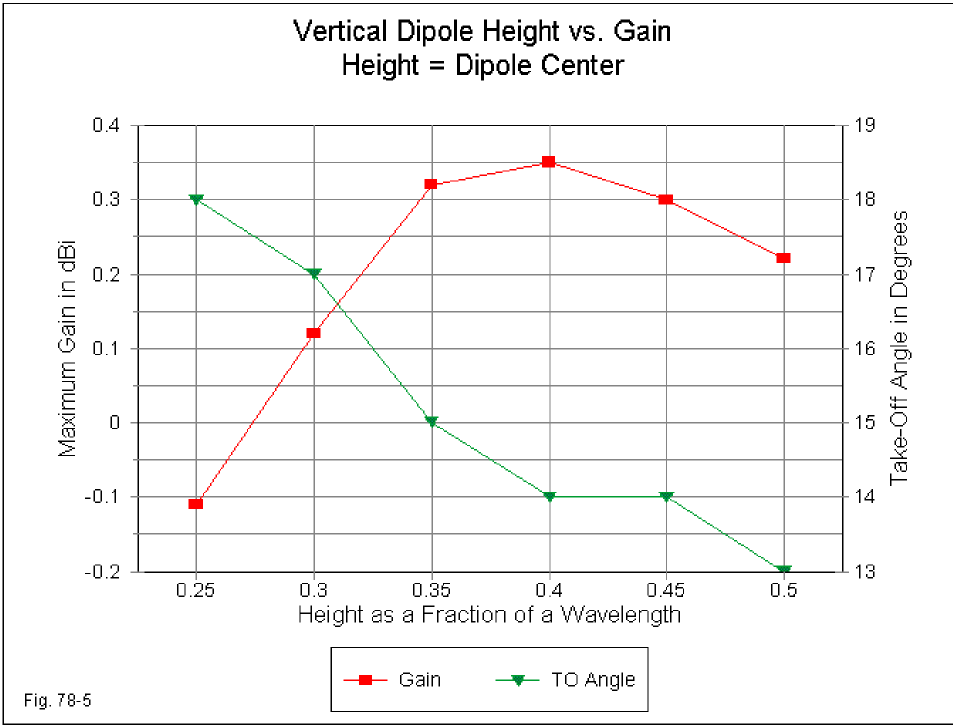

Fig. 78-6 provides 3 elevation patterns that show why this decrease occurs. The second lobe of a vertical dipole does not emerge as a narrow-beamwidth lobe, but instead as a large region of radiation (or reception sensitivity). At a height of 0.5-λ, the second lobe–even though weaker in terms of maximum gain–contains a great deal of the antenna's energy, as indicated by its large area. Remember that this elevation pattern would be the same regardless of the azimuth bearing, so in 3-dimensional terms, the second lobe already dominates the vertical dipole radiation pattern. The only source for that large increase in energy is from the lower lobe.

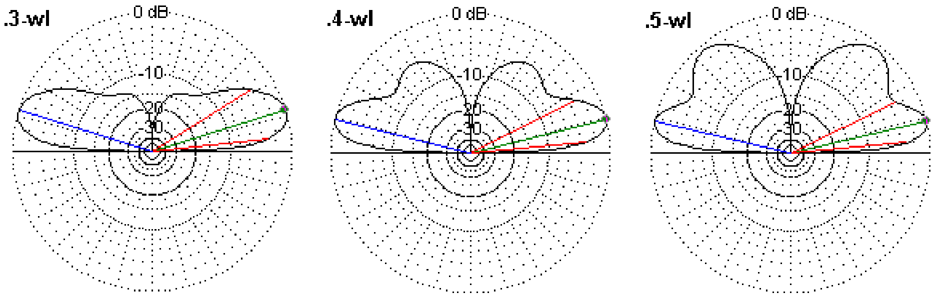

Elevation Patterns of the Vertical Dipole as Its Center Passes Through the Height of Maximum Gain in the Lower Lobe

Fig. 78-6

Lobe development for vertically polarized antennas is so different from the lobe development of horizontally polarized antennas that it requires detailed study, if one is to acquire reasonable expectations of vertical antenna behavior. These initial systematic exercises only form a start to the process.

E. Element Length

When we examined horizontal wires, we explored length changes in small increments. For our vertical dipole, we shall use much larger increments. First, set the center of the 1" (25.4-mm) dipole at a height of 0.8-λ (110.05' or 33.54 m). This height will allow us to extend each end of the antenna in 0.125-λ (17.20' or 5.24-m) increments, thus extending the total antenna length in quarter-wavelength increments. We shall start with the free-space resonant length, which is 0.48-λ, just shy of the perfect 0.5-λ mark, but using the resonant length will start us on familiar ground. The longest antenna length that we shall examine, 1.5-λ, will still clear the ground by 0.05-λ without moving the antenna's center point. See model 78-5.

For each change of length, we shall increase the number of segments by 10. The resulting segment lengths will therefore be close to the same for each new model. If we perform the exercise, we obtain a table that should resemble the following one.

Extending the Vertical Dipole Length

Length	Gain	TO Angle	Source Impedance
WL	dBi	degrees	R +/- jX Ohms
0.50	2.99	34	72.62 - j 0.09
0.75	2.45	32	497.0 - j 829.9
1.00	2.05	10	1922 - j 1621
1.25	2.62	9	144.6 - j 612.8
1.50	5.65	41	135.8 + j 35.85

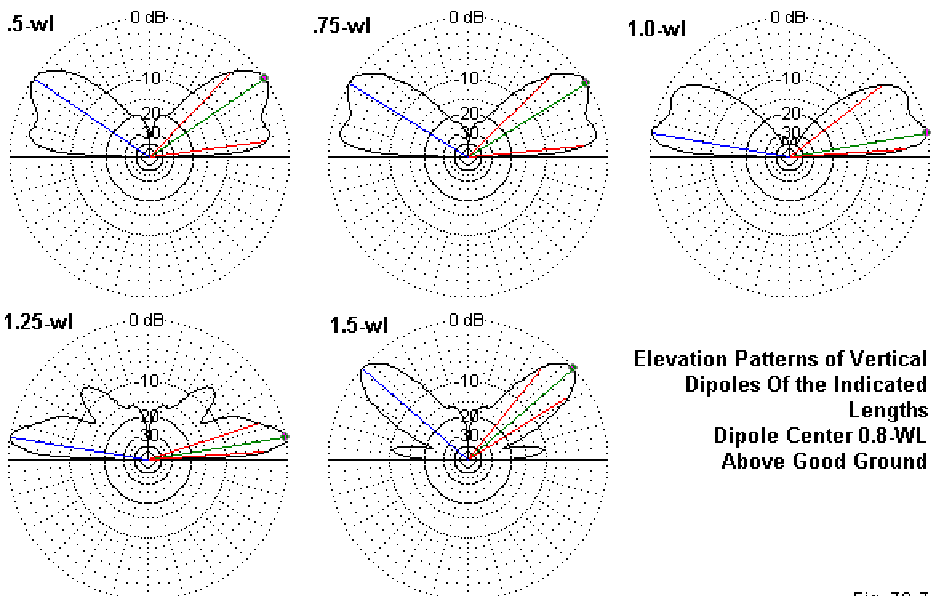

Elevation Patterns of Vertical Dipoles Of the Indicated Lengths
Dipole Center 0.8-WL Above Good Ground

Fig. 78-7

Fig. 78-7 can assist us in interpreting the data by relating it to the corresponding elevation patterns. The first two antenna lengths have high elevation angles, indicating that the maximum gain is in the second lobe. However, by a length of 1 λ, the maximum gain lies in the lowest lobe. Maximum low-angle gain appears with a length of about 1.25 λ. When we extend the length further, the lowest lobe almost disappears, and virtually all of the energy appears in the upper lobe that we just saw emerging with the 1.25-λ version of the antenna.

We may correlate in a general way the information in this table and figure with what we may already know about horizontal wires. In that arena, antennas maintained a broadside azimuth lobe up through and past a length of 1 λ. As we increase the length of the horizontal antenna, the broadside lobe continues to increase in strength and to narrow in beamwidth, although new lobes gradually appear at angles to the main broadside bearing. By the time we reach a length of 1.5 λ, the broadside lobe has severely diminished as the angular lobes dominate the pattern.

Turning the array on end to make a center-fed vertical antenna creates a comparable set of radiation phenomena, but translated to the elevation pattern and taking ground reflections into account in lobe formation. We achieve maximum low-angle gain at about 1.25 λ. At a length of 1.5 λ, the antenna becomes almost useless for low angle communications. Since vertical doublets are sometimes used as multi-band antennas, the lesson is not to use one that is longer than about 1.25-λ at the frequency of operation. If you find it necessary to operate where the antenna would be longer, it is likely time to set up a second vertical dipole.

F. Ground Quality

Because vertically polarized radiation tends to enter more deeply into the ground than horizontally polarized antenna radiation, verticals tend to be more sensitive to changes in the quality of the ground. Therefore, let's do a small survey of the effects of ground quality on antenna performance with our 1" (25.4-mm) vertical dipole. We shall use the same categories of ground quality that we employed for the horizontal wire. You may modify model 78-4 for these tests.

Some Useful Soil Types

Soil Type	Conductivity S/m	Permittivity (Dielectric Constant)
Very Poor	0.001	5
Poor	0.002	13
Good	0.005	13
Very Good	0.0303	20

To see whether height above ground makes a difference in the range of performance from the best to the worst soils, we shall perform the trial twice. The first test will place the center of the dipole at a height of 0.25-λ, and the second will place the center at a height of 0.5-λ (the highest level at which the lower lobe dominates over good ground). We shall record the gain, TO angle, and source impedance and arrive at a table that resembles the following one.

Changes of Vertical Dipole Performance with Ground Quality

Center Height: 0.25-Wavelength

Soil Type	Gain dBi	TO Angle degrees	Source Impedance R +/- jX Ohms
Very Poor	-.74	21	91.80 + j 1.63
Poor	0.22	19	96.04 + j 5.35
Good	-.11	18	98.16 + j 5.20
Very Good	1.94	15	101.7 + j 8.80

Center Height: 0.5-Wavelength

Soil Type	Gain dBi	TO Angle degrees	Source Impedance R +/- jX Ohms
Very Poor	1.37	16	69.97 + j 0.60
Poor	1.13	14	69.26 + j 0.35
Good	0.22	13	68.98 + j 0.49
Very Good	1.25	10	68.13 + j 0.21

At the lower height, the source impedances show a maximum variation of 10 Ω resistance and j7 Ω reactance. At the higher level, the source impedance differences are under 2 Ω resistive and less than j0.5 Ω reactive. This data provides the suggestion that the higher above ground that we place a vertical dipole, the less the effect of the ground in the immediate area of the antenna on the source impedance.

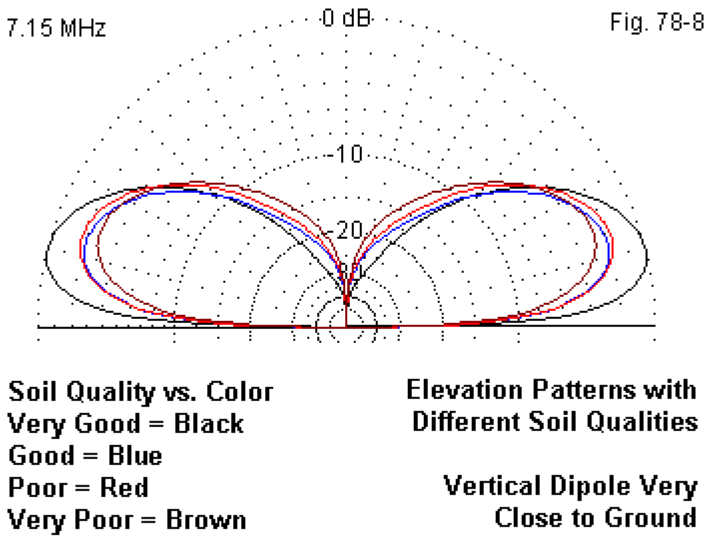

To gain a handhold on the gain and TO angle data, **Fig. 78-8** provides overlaid patterns of the lower-level antenna over the 4 ground types. We can clearly see the increase in TO angle with a decrease in soil quality. The gain is another matter, since the table shows shifts above and below 0 dBi. However, except for the gain over very good soil, the actual patterns are tightly clustered. However, the gain over good soil is lower than the gain over poor soil, which may initially seem unexpected. NEC calculates the effects of ground quality by creating a single composite value from the conductivity and permittivity values in the tables. The method of combining them results in a slightly higher far-field loss for good soil than for poor soil. Operationally, the difference could not be noticed, assuming that we could ascertain that our soil in fact met the condition for either good or poor soil in the table.

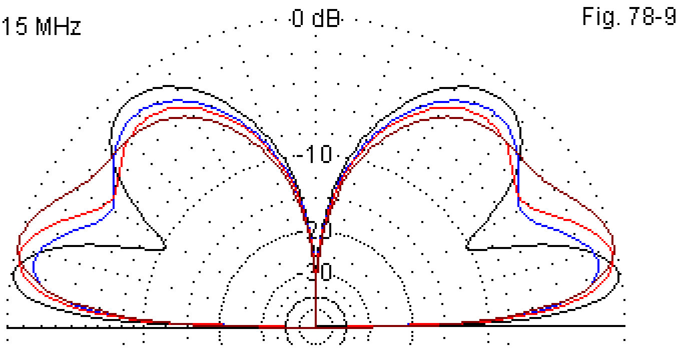

Soil Quality vs. Color
Very Good = Black
Good = Blue
Poor = Red
Very Poor = Brown

Elevation Patterns with
Different Soil Qualities

Vertical Dipole with Source
1/2-WL above Ground

Fig. 78-9 overlays the elevation patterns for the upper-level antenna over each of the 4 soil types. The entire series is interesting, since it samples patterns with two elevation lobes. Perhaps the first notable feature is the face that, if the soil is very good, then the lobe structure of the elevation pattern is more distinct than for any of the lesser soil qualities. We see the familiar increase in TO angle with decreasing soil quality. As well, the good soil pattern has lower gain than the poor soil pattern. However, what may surprise us most is that the highest gain occurs with the antenna over very poor soil. The advantages of finding a location with very good soil dwindle as we elevate the antenna further above the ground.

We may fairly ask whether a ground radial system beneath the vertical dipole will improve its performance. Unfortunately, neither NEC-2 nor MININEC permit buried radials. The closest that we can come in these programs is to place a radial system at about 0.001-λ above ground, a procedure available in NEC, but generally not recommended for MININEC. We shall use 64 radials to create a radial system about as large as amateurs ever use, larger than most in operation, but shy of commercial broadcast standards. Smaller radial systems will have lesser effects than those shown, but larger ones will not change the results significantly. With the radials in place, we can re-run the trials for both the lower and higher antenna positions over the 4 soil types. See models 78-6 and 78-7. The table we develop will be similar to the following one.

Changes of Vertical Dipole (Plus Radials) Performance with Ground Quality

Center Height: 0.25-Wavelength

Soil Type	Gain dBi	TO Angle degrees	Source Impedance R +/- jX Ohms
Very Poor	-.20	21	85.88 + j 11.60
Poor	0.56	19	90.60 + j 10.75
Good	0.18	18	91.68 + j 8.88
Very Good	1.95	15	98.69 + j 8.00

Center Height: 0.5-Wavelength

Soil Type	Gain dBi	TO Angle degrees	Source Impedance R +/- jX Ohms
Very Poor	1.41	16	70.33 + j 0.71
Poor	1.17	14	69.50 + j 0.44
Good	0.26	13	69.17 + j 0.64
Very Good	1.25	10	68.14 + j 0.32

In no case did the radial system model change the TO angle of any of our trials. At the higher level, the maximum impedance difference made by the radials was about 1/3-Ω. The maximum gain difference was 0.04 dB. Hence, the radials prove to be ineffective in improving the performance of a vertical dipole placed a half-wavelength over ground at its center, with the tip about 1/4-λ above ground.

The lower antenna shows some signs of improvement for soils worse than very good, where differences are not significant with and without the radials. Gain increases with decreasing soil quality, with a maximum improvement of about 0.5-dB for very poor soil. We would expect more significant changes in source impedance, since it is largely a function of soil in the immediate antenna area. Here we find that the source resistance decreases by about 6 Ω on average, suggesting lower ground losses.

As a side note, we may re-run the lower-level antenna over a 64-radial field buried a half-foot under the soil, if we have NEC-4. I am adding this exercise, since it provides a check on the adequacy of the model that uses a slightly elevated field to simulate buried radials. Our buried radial version produces the following results. See models 78-8 and 78-9.

Changes of Vertical Dipole (Plus Buried Radials) Performance with Ground Quality

Center Height: 0.25-Wavelength

Soil Type	Gain dBi	TO Angle degrees	Source Impedance R +/- jX Ohms
Very Poor	-.02	22	89.42 + j 15.40
Poor	0.71	19	95.29 + j 15.00
Good	0.35	18	96.14 + j 13.16
Very Good	2.09	15	100.7 + j 11.75

The buried radial system show less change in source resistance relative to the antenna with no radials than did the system with elevated radials. However, the effects upon the reactance result in a relatively uniform “detuning” effect, with similar reactance levels for all 4 soil types. Gain increases vary from 0.15 dB for very good soil to 0.72 dB for very poor soil. These values do not change for moderate changes in the depth of the radial field.

The result is that the NEC-2 simulated buried radial field only partially captures the effects of buried radials as modeled in NEC-4. For some operational planning and analysis needs, the NEC-2 radials may be perfectly satisfactory; for other needs, they may fall short. A final reminder is in order: the 64-radial field is large. Any smaller fields will have lesser affects upon the performance of the low-level vertical dipole.

Conclusion

We have run a number of systematic modeling studies on vertical dipoles to become familiar with their properties. A more complete set of exercises would include the same trials for vertical dipoles for many frequencies, from MF through at least high HF. As well, there are numerous other systematic tests that are possible with the modeling software for this basic antenna. This episode simply shows a few of the many paths of study that are possible in the process of developing reasonable expectations of the vertical dipole–and antennas based upon it.

However, as incomplete as the work may be, we shall move on. There is another basic vertical antenna type that needs attention long before we look at more complex antennas: the vertical monopole. That will be our subject next time.

79. Developing Antenna Expectations Using Modeling Software 2B: Vertical Monopoles

In the last episode, we examined the vertical dipole. This month, we shall explore its half-brother, the vertical monopole. Actually, we shall divide our work in two, examining fraternal twins: the elevated vertical monopole with an attached ground plane and the ground-mounted vertical monopole with a ground plane on or under the soil. By starting with the elevated monopole, we can begin the sampling as we did for every other episode in this series: in free space.

As always, we shall look systematically at a number of antenna properties that modeling software can unfold for us.

- A. Elevated vertical monopole
    1. Monopole development
    2. Height above ground
    3. Ground quality
- B. Ground-mounted monopole
    1. Perfect vs. lossy ground
    2. Radial density
    3. Buried radials
    4. Radial length
    5. Vertical length

Coverage will be incomplete, but by combining our explorations with those you have acquired from past episodes, you can produce your own complete survey.

A. Elevated Vertical Monopoles

Elevated vertical monopoles generally consist of a vertical element approximately 1/4-λ long. To the base of this element goes the center conductor of a coaxial feedline cable. The braid of the cable connects to a symmetrical set of radials extending usually at right angles to the vertical element. Because we think of the coaxial cable braid as being grounded and serving as a shield, we often think of the antenna as consisting of a vertical radiating element and a relatively inert "counterpoise." Nothing could be farther from the truth. Every part of the antenna structure radiates and is active in yielding the performance that emerges from a vertical monopole.

1. Monopole Development

To understand the elevated vertical monopole, we may begin where we left off last month: with a vertical dipole. Then we can proceed to develop the vertical monopole out of that antenna, as suggested by **Fig. 79-1**.

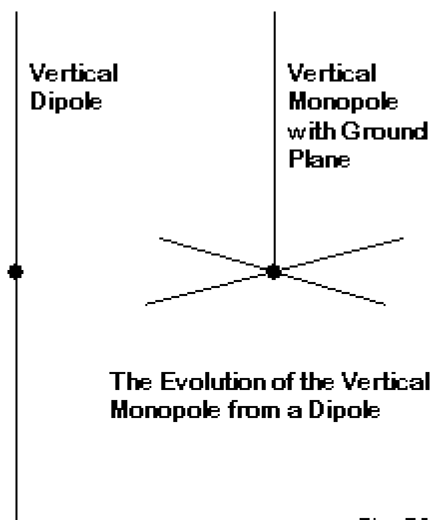

Fig. 79-1

Let's begin our work on 2-meters, 146 MHz, to be more precise. Verticals are used at all frequencies, from LF through UHF, so a VHF example is suitable for our work. We shall use 0.25" (6.35-mm) aluminum as our material for both the vertical element and, eventually, for ground plane radials. Since we wish to have a baseline against which to compare our development, let's use the vertical dipole. In free space, a resonant 1/2-λ vertical dipole will have the properties shown in the following brief table. See model 79-1.

Vertical Dipole: 146 MHz

Diameter:	0.25"	6.35 mm
Length:	38.1"	967.74 mm
Free-space gain	2.13 dBi	
Source impedance		
R +/- jX:	72.11 + j 0.35 Ohms	

For all of our work on 2 meters, we shall expressed dimensions in inches and millimeters. My tables emerge from NEC-4 models, so the exact figures produced by your model may differ slightly. But as always, the trends will remain good for any version of NEC-2 or MININEC. The patterns for the free-space vertical dipole are identical to those we discussed in the preceding column.

We may view a vertical monopole with a ground plane attached as simply an adapted vertical dipole. We retain the upper portion of the dipole–about 1/4-λ long–and revise the lower half of the vertical element. Instead of a single wire, we construct a symmetrical set of spokes or radial elements, connected together at the source and extending at right angles to the upper portion of the element. We may use any number of radial elements, but 4 have proven sufficient for highly predictable performance.

In constructing our initial vertical monopole, we shall use a fixed vertical length that is 1/2 the length of the vertical dipole. Then we shall add 4 radials. The radial lengths will be equal and set to achieve 2 goals. First, we wish to achieve resonance. Second, we wish the current to divide equally, not only among the radials, but also between the two halves of the assembly. The current at the base of the vertical element, where we place the modeling source, should equal the sum of the currents on the innermost segments of the radials. The result of our work will resemble the following model in both dimension and performance. See model 79-2.

First Model: Vertical Monopole with 4 Radials: 146 MHz

Diameter:	0.25"	6.35 mm
Vertical Length:	19.05"	483.87 mm
Radial length:	23.7"	601.98 mm
Free-space gain	1.01 dBi	
Relative radial current:	0.249	
Source impedance		
R +/- jX:	23.17 + j 0.12 Ohms	

The table should raise many questions. The first concerns a mythology attaching to vertical monopoles that lists their resonant source impedance as about 35-36 Ω. That value holds true of 1/4-λ vertical radiators over and connected to perfect ground. However, the elevated vertical monopole with ground plane has a much lower impedance. What we build, we can rebuild as soon as we examine a second question: Why is the gain so low?

A conventional and wrong answer to this question is that only the vertical portion of the antenna is radiating. In fact, all parts of the antenna radiate. However, the symmetrical portion of the assembly radiates in such a way, due to the symmetry of the radials, that the radiation almost cancels. See **Fig. 79-2**.

The “azimuth” or H-plane pattern shows the total far field along with its horizontal and vertical components. The vertical component is invisible behind the black line showing the total field. The horizontal component appears in blue at the center of the pattern, in the form of 8 very small lobes. It is the remnant calculable radiation after cancellation among the fields produced by each of the 4 radials. Over ground, the horizontal component of the total field will be slightly stronger, but never strong enough to alter the dominantly vertical polarization of the antenna.

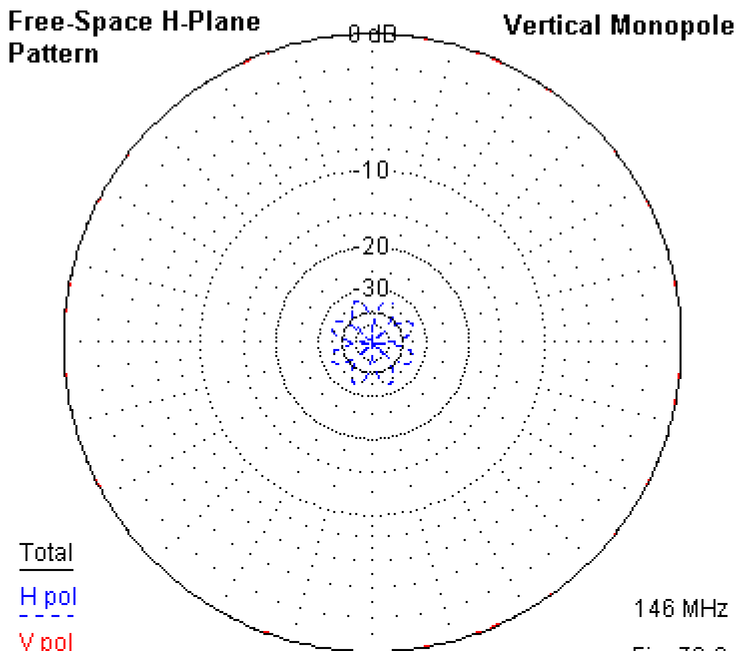

Fig. 79-2

Our initial model of the vertical monopole actually has radials that are longer than the vertical element. We can approach more conventional dimensions by lengthening the vertical element a bit and shortening the radials. The work would result in the following model–and its performance. See model 79-3.

Second Model: Vertical Monopole with 4 Radials: 146 MHz

Diameter:	0.25"	6.35 mm
Vertical Length:	20.15"	511.81 mm
Radial length:	19.00"	482.60 mm
Free-space gain	1.34 dBi	
Relative radial current:	0.250	
Source impedance		
R +/- jX:	24.66 - j 0.30 Ohms	

The model achieves an almost perfect current equality between the upper and lower halves of the assembly. It also yields a vertical element a bit longer than the radials. However, the source impedance remains under 25 Ω at resonance.

We did increase the gain by about a third of a dB, a function of lengthening the vertical portion and shortening the radials. Perhaps we can further lengthen the vertical element and achieve the "ideal" 35-Ω vertical monopole. The results appear in the following table. See model 79-4.

Third Model: Vertical Monopole with 4 Radials: 146 MHz

Diameter:	0.25"	6.35 mm
Vertical Length:	23.45"	595.63 mm
Radial length:	10.00"	254.00 mm
Free-space gain	1.68 dBi	
Relative radial current:	see text	
Source impedance		
R +/- jX:	34.94 + j 0.51 Ohms	

The vertical element is longer and achieves a higher gain than the preceding vertical monopole models. However, the vertical portion of the assembly is not a resonant 1/4-λ element. Rather, it is longer than 1/4-λ, as indicated by the fact that the current peaks above the feedpoint segment in the model. Note that to do this analysis, we are examining data that we have not checked with other models in this series of exercises: the element current. There is no intrinsic harm or fault attached to this situation–only a name change. Rather than being the analog of a vertical dipole, the new monopole is an analog of an off-center-fed 1/2-λ element.

Since we have a procedure for producing a 35-Ω monopole assembly, we may as well go all the way to a 50-Ω assembly. The results should resemble those in the following table, as we continue to extend the vertical element and shrink the length of the radials. See model 79-5.

Fourth Model: Vertical Monopole with 4 Radials: 146 MHz

Diameter:	0.25"	6.35 mm
Vertical Length:	26.30"	668.02 mm
Radial length:	6.25"	158.25 mm
Free-space gain	1.83 dBi	
Relative radial current:	see text	
Source impedance		
R +/- jX:	50.55 - j 0.09 Ohms	

The antenna is highly off-center-fed, since the current reaches its peak value about 20% of the way up the vertical element. We achieved a 50-Ω source impedance. However, you may find that the dimensions are a bit more finicky to pick out as we shorten the radials to about a third of the length of those used in the initial model.

The exercise is designed to remove some common misconceptions about elevated vertical monopoles. The vertical monopole can be derived from the vertical dipole without reference to ground, either real or perfect. The H-plane pattern establishes that all parts of the assembly are active radiators, although the radiation from the radials almost cancels completely. We can make the monopole–within the initial 1/2-λ total size–any length we wish in order to effect a desired source impedance, and the resulting increase in vertical element length tends to increase the overall gain of the assembly.

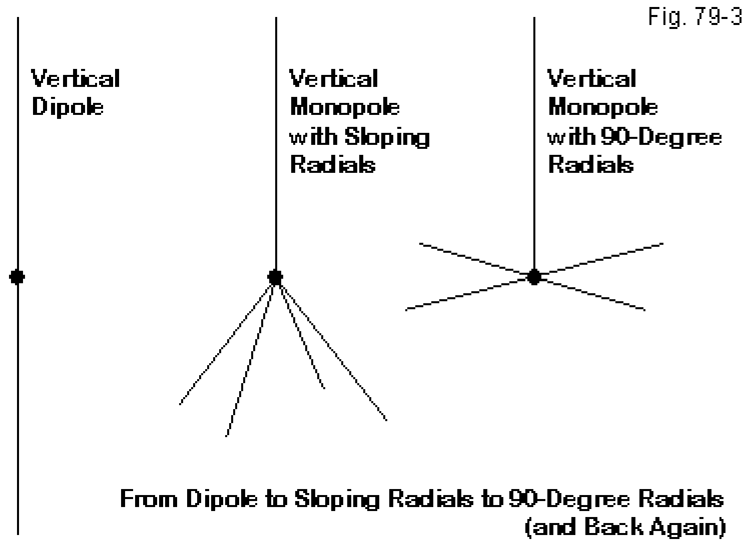

Before we leave free space for an environment closer to the ground, let's examine an intermediate step between the vertical dipole and the vertical monopole with radials extending at right angle from the vertical element. We may slope the radials at any angle downward from the right-angle plane, as suggested by the middle portion of **Fig. 79-3**. If we select an angle of about 45°, we can obtain a vertical monopole that takes up less radial room while using a shorter vertical element. As well, the array will have a 50-Ω resonant impedance, equal current division between upper and lower parts, and a slightly higher gain than we have so far obtained. The following table summarizes the design. See model 79-6.

Vertical Monopole with 4 Sloping Radials: 146 MHz

Diameter:	0.25"	6.35 mm
Vertical Length:	18.70"	474.98 mm
Radial length (see text):	18.50"	469.90 mm
Free-space gain	1.98 dBi	
Relative radial current:	0.251	
Source impedance		
R +/- jX:	51.24 + j 0.48 Ohms	

Although the radials are 18.5" (469.9 mm) long, they use only 13.08" (332.23 mm) distance from the vertical centerline of the assembly. Of course, they also extend downward by the same distance, since we set them at a 45° downward angle. Sloping radials are a standard technique in vertical monopole construction to obtain a system that shows a good match to common 50-Ω coaxial cables.

Even though the vertical element is shorter than the other 50-Ω model, we obtain slightly higher gain. Actually, the vertical element in this model does not end at the feedpoint or base of the exactly vertical element. It extends downward to the lower tips of the sloping radials.

As **Fig. 79-4** shows, the horizontal component of radiation from the radials remains well canceled. However, the radials also have a vertical dimension, and the radiation in that plane does not cancel. Rather, it contributes to the overall vertically polarized radiation of the entire assembly from top to bottom. Not only are the radials not an inert counterpoise, they are an essential active ingredient in the vertical monopole and necessary to make it function in the desired manner.

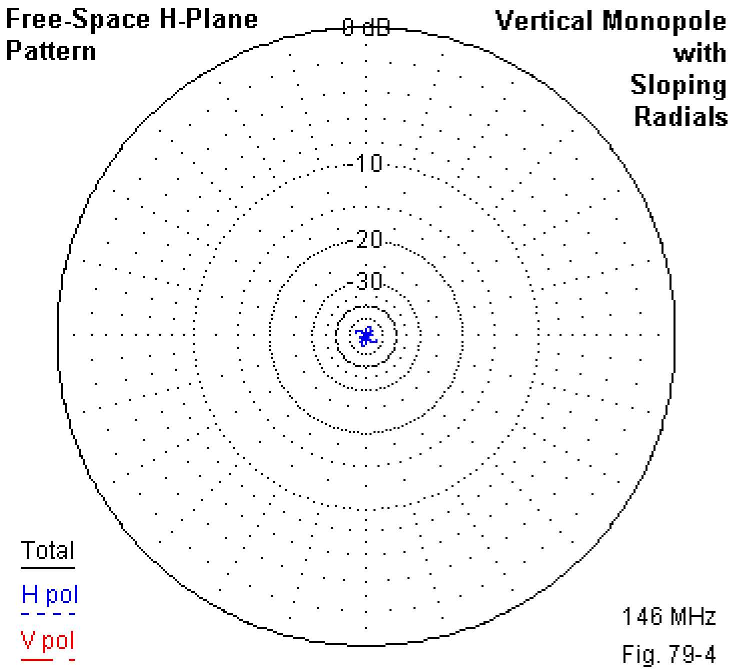

Fig. 79-4

2. Height above Ground

We shall omit from these notes certain exercises that you should perform for yourself. For example, check the performance of the vertical monopole in free space using various materials, as we did for the vertical dipole. In addition, perform frequency sweeps across the 4 MHz of the 2-meter band for each model to determine the operating bandwidth, not only relative to SWR, but also with respect to other performance parameters. To save a bit of column space for ground-mounted vertical monopoles, we shall leap to an examination of the vertical monopole at various heights above ground.

For the exercise, we shall use the version of the monopole with a 20.15" (511.81-mm) vertical element. From that model, we obtained a free-space gain of 1.34 dBi and a source impedance of 24.66 - j 0.30 Ω. Our first test will cover a broad swath: from 0.5 λ to 5 λ in height in 0.5-ë increments. This coverage reflects the fact that VHF vertical monopoles are used at many heights, depending upon operating circumstances. For reference, 1 λ at 146 MHz is 6.737' or 2.053 m. We shall use good ground (conductivity: 0.005 S/m; permittivity: 13). The antenna height will reflect the distance between ground and the base or feedpoint of the assembly. The results yield the following table.

Vertical Monopole Performance vs. Height Above Ground: 146 MHz

Height Above Ground			Gain	TO Angle	Source Impedance
WL	Feet	Meters	dBi	degrees	R +/- jX Ohms
0.5	3.368	1.027	1.42	45.3	25.04 + j 0.43
1.0	6.737	2.053	2.61	9.1	24.72 - j 0.08
1.5	10.105	3.080	3.65	7.0	24.69 - j 0.19
2.0	13.474	4.107	4.33	5.6	24.68 - j 0.23
2.5	16.842	5.133	4.81	4.7	24.67 - j 0.26
3.0	20.210	6.160	5.16	4.1	24.67 - j 0.27
3.5	23.579	7.187	5.42	3.6	24.67 - j 0.28
4.0	26.947	8.213	5.63	3.2	24.67 - j 0.28
4.5	30.316	9.240	5.79	2.8	24.67 - j 0.29
5.0	33.684	10.267	5.93	2.6	24.66 - j 0.29

The table of performance values vs. height uses an elevation angle increment of 0.1° rather than the more usual 1.0° increment. As we raise an antenna above 1 λ, the rate of change of TO angle with each change of height decreases. If we want to know the maximum gain, using 1° angle intervals may not yield a reliable answer, since the width of the lobe may be narrow, and a few tenths of a degree difference in angle may show as much as a half-dB difference in gain. The higher the antenna, the more critical it becomes to use the finest elevation angle increment available on the software.

The vertical monopole shows nothing unexpected. The source impedance is virtually constant, regardless of height within the table's range. The lowest lobe is strongest for all but the 0.5-λ height, and the progressions of gain and TO angle are normal in every way. Use model 79-7, modified as needed, for these runs.

We should investigate the performance of the same vertical monopole in the lower height region, using heights comparable to those used with the vertical monopole in the preceding column. The results appear in the following table, although the physical heights are listed in terms of inches and millimeters. For reference, at 146 MHz, a wavelength is 80.8415" or 2053.37 mm.

Vertical Monopole Performance vs. Height Above Ground: 146 MHz

Height Above Ground			Gain	TO Angle	Source Impedance
WL	Inches	mm	dBi	degrees	R +/- jX Ohms
0.25	20.21	513.3	1.25	16.0	23.19 - j 2.06
0.35	28.29	718.7	1.26	14.1	23.28 + j 0.08
0.45	36.38	924.0	1.19	13.2	24.55 + j 0.67
0.55	44.46	1129.4	1.79	42.4	25.28 - j 0.03
0.65	52.55	1334.7	2.29	37.6	25.06 - j 0.65
0.75	60.63	1540.0	2.57	33.7	24.51 - j 0.68
0.85	68.72	1745.4	2.63	35.9	24.33 - j 0.29
0.95	76.80	1950.7	2.53	27.7	24.58 - j 0.05
1.05	84.88	2156.0	2.71	8.7	24.83 - j 0.16

As we did in the first table, we used good ground beneath the vertical monopole for the test. The range of source resistance values is only 2.09 Ω, and the range of source reactance is only 2.73 Ω, despite the great range of heights. The antenna shows a high TO angle from a height of 0.55 λ through a height of 0.95 λ. You may wish to compare this table with the corresponding table for the vertical dipole in the last episode, understanding that the heights in the two tables mean two different things. The vertical dipole heights mark the height of the dipole center, while the monopole heights mark the base of the antenna. However, in both cases, the height represents the antenna feedpoint.

For both antennas, 0.55-λ marks the beginning of the high TO angle or the dominance of the second elevation lobe. However, the vertical dipole does not return to the dominance of the lowest lobe within the limit of the table, 1.25 λ. Still, the tables are not directly comparable in detail, since one antenna is for 7.15 MHz and the other is for 146 MHz. You may wish to create either a 146-MHz vertical dipole or a 7.15-MHz vertical monopole to produce a more exacting comparison.

3. Ground Quality

There are some correlations between the behavior of a vertical dipole and an elevated vertical monopole, but they are not universal. Hence, we cannot assume that the behavior of the vertical monopole over different ground qualities will replicate the work we did with the dipole. We need to give the monopole its own trials.

For this test, we shall alter the vertical monopole to one for which the trials might be more useful in guiding practical antenna work. We shall use a 10-meter (28.4-MHz) vertical monopole with a vertical element that is 8.75' (2.667 m) long with a 1" (25.4-mm) diameter. The radials will be 0.25" (6.35 mm) in diameter and 8.0' (2.438 m) long. The material is aluminum. At 28.4 MHz, a wavelength is 34.63' (10.56 m), and we find 10-meter verticals mounted at all heights from near the ground to a full wavelength above the ground (usually on rooftops). Therefore, we shall check our vertical monopole at base heights of 0.25 λ, 0.5 λ, 0.75 λ, and 1.0 λ. Use model 79-8, modified as necessary.

We shall use the same ground qualities as in the past, as shown in the following table.

Some Useful Soil Types

Soil Type	Conductivity S/m	Permittivity (Dielectric Constant)
Very Poor	0.001	5
Poor	0.002	13
Good	0.005	13
Very Good	0.0303	20

With these soil qualities, we obtained the following results for the 10-meter vertical monopole.

Changes of Vertical Monopole Performance with Ground Quality

Base Height: 0.25-Wavelength

Soil Type	Gain dBi	TO Angle degrees	Source Impedance R +/- jX Ohms
Very Poor	1.11	19	23.24 - j 0.70
Poor	1.29	16	23.05 - j 1.34
Good	1.04	16	22.95 - j 1.34
Very Good	0.73	14	22.63 - j 1.76

Base Height: 0.5-Wavelength

Soil Type	Gain dBi	TO Angle degrees	Source Impedance R +/- jX Ohms
Very Poor	2.01	15	24.72 + j 0.96
Poor	1.54	46	24.75 + j 1.21
Good	1.64	45	24.79 + j 1.21
Very Good	2.57	44	24.89 + j 1.38

Base Height: 0.75-Wavelength

Soil Type	Gain dBi	TO Angle degrees	Source Impedance R +/- jX Ohms
Very Poor	3.09	12	24.29 + j 0.01
Poor	2.70	34	24.28 + j 0.10
Good	2.76	33	24.26 + j 0.10
Very Good	3.83	32	24.21 + j 0.23

Base Height: 1.0-Wavelength

Soil Type	Gain dBi	TO Angle degrees	Source Impedance R +/- jX Ohms
Very Poor	3.81	10	24.46 + j 0.62
Poor	2.71	9	24.46 + j 0.69
Good	2.64	26	24.47 + j 0.69
Very Good	3.83	25	24.50 + j 0.74

Although the source impedance is stable at every height over the range of soil types, it grows perceptibly more stable as we increase the height. The chief interesting elements in the table are the gain and corresponding TO angle values. At 0.25-λ, the lower lobe dominates for every soil types. However, above the height, only over very poor soil does the lower lobe dominate. As we move upward with the antenna base, we see a gradual return to lower lobe domination from worse to better soils, but the table only suggests the situation. You may wish to do further trials at 1.25 λ and above to discover at what point the lower lobe returns to domination for good and very good soils.

The gain values are also interesting, since they do not correlate directly with soil type. At heights from 0.5 λ to 1.0 λ, the antenna over very poor soil is superior to all but very good soil, and at the lowest height shown, poor soil takes gain honors. The differences are of only marginal operational interest–much less interest than the TO angle–but the trends will likely seem surprising relative to common assumptions about vertical monopoles.

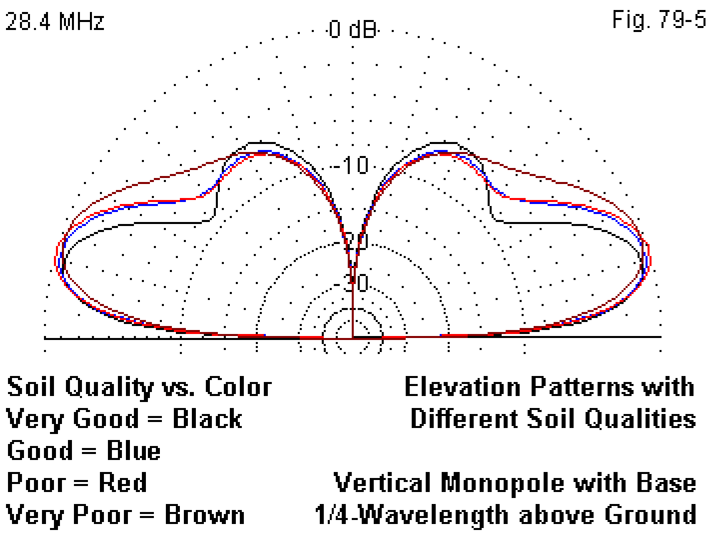

To better gauge the importance of the tabular data, you may wish to overlay elevation patterns at each height for the 4 soil types. **Fig. 79-5** shows the patterns at a height of 0.25-λ above ground. As in all of the overlays that you will obtain from these trials, the patterns for good and poor soil are virtual clones of each other. The pattern for very good soil shows the more distinct differentiation of the lower and the emerging second lobe. In contrast, the pattern for very poor soil does not show a distinct second lobe at all. In all cases, the vertical beamwidth is large enough that there is likely to be little detectable difference in the performance of the antenna with a change in soils.

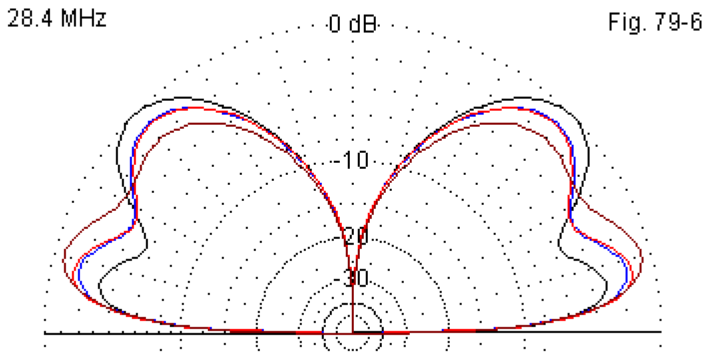

Soil Quality vs. Color
Very Good = Black
Good = Blue
Poor = Red
Very Poor = Brown

Elevation Patterns with Different Soil Qualities

Vertical Monopole with Base 1/2-Wavelength above Ground

As we move to a height of 0.5-λ above ground, **Fig. 79-6** provides the relevant elevation patterns. Only over very poor soil is the development of the second lobe sufficiently retarded to allow the lower lobe to dominate in terms of maximum gain. As we improve soil quality, the upper lobe increasingly dominates over the lower lobe. Over poor and good soils, there is not a very great difference in the maximum gain for each lobe. However, over very good soil, the high-angle lobe has a considerable advantage over the lower lobe. As well, since all of the plots use the same gain scale, the lower lobe of the “very-good soil” pattern is weaker than for the other antenna environments.

In **Fig. 79-7**, we can find the first emergence of the third lobe, although it is not clearly identifiable in the pattern for very poor soil. In that pattern, the lowest lobe continues to have the maximum gain. In all of the patterns, the lower two lobes have begun to merge. Over poor and good soil, the two parts of the merged lobe have nearly the same strength. However, over very good soil, the lower component of the merged elevation lobe remains considerably weaker than the upper lobe. Hence, higher-angle radiation (and reception) dominates the antenna's performance.

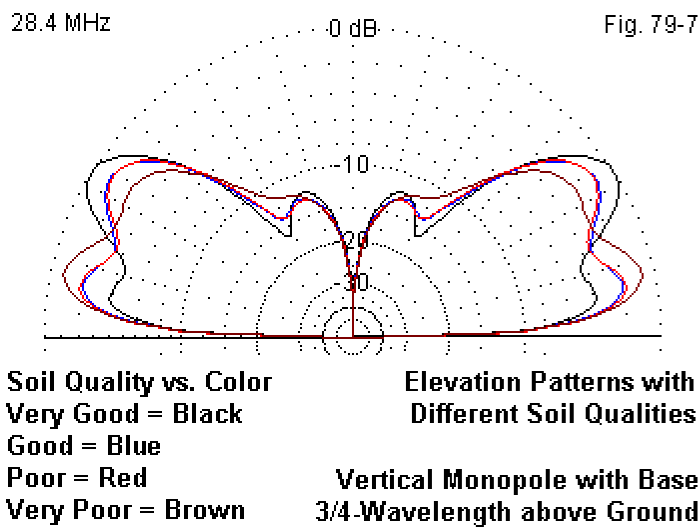

In our final set of overlaid patterns–**Fig. 79-8**–at 1.0 λ above ground, we find that the third lobe has become very distinct in all of the patterns. Over good and poor soil, the merged lower lobes have very nearly equal strength–too near to make a difference. However, the pattern for very poor soil continues to show the clear dominance of the lowest lobe–virtually to the same degree that over very good soil, the upper lobe continues to dominate. Indeed, one must wonder how high one might have to raise the antenna over very good soil before the TO angle comes down to the level of the lower lobes of the patterns over other soil types.

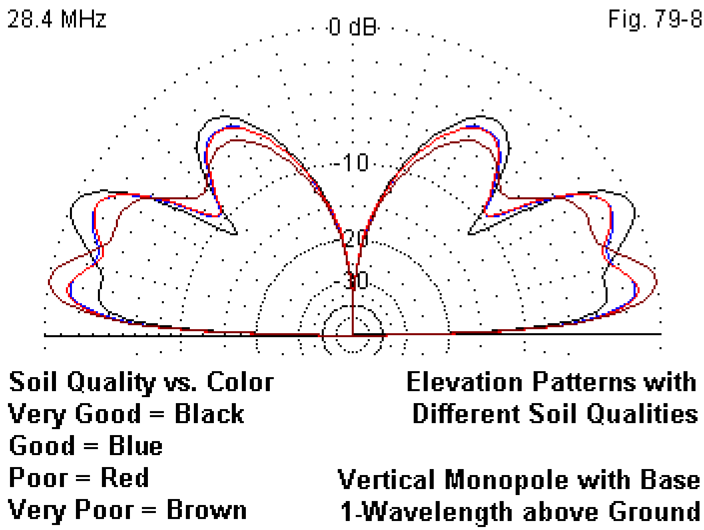

These patterns should accomplish two goals. First, they should serve to question some of the assumptions that we may be inclined to bring to the study of vertical monopoles. With the proper systematic use of our modeling software, we may set aside assumptions and allow the data to develop as it will. Second, the patterns should prepare us for the highly complex sets of elevation lobes that we encounter when taking patterns of antennas set at considerable heights, when measured in terms of wavelengths.

We have spent considerable space looking at elevated vertical monopoles, and still many questions remain for you to explore on your own. What is the effect of using either fewer or more radials in the ground-plane system? What is the effect of the relative diameters of the vertical element and the radials on the required lengths of each for resonance? How would a vertical monopole with sloping radials perform at various heights and over different soils? Would it perform more like a vertical dipole or like the vertical monopoles that we have explored in this column? Are there any frequency-related performance differences that we might detect by using directly scaled antennas? These are only a few of the questions unanswered by this small beginning in the systematic study of elevated vertical monopoles.

I had hoped to include in this episode a considered look at ground-mounted vertical monopoles. There are not only questions of performance expectations to develop, but as well a host of modeling questions to consider. Hence, to be fair to the ground-mounted vertical monopole, I shall have to wait until next time. Until then, you have time to work on the unanswered questions that I left behind for elevated vertical monopoles.

80. Developing Antenna Expectations Using Modeling Software 2C: Vertical Monopoles

In the preceding episode, we began our investigation of vertical monopoles by looking at elevated versions of the antenna. However, as our general work outline showed us, the elevated vertical monopole is but one of the two ways we use the antenna. At lower frequencies ranging from LF and VLF up through the lower HF region, we often use them with one end at ground level and with a buried system of radials. So we still have half a project to finish.

The overall project had this structure:

A. Elevated vertical monopole
   1. Monopole development
   2. Height above ground
   3. Ground quality
B. Ground-mounted monopole
   1. Perfect vs. lossy ground
   2. Radial density
   3. Buried radials
   4. Radial length
   5. Vertical length

Even though we could only sample some of the many systematic questions relating to the properties of elevated vertical monopoles, we have to move onward. This series is not designed to answer all questions that contribute to a set of reasonable expectations of antenna types. Instead, it is designed to show some of the principles of systematic study that will let you continue the process of gathering data in ways that make sense of antenna performance patterns. We shall be similarly incomplete this month.

B. Ground-Mounted Monopole

The ground-mounted vertical (monopole) was once considered one of the most basic of all antennas. More recently, we have come to see it as an extension or a modification of the dipole, with the radial system substituting for the lower half of the dipole. However, because the ground plays such a significant role in the performance of the antenna, we shall not start in the same place that we began with all of the other antennas that we have so far explored. Instead of beginning in free space, we shall begin with a perfectly reflecting ground.

1. Perfect vs. Lossy Ground

In both NEC and MININEC, if we place a vertical element in contact with a perfect ground, the program will calculate the properties of the antenna by creating an image antenna that extends mathematically below the ground surface by an equal length. The left sketch in **Fig. 80-1** shows the general situation.

A perfect ground will totally reflect the radiation striking it, thus doubling the power in the radiated field. To see the image antenna effects in action, let's create a 7.05-MHz vertical monopole made from 2" (50.8-mm) aluminum. We shall give it a length of 33.25' (10.135 m). For this exercise, let's use 30 segments. NEC-4 returns a maximum gain of 5.14 dBi with a source impedance of 35.94 - j 0.13 λ. See model 80-1.

As shown in the middle portion of **Fig. 80-1**, the 1/4-λ vertical element plus its image is equivalent to a 1/2-λ vertical dipole in free space–except for the source impedance. If we create such a dipole for 7.05 MHz from the same materials, making it 66.5' (20.27 m) long, we obtain a source impedance of 71.84 - j 0.58 Ω. The very slight difference between the reported impedance and double the 1/4-λ impedance stems from the slight shift we had to make in the position of the source. The monopole source is on the lowest segment of the physical antenna, which places it slightly above ground. We assigned the dipole 61 segments, placing the source at its exact center, which corresponds to the ground level (Z=0) for the monopole. See model 80-2.

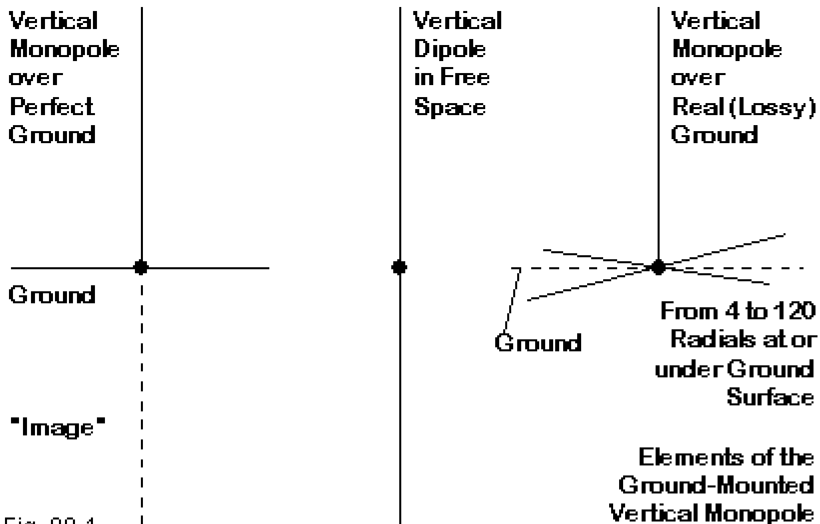

Fig. 80-1

Because the dipole has no reflections to double the radiated power of its far field, we should expect the field strength to be 1/2 the level of the monopole over perfect ground. So, instead of a field strength of 5.14 dBi, the dipole in free space reports 3 dB less, or 2.13 dBi.

To simplify models of vertical monopoles, modelers have in the past simply placed the monopoles in contact with the ground using MININEC. (NEC-2 and NEC-4 return completely useless reports under the same conditions.) The practice was so widespread that the EZNEC version of NEC incorporated the MININEC ground as a user-selected option. To understand the operation of the MININEC ground, let's place our monopole from the ground up using the MININEC ground system. As in past episodes, we shall use the following samples of ground quality as trials for our simple monopole model.

Some Useful Soil Types

Soil Type	Conductivity S/m	Permittivity (Dielectric Constant)
Very Poor	0.001	5
Poor	0.002	13
Good	0.005	13
Very Good	0.0303	20

Running the model through these sample ground qualities, we obtain the following performance. See model 80-3 (for EZNEC only).

Changes of Vertical Monopole Performance with Ground Quality: MININEC Ground

Soil Type	Gain dBi	TO Angle degrees	Source Impedance R +/- jX Ohms
Very Poor	-1.76	29	35.94 - j 0.13
Poor	-0.28	27	35.94 - j 0.13
Good	-0.03	26	35.94 - j 0.13
Very Good	1.95	21	35.94 - j 0.13

We obtain a plausible-looking chart of gain values and TO angles. However, the source impedance remains the same for every value. The MININEC ground system always uses the source impedance for a perfect ground as one of its simplifying features, remembering that it was developed for early PCs with very limited memory resources. Hence, it cannot tell us whether the source impedance changes with ground quality. We cannot know from the MININEC ground system whether we need to adjust the length of the monopole to bring it to resonance for a given ground quality.

The MININEC ground system does let us make an important contrast, one that will hold true for every trial in this episode. **Fig. 80-2** shows the difference between a pattern taken over perfect ground and one taken over a real (MININEC) ground. The lower part of the figure represents all of the elevation patterns that we shall encounter. The only differences will be in the maximum gain and the TO angle as we move from one trial to another. As long as we stick to our 1/4-λ vertical monopole, we shall see the lower elevation pattern.

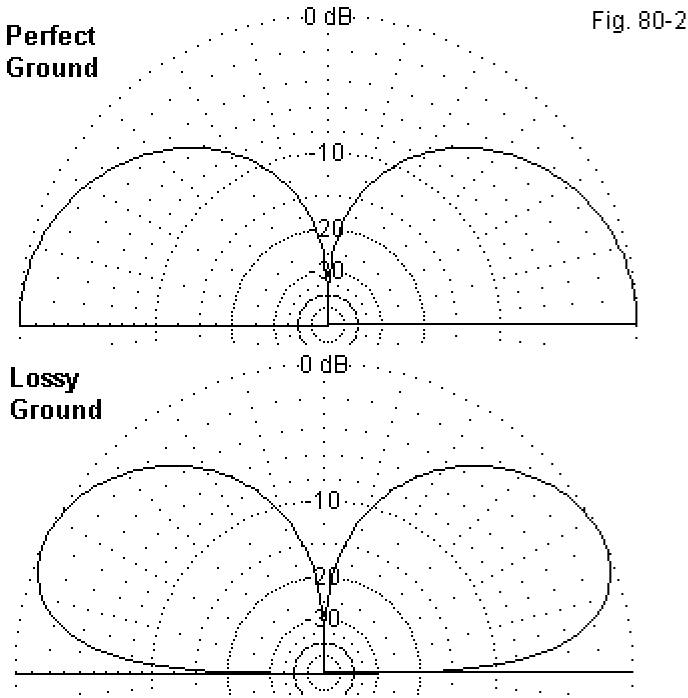

Elevation Patterns of a Ground-Mounted Vertical Monopole Over Perfect and Lossy Ground

2. Radial Density

The use of a MININEC ground cannot capture the fact that the performance of a vertical monopole will change according to the size of the radial field that we add to the base of the monopole, as shown in the far right portion of **Fig. 80-1**. The radials, normally at or below the ground surface of a ground-mounted vertical monopole, are an essential ingredient to the antenna's performance with respect both to its source impedance and its far-field strength. We should now be on the verge of appreciating that the performance of a ground-mounted vertical monopole is a function of a complex interaction among the physical properties of the antenna, the ground quality, and the number and type of radials that we place at its base.

NEC-2 does not permit a wire to extend below ground level (Z=0). Therefore, the program cannot directly model a buried radial system. However, to simulate a buried radial system, the standard procedure is to create the radial set with the antenna and its radials raised about 0.001-λ above ground. This level is at or close to the absolute proximity permitted under NEC for wires above a Sommerfeld ground calculating system. (Do not use the simpler reflection coefficient system.)

For our 7.05-MHz monopole, we shall raise it by only 0.4" (10.16 mm) above ground. To the antenna base, we shall add radial systems using various numbers of radials. To be systematic about the matter, we shall use the progression 4, 8, 16, 32, and 64 radials. Broadcast systems use 120 radials with shorter radials between the longer ones, but a 64-radial system is about as large as amateur systems get. Besides, 64 radials, set up as we shall prescribe, will result in models with more than 1900 segments. See models 80-4 through 80-8.

We shall not change the length of the monopole, but instead track what happens as we change the number of radials and the soil quality. We need to set a length for the radials. Each one will be–for the sake of our initial trials–0.25-λ long, that is, 34.88' or 10.63 m. (We shall look at the question of radial length before we have finished the episode.) For reasons having to do with subsequent trials, we shall assign 30 segments to each radial, as well as to the monopole, so that all segments are about the same length, close to 12" (0.3 m).

If we create the models using each of the specified number of radials and run the model over the 4 sample ground qualities, we obtain a table that resembles the following one.

Vertical Monopole Performance with Ground Quality and Number of Radials: NEC-2

4 Radials

Soil Type	Gain dBi	TO Angle degrees	Source Impedance R +/- jX Ohms
Very Poor	-2.64	29	46.57 + j 27.66
Poor	-2.13	27	59.43 + j 64.93
Good	-3.31	26	81.51 + j 63.16
Very Good	-3.09	21	114.0 + j 97.64

8 Radials

Soil Type	Gain dBi	TO Angle degrees	Source Impedance R +/- jX Ohms
Very Poor	-1.67	29	36.19 + j 4.73
Poor	-0.65	27	40.48 + j 20.35
Good	-1.40	26	49.86 + j 21.27
Very Good	-1.01	21	69.18 + j 43.57

16 Radials

Soil Type	Gain dBi	TO Angle degrees	Source Impedance R +/- jX Ohms
Very Poor	-1.28	29	33.44 - j 3.90
Poor	-0.18	27	35.55 + j 3.53
Good	-0.59	26	40.06 + j 3.94
Very Good	0.20	21	51.69 + j 14.66

32 Radials

Soil Type	Gain dBi	TO Angle degrees	Source Impedance R +/- jX Ohms
Very Poor	-1.05	29	30.61 - j 6.90
Poor	0.08	27	33.16 - j 2.89
Good	-0.15	26	35.54 - j 3.14
Very Good	1.09	21	41.64 + j 1.37

64 Radials

Soil Type	Gain dBi	TO Angle degrees	Source Impedance R +/- jX Ohms
Very Poor	-0.89	29	29.66 - j 7.48
Poor	0.24	27	32.08 - j 4.73
Good	0.06	26	33.70 - j 4.99
Very Good	1.51	21	47.39 - j 2.82

The table shows that for any number of radials, the elevation angle of maximum radiation–the TO angle–varies only with the soil quality. As we add radials, the source resistance descends and compresses, so that the wide range we see with few radials becomes a narrow range with many radials. The source reactance, which was always inductive with only 4 radials, is always capacitive with 64 radials. However, we should also note that some of the source impedance values drop below the 35-Ω level that we encountered with a perfect ground. There is an old rule of thumb that suggests a way to account for losses to ground in a vertical monopole. Any portion of the source resistance that is above 35-36 Ω is simply a loss function. However, the models suggest to the contrary that the relationship may not be so simple as that, since some source resistance values are below the ideal level. In fact, the source resistance for very poor soil and 64 radials begins to approach the level that we encountered for an elevated monopole with radials.

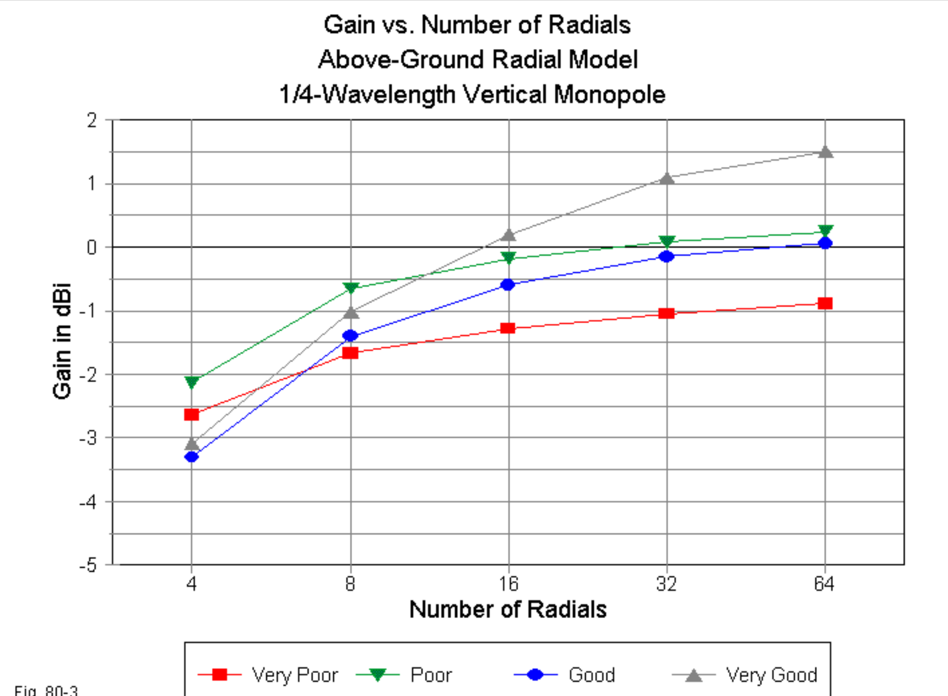

Fig. 80-3

Of course, the gain reports will not support a suggestion that very low source resistance values mean high efficiency from our vertical monopole. **Fig. 80-3** tracks the gain values from the table for each of the ground qualities as we increase the number of radials. Note that the gain performance of the monopole over poor soil is always slightly better than over good soil. As well, the performance over very good soil shows a much steeper curve so that, with fewer than 16 radials, the gain is lower than with some of the worse soil qualities.

If we remember that we created these models as an above ground simulation of a buried radials system, we can pose a valid question: how reliable is this simulation? This question is not so simple as it seems. The effects of ground on vertical monopoles have been under continuous study since the earliest days of radio. Even the best modeling systems are under scrutiny in the quest for a more perfect understanding of ground effects and the ideal radial system. At best, in our trials, we can only demonstrate a superior model of the monopole and its radials. We cannot reach an absolutely final answer.

3. Buried Radials

Unfortunately, the only way to create a superior model of the ground-mounted vertical monopole with a buried radial system is to use NEC-4, which is outside the reach of most casual modelers. However, NEC-4 does permit the use of wires below ground. In conjunction with the Sommerfeld ground calculating system, the model promises to yield more accurate results than a scarcely elevated substitute. However, should the Sommerfeld (S-N) system undergo refinement as a means of calculating ground effects, then even these models will yield better results in future modeling software.

Fig. 4 shows what is necessary to develop a buried radial system. NEC requires that a wire or segment junction coincide with the ground (Z=0). The wire or segment from ground down to the level of the junction of radials plays a critical role in the model. The segment just above ground is where we place the source, and to obtain reliable results, this segment should be the same length as the segments adjacent to it. If we do not use segment length tapering, the distance from the ground down to the radials thus determines the length of the segments in the vertical monopole. We shall use 66 segments, since we shall place the buried radials 0.5' (0.15 m) below ground. In fact, moving the radial depth tends to change the results by insignificant amounts for a fairly wide range of depths. Hence, the half-foot depth represents a reasonable compromise between reflecting actual practice in setting radials and relatively manageable model sizes. Because the radials are symmetrical, we can use a reduced segmentation density. In fact, we shall retain the 30-segment-per-radial density that we used for the elevated system.

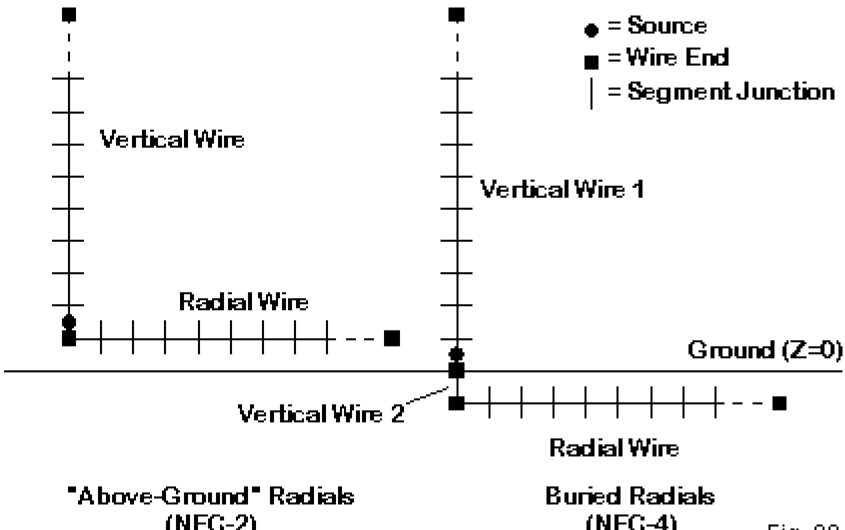

Fig. 80-4

If we set up the models according to this scheme and run them through the sample soil qualities, we obtain the following table of results. See models 80-9 through 80-13, but for NEC-4 only.

We may first notice that the TO angles have not changed, with the one exception of 4 radials with very poor soil. Our second notice should go to the source impedances. With few radials, the buried-radial model reverses the source impedance situation with respect to values for very good and very poor soil. Internally to the table, the 16-radial level marks a turning point in the source resistance reports.

Vertical Monopole Performance with Ground Quality and Number of Radials: NEC-4

4 Radials

Soil Type	Gain dBi	TO Angle degrees	Source Impedance R +/- jX Ohms
Very Poor	-4.62	30	97.95 + j 27.77
Poor	-2.85	27	69.26 + j 6.64
Good	-2.53	26	67.02 + j 12.35
Very Good	0.35	21	52.55 + j 12.79

8 Radials

Soil Type	Gain dBi	TO Angle degrees	Source Impedance R +/- jX Ohms
Very Poor	-2.49	29	57.61 + j 22.66
Poor	-1.73	27	57.59 + j 8.47
Good	-1.49	26	54.66 + j 11.89
Very Good	0.81	21	47.47 + j 10.82

16 Radials

Soil Type	Gain dBi	TO Angle degrees	Source Impedance R +/- jX Ohms
Very Poor	-1.32	29	40.34 + j 11.40
Poor	-0.63	27	46.71 + j 10.16
Good	-0.64	26	45.81 + j 9.69
Very Good	1.19	21	43.76 + j 9.23

32 Radials

Soil Type	Gain dBi	TO Angle degrees	Source Impedance R +/- jX Ohms
Very Poor	-0.91	29	34.52 + j 4.58
Poor	0.09	27	38.55 + j 7.91
Good	-0.07	26	39.69 + j 7.38
Very Good	1.50	21	40.89 + j 7.99

64 Radials

Soil Type	Gain dBi	TO Angle degrees	Source Impedance R +/- jX Ohms
Very Poor	-0.78	29	32.47 + j 1.54
Poor	0.34	27	35.00 + j 5.20
Good	0.16	26	36.53 + j 5.12
Very Good	1.70	21	38.76 + j 6.91

With fewer radials, the source resistance goes up as soil quality goes down. With more than 16 radials, the trend reverses. All reactances are inductive for two reasons. First, the height above ground of the vertical is unchanged, even though we added a small subterranean section to the antenna. Second, the source position is slightly higher up on the total vertical length from the radials to the tip. Nonetheless, as we add more radials, the ground-mounted vertical monopole comes very close to resonance over any soil quality, with under j 7 Ω reactance as the 64-radial worst case.

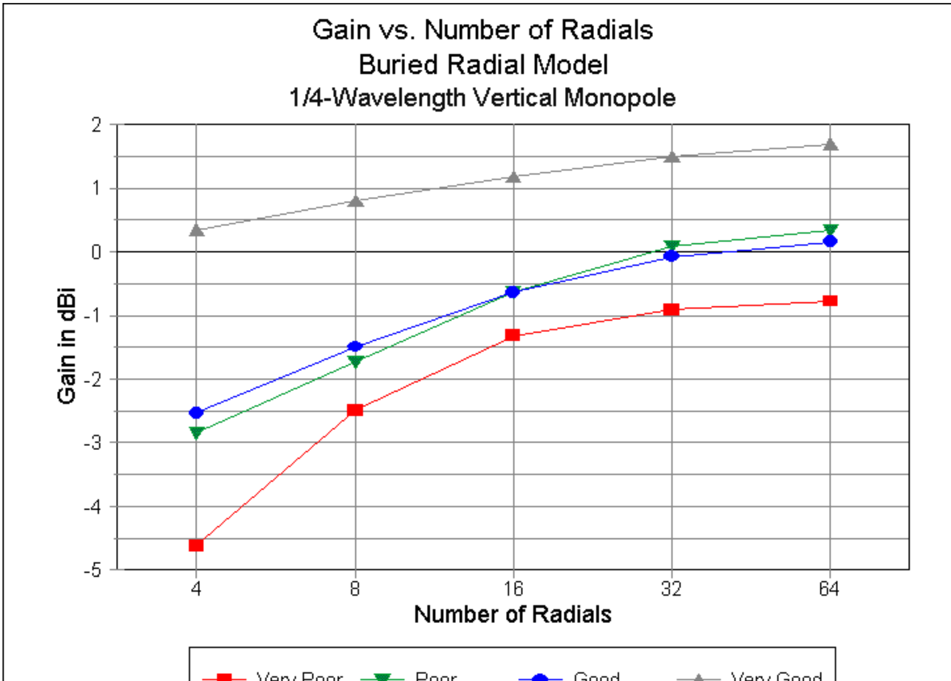

Fig. 80-5

Fig. 80-5 extracts the gain data for a visual presentation. When we compare it to the data from the above ground radial models, we see some clear differences. Even though the above ground version did not record the cross-over in gain advantage between poor and good soils at the 16-radial mark (corresponding to the changeover point for the source resistance values), these two soil levels show the highest correlation between the two graphs. The most significant changes occur with respect to very good and very poor soil. The values for very good soil maintain an advantage over other soil qualities and the curve is much shallower than with the above ground reports. In contrast, with buried radials and very poor soil, we find a steeper curve and values always at the bottom of the scale.

It is likely that the buried-radial models return more reliable results than their NEC-2 above ground simulation. The gain and source impedance reports tend to be closer to intuitions, although intuition would be a poor guide with respect to the middle of the scale, where poor soil sometimes outperforms good soil by a small margin (that is not operationally significant). We should note once more that the inter-relationship among the physical antenna structure, the soil quality, and the number of radials is further complicated by source resistance values that fall noticeably below the perfect-ground value. Finally, you may wish to compare the results in both sets of tables with the recorded when using a MININEC ground without a radial system.

4. Radial Length

Throughout the trials that we have been performing, we used radials that were exactly 1/4-λ at 7.05 MHz. One continuing discussion concerning ground-mounted vertical monopoles concerns the ideal length for radials. As we have seen, we cannot obtain absolute answers to such questions, but we can see what models have to report on the subject. Let's take the 16-buried-radial model (80-11) and test it for radials of varying length, ranging from 0.10-λ to 0.40-λ. We can, for demonstration purposes only, use only good and very poor soils for our sampling, leaving other options for further exploration as something you can do yourself. We shall retain our 0.25" (6.25-mm) radials and segmentation density, which means that the models will grow larger with every increase in radial length. The results should resemble the following table.

Effects of Radial Length on Vertical Monopole Performance

Good Soil

Length WL	Gain dBi	TO Angle degrees	Source Impedance R +/- j X Ohms)
.10	-1.30	26	47.12 - j 0.85
.15	-0.87	26	43.92 + j 4.80
.20	-0.72	26	44.58 + j 8.29
.25	-0.74	26	45.82 + j 9.69
.30	-0.57	26	46.95 + j 10.17
.35	-0.51	26	47.83 + j 10.07
.40	-0.48	26	48.36 + j 9.63

Very Poor Soil

Length WL	Gain dBi	TO Angle degrees	Source Impedance R +/- j X Ohms)
.10	-3.10	29	46.94 - j 17.96
.15	-2.40	29	40.94 - j 7.64
.20	-1.76	29	37.77 + j 1.90
.25	-1.32	29	40.33 + j 11.40
.30	-1.18	30	47.76 + j 15.52
.35	-1.13	30	53.84 + j 13.71
.40	-1.06	31	56.34 + j 9.68

In both trials, we see a regular and smooth improvement in gain performance with longer radials, although the range is less with good soil than with very poor soil. There are in the models no special lengths within the range tested. The TO angle over good soil remains constant, although over very poor soil, the angle begins to increase slowly as we extend the radial length above 0.25-λ.

Both tables show that with radials about 0.30-λ, the inductive reactance reaches a maximum. Source resistance shows minimum values, but at slightly different radial lengths: for good soil, at 0.15-λ, for very poor soil, at 0.20-λ. These are minor phenomena, more of numerical interest than operational significance. Indeed, IF the models are reasonably accurate predictors of antenna behavior with varying radial lengths, then it is likely that the exact radial length will not affect antenna performance significantly so long as all radials are the same length and as symmetrically laid out as feasible.

5. Vertical Length

When we encounter initial textbook discussions of ground-mounted vertical monopoles, the authors treat us to graphical elevations patterns related to the length of the vertical monopole above ground. Inevitably, the patterns show a significant gain advantage to using a monopole that is 0.625 λ. Let's replicate those patterns over perfect ground. Then let's go a step farther and perform the same set of trials over good ground with our 16-radial buried system (model 80-11). We shall not change general parameters of the model, using 1/4-λ radials. Our goal will be to understand why some broadcast antenna engineers prefer in fact not to use the longer monopole (beyond the fact that such a monopole represents a very tall structure to maintain in the AM broadcast frequency range).

The results of our trials at 7.05 MHz will look like those in the following table.

Effects of Vertical Length on Vertical Monopole Performance

	Length WL	Gain dBi	TO Angle degrees	Source Impedance R +/- j X Ohms)
Perfect Ground				
	.25	5.14	--	35.94 - j 0.13
	.375	5.83	--	269.9 + j 372.4
	.50	6.95	--	6762. - j 664.9
	.625	8.04	--	64.09 - j 253.9
	.75	6.61	46	59.14 + j 26.59
Good Soil				
	.25	-0.64	26	45.83 + j 9.71
	.375	-0.06	22	308.3 + j 380.0
	.50	0.53	18	5859. - j 669.4
	.625	0.73	15	64.65 - j 235.5
	.75	4.14	45	73.26 + j 34.47

With an aluminum vertical, the 5/8-λ vertical over perfect ground shows a 2.9-dB advantage over the 1/4-λ vertical. However, when we transplant the verticals to merely good soil, the gain advantage of the longer version shrinks to less than 1 dB. We may note the lower TO angle of the longer vertical and still think that we should use it. For that reason, we should also explore the elevation patterns themselves over both perfect and merely good ground.

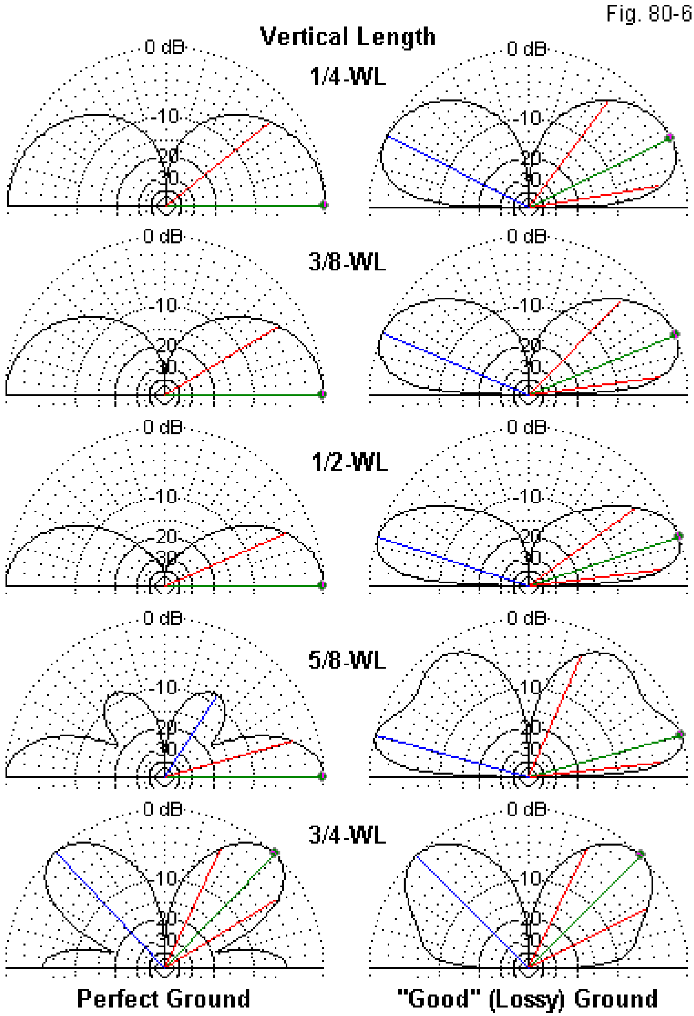

Vertical Monopoles of Different Lengths Over Perfect Ground and Over Lossy Ground with 16 Buried Radials

We can trace the pattern development in **Fig. 80-6**. From a vertical length of 1/4-λ up to 1/2-λ, the patterns over good soil track well with the patterns over perfect ground. However, at a length of 5/8-λ, the very modest secondary lobes of the pattern over perfect ground take a different turn. They become very large regions of high angle radiation. Much of the energy that–over perfect ground–extended the lower lobe has now moved into the second lobe. Little wonder that engineers who do not wish to cause interfering skip signals at night in the AM BC band opt for a shorter length of vertical monopole. Even for amateur use, the 5/8-λ monopole may increase short-range noise and interfering signals without commensurate improvements in long-range performance.

The 0.625-λ vertical monopole is the analog of the 1.25-λ vertical dipole. Two episodes ago, we saw that increasing the dipole length to 1.5 λ virtually eliminated low angle radiation and redirected energy at very high angles. The same effect holds true for ground-mounted vertical monopoles that we extend to 0.75-λ. As the bottom patterns in **Fig. 80-6** show clearly, even the version over perfect ground shows the angle of the main lobes to be very high. The version over good soil eliminates virtually all low-angle radiation.

Conclusion

Although we seem to have covered a wide territory in our investigation of ground-mounted verticals, we have omitted many facets of what a truly thorough study might accomplish. We did not look at the effects of using different combinations of vertical element diameters with equally varied radial diameters. We did not investigate the effects of different materials on monopole performance. Even where we sampled different soil qualities, we often left gaps in the coverage.

However, we have progressed far enough for you to proceed individually to do a more thorough exploration. Indeed, the principles of systematic exploration of antenna properties via models apply to any number of antenna types, both simple and complex: parasitic arrays, phased arrays, closed geometries (vertical and horizontal loops, etc.), and even systems of multiple antennas. In some cases, such as horizontal arrays that are well elevated above ground, the results will be as authoritative as one might wish. In other cases, such as ground-mounted verticals, they will be useful, suggestive, and helpful, without necessarily being without contest from new developments in the understanding of how complex factors combine to yield antenna performance.

In virtually all cases, the exercises will not only contribute to our understanding of the subject antenna types. As well, they will help us overcome numerous misconceptions, presumptions, myths, and assumptions that we carry to our antenna work. These are some of the key roadblocks to developing reasonable expectations of antenna performance, the goal of using modeling as a means to understanding better what antennas can do.

81. Appreciating the EK Command

In episode 51, we encountered the inaccuracies that result in NEC-2 from too low a ratio between the segment length (Ls) and the wire radius (R). In the example, we used the following model, outlined in **Fig. 81-1**, to track the differences between NEC-4 results and NEC-2 results. See model 81-1.NEC.

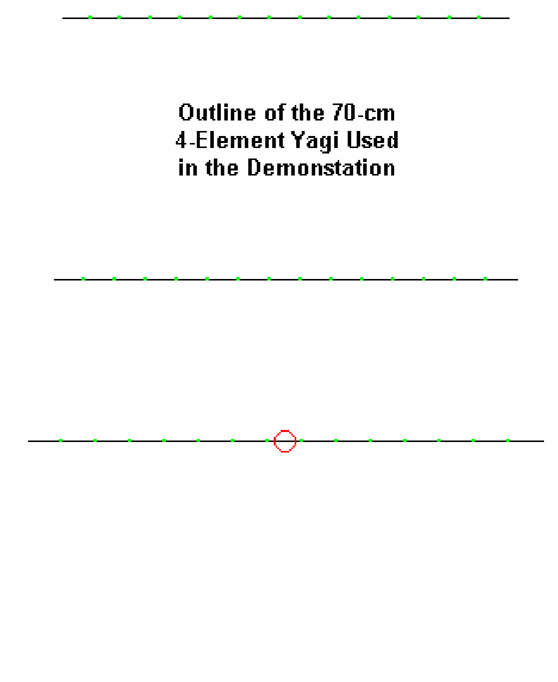

Fig. 81-1

```
W4RNL 432 WB Yagi                                          Frequency = 432  MHz.
Wire Loss: Aluminum -- Resistivity = 4E-08 ohm-m, Rel. Perm. = 1
              --------------- WIRES ---------------
Wire Conn. --- End 1 (x,y,z : in)  Conn. --- End 2 (x,y,z : in)   Dia(in) Segs
1             0.000, -6.575,  0.000          0.000,  6.575,  0.000 5.00E-01  15
2             5.807, -6.083,  0.000          5.807,  6.083,  0.000 5.00E-01  15
3             9.626, -5.453,  0.000          9.626,  5.453,  0.000 5.00E-01  15
4            15.748, -5.256,  0.000         15.748,  5.256,  0.000 5.00E-01  15
```

The average segment length is about 0.8", while the diameter is 0.5", for a length-to-radius (Ls/R) ratio of 3.2:1. The following table records the modeled performance data from 420 to 250 MHz for the 4-element wide-band Yagi design.

Wide-Band 4-Element Yagi for 420-450 MHz

Core	Freq. MHz	Free-Space Gain dBi	Front-Back Ratio dB	Source Impedance R +/- jX Ohms	50-Ohm SWR
NEC-4D	420	9.12	11.56	45.81 - j 2.99	1.114
	430	9.23	12.14	56.30 + j 1.51	1.130
	440	9.34	12.73	61.22 - j 2.38	1.230
	450	9.55	14.31	49.47 - j 7.28	1.158
NEC-2	420	9.17	11.69	47.77 - j 1.14	1.053
w/o EK	430	9.27	12.20	58.14 + j 1.51	1.166
	440	9.40	12.92	59.93 - j 4.57	1.221
	450	9.64	14.99	42.72 - j 6.56	1.236
NEC-2	420	9.12	11.52	45.64 - j 2.99	1.120
w EK	430	9.23	12.11	56.12 + j 1.64	1.130
	440	9.35	12.72	61.11 - j 2.20	1.230
	450	9.55	14.29	49.40 - j 7.23	1.160

The last portion of the table records the data we obtain when we implement the EK or extended thin-wire kernel command (EK). The use of this command restores the performance reports to good alignment with NEC-4 results. Hence, we should learn how, when, and why to use the EK command in NEC-2, as well as why it is unnecessary in NEC-4.

How: The easiest step in the process is implementing the EK command. Immediately following the GE (geometry end command), we may write a new line:

```
EK 0
```

The line changes the approximation of the electrical field integral equation in the core calculations from the thin-wire kernel to the extended thin-wire kernel. Unfortunately, some entry-level versions of NEC-2 do not give the user the option of using the extended kernel, although NEC2GO does implement it automatically whenever the wire radius exceeds a certain ratio to the segment length. Programs that allow the user to write his or her own model file, such as NEC-Win Pro, provide for the use of the extended thin-wire kernel whenever the modeler deems it necessary. For a simple sample dipole, the model file will have the following appearance. See model 81-2.NEC.

```
CM NEC-WIN Example
CM Simple dipole antenna in Free Space
CM Optimized for resonance at 300 MHz
CE
GW 1 9 0 -.2418 0 0 .2418 0 .0537
GS 0 0 1
GE 0 -1 0
EK 0
EX 0 1 5 0 1 0
FR 0 1 0 0 300 1
RP 0 181 1 1000 -90 0 1 1
RP 0 1 360 1000 90 0 1 1
EN
```

Why: The information necessary to appreciate the significance of the extended thin-wire kernel in NEC-2 appears early on in the user portion of the manual. “In the thin-wire kernel, the current on the surface of a segment is reduced to a filament of current on the segment axis. In the extended thin-wire kernel, a current uniformly distributed around the segment is assumed. The field of this current is approximated by the first two terms in a series expansion of the exact field in power of a^a [where *a* is the wire radius]. The first term in the series– which is independent of *a*– is identical to the thin-wire kernel, while the second term extends the accuracy for larger values of *a*. Higher order approximations are not used because they would require excessive computation time."

"In either of these approximations, only currents in the axial direction on a segment are considered, and there is no allowance for variation of the currents around the wire circumference. The acceptability of these approximations depends on both the value of a/λ and the tendency of the excitation to produce circumferential current or current variation. Unless (2*pi**a*)/λ is much less than 1, the validity of these approximations should be considered." One potential arena in which the validity of these approximations may be tested is the modeling of a boom connected directly to the parasitic elements of a Yagi antenna. In practice, the connection or the very close proximity of a boom to the parasitic elements alters the required length of the elements to preserve array performance. However, in NEC-2 and NEC-4–when modeled within the other limitations of the software–the boom has no effect upon the parasitic elements. The result strongly suggests that boom-to-element effects are functions of variations in circumferential currents, which NEC does not take into account. A fuller account of this phenomenon is a subject for another episode in this series.

The NEC-2 manual goes on. "The accuracy of the numerical solution for the dominant axial current is also dependent on [the ratio of segment length to radius or Ls/R]. Small values of [Ls/R] may result in extraneous oscillation in the computed current near free wire ends, voltage sources, or lumped loads. Use of the extended thin-wire kernel will extend the limit on [Ls/R] to smaller values than are permissible with the normal thin-wire kernel." In general, Ls/R must be greater than 8 for errors under 1% for the normal thin-wire kernel. This amounts to a segment length-to-wire-diameter ratio of 4:1, for programs that input wire thickness as a diameter. The manual notes that "reasonable solutions" have been obtained for the normal thin-wire kernel for Ls/R values down to about 2, with equally "reasonable solutions" for the extended thin-wire kernel for Ls/R values down to about 0.5. However, exact specification of the geometries involved does not appear. Hence, the most general guidance one might give is to use the EK command to implement the extended thin-wire kernel whenever the value of Ls/R goes below 8 (or a segment-length-to-wire-diameter ratio of 4). For straight-wire elements, the limit to Ls/R may be between 2 and 1 for very reliable results.

There are numerous other facets of extended thin-wire kernel implementation noted in the manual. For example, the normal thin-wire kernel is used–even if the EK command is implemented–at wire bends, such as those encountered in closed and nearly closed antenna geometries. Delta, quad, and Moxon rectangle geometries are samples of such antennas. At bends, the modeler should avoid very small values of Ls/R so that the surface of one wire at the junction does not penetrate into the central region of the other wire, a condition that "generally leads to severe errors."

Why EK is not used in NEC-4: The NEC-4 manual provides a chapter outlining the differences between NEC-3 and NEC-4. Over the range of considerations relevant to the use of EK in NEC-2, NEC-3 is essentially the same as NEC-2–but is different in other respects. In NEC-4, "the thin-wire approximation is now implemented with the current treated as a filament on the wire surface and the boundary condition enforced on the wire axis."

"With the boundary condition enforced on the wire axes, the openings at wire ends should be closed with end caps. This is particularly important when the ratio of segment length to radius is on the order of 2 or less. Wire ends are closed with flat caps in NEC-4, with the current and charge density assumed continuous from the wire onto the cap." NEC-4 also includes optional caps for use with voltage sources with equally low values of Ls/R. "This approximate treatment was found to be about as effective as the extended thin-wire kernel included as an option in [NEC-2 and] NEC-3. The extended thin-wire kernel option (EK card) has been dropped from NEC-4."

The NEC-4 thin-wire kernel appears at first sight to replicate the extended thin wire kernel of NEC-2 and NEC-3. Hence, results seemingly should be identical. However, the implementation of wire end caps and other alterations to the solution algorithms for wires tells us otherwise. Rather, expect results to be very close.

For relatively thin, straight wires having long segment lengths, where Ls/R is more than 8, there will be almost no difference between NEC-2 and NEC-4, even without implementing the extended thin-wire kernel in NEC-2. For values of Ls/R between 8 and 2, NEC-2 with EK and NEC-4 will normally show very close results. However, as the value of Ls/R passes 2 on its way downward, expect larger differences.

I have quoted directly from the NEC-2 and NEC-4 manuals because many users of antenna modeling software simply do not read them. As well, the self-consistent language within those manuals is guidance against misinterpretation of what the manuals record about the basis for NEC core operations. However, what we have been reviewing are simply the most relevant extracts from the fuller treatment provided by the manuals to cover not only the situation surrounding the EK card, but as well overall core operations. Hence, I fully recommend that every user of NEC-2 or NEC-4 (or even NEC-3) gradually become fully conversant with the provisions of the manuals. They were not written for the purpose of being supplanted by a series of one-line or more-easily remembered summary statements. Such statements may be useful at the beginning, but are never the ultimate end of understanding both the capabilities and the limitations of the cores.

When: I have provided some general recommendations on when to invoke the EK card, where "when" means "at what Ls/R value." However, we might pause to go through a pair of small exercises in order to appreciate better the high generality of those recommendations.

9-Segment 300-MHz Dipole Used in
the EK Deomonstration

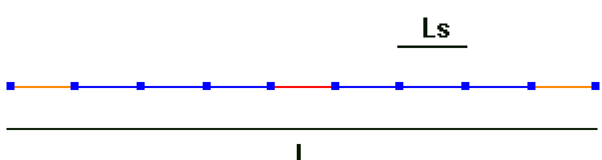

Fig. 81-2

The first exercise involves a simple dipole, the model for which I showed earlier. **Fig. 81-2** outlines the dipole. Nothing in the dipole will change except the radius of the one wire that makes up the model. Beginning with a radius of 0.0001 meters (0.1 mm), we shall increase the radius until we reach levels that allow us to create segment-length-to-radius values in the range from 4:1 down to 1:1. Since we shall not change the wire length, every increase in radius will carry us theoretically further from the initial resonance of the antenna. This move is intentional, since once we have significant reactance in the source impedance, differences created by running the model under various conditions will become more graphic.

Because we shall begin with a 1/2-λ resonant dipole, we should not expect much change in the gain or variation among models with respect to gain. Resonant dipoles change gain only very slowly with changing conditions, a common feature of most simple antennas resonated for a high source current. Therefore, the source impedance values will be our primary window on the differences. We shall run them without the EK card in both NEC-2 and NEC-4, and also with the EK card in NEC-2. All models were run on NSI's GNEC package, which contains both NEC-2 and NEC-4 cores. The following table captures the results.

Certain results appear incontestable. First, wherever there is a difference among the results, the NEC-2-with-EK data are closer to the NEC-4 data than are the data from NEC-2-without-EK. Second, the values for a ratio of segment length to radius of 1.0 are sufficiently variable as not to be able to say which values are more reliable than the others. From the table alone, without external verification, it would even be presumptuous to assert that the NEC-4 values are the most reliable. At all other values, we have much more confidence in the coincidence between NEC-4 and NEC-2-with-EK.

The more difficult question to answer is when to implement the EK card in NEC-2. For Ls/R values above 5.37, the EK card is certainly unnecessary for the dipole. Even at the radius of 0.01 m, the NEC-2 results seem equally separated from the NEC-4 results, although in opposite directions. There is a change when we simply reduce the Ls/R value from 5.37 down to 4.0: the NEC-2-with-EK results are clearly more coincident with the NEC-4 results than NEC-2-without-EK. Hence, a segment-length-to-radius ratio in the range of 6 down to 4 seems an appropriate changeover to the use of EK for NEC-2 users.

Coincidence between NEC-2-EK results and NEC-4 is not always a decisive reason for implementing the EK card in NEC-2. Consider, for example, a simple quad loop, such as the one outlined in **Fig. 81-3**. The EK version of the model follows. See model 81-3.NEC.

A Dipole in NEC-4 and in NEC-2 With and Without EK

Constants: Free-Space Environment; Frequency: 300 MHz
Length: 0.4836 m; Segments: 9; Segment Length: 0.5373 m
Ls = segment length; R = radius

Wire Radius: 0.0001 m	Ls/R: 537	
Core	Gain (dBi)	Source Impedance (R+/-jX Ohms)
NEC-4	2.12	72.080 - j 0.001
NEC-2 w/o EK	2.12	72.079 - j 0.002
NEC-2 w EK	2.12	72.079 - j 0.002
Wire Radius: 0.001 m	Ls/R: 53.7	
Core	Gain (dBi)	Source Impedance (R+/-jX Ohms)
NEC-4	2.13	75.629 + j16.514
NEC-2 w/o EK	2.13	75.628 + j16.515
NEC-2 w EK	2.13	75.222 + j16.490
Wire Radius: 0.01 m	Ls/R: 5.37	
Core	Gain (dBi)	Source Impedance (R+/-jX Ohms)
NEC-4	2.18	91.469 + j32.379
NEC-2 w/o EK	2.18	92.039 + j33.316
NEC-2 w EK	2.18	90.677 + j31.667
Wire Radius: 0.0134 m	Ls/R: 4.00	
Core	Gain (dBi)	Source Impedance (R+/-jX Ohms)
NEC-4	2.20	95.680 + j30.113
NEC-2 w/o EK	2.20	97.272 + j32.149
NEC-2 w EK	2.20	94.637 + j30.042
Wire Radius: 0.0179 m	Ls/R: 3.00	
Core	Gain (dBi)	Source Impedance (R+/-jX Ohms)
NEC-4	2.22	99.783 + j23.974
NEC-2 w/o EK	2.22	103.832 + j27.652
NEC-2 w EK	2.22	98.657 + j25.572
Wire Radius: 0.0269 m	Ls/R: 2.00	
Core	Gain (dBi)	Source Impedance (R+/-jX Ohms)
NEC-4	2.26	102.414 + j 5.134
NEC-2 w/o EK	2.27	114.262 + j 9.213
NEC-2 w EK	2.27	102.410 + j12.229
Wire Radius: 0.0537 m	Ls/R: 1.00	
Core	Gain (dBi)	Source Impedance (R+/-jX Ohms)
NEC-4	2.38	51.890 - j46.292
NEC-2 w/o EK	2.43	54.146 - j58.430
NEC-2 w EK	2.47	86.345 - j31.830

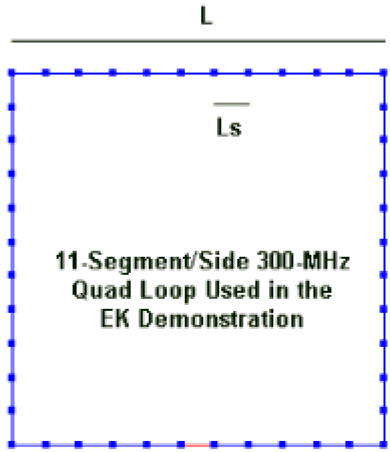

Fig. 81-3

```
CM Quad Loop
CE
GW 1,11, -0.1324,0,-0.1324, 0.1324,0,-0.1324, 0.0001
GW 2,11, 0.1324,0,-0.1324, 0.1324,0,0.1324, 0.0001
GW 3,11, 0.1324,0,0.1324, -0.1324,0,0.1324, 0.0001
GW 4,11, -0.1324,0,0.1324, -0.1324,0,-0.1324, 0.0001
GS 0 0 1
GE 0
EK 0
EX 0 1 6 0 1 0
FR 0 1 0 0 300 1
RP 0 1 360 1000 89 0 1
RP 0 181 1 1000 -90 0 1 1
EN
```

The loop is set for 300 MHz, with initial side lengths that are 0.2648 m, with 11 segments per side. With the initial wire radius of 0.0001 m, the segment lengths are 0.0241 m. As we increase the radius of the wire, the loop will drift farther from resonance. Since the geometry is closed, the loop will show capacitive reactance as we enlarge the wire (in contrast to the increasing inductive reactance of a straight wire under similar conditions). We can tabulate the results of modeling in NEC-2, NEC-2-without-EK, and NEC-2-with-EK.

Variations of both gain and source impedance begin to appear with a segment-length-to-radius ratio of 5:1. Down to a ratio of about 2:1, the pair of NEC-2 results are closer to each other than either is to the NEC-4 result. The most likely reason for this divergence from the type of results we obtained from the straight dipole is the conditions of the model and how each core handles them. The NEC-4 applies its revised algorithm to all segments and junctions of the loop. The simplified thin-wire kernel of NEC-2 also applies to each segment and wire junction. Hence, we expect some divergence of results relative to NEC-4. The EK version of NEC-2 does not apply the extended thin-wire kernel to junctions of wires that are at an angle–the bent-wire case. As a consequence, its reports will coincide with neither NEC-4 nor NEC-2-without-EK.

A Quad Loop in NEC-4 and in NEC-2 With and Without EK

Constants: Free-Space Environment; Frequency: 300 MHz
Side Length: 0.2648 m; Segments: 11; Segment Length: 0.0241 m
Ls = segment length; R = radius

Wire Radius: 0.0001 m		Ls/R: 241
Core	Gain (dBi)	Source Impedance (R+/-jX Ohms)
NEC-4	3.30	125.46 - j 1.213
NEC-2 w/o EK	3.30	125.46 - j 1.207
NEC-2 w EK	3.30	125.46 - j 1.207
Wire Radius: 0.001 m		Ls/R: 24.1
Core	Gain (dBi)	Source Impedance (R+/-jX Ohms)
NEC-4	3.29	119.53 - j52.554
NEC-2 w/o EK	3.29	119.58 - j52.323
NEC-2 w EK	3.29	119.58 - j52.322
Wire Radius: 0.0048 m		Ls/R: 5.00
Core	Gain (dBi)	Source Impedance (R+/-jX Ohms)
NEC-4	3.28	106.48 - j86.861
NEC-2 w/o EK	3.26	107.84 - j83.170
NEC-2 w EK	3.26	108.21 - j83.076
Wire Radius: 0.006 m		Ls/R: 4.00
Core	Gain (dBi)	Source Impedance (R+/-jX Ohms)
NEC-4	3.28	102.50 - j91.561
NEC-2 w/o EK	3.25	104.60 - j86.457
NEC-2 w EK	3.25	105.33 - j86.268
Wire Radius: 0.008 m		Ls/R: 3.00
Core	Gain (dBi)	Source Impedance (R+/-jX Ohms)
NEC-4	3.29	95.571 - j97.117
NEC-2 w/o EK	3.20	99.146 - j89.857
NEC-2 w EK	3.22	100.91 - j89.398
Wire Radius: 0.012 m		Ls/R: 2.00
Core	Gain (dBi)	Source Impedance (R+/-jX Ohms)
NEC-4	3.31	80.679 - j102.15
NEC-2 w/o EK	3.20	87.361 - j92.323
NEC-2 w EK	3.16	93.264 - j90.958
Wire Radius: 0.0241 m		Ls/R: 1.00
Core	Gain (dBi)	Source Impedance (R+/-jX Ohms)
NEC-4	3.32	37.507 - j80.703
NEC-2 w/o EK	3.11	43.091 - j78.095
NEC-2 w EK	2.58	81.412 - j80.556

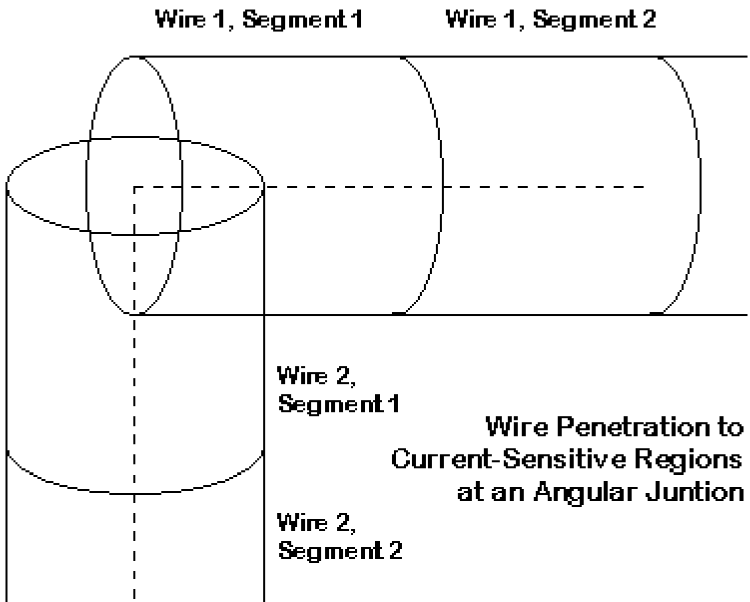

Fig. 81-4

As we increase the wire radius, the surface of one wire at a junction penetrates farther into the central region of the other wire segment forming the junction, as suggested by the simple sketch in **Fig. 81-4**. As the penetration reaches a region where it alters the current calculation, the results grow less reliable. Between ratios of 5:1 and 3:1, we encounter a growing variance among the reports, with no internal guidance as to which one may be the more nearly correct. In just the region that the EK card in NEC-2 provided significant modeling assistance in terms of the accuracy of results, it proves to be of little assistance with closed geometries and other bent-wire configurations without external means of verification.

The use of the EK card with NEC-2 thus finds its best range of uses with straight-wire elements of uniform diameter. For segment-length-to-radius ratios between 8:1 and 2:1, it yields results that are consistent with those emerging from NEC-4. Perhaps one day we shall see the EK facility appear as a user option on most entry-level NEC-2 software. More and more entry level NEC-2 software is implementing the command automatically as the ratio of segment length to radius grows smaller. However, the exact ratio of implementation remains a programmer option.

82. The Nature and Adequacy of NEC Correctives

NEC has a number of correctives for special situations. The most notable of these situations involves the ratio of segment length to wire radius. In NEC-2, whenever the radius is greater than about 1/4 the segment length, the NEC-2 manual recommends the use of the EK command, which invokes the extended thin-wire kernel. We examined that feature of NEC-2 in the last episode. We also noted that NEC-4 revised the algorithms for determining the currents on wire segments so as to do away with the need for the EK command.

The most noted external corrective for NEC-2 involves the inherent weakness of the program for dealing with elements having a tapered diameter, as illustrated in **Fig. 82-1**.

Fig. 82-1

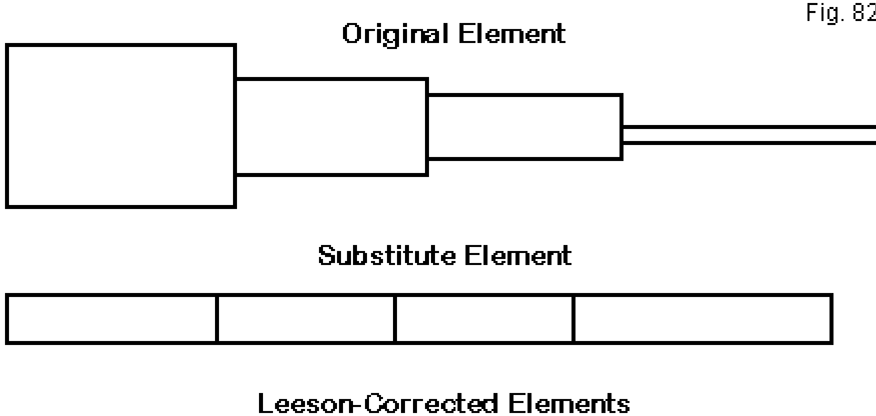

The most commonly used corrective system was developed by Leeson and involves the use of substitute uniform-diameter elements. The substitute elements involve a reasonably complex procedure that begins with the detection of the element ends and hence the determination of the range of wires over which the corrective will be applied. The wires must be linear and symmetrical about a center coordinate. The exception is a monopole wire in contact with the ground with its source (if any) on the segment adjacent to the ground. The wire with two ends must place any sources or loads on the center segment. Moreover, the corrective is valid for only a restricted frequency range, usually prescribed as being within about 15% of the element being 1/2-λ. Most programs (such as EZNEC and NEC-Win Plus) simply refuse to invoke the correctives if the element does not meet any one of the limiting criteria. Although the standard case for the application of Leeson correctives is the downward taper of element diameter, as portrayed in **Fig. 82-1**, the correctives will also work with bi-conical antennas composed of stepped diameter elements.

The adequacy of the Leeson correctives is dependent upon a number of factors. One of those factors is the uniformity of segment length along the substitute element. If we model a physical element exactly, we often find a mixture of long, short–and sometimes very short–sections of element for the various element diameters. There is a tendency among modelers to under-segment the longer wires in the element relative to the shorter wires. Consider the situation in **Fig. 82-2**.

In this example, the short center section uses a single segment, followed in the next wire by longer segments, etc. The application of the Leeson correctives normally pre-calculates a total element length for the substitute element, using the calculated uniform diameter that achieves an element having the same electrical characteristics as the original tapered-diameter element. Then the program will calculate the length of wires that substitute for each of the original wires. The program will normally use for each new wire the same number of segments as specified for the tapered diameter wire. The resulting element will be as uniform or non-uniform in segment length as the originally specified element.

Fig. 82-2

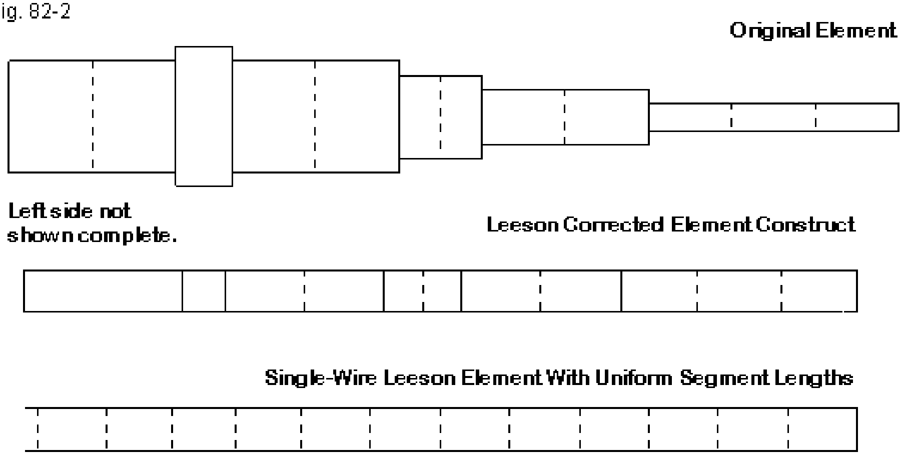

The new algorithms of NEC-4 ostensibly did away with the need for using the Leeson corrections. For many cases, NEC-4 produces virtually identical results to those of NEC-2 with the Leeson correctives invoked. However, NEC-4's new algorithms are not without limits. If the rate of diameter change is too great or if the overall decrease in diameter is too large along the overall length of the element, NEC-4 will tend to over estimate the gain of the element and underestimate the source impedance, if that element is driven.

We may illustrate the situation for virtually all of the limitations by running a pair of contrasting elements through all of the available options. We shall begin with a "low-taper" element that I extracted from a multi-element Yagi design for 20 meters. I isolated the driven element of the array, but made no attempt to resonate it in isolation, relative to its resonant length within the array. Hence, the element will show some feedpoint reactance.

The following EZNEC description of the element shows the free-space environment used for the comparisons. However, it was necessary to run the element in a variety of programs, including NEC-Win Pro, GNEC, and EZNEC, in order to cover all of the possibilities. See models 82-1 through 82-3.

lo-taper element Frequency = 14.175 MHz
Wire Loss: Aluminum (6061-T6) -- Resistivity = 4E-08 ohm-m, Rel. Perm. = 1

--------------- WIRES ---------------

No.	End 1 Conn.	X	Y	Z	End 2 Conn.	X	Y	Z	Dia (in)	Segs
1		-205.95,	79.8,	0	W2E1	-156,	79.8,	0	0.625	4
2	W1E2	-156,	79.8,	0	W3E1	-120,	79.8,	0	0.75	3
3	W2E2	-120,	79.8,	0	W4E1	-72,	79.8,	0	0.875	4
4	W3E2	-72,	79.8,	0	W5E1	72,	79.8,	0	1	13
5	W4E2	72,	79.8,	0	W6E1	120,	79.8,	0	0.875	4
6	W5E2	120,	79.8,	0	W7E1	156,	79.8,	0	0.75	3
7	W6E2	156,	79.8,	0		205.95,	79.8,	0	0.625	4

(Column headings: End 1 Coord. (in); End 2 Coord. (in).)

Total Segments: 35

-------------- SOURCES --------------

No.	Specified Pos. Wire #	% From E1	Actual Pos. % From E1	Seg	Amplitude (V/A)	Phase (deg.)	Type
1	4	50.00	50.00	7	1	0	I

Ground type is Free Space

The segmentation along the element is relatively uniform. For wires 1-4, the segment lengths are 12.49", 12", 12", and 11.07". As well, the long center section of the element with 13 uniform length segments ensures that the segments adjacent to the source segment are the same length as the source segment. The diameter steps are a uniform 0.125" drop per step.

Now let's run this element through all of the available combinations of corrected and uncorrected situations that we can generate with the NEC-2 and NEC-4 cores. Our results should resemble those in the following table.

Low-Taper Element Free-Space Gain and Source Impedance

Core and Condition	Gain (dBi)	Impedance (R+/-jX Ohms)
NEC-2		
1. No internal or external correctives	2.20	76.49 + j 19.23
2. EK command invoked	2.20	76.78 + j 19.21
3. Leeson correctives invoked	2.14	74.68 + j 11.85
4. Resubstitution of a single wire with the Leeson diameter, length, and total number of segments	2.14	74.69 + j 11.94
NEC-4		
1. No internal or external correctives	2.17	76.14 + j 12.84
2. Resubstitution of a single wire with the Leeson diameter, length, and total number of segments	2.14	74.69 + j 11.94

In NEC-4 programs that permit the use of Leeson corrections (such as EZNEC Pro/4), there is rarely any difference between corrected NEC-2 and corrected NEC-4. The Leeson corrections apply only to modeling situations in which there is no inherent difference in the performance of the two cores.

Given the relatively gentle taper of the element, even the NEC-2 results are not dramatically off the mark. However, note that the "raw" NEC-4 results are only about halfway home in the estimation of gain, although they are quite close in the estimation of the source impedance. Of course, the standard for these remarks is the Leeson correction result, which is presumed accurate here and has tested accurate in innumerable physical antenna designs.

For our second example, let's use a much more highly tapered element, extracted from another multi-element array. The element model employs a short, fat center section simulating the boom-to-element assembly. Our concern in this exercise is not the adequacy of that technique, but its consequences for the element model. See models 82-4 through 82-6.

hi-taper element Frequency = 14.175 MHz

Wire Loss: Aluminum (6061-T6) -- Resistivity = 4E-08 ohm-m, Rel. Perm. = 1

--------------- WIRES ---------------

No.	End 1 Conn.	Coord. (in) X	Y	Z	End 2 Conn.	Coord. (in) X	Y	Z	Dia (in)	Segs
1		-203.5,	72,	0	W2E1	-138,	72,	0	0.5	8
2	W1E2	-138,	72,	0	W3E1	-96,	72,	0	0.625	6
3	W2E2	-96,	72,	0	W4E1	-48,	72,	0	0.75	6
4	W3E2	-48,	72,	0	W5E1	-4,	72,	0	0.875	5
5	W4E2	-4,	72,	0	W6E1	4,	72,	0	3.419	1
6	W5E2	4,	72,	0	W7E1	48,	72,	0	0.875	5
7	W6E2	48,	72,	0	W8E1	96,	72,	0	0.75	6
8	W7E2	96,	72,	0	W9E1	138,	72,	0	0.625	6
9	W8E2	138,	72,	0		203.5,	72,	0	0.5	8

Total Segments: 51

-------------- SOURCES --------------

No.	Specified Pos. Wire #	% From E1	Actual Pos. % From E1	Seg	Amplitude (V/A)	Phase (deg.)	Type
1	5	50.00	50.00	1	1	0	V

Ground type is Free Space

Ideally, the segment lengths adjoining the source segment (Wire 5) should be the same length as the source segment. However, the segment lengths for wires 1 through 5 read as follows: 8.19", 7", 8", 8.8", 8". Achieving the desired result would require additional segments on an already large model (when we add all of the other elements of the original array). We are blocked from further segmenting the short, fat source wire, because the segment-length-to-radius ratio is already 4.68:1. Adding a segment each to wires 4 and 6 would have resulted in a segment length as much below the segment length on Wire 5 as the present segmentation places the length above that of the center segment in the element.

Let's see what happens to the results for this model when we run it through the same set of core runs that we used for the low-taper element.

-

High-Taper Element Free-Space Gain and Source Impedance

Core and Condition	Gain (dBi)	Impedance (R+/-jX Ohms)
NEC-2		
1. No internal or external correctives	4.30	45.33 + j 2.51
2. EK command invoked	4.37	44.56 + j 2.48
3. Leeson correctives invoked	2.16	68.88 - j 11.44
4. Resubstitution of a single wire with the Leeson diameter, length, and total number of segments	2.12	69.59 - j 11.52
NEC-4		
1. No internal or external correctives	3.06	59.14 - j 6.17
2. With the VC command invoked	2.95	60.57 - j 6.26
3. Resubstitution of a single wire with the Leeson diameter, length, and total number of segments	2.12	69.58 - j 11.53

The wholesale inability of raw NEC-2 to handle the highly tapered element is evident. I invoked the EK command in the NEC-2 sequence of results simply to demonstrate that the EK command is not a substitute for the Leeson corrections. If we skip to the NEC-4 results, we find that the very high taper and other limitations of the element model also yield results that are well off the mark set by invoking the Leeson corrections. Once more, the gain report is about halfway between the NEC-2 report and the Leeson report. However, the source impedance report is about 2/3 the way home–a function of the fact that one figure is recorded in dB while the other uses a non-logarithmic adjustment. Raw NEC-4 shows an average gain test value of 1.235 for the element. The adjusted gain would be 2.14 dBi, much closer to the Leeson value.

Unlike the low-taper element case, the high-taper element does show a difference between the results for the modeled element and for a one-wire substitute element with the same length, diameter, and total number of segments as the programmed set of wires. The difference is not great, since some pains were taken to equalize segment lengths as best one could within the original model. Less careful segmentation–as is commonly used in casual modeling of large arrays with tapered diameter elements–would have yielded a higher disparity between the programmed Leeson element and the 1-wire equivalent element.

Because the highly tapered element has a short, fat center section with a segment-length-to-radius ratio of only 4.68:1, I added an entry to the NEC-4 list. One run of the model invokes a new command in NEC-4 labeled VC, for voltage cap. For the element that we have been testing, the invocation of the new command produces noticeable but not very large differences relative to raw NEC-4. See models 82-8.NEC and 82-9.NEC in NEC-4 only

NEC-4 introduces wire-end caps as a standard part of the overall calculations. At a voltage source segment or at segments with impedance loads, NEC-4 makes it optional for the user to introduce segment end caps “to reduce the excitation of the inside of the wire at these points.” **Fig. 82-3** shows the general situation at a voltage source.

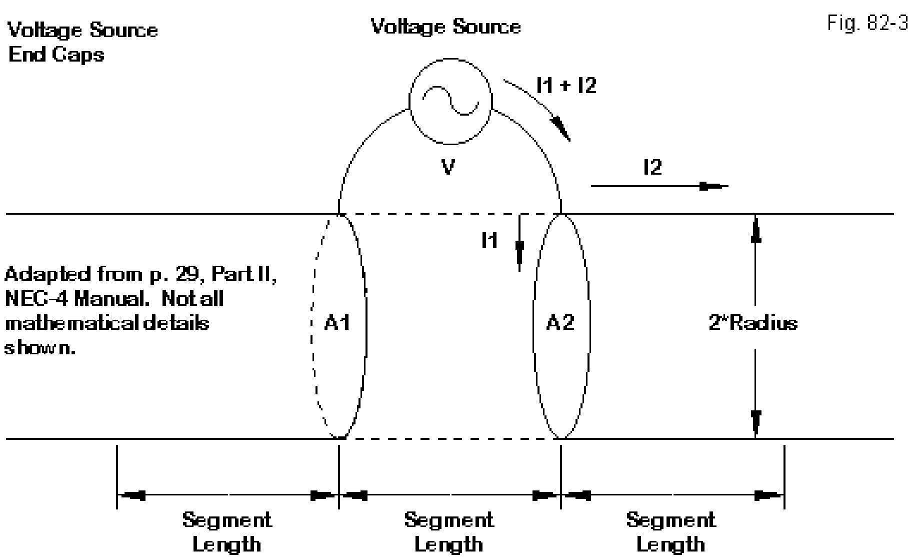

The sketch is adapted from Part II (page 29) of the NEC-4 manual and does not show all mathematical detail. Its purpose is to acquaint you with the general situation at the voltage source with respect to the caps forming the inside ends of the wire segments on either side of the source segment. See the NEC-4 manual for full mathematical details.

To employ these end caps, we need only place a simple program control card in the deck:

```
VC
```

The end caps become important for small segment-length-to-radius values. As the ratio goes below 2:1 and continues to shrink, the imaginary part of the current and the real part of the charge will go into oscillation without the use of end caps. Because a source that is near to the end of a wire may show an error in the source voltage, the end caps have been made optional by introducing them via the VC command.

For the average user of NEC, the question that is often preliminary to matters of mathematical refinement is at what point the use of the VC command will begin to show differences from the same model without using the VC command. To provide a sample answer, we may return to the dipole that we have used in other episodes. The NEC input file for this dipole is quite simple; see model 82-6.

```
CM NEC-WIN Example
CM Simple dipole antenna in Free Space
CM Optimized for resonance at 300 MHz
CE
GW 1 9 0 -.2418 0 0 .2418 0 .0001
GS 0 0 1
GE 0 -1 0
VC
EX 0 1 5 0 1 0
FR 0 1 0 0 300 1
RP 0 181 1 1000 -90 0 1 1
RP 0 1 360 1000 90 0 1 1
EN
```

The 9-segment free-space dipole is initially resonant at 300 MHz. Let’s catalog the gain and source impedance reports as we enlarge the radius of the antenna without altering any other factors. The only difference between the non-VC and VC models is the absence of the VC line in the former.

Gain and Source Impedance of a Dipole With and Without the VC Command

Wire Radius	Segment-Length-to-	Without VC		With VC	
(meters)	Radius Ratio	Gain (dBi)	Source Z	Gain (dBi)	Source Z
0.0001	537:1	2.12	72.08 - j 0.00	2.12	72.08- j 0.00
0.001	53.7:1	2.13	75.63 + j16.51	2.13	75.63 + j16.52
0.01	5.37:1	2.18	91.47 + j32.38	2.15	91.57 + j33.10
0.0134	4:1	2.20	95.68 + j30.11	2.15	95.71 + j31.69
0.0179	3:1	2.22	99.78 + j23.97	2.14	99.71 + j27.48
0.0269	2:1	2.26	102.41 + j5.13	2.10	103.60 + j15.82
0.0537	1:1	2.38	51.89 - j46.29	1.93	99.00 - j17.25

As the ratio reaches the 4-6:1 level, we can clearly see an effect upon the gain report with and without the use of the VC command. Without the VC command, the gain report increases steadily. In contrast, with the VC command invoked, the gain reaches a peak value and then descends. Except for the 1:1 segment-length-to-radius ratio value, there is little difference in the source impedance reports. However, for the very small ratio, the source impedance difference is considerable. The non-VC report represents a precipitous drop in resistance and a rapid shift in the reactance. With the VC command invoked, the resistance remains in the general range of the preceding reports, with a milder shift in reactance.

The test dipole used only 9 segments, a segmentation density one might consider below true convergence. So we may reset the dipole example for a segment-length-to-radius ratio of 1.5:1. We may sample a number of different levels of segmentation by simply altering the radius so that it is always 2/3 the segment length. The results of this exploration form an interesting table.

Constant Dipole Length and Segment-Length-to-Radius Ratio

No.	Segment	Radius	Without VC		With VC	
Segs	Length (m)	(m)	Gain (dBi)	Source Z	Gain (dBi)	Source Z
9	0.0537	0.0358	2.30	95.83 - j 17.52	2.05	104.00 + j 3.81
15	0.0322	0.0215	2.20	129.68 - j 34.52	2.09	141.40 - j 8.96
25	0.0193	0.0129	2.13	182.40 - j118.85	2.09	224.11 - j 92.56
41	0.0118	0.0079	2.11	215.06 - j258.65	2.09	292.31 - j262.77

With the VC command invoked, the gain stabilizes very rapidly with the increase in the number of segments and a constant segment-length-to-radius ratio. Without the VC command in use, the gain descends with increasing numbers of segments toward the "with-VC" value. The source impedance values follow the same general trends, but show noticeably different values are each level.

At the same time as the results appear to be converging, the average gain test (AGT) values also approach closer to 1.000. However, with the lowest segmentation level and no VC command, the AGT value is 1.0148. With the AGT command in use, the corresponding AGT value is 0.9591. The two sets of AGT values approach 1.000 from opposite directions, and the use of the VC command results in a slightly poorer AGT value than without the command in use. A similar pattern holds for the first sample that we took. Without the VC command in use, we obtained a gain report of 2.38 dBi with a source impedance of about 52 - j46 Ω. With the VC in use, the gain report was 1.93 dBi with an impedance of 99 - j17 Ω. Although the VC report appeared more closely tied to the preceding ratios of segment length to radius, the non-VC AGT value was 1.0315, while the VC value was 0.9330, about twice as distant from the ideal value.

The VC command, then, yields results that are not self-interpreting or wholly consistent with other markers that one normally uses to develop a sense of model adequacy. In general, then, the VC source wire-end cap command should only be used where there are experimental results with which to correlate the results. The NEC-4 manual notes that the "voltage-source end caps have been made optional until their effect is better understood."

83. Insulated Wires: The NEC-2 Way

In episode #50 of this series, I called attention to the IS (Insulated Sheath) card introduced into NEC-4. The program control command provides a means to factor into a model the effects of the conductivity and permittivity of insulation wrapped around a wire. Assuming a high insulating effect—that is, a very low conductivity—the physical shortening effects of insulation on a wire for a given frequency are functions of the permittivity (relative dielectric constant) and thickness of the insulation.

NEC-4 and IS

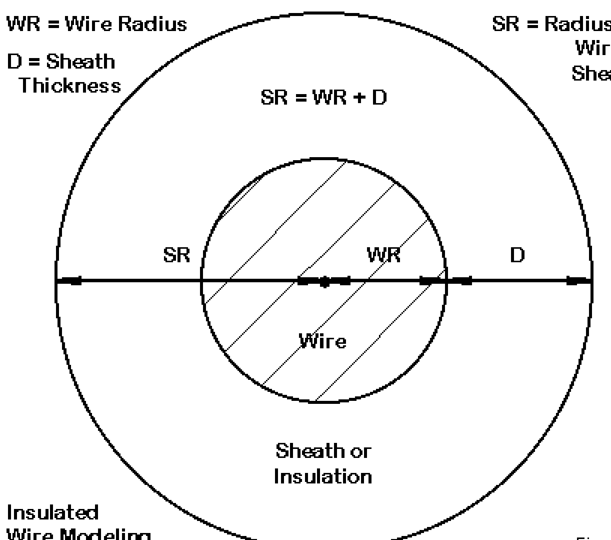

Fig. 83-1

Fig. 83-1 shows the situation of an insulated wire. For NEC modeling, there are two radii of interest. One is the radius of the conducting wire (WR). The second is the radius of the wire-plus-insulation (SR). The difference in the two radii is the thickness of the insulation (D). In NEC-4, we can enter the required data in the IS command and obtain automatic calculation of the effects of the insulation. By comparing, for example, the resonant length of a bare wire and a wire with a given type and thickness of insulation, we can obtain the velocity factor of the insulated wire in antenna (not in transmission-line) service. See column 50 for some ranges of velocity factors that apply to typical types and depths of insulation.

I do not presently have access to a handy list of relative dielectric constant values for wire insulations that we commonly encounter. One of the few guides available comes from the checking sources like *Passive Electronic Component Handbook*, 2nd Ed, edited by Charles A. Harper (McGraw-Hill, 1997). The capacitor chapter provides an interesting—although not wholly relevant—list of plastics used as capacitor dielectrics, along with their approximate dielectric constants. Some of these same plastics are used for wire insulation.

Material	Approx. Permittivity
Polyisobutylene	2.2
Polytetrafluoroethylene (PTFE)	2.1
Polyethylene terepthalate (PET)	3.0-3.2
Polystyrene (PS)	2.5
Polycarbonate (PC)	2.8-3.0
Polysulfone (PSU)	2.8-3.2
Polypropylene (PP)	2.2

Common plastics, then, appear to have a range of relative permittivity values between 2 and 3. In contrast, the permittivity of a vacuum is by definition 1.0, and air is 1.0006. If we specify a relative permittivity value of 1.0 for any sheath, no matter how thick, we obtain the performance of bare wire.

Fig. 83-2 shows—at the top—the model for a resonant 30-MHz dipole using 2-mm diameter copper wire in free space. In this model, the wire has a 2-mm-thick insulating sheath with a permittivity of 2.25. The model shows the length of the dipole when brought to resonance. The dipole half-length of 2.302 m contrasts to the bare-wire half-length of 2.416 for resonance. The result is a velocity factor of 0.957.

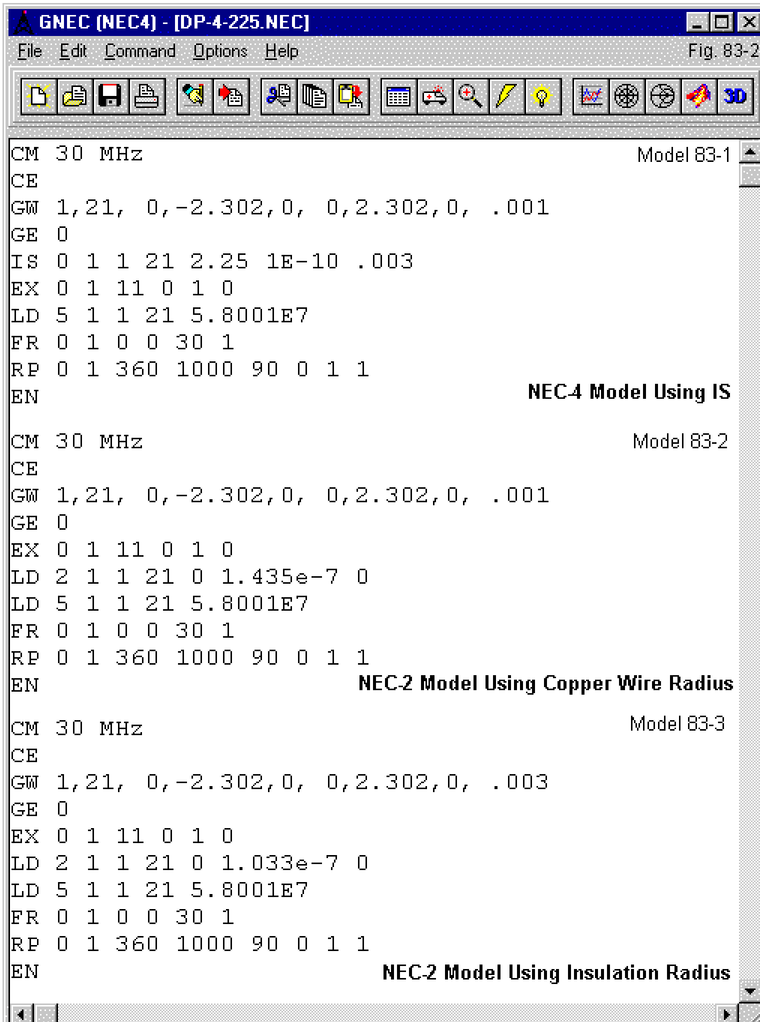
GNEC (NEC4) - [DP-4-225.NEC]
File Edit Command Options Help
Fig. 83-2
CM 30 MHz
CE
GW 1,21, 0,-2.302,0, 0,2.302,0, .001
GE 0
IS 0 1 1 21 2.25 1E-10 .003
EX 0 1 11 0 1 0
LD 5 1 1 21 5.8001E7
FR 0 1 0 0 30 1
RP 0 1 360 1000 90 0 1 1
EN
Model 83-1
NEC-4 Model Using IS
CM 30 MHz
CE
GW 1,21, 0,-2.302,0, 0,2.302,0, .001
GE 0
EX 0 1 11 0 1 0
LD 2 1 1 21 0 1.435e-7 0
LD 5 1 1 21 5.8001E7
FR 0 1 0 0 30 1
RP 0 1 360 1000 90 0 1 1
EN
Model 83-2
NEC-2 Model Using Copper Wire Radius
CM 30 MHz
CE
GW 1,21, 0,-2.302,0, 0,2.302,0, .003
GE 0
EX 0 1 11 0 1 0
LD 2 1 1 21 0 1.033e-7 0
LD 5 1 1 21 5.8001E7
FR 0 1 0 0 30 1
RP 0 1 360 1000 90 0 1 1
EN
Model 83-3
NEC-2 Model Using Insulation Radius

In episode 50, I cataloged a considerable mass of baseline data for the IS command using the 30-MHz dipole. I took three cases involving a 2-mm diameter wire: with 0.5-mm, 1.0-mm, and 2.0-mm thick insulation. I then systematically ran each physical situation through permittivities from 0 through 3 in 0.25 steps. My goal was to develop a series of curves for various ways of looking at the data for the progression of insulation thickness that had a 1-2-4 progression. Part of that work was to develop data on the 30-MHz dipole's resonant length and resonant impedance for each permittivity level.

These two data categories will be useful to us when we examine an alternative means of handling insulated wires that is equally applicable to any form of NEC.

Insulation through LD2

Although NEC-2 does not have anything to equal the simplicity of an IS command, it is possible to simulate the effects of wire insulation by using the LD 2 command. The commands LD 0 through LD 3 specify lumped loads of either series or parallel R-L-C types. (LD 4 is the R-X load, while LD 5 is the command used to specify the conductivity of the wire, where no entry indicates a perfect or lossless wire.) In early episodes of this series, we have worked in detail with the use and limitations of both series and parallel loads that specify the capacitance or the inductance in basic units—the LD 0 and LD 1 commands. However, for most modeling situations, there seems to be little application for the LD 2 and LD 3 commands, which also specify either series of parallel R-L-C circuits. However, these commands use distributed values, specified as farads/meter or henrys/meter.

We shall be employing the LD 2 series circuit, but use only one value: the inductance value in distributed form. The premise is simple: an insulated sheath around a wire acts very much like a distributed inductance along the wire in terms of shortening the required physical length for a given electrical length. Since LD loads are non-radiating, whether lumped or distributed, the use of the LD 2 load has no affect on the performance pattern of the antenna except as the physical wire length has an affect.

The middle portion of **Fig. 83-2** shows the direct substitution of an LD 2 command card for the IS command.

```
LD          2    1       1          21     0  1.033e-7   0
Command   Type   Tag   Start Seg   End Seg   R      L       C
```

The expanded version of the LD 2 line identifies the individual entries. Note that for this type of entry, we select all of the segments on the wire to apply the following series R-L-C values uniformly along the length. The value of the required inductance in H/m is in the order of E-07, that is, in the ballpark that surrounds a tenth of a uH/m. The exact amount that I placed in the LD 2 line was the amount required to resonate the dipole at the same length and frequency as the IS card. I called the dipole resonant if the reactance was under +/-0.2 Ohms. By a series of modeling exercises, I was able to replace all of the IS commands from episode 50 with LD2 commands with L/m values for the three cases and for all permittivities from 0 through 3. Then I made a table.

The table actually has more data than we yet have use for, but we may examine most of the lines. The “Permittivity” line in each of the 3 sections lists the range and increments of dielectric constants covered by the exercise. The “DP Length” line shows the half-length in meters. The “Zres IS” line records the resonant impedance or feedpoint resistance for each dipole length and permittivity level.

The next line—”A:L/m”—records the value of distributed inductance required to bring the dipole back to resonance after removing the IS line. The following line lists the resonant impedance recorded from the model that used that specified value of L/m. As you will note, there is a slight but no where close to debilitating difference in the Zres numbers that emerge from the use of the IS command and from the use of the LD 2 command to simulate wire insulation.

You may create from the specified lines of the table a chart that correlates insulation permittivity and thickness on the one hand and usable model values for LD 2 commands to simulate in NEC-2 the increments of insulation covered. 2-mm diameter (1-mm radius; 0.0787" diameter) wire is about half way between AWG #14 (0.0641") and AWG #12 (0.0808"). The indicated L/m value should cover both wire sizes and associated insulation. Remember to use the center portion of **Fig. 83-2** as a model-construction guide. It should especially remind you to multiply each of the values shown in the table by E-07.

Data Table: Comparison of NEC-4 IS Values to NEC-2 LD 2 Values

Copper wire radius 1 mm for all cases.- TH = insulation thickness. "Radius" = insulation radius.
A:L/m = required inductance for 1-mm radius wire. B:L/m = required inductance for 3-mm wire.
C:L/m = calculated value of required inductance. All L/m values = H/m * E-07.

TH=0.5 mm; Radius=1.5 mm									
Perm	1	1.25	1.5	1.75	2	2.25	2.5	2.75	3
DP Length	2.416	2.4	2.391	2.383	2.378	2.374	2.371	2.368	2.366
Zres IS	72.536	71.665	71.238	70.794	70.552	70.355	70.215	70.052	69.961
A:L/m	0	0.185	0.293	0.393	0.452	0.503	0.54	0.577	0.603
Zres 1-mm	72.536	71.65	71.15	70.73	70.45	70.24	70.07	69.91	69.8
B:L/m	-0.06	0.12	0.22	0.31	0.37	0.415	0.45	0.483	0.51
Zres1.5mm	72.59	71.72	71.23	70.79	70.52	70.3	70.14	69.97	69.87
C:L/m	-0.0876	0.0929	0.2119	0.2974	0.3617	0.4116	0.4515	0.4842	0.5114
TH=1.0 mm; Radius=2.0 mm									
Perm	1	1.25	1.5	1.75	2	2.25	2.5	2.75	3
DP Length	2.416	2.391	2.373	2.36	2.351	2.345	2.339	2.333	2.33
Zres IS	72.536	71.262	70.306	69.618	69.172	68.915	68.605	68.256	68.142
A:L/m	0	0.295	0.515	0.677	0.793	0.867	0.945	1.022	1.06
Zres 1-mm	72.54	71.16	70.18	69.48	69	68.67	68.35	68.02	67.86
B:L/m	-0.1	0.165	0.36	0.505	0.61	0.675	0.745	0.815	0.85
Zres 2-mm	72.71	71.34	70.35	69.64	69.17	68.83	68.51	68.19	68.03
C:L/m	-0.1498	0.1574	0.3623	0.5085	0.6183	0.7036	0.7719	0.8277	0.8743
TH=2.0 mm; Radius=3.0 mm									
Perm	1	1.25	1.5	1.75	2	2.25	2.5	2.75	3
DP Length	2.416	2.375	2.348	2.328	2.313	2.302	2.292	2.284	2.278
Zres IS	72.536	70.405	69.046	68.029	67.275	66.754	66.235	65.829	65.551
A:L/m	0	0.49	0.83	1.088	1.285	1.435	1.57	1.68	1.76
Zres 1-mm	72.54	70.29	68.83	67.76	66.96	66.38	65.86	65.42	65.1
B:L/m	-0.162	0.25	0.53	0.745	0.91	1.033	1.142	1.235	1.303
Zres 3-mm	72.96	70.71	69.24	68.16	67.36	66.77	66.22	65.8	65.48
C:L/m	-0.2373	0.2495	0.5742	0.806	0.9797	1.1152	1.2234	1.3119	1.3857

You can roughly approximate these values by knowing the insulation thickness, the wire size, and the relative permittivity of the insulation. You can pre-calculate the required values from the following rough equation:

$$L/m = 2.267E{-}07 \cdot \left(1 - \frac{1}{\varepsilon}\right) \cdot \ln\left(\frac{R}{r}\right) \qquad (1)$$

L/m is the distributed inductance in henrys/meter, epsilon is the permittivity of the insulation, R is the radius of the wire-plus-insulation, and r is the radius of the wire itself. The equation is especially good for permittivity values between 2 and 3, the normal range of insulation dielectric constant for most wire used by radio amateurs. However, the final constant (2.267) is an average between the lowest and highest values required to cover all of the required values of L/m in the table. Within the range of the table, calculated values at the extremes reach an error of +/-6%. However, a 6% error in the LD 2 command inductance entry still provides a model that is off resonance only by about 3 to 4 Ohms of reactance. Hence, the calculation may still be quite serviceable for practical applications.

The value of L/m actually undergoes inflation with increases in both the ratio of radii and permittivity. The approximate rate of expansion is roughly equal to the product of those 2 values to the 12th root. So you may obtain a further bit of accuracy by using this variant of the roughest equation:

$$L/m = 2E{-}07 \cdot \left(\sqrt[12]{\frac{R}{r} \cdot \varepsilon} \right) \cdot \left(1 - \frac{1}{\varepsilon} \right) \cdot \ln\left(\frac{R}{r} \right) \qquad (1A)$$

The use of the expansion factor on the equation's constant results in maximum errors for L/m of less than 2% across the range of calibration. For most combinations of radii ratios and permittivities, the error is less than 0.5%.

Of course, the error notes for equations 1 and 1A are not a comparison to a physical antenna, but a correlation of LD 2 values of L/m to NEC-4 IS results for the range of radii and permittivity in the original table for a 2-mm copper dipole at the test frequency. In both the initial approximation and the version of the equation with the expansion adjustment, the second term ensures that the value of L/m goes to zero when the permittivity goes to 1, the condition of a bare wire. As well, the final term ensures that the value of L/m goes to zero when R and r are equal, again, the condition of a bare wire.

Equations 1 and 1A are *ad hoc* adjustments of a somewhat different equation developed by Alexander Yurkov, RA9MB. We shall look at his alternative as our next step in providing a substitute for the IS command for NEC-2 users.

The RA9MB/UA3AVR Insulated Wire Simulation

Yurkov took a different tack in developing his modeling aid for insulated wires. He calculated the effect of insulation, taking the entire wire-plus-insulation radius as his basic unit. Examine the lowest model in **Fig. 83-2**. Note that the wire radius is not the copper wire radius of 1 mm, but the insulation outer radius of 3 mm. In the LD 2 line, note that the value of distributed inductance is considerably different from the value used in the middle model. (The middle model retained the wire size as originally specified.)

$$L/m = 2E\text{–}07 \cdot \left(1 - \frac{1}{\varepsilon \cdot k_{abs}^2}\right) \cdot \ln\left(\frac{R}{r}\right) \qquad (2)$$

Equation 2 uses the same terms as equation 1. However, the Yurkov adds a term, the square of k_{abs}. The term "k_{abs}" stands for an "absolute velocity factor" and uses the value 0.95 in applications of the equation. Yurkov's original equation also employs a complex first term that he labels μ_0. However, Dimitry Federov, UA3AVR, modified the equation for use in NEC models by dividing that term by values that simplified the left-most term of the equation to the form used in equation 2. For further information on the Yurkov equation and its foundations, you may visit http://www.qsl.net/ua3avr/Read_me_Eng.htm.

As an exercise, I took the models used in the first two steps of the data table and modified the GW lines to reflect the larger wire radius required by the Yurkov equation. I then varied the value of "B:L/m" until the dipole was once more resonant for each case and increment of permittivity. I recorded the resulting resonant impedance as "Zres 1.5" (or "Zres 2" or Zres 3", depending upon the case).

The final line of the data table lists "C:L/m," the values of distributed inductance calculated directly from equation 2.

We can summarize the differences between the Yurkov equation and my rough variant in this way. Yurkov's equation is based on solid foundations. However, it requires that the user alter the wire radius from its wire value to a value equal to the insulation radius. For most real cases, that change will make no significant difference to the reported data. However, it does result in a requirement to introduce a negative inductance for permittivity values of 1 and just above 1 in order to restore the dipole to resonance. Thickening the wire changes both the skin effect and the resonant length so as to require a capacitive reactance for resonance with the fixed dipole lengths used. Note that NEC will handle at least small values of inductance in negative numbers. On the other hand, my initial rough equation has a narrower range within which it yields accurate values, although the version including expansion is at least as accurate as the Yurkov equation over the test range in correlations with the results of NEC-4 models using the IS command. In addition, equations 1 and 1A retain the original wire radius in the model. Which version you employ will make little difference practically and may well turn out to be a function of which equation you are most comfortable solving and which modeling technique (applying the original or the adjusted wire radius) you are most comfortable using.

How Confident Should We Be in the NEC-2 LD 2 Simulation of Insulated Wires?

Tabular data often does not lend itself to evaluations indicated by our lead question. Perhaps we can better judge our confidence level in the Yurkov substitution method by graphing the data. Note that we have no external baseline of empirical data. So we shall be comparing the results obtained by the NEC-4 IS command with the substitute methods of handling insulated wires. We shall proceed on a case-by-case basis, beginning with the thinnest insulation.

Fig. 83-3 has 3 lines. The red line indicates the required values for L/m to restore the dipole to resonance based on the original use of the IS command in NEC-4. These values are based on retaining the specified wire radius as it was in the original NEC-4 IS model. The green line indicates the values of inductance required if we increase the wire radius to the value indicated by the insulation radius. In this case, the radius increases from 1 mm to 1.5 mm. The blue line records the values of L/m calculated from the Yurkov equation.

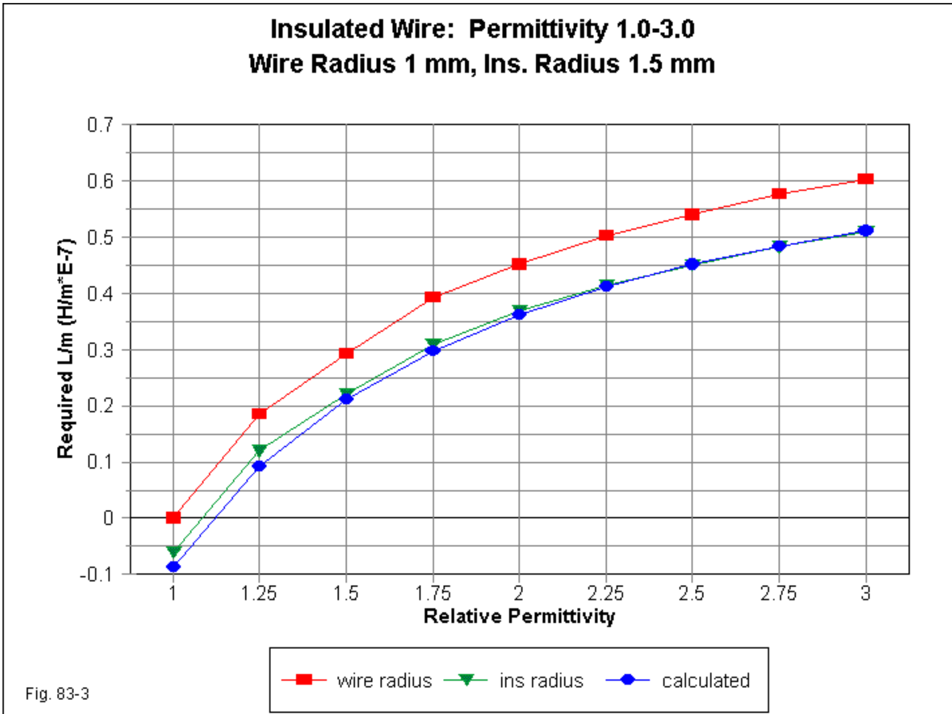

Fig. 83-3

Two trends are equally important in this graph. First, all three curves are closely parallel, indicating the general validity of either procedure in simulating an insulated wire. However, at very low values of permittivity, the enlarged conductor radius of the Yurkov method results in required values of L/m that are less than zero. This situation represents a limit to the application of the Yurkov equation, since a permittivity of 1 should yield the same results as a bare wire (under the condition that the conductivity is so low as to be negligible). However, most applications will never encounter this situation.

The second trend involves the modeled values of L/m and the values of L/m calculated from the Yurkov equation. The two lines are too close together to yield differences in modeling results that could be called significant.

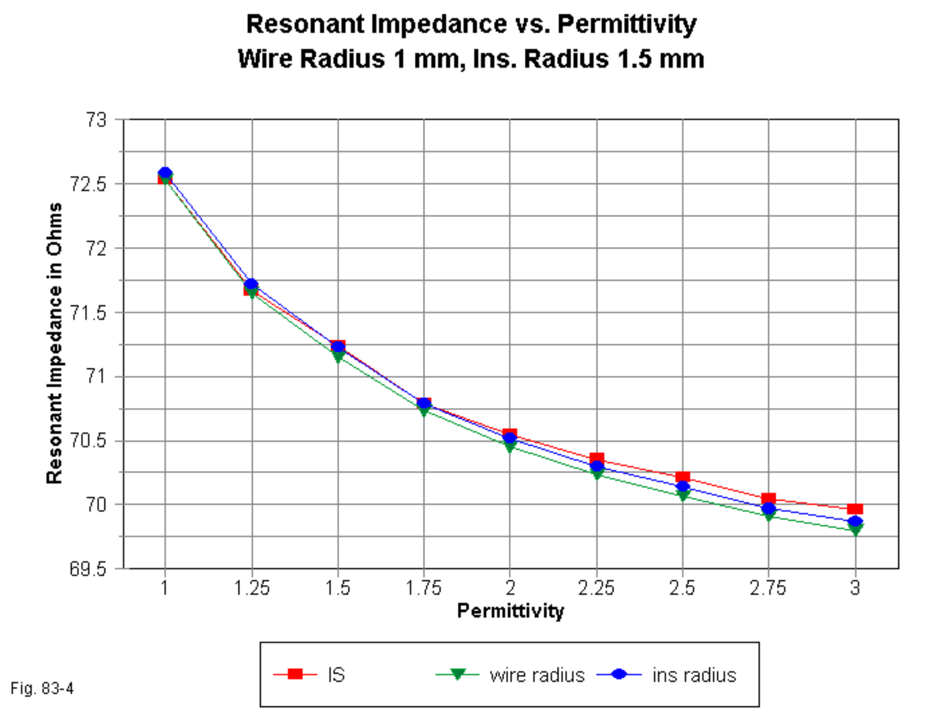

Fig. 83-4

Fig. 83-4 tracks the 30-MHz dipole resonant impedance under three conditions. The red line indicates the resonant impedance using the original NEC-4 model with the IS command. The green line indicates the resonant impedance using the 1-mm radius wire and the associated LD 2 command entries. The blue line provides values of resonant impedance using the increased radius and the required values of L/m in the LD 2 command. The three lines correspond to the upper, middle, and lower models in **Fig. 83-2**.

Perhaps the most telling note that we can make for this graph is this one: at widest divergence, the modeled resonant impedance values vary among all three lines by less than 0.25-Ohm relative to a median value of nearly 70 Ohms.

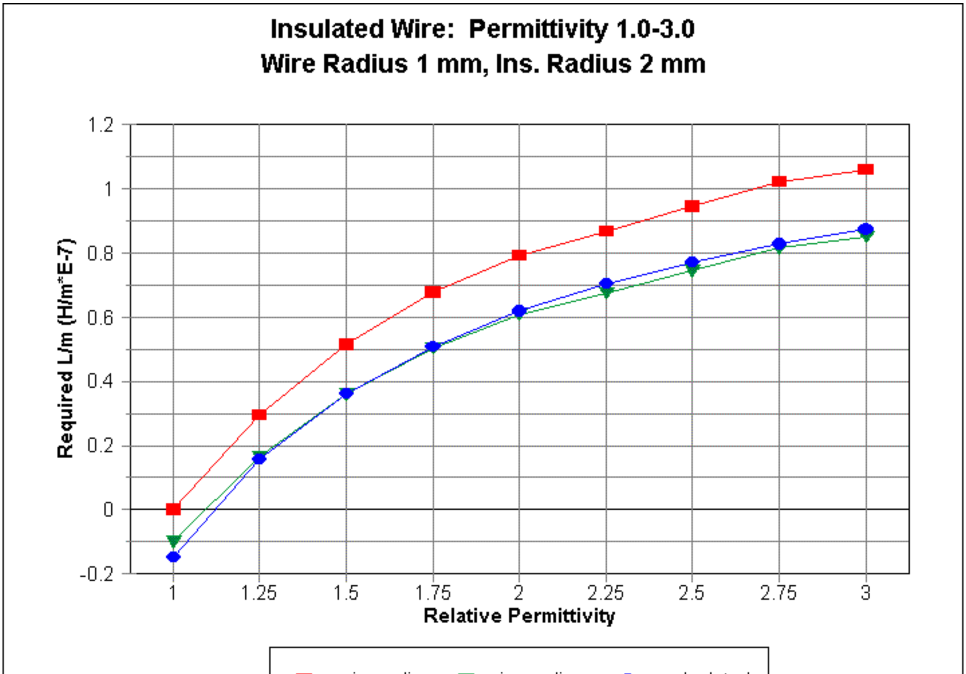

Fig. 83-5

Fig. 83-3 and **Fig. 83-4** tracked the data for the thinnest insulation—0.5 mm. **Fig. 83-5** and **Fig. 83-6** track the data for the next level of insulation thickness: 1.0

mm. **Fig. 83-5** provides information on the values of L/m for the same three situations described for **Fig. 83-3**. Once more, the curve for the 1-mm wire parallels the curves for the 2-mm wire, with the latter pair of curves dipping below an L/m value of zero for the lowest permittivity level. Again, the calculated and modeled values of L/m for the Yurkov case are too close together to represent any significant difference.

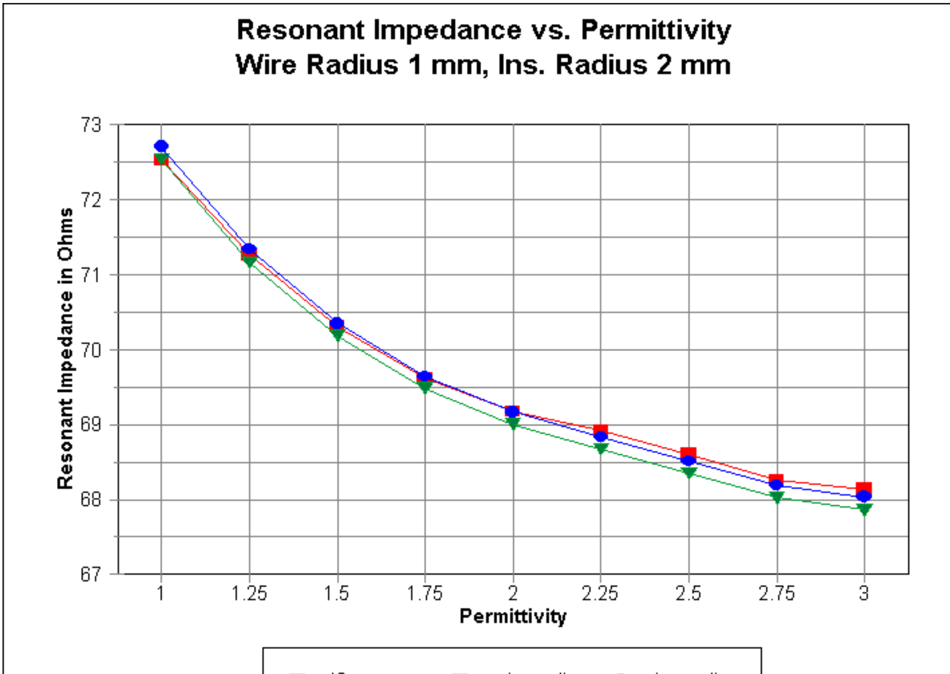

Fig. 83-6

Fig. 83-6 tracks the three defined resonant impedance cases, in parallel to **Fig. 83-4**, but for the middle insulation thickness. Once more, the three lines are within about a quarter-Ohm of each other at their widest divergence. However, there is a systematic variance between the values that emerge from using the IS command and those emerging from use of the LD 2 simulation when using the same wire radius in the GW line. This condition suggests a difference between the two methods for simulating the effects of insulation, but not a difference that should create a level of variance that has practical implications for the average wire antenna builder.

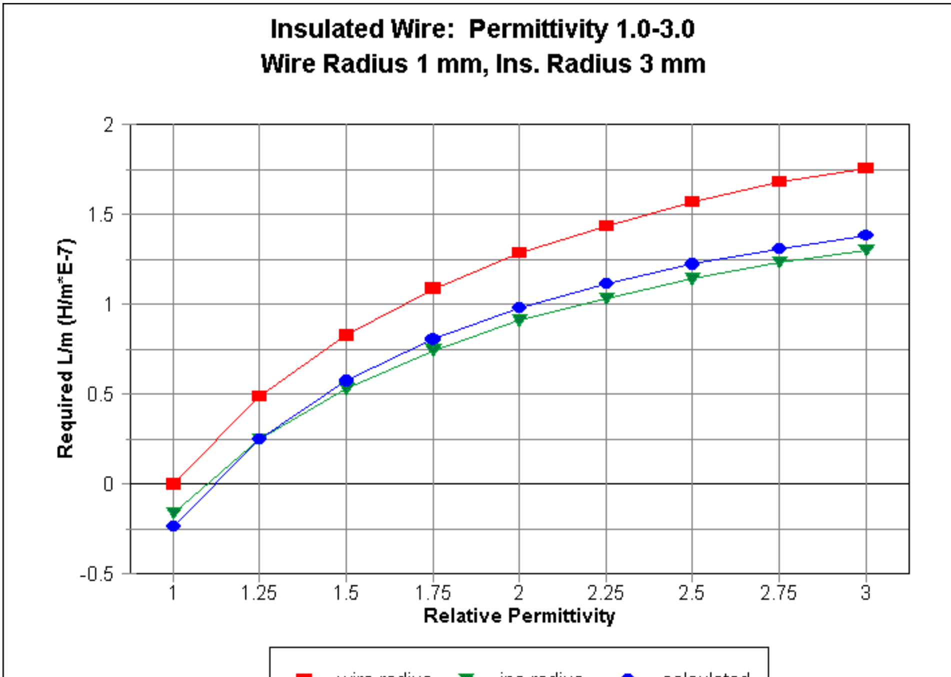

Fig. 83-7

Fig. 83-7 and **Fig. 83-8** track the same two data sets for the thickest insulation: 2 mm. The L/m traces show the same parallel development. However, the values calculated from the Yurkov equation and the values required by the model to restore the 3-mm radius wire to resonance begin to diverge at both ends of the permittivity range covered. The final sets of values for the green and blue lines at a permittivity of 3 differ by about 6%. However, for the 30-MHz dipole, that divergence yields an impedance that is off-resonance by only about 3.5 Ohms of reactance. For practical applications, construction variables would normally mask this difference.

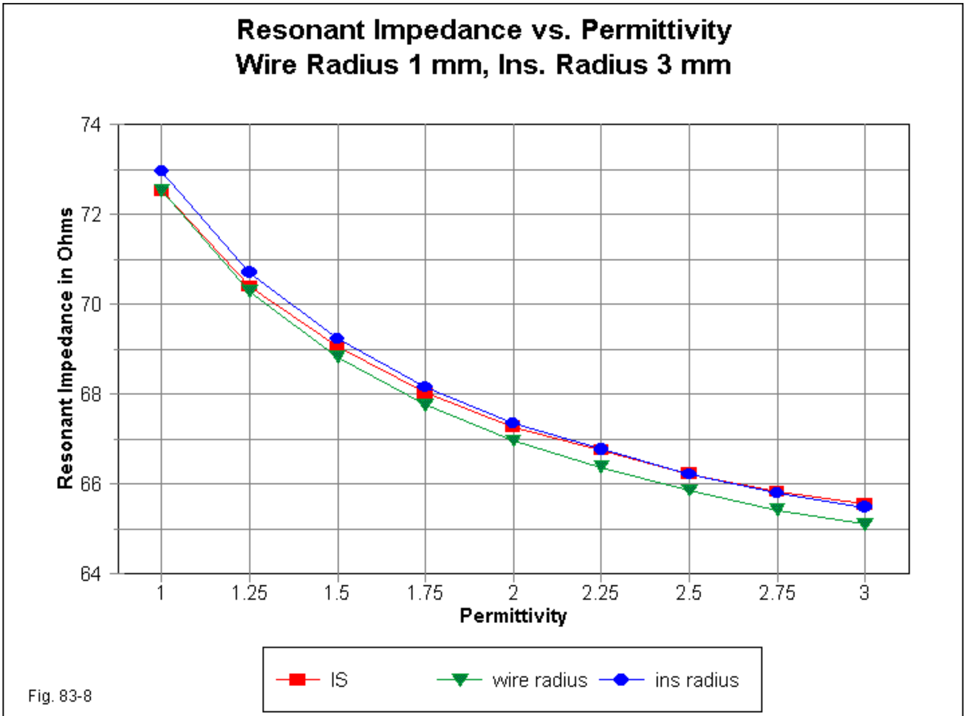

Fig. 83-8

In **Fig. 83-8**, we have the traces for the three resonant impedance situations: the original IS model, the direct substitution of an LD 2 command for the IS command, and the use of the insulation radius as in the Yurkov equation. The latter two cases parallel each other with a maximum separation of about a third of an Ohm. Interestingly, the original IS model shows resonant impedance values that begin by tracking the direct replacement model and end by tracking the Yurkov model.

Conclusion

We began the series of graphs with the question of to what degree we might have confidence in using either equation 1 (or 1A) or equation 2 as NEC-2 substitutes for the IS command that is available in NEC-4. Over the range of tests covered by this exercise, the general answer is that we can have high confidence in the use of the LD 2 simulation for virtually all practical applications. It yields results that are—to a high degree—consistent with those produced by the NEC-4 IS command.

However, we need to enter a caution here. These initial tests cover only a single dipole. They do not cover all frequencies at which we generally use insulated wire for antennas—generally the HF range. Nor do the tests cover closed loops. These notes are not designed to fully validate the method, but only to show some of the procedures that might be used to validate the method for a given modeling situation. As well, these notes do not validate the substitute method against the physical realities of antennas, but only against the NEC-4 results when using the IS facility.

We should also be aware of a second caution. We noted that equation 1 shows about a 6% potential error in the value of L/m at the extremes of its range of application. Equation 1A, of course, shows a much lower level of potential error, a maximum of 2% for the test range. The Yurkov equation shows limitations at the upper end of application to the same degree as equation 1. At the lower end of application—with very low values of permittivity—it also has a limit. Within the range of insulation thicknesses used in this exercise and within the range of permittivities covered, the limitations are no barrier to practical applications. Indeed, practical values of both insulation permittivity and insulation thickness generally fall within the limits of the exercise.

There are, however, specialized applications that fall well outside the limits of the exercise. The general confidence that we can place on these simulation techniques may not carry over to such applications. Since both equations show trends toward divergence from the IS command models at the extremes of the test range, it is probable that further divergence will appear as we move well outside the test range of values. Hence, all such applications would require independent validation of whatever modeling technique is used to simulate insulated wires against the physical realities of antenna construction.

Addendum: Why the Technique Has Limited Application

Jack Louthan of TeriSoft has provided a simple and direct explanation of why the technique illustrated above has limited application. For example, it provides in the form given a reasonable output impedance value for a simple dipole, but the results for a closed loop show a significant divergence between IS-based and workaround-based results. In calculating the E-field for each segment in a model NEC calculates a "cosine" component, a "sine" component, and a "constant" component. NEC then sums the three fields to arrive at a total field value for each segment.

LD commands modify the "constant" component of the E-field calculation, whereas IS commands (in NEC-4) modify the "cosine" component. As a consequence, any workaround formulation will result in satisfying only a limited range of geometries. The workaround shown is applicable only to linear elements—and likely only to applications in which the element is in the vicinity of 1/2 wavelength.

These notes are directed toward users of existing NEC-2 codes. NEC-2 exists under numerous modifications, since it is readily available in the public domain. NEC-4 remains proprietary. Some software writers have adapted the NEC-4 IS command input to the NEC-2 framework and thus provide direct insulated wire or sheath inputs. Wherever the IS input is available, you should use it, since the results will be considerably more accurate for more antenna geometries than any workaround.

The concept of a workaround within NEC itself covers a broad territory, since it is not so much a fundamental idea within the program as a set of techniques brought to the program by modelers. At the trivial end of the scale, we may use the term in connection with complex straight-wire only structures that we create when some of the more complex commands within NEC are not available to us. Hence, we may create circles from 20 wires instead of using a single GA command. We might use equations to develop an "all-GW" helix rather than using the GH command. Programs such as NEC-Win Synth and EZNEC use this method extensively, with Synth being able to create structures for which there are no single NEC commands.

We also apply to terms to cases in which we overcome a limitation within the core by judicious modeling. For example, we can overcome MININEC's difficulty with angular junctions by increasing the number of segments per unit of physical length. We can center a source along a straight wire with an even number of segments within NEC by using split sources on adjacent segments. Many of these workarounds appear within the notes in this series.

At the most extreme end of the scale, we can partially replicate reality by judicious experimentation with the available commands. This episode has shown one such case. Another case is the use of the insulated sheath to simulate twinlead transmission lines. Since we cannot accurately replicate the flat insulation directly between wires, we often simply alter the insulation on the transmission-line wires until it exhibits the correct velocity factor. The interactions between the fields of the two wires may not be exactly the same for real twinlead and the simulation, but the accuracy is often satisfactory for most analytical purposes.

Workarounds are a valuable collection of tools in the modeler's kit. However, like all useful tools, we must use them with care and keep them sharply calibrated if we are to rely on the results of using them.

84. GA: Creating and Moving Arcs

In episode 69 of this series, I showed a way to create approximations of circles that used up to 16 sides via the equations facility of NEC-Win Plus. In that exercise, I was not only showing some easy techniques of polygon formation, but as well comparing the quality of circle approximations. The basic equations-page facet of the model appears in **Fig. 84-1**. Note that I have translated the dimensions from the original ones in inches for 146 MHz into meters for 300 MHz.

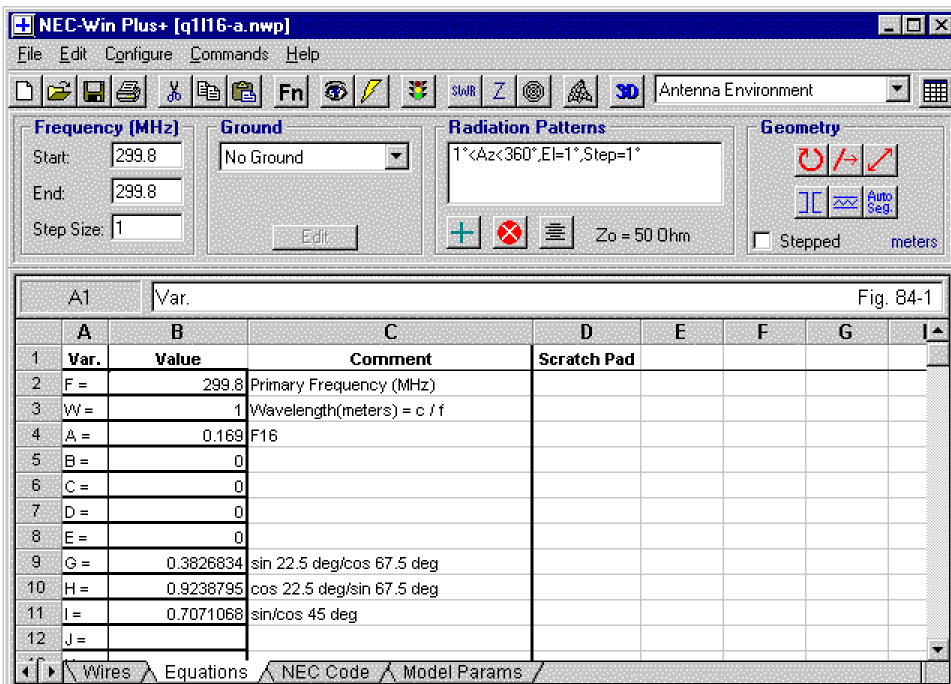

Although the Equations page appears simple enough, the model itself requires 16 wire and 48 segments, at 3 segments per wire. A standard ASCII NEC input file for the formulation appears in **Fig. 84-2**. See models 84-1 (.NWP only) and 84-2 (.NEC only).

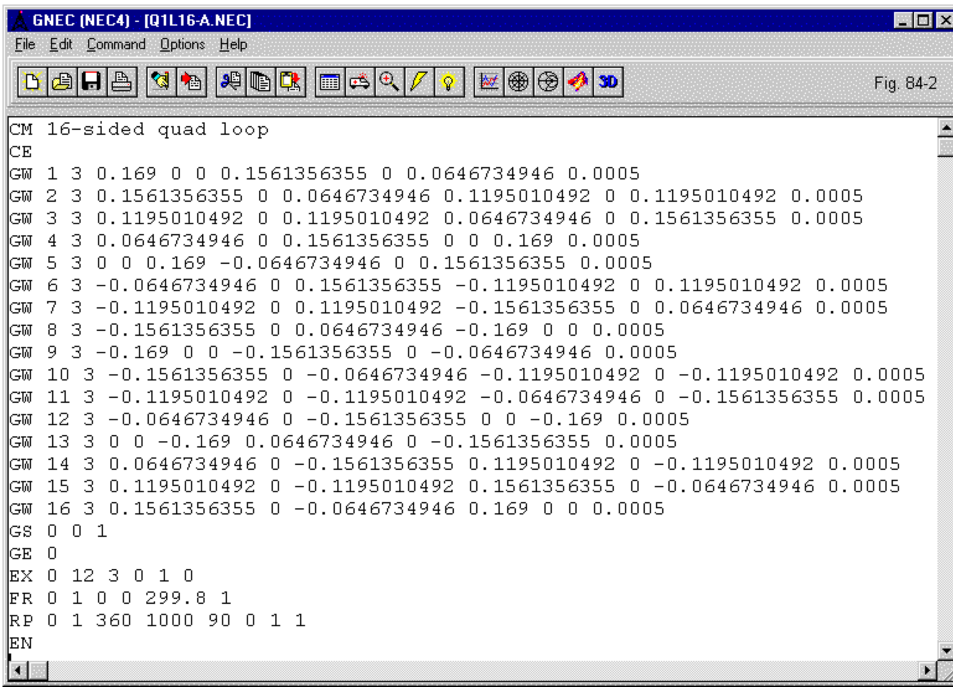


```
CM 16-sided quad loop
CE
GW 1 3 0.169 0 0 0.1561356355 0 0.0646734946 0.0005
GW 2 3 0.1561356355 0 0.0646734946 0.1195010492 0 0.1195010492 0.0005
GW 3 3 0.1195010492 0 0.1195010492 0.0646734946 0 0.1561356355 0.0005
GW 4 3 0.0646734946 0 0.1561356355 0 0 0.169 0.0005
GW 5 3 0 0 0.169 -0.0646734946 0 0.1561356355 0.0005
GW 6 3 -0.0646734946 0 0.1561356355 -0.1195010492 0 0.1195010492 0.0005
GW 7 3 -0.1195010492 0 0.1195010492 -0.1561356355 0 0.0646734946 0.0005
GW 8 3 -0.1561356355 0 0.0646734946 -0.169 0 0 0.0005
GW 9 3 -0.169 0 0 -0.1561356355 0 -0.0646734946 0.0005
GW 10 3 -0.1561356355 0 -0.0646734946 -0.1195010492 0 -0.1195010492 0.0005
GW 11 3 -0.1195010492 0 -0.1195010492 -0.0646734946 0 -0.1561356355 0.0005
GW 12 3 -0.0646734946 0 -0.1561356355 0 0 -0.169 0.0005
GW 13 3 0 0 -0.169 0.0646734946 0 -0.1561356355 0.0005
GW 14 3 0.0646734946 0 -0.1561356355 0.1195010492 0 -0.1195010492 0.0005
GW 15 3 0.1195010492 0 -0.1195010492 0.1561356355 0 -0.0646734946 0.0005
GW 16 3 0.1561356355 0 -0.0646734946 0.169 0 0 0.0005
GS 0 0 1
GE 0
EX 0 12 3 0 1 0
FR 0 1 0 0 299.8 1
RP 0 1 360 1000 90 0 1 1
EN
```

You may wish to review column #69 for further details of the technique, especially if you do not have access to a version of NEC-2 having the complete command set. In this column, I want to review one of those seemingly more esoteric commands. As a sample, examine **Fig. 84-3**, which contrasts the 16-sided simulation of a circle with one having 90 sides with 1 segment per side. Obviously, the right-hand view of the antenna is much closer to a "perfect" circle–perhaps even more perfect than anything we might build. The question for this column is how we can build the circle.

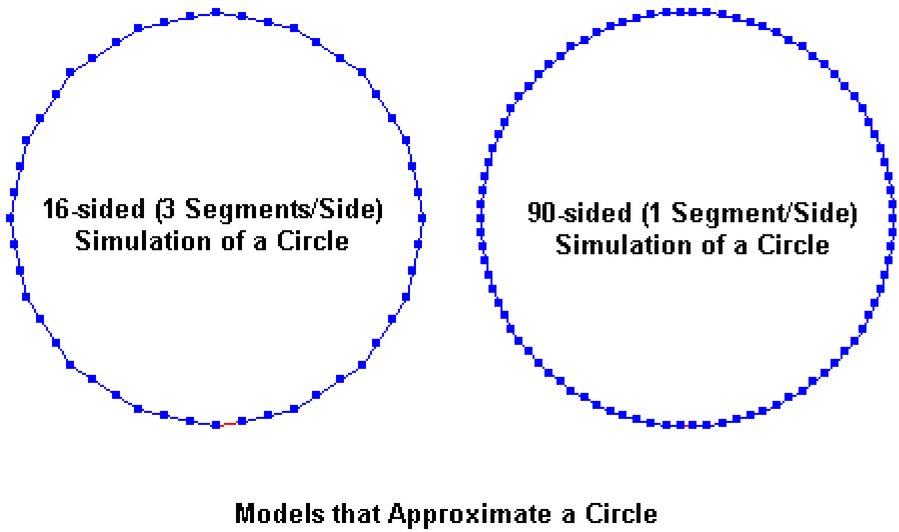

Fig. 84-3

The requisite command is GA, Wire Arc Specification. The line is the same in both NEC-2 and NEC-4 and has the following appearance:

```
GA      1      5      10      50      75      .001
        I1     I2     F1      F2      F3      F4
        ITG    NS     RADA    ANG1    ANG2    RAD
```

The line begins (after the identification of the command) with the tag (or wire) number, followed by the number of segments: the two occupy the two integer places. All of the segments will have the same tag number, although constructing the arc with just the GW facility would give each segment a new wire or tag number, since each segment will have a different angle as well as coordinate set.

RADA specifies the radius of the arc relative to a perfect circle with its center at 0, 0, 0 on the coordinate system. The radius axis is relative to the Y-axis and hence will take a positive X value. The arc extends from ANG1 through ANG2 as measured relative to the X-axis in the +/-Z direction around the Y-axis. Both ANG1 and ANG2 are in degrees. The angles move clockwise relative to the X-axis. RAD is the radius of the wire.

Therefore, the sample line specifies Tag 1 with 5 segments. The arc radius is ten (units of measure). The arc extends between 50° and 75° “vertically,” that is, from 50° from the X-axis to 75° relative to the X-axis. You may, if you wish in a free-space model, begin with a negative angle.

Since we are not limited in segment length, except by the rules governing segment-length-to-wire-radius ratios, we can in principle create very close approximations of smooth arcs simply by increasing the number of segments in the GA command. The GA command gives us the ability to fabricate some interesting structures, so let’s take a few steps in that direction.

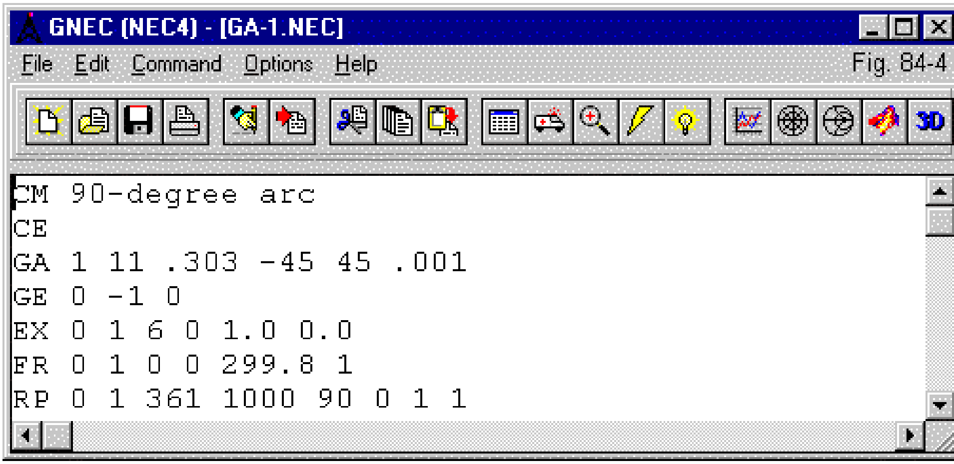

First, we shall create a simple 90° arc using the specifications shown in the GA line in **Fig. 84-4**. Here we create a simple arc with 11 segments. Note that the arc extends from -45° to +45°. The radius of 0.303 meters is not accidental. It yields a nearly resonant dipole when fed at segment 6 at the frequency specified in the FR line. In the E-plane, the gain is just under 2 dB, with a feedpoint impedance of about 65 Ω. These values will be sensible to anyone who has modeled an inverted-Vee wire antenna, which brings its ends toward each other, but with straight-line legs. See model 84-3.

The individual segments within Tag 1 are more interesting than the straight-line segments of an inverted-Vee, as evidenced by the extract from the NEC output report.

```
- - - - SEGMENTATION DATA - - - -

COORDINATES IN METERS

I+ AND I- INDICATE THE SEGMENTS BEFORE AND AFTER I
```

SEG. NO.	COORDINATES OF SEG. CENTER X	Y	Z	SEG. LENGTH	ORIENTATION ANGLES ALPHA	BETA	WIRE RADIUS	CONNECTION DATA I-	I	I+	TAG NO.
1	0.22841	0.00000	-0.19792	0.04323	49.09091	0.00000	0.00100	0	1	2	1
2	0.25425	0.00000	-0.16340	0.04323	57.27273	0.00000	0.00100	1	2	3	1
3	0.27492	0.00000	-0.12555	0.04323	65.45455	0.00000	0.00100	2	3	4	1
4	0.28999	0.00000	-0.08515	0.04323	73.63636	0.00000	0.00100	3	4	5	1
5	0.29915	0.00000	-0.04301	0.04323	81.81818	0.00000	0.00100	4	5	6	1
6	0.30223	0.00000	0.00000	0.04323	90.00000	0.00000	0.00100	5	6	7	1
7	0.29915	0.00000	0.04301	0.04323	81.81818	180.00000	0.00100	6	7	8	1
8	0.28999	0.00000	0.08515	0.04323	73.63636	180.00000	0.00100	7	8	9	1
9	0.27492	0.00000	0.12555	0.04323	65.45455	180.00000	0.00100	8	9	10	1
10	0.25425	0.00000	0.16340	0.04323	57.27273	180.00000	0.00100	9	10	11	1
11	0.22841	0.00000	0.19792	0.04323	49.09091	180.00000	0.00100	10	11	0	1

Note that the X-coordinate for the center of the 6th segment is 0.30223, although we specified a radius of 0.303. The deficit is due to the fact the segment 6 is a straight wire that cuts off very slightly the curve of a true arc. As the Seg. Length column shows, the command calculates the arc so that all segments have the same length.

The orientation of the arc is not especially useful. However, we may move it anywhere we wish via the GM command. Suppose that we wish to point the open side of the arc straight up and bring the bottom of the arc to a ground or Z=0 level. We can use the GM command shown in **Fig. 84-5** and in model 84-4.

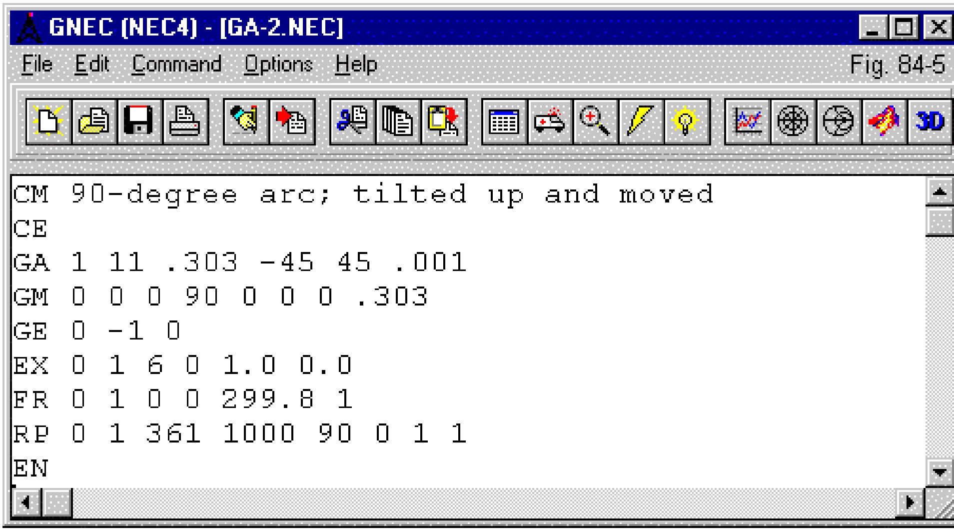
GNEC (NEC4) - [GA-2.NEC]
File Edit Command Options Help
Fig. 84-5
CM 90-degree arc; tilted up and moved
CE
GA 1 11 .303 -45 45 .001
GM 0 0 0 90 0 0 0 .303
GE 0 -1 0
EX 0 1 6 0 1.0 0.0
FR 0 1 0 0 299.8 1
RP 0 1 361 1000 90 0 1 1
EN

```
                    - - - - SEGMENTATION DATA - - - -

                          COORDINATES IN METERS

              I+ AND I- INDICATE THE SEGMENTS BEFORE AND AFTER I

 SEG.   COORDINATES OF SEG. CENTER     SEG.     ORIENTATION ANGLES    WIRE    CONNECTION DATA   TAG
 NO.      X         Y         Z       LENGTH     ALPHA      BETA     RADIUS    I-    I    I+    NO.
   1  -0.19792   0.00000   0.07459   0.04323  -40.90909   0.00000   0.00100    0    1    2     1
   2  -0.16340   0.00000   0.04875   0.04323  -32.72727   0.00000   0.00100    1    2    3     1
   3  -0.12555   0.00000   0.02808   0.04323  -24.54545   0.00000   0.00100    2    3    4     1
   4  -0.08515   0.00000   0.01301   0.04323  -16.36364   0.00000   0.00100    3    4    5     1
   5  -0.04301   0.00000   0.00385   0.04323   -8.18182   0.00000   0.00100    4    5    6     1
   6   0.00000   0.00000   0.00077   0.04323    0.00000   0.00000   0.00100    5    6    7     1
   7   0.04301   0.00000   0.00385   0.04323    8.18182   0.00000   0.00100    6    7    8     1
   8   0.08515   0.00000   0.01301   0.04323   16.36364   0.00000   0.00100    7    8    9     1
   9   0.12555   0.00000   0.02808   0.04323   24.54545   0.00000   0.00100    8    9   10     1
  10   0.16340   0.00000   0.04875   0.04323   32.72727   0.00000   0.00100    9   10   11     1
  11   0.19792   0.00000   0.07459   0.04323   40.90909   0.00000   0.00100   10   11    0     1
```

The GM line specifies that we rotate the arc 90° around the Y-axis so that the wire ends are upward. That rotation will bring the bottom of the arc below Z=0, so we may raise it on the Z-axis by the radius of the arc. The resulting segmentation table appears in the model output report.

We can see from the table that the ends of the arc are stretched symmetrically across the Y-axis from -X to +X. Segment lengths remain unchanged by the translation and rotation exercise. However, note the Z-value for Segment 6. Instead of being zero, it is 0.00077. A true arc would rest at Z=0. However, because segment 6 is a straight line, it remain shy of zero by the same amount that the identical position in the first model remained shy of the specified arc radius. For both models, note that the alpha orientation angle increases by 8.18182° with each segment. **Fig. 84-6** provides NEC-Vu representations of the two arcs. Note that in the right-hand case, the axes are conventionalized to the center of the sketch and do not show the fact that the entire arc is above Z=0.

Fig. 84-6

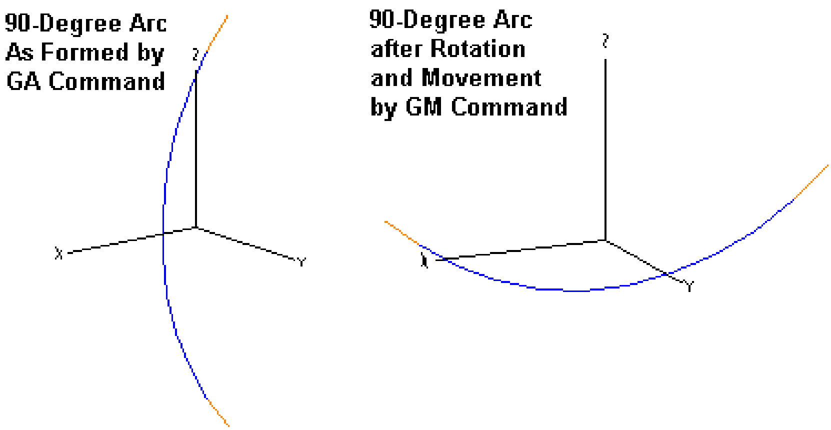

Creating and Positioning an Arc via GA and GM Commands

So far, we have been exercising the GA and GM commands only far enough to orient us to their use to create and position a desired arc. We have not yet built anything interesting. Let's build something. See model 84-5.

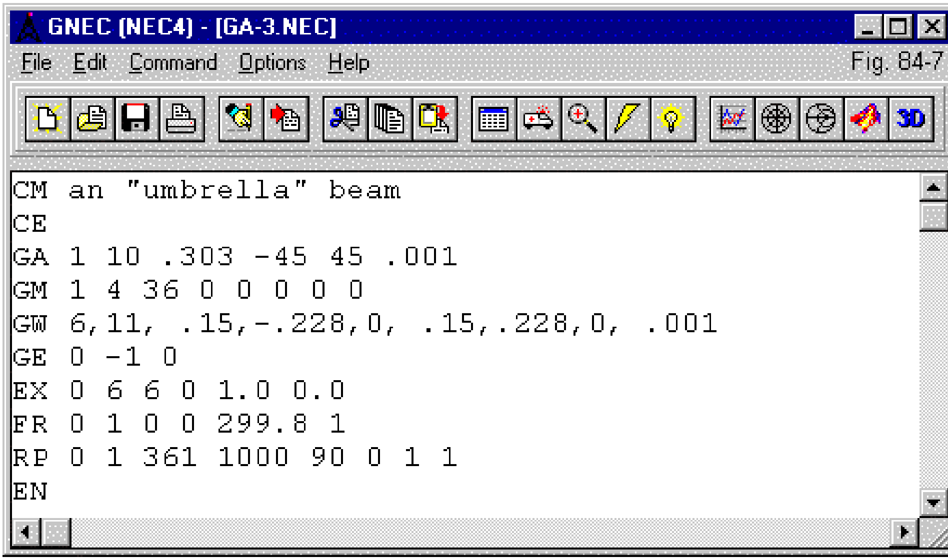


```
CM an "umbrella" beam
CE
GA 1 10 .303 -45 45 .001
GM 1 4 36 0 0 0 0 0
GW 6,11, .15,-.228,0, .15,.228,0, .001
GE 0 -1 0
EX 0 6 6 0 1.0 0.0
FR 0 1 0 0 299.8 1
RP 0 1 361 1000 90 0 1 1
EN
```

Fig. 84-7 shows the model of an "umbrella" reflector with a dipole driver. We recognize the GA line. The only difference between this line and our first model is that the number of segments is 10. The reduction is to place a segment junction at the center of the arc. The significant line is the GM command. It specifies that we shall increment the tag numbers by 1 and create 4 new structures identical to the entirety of the first. The third entry in the line specifies a rotation angle of 36° for each new structure around the X-axis. By this means, we can create 5 full arcs or a 10-spoke "umbrella." Since we gave each arc 10 segments, each arc will join at the junction of segments 5 and 6. **Fig. 84-8** shows the results of our modeling.

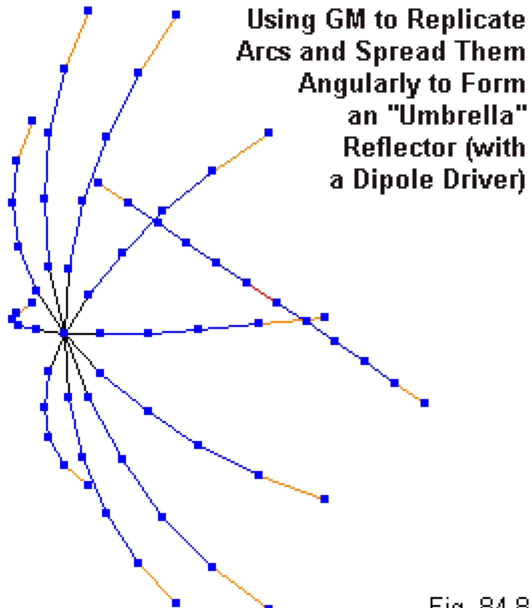

Fig. 84-8

For this model, the umbrella ribs represent a reflector. Hence, the GW line with the tag number of 6 sets a near-resonant dipole ahead of the umbrella. For this exercise, I have not optimized the position of the driver relative to the reflector. Nor have I experimented with optimizing the arc size for maximum performance from the array.

Nevertheless, even this rough and ready construct exhibits a reasonable 2-element parasitic beam pattern, as revealed by **Fig. 84-9**. The free-space gain is 5.1 dBi, with a 9.9-dB front-to-back ratio. The feedpoint impedance is 61 Ω resistive, since the spacing between the reflector and the driver center is about 0.75-λ.

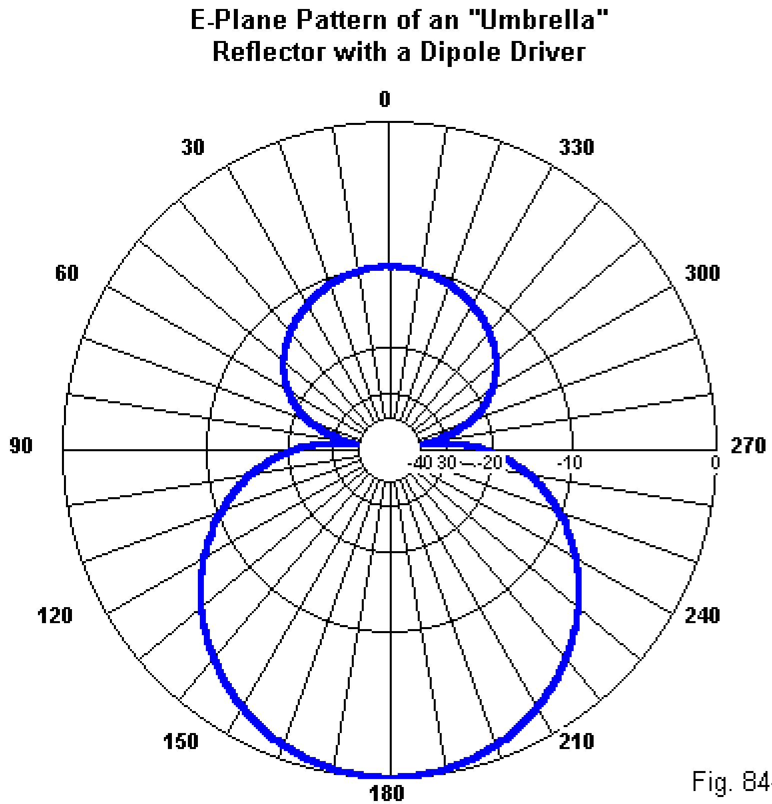

Fig. 84-9

Note that we have achieved this performance even though the reflector is circular rather than parabolic and is even smaller across than the dipole driver. The possibilities for experimenting with other radii of reflector arcs as well as different distances between the reflector and driver centers are nearly endless. Included in these experiments would be the reduction in the number of ribs or arcs, since only the two arcs most closely aligned with the driver carry significant current.

It is now time to use GA to create a complete circle, as promised at the beginning of this exercise. To make a complete circle with 90 segments, we need only modify our very first model, as shown in **Fig. 84-10** and in model 84-6.

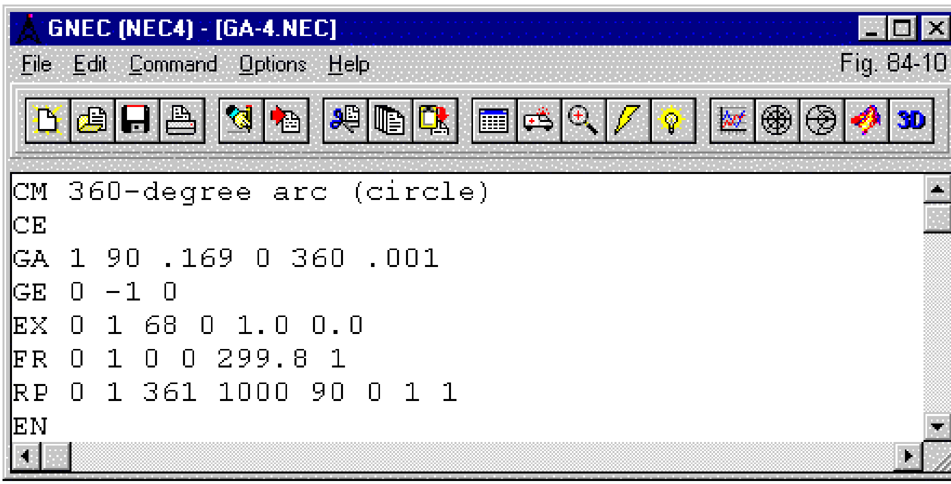

In this GA line, we specify a full 360° arc, that is, a circle. For simplicity, I specified ANG1 as 0 and ANG2 as 360. The arc has the 90 segments shown back in **Fig. 84-3**, with a source on the bottom-most segment (Segment 68, as noted in the EX line of the model). Let's run this model and compare the results with those that we obtained from the 16-sided approximation of a circular quad element.

Comparison of a 16-Sided and a 90-Sided Approximation of a Resonant Circular Loop

Model	Free-Space Gain dBi	Feedpoint Impedance R +/- jX Ohms
16 sides	3.63	140.2 + j 0.0
90 sides	3.68	142.3 - j 0.7

Given that a square loop shows a gain of about 3.39 dBi with a resonant feedpoint impedance of about 125 Ω, we see that the closer approximation of a true circle continues the upward progression of values. However, the values differ by less than 1.5%, making the 16-sided approximation a fair representation of a circle. On the other hand, given the simplicity of the circular loop using the GA command, the original method of creating the 16-sided figure now seems cumbersome.

Single quad loops have applications, but multi-element quad beams are more common, at least for amateur-band operations. Let's take one final construction step and compare a pair of typical 2-element quad beam models.

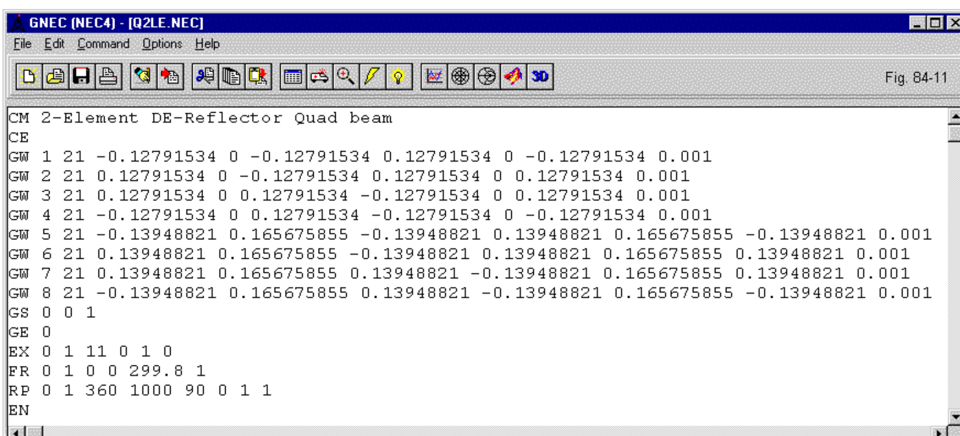


```
CM 2-Element DE-Reflector Quad beam
CE
GW 1 21 -0.12791534 0 -0.12791534 0.12791534 0 -0.12791534 0.001
GW 2 21 0.12791534 0 -0.12791534 0.12791534 0 0.12791534 0.001
GW 3 21 0.12791534 0 0.12791534 -0.12791534 0 0.12791534 0.001
GW 4 21 -0.12791534 0 0.12791534 -0.12791534 0 -0.12791534 0.001
GW 5 21 -0.13948821 0.165675855 -0.13948821 0.13948821 0.165675855 -0.13948821 0.001
GW 6 21 0.13948821 0.165675855 -0.13948821 0.13948821 0.165675855 0.13948821 0.001
GW 7 21 0.13948821 0.165675855 0.13948821 -0.13948821 0.165675855 0.13948821 0.001
GW 8 21 -0.13948821 0.165675855 0.13948821 -0.13948821 0.165675855 -0.13948821 0.001
GS 0 0 1
GE 0
EX 0 1 11 0 1 0
FR 0 1 0 0 299.8 1
RP 0 1 360 1000 90 0 1 1
EN
```

Fig. 84-11 shows a NEC model of an optimized 2-element square quad beam for 299.8 MHz in free space with no element loading. The square quad beam model requires 8 wires (with 21 segments each in this model). For ease of modification, the model driver element is centered at X=0, Y=0, and Z=0, with the reflector spaced along the Y-axis. Modifying this array requires that we change at least 8 values to change the length or circumference for each element. See model 84-7. Alternatively, one might develop a set of equations and use variables for the element corner positions and for the reflector position relative to the driver. However, the modeling software must have a model by equation facility to do this. In fact, this model was derived from a more complex set of equations for which the user need enter only the design frequency and the element diameter. However, those equations do not cross over into the .NEC format input file. So the user must employ (at the time of writing) 2 programs–one with equation and variable facilities and one able to work in NEC-4 in this case.

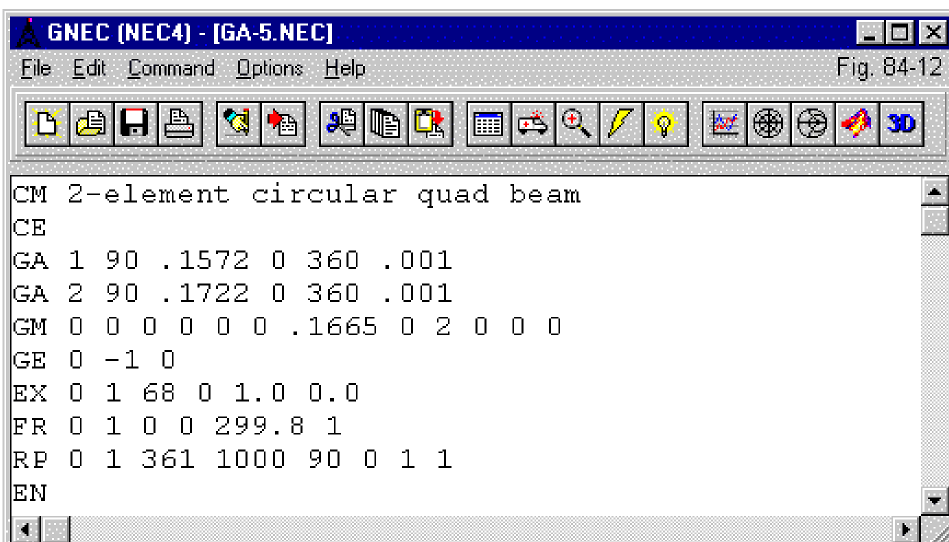

In **Fig. 84-12**, we have a circular quad that uses the GA command to create the two requisite circles of wires. The driver line is simply a revision of our earlier single element circular loop. The reflector line begins with a circular loop created by the GA command and then uses the GM command to move the loop (Tag 2) the proper distance from the driver. Each loop has 90 segments. See model 84-8.

Fig. 84-13 compares the two structures. The square quad beam has 168 segments using 8 wires or tags. The circular quad beam has 180 segments in two tags. However, as the models indicate, the circular structure has only 3 values that might require modification after the initial formation of the model. To change the driver circumference–and the length of every wire segment within it–we need change only the value of the driver (Tag 1) radius. A similar operation on Tag 2 changes the reflector size. We can change the element spacing simply by altering the GM card Y-axis translation value. In effect, we may easily optimize the design of circular quad beams because the variables are built into the GA and GM commands.

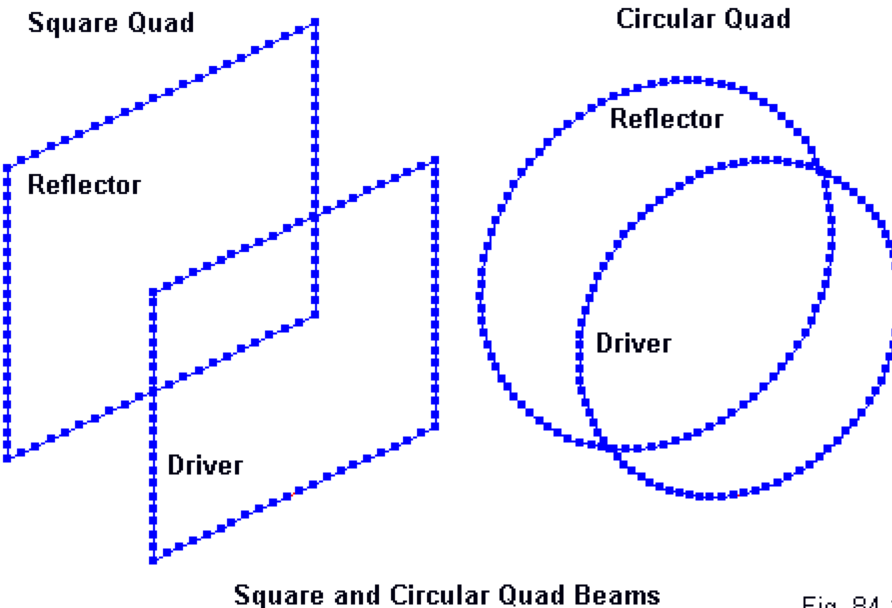

Fig. 84-13

In episode 69, I suggested that the slight (0.3-dB) gain advantage of a circular loop over a square loop would be a 1-time matter. We should not expect to see the gain advantage increase arithmetically with every parasitic loop that we might add to a more elaborate quad. The following table tends to confirm the suggestion, since it presents the result of hand optimizing the circular quad beam for driver resonance and for maximum front-to-back ratio (in excess of 40 dB) at the design frequency.

Comparison of 299.8-MHz 2-Element Square and Circular Quad Beams in Free-Space

Quad	Driver Cir. meters	Reflector Cir. meters	Space meters	Gain dBi	Front-Back Ratio dB	Feedpoint Impedance R +/- j X Ohms
Square	1.0233	1.1159	0.1657	7.17	46.25	142.2 - j 1.3
Circular	0.9877	1.0820	0.1665	7.37	42.17	160.2 - j 0.4

Immediately apparent is the fact that the circumference of the circular elements is smaller than the circumference of the square elements for equivalent performance properties. If you examine the current distribution on the square elements, you may discover part of the reason. At the square quad loop corners, we find a higher current level than would be found on a pair of 1/2-λ linear elements at equivalent positions. In contrast, the current distribution takes on a smoother curve with the circular loops. In addition to using elements with smaller circumference values, the circular loop requires slightly wider spacing than its square counterpart. Both models use a 0.001-m wire radius.

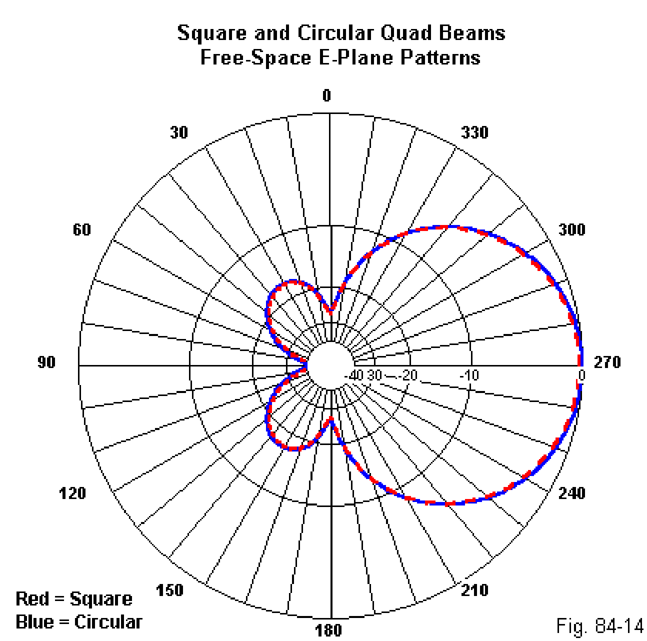

Fig. 84-14

As was the case with the single loops, the circular array has a higher resonant feedpoint impedance than the square quad beam, about 13% higher. The 180° front-to-back ratios are comparable. The circular quad beam has a gain advantage of only 0.2 dB over its square comparator. **Fig. 84-14**–the free-space E-plane patterns for both arrays–suggests that the difference is operationally insignificant.

The performance of a parasitic array is a complex interaction of element diameter, size (circumference), and spacing. Hence, one might be able to tweak the values for slightly better performance out of either quad. However, such improvements would not likely translate into actual performance from a physical version of the antenna, since construction variables would tend to be larger than the percentage of change made to any of the variables in the design. The bottom line is that the shape we choose for a quad beam is more a function of mechanical demands at any given frequency than it is of the electrical superiority of one shape over another.

However, deciding quad array matters is secondary in this exercise. Our basic premise was that the GA command–especially when combined with the GM command–gives us the ability to construct interesting and potentially useful structures. It does so in a manner that allows easy user control over design modifications, which is always a desirable feature of a model. The umbrella reflector and the 2-element circular quad beam are but two samples that help demonstrate the ease of construction and modification.

In the course of this series, we have had occasion to cover many of the geometry commands that are not normally available on entry-level software. However, several still remain as potential subjects for future columns.

85. Electrical Fields at a Power Level and Distance

There are occasions on which the modeler needs to know the strength of a radiated electrical field using a specific power level and a specific distance from the antenna. If the antenna structure is centered at the coordinate system origin, that is, where X, Y, and Z equal zero, we can develop this information within NEC in a straightforward manner. However, the task requires more than one step.

The following exercises will develop those steps in two ways, paying special attention to the RP (pattern request) and the EX (excitation) commands.

Consider the following simplified model of a 1/4-λ monopole with 4 buried short radials.

```
CM 1/4-wl gp 4r
CE
GW 1,30,0.,0.,10.135,0.,0.,0.,.0254
GW 2,1,0.,0.,0.,0.,0.,-.1524,.0254
GW 3,10,0.,0.,-.1524,3.292,0.,-.1524,.003175
GW 4,10,0.,0.,-.1524,0.,3.292,-.1524,.003175
GW 5,10,0.,0.,-.1524,-3.292,0.,-.1524,.003175
GW 6,10,0.,0.,-.1524,0.,-3.292,-.1524,.003175
GE -1
FR 0,1,0,0,7.05
GN 2,0,0,0,13.,.005
EX 0,1,30,0,1.414214,0.
RP 0,181,1,1000,90.,0.,-1.,0.,0.
EN
```

The dimensions are the metric equivalents of a 2" diameter main element and of 0.25" diameter radials. **Fig. 85-1** shows the outline of the antenna from two perspectives.

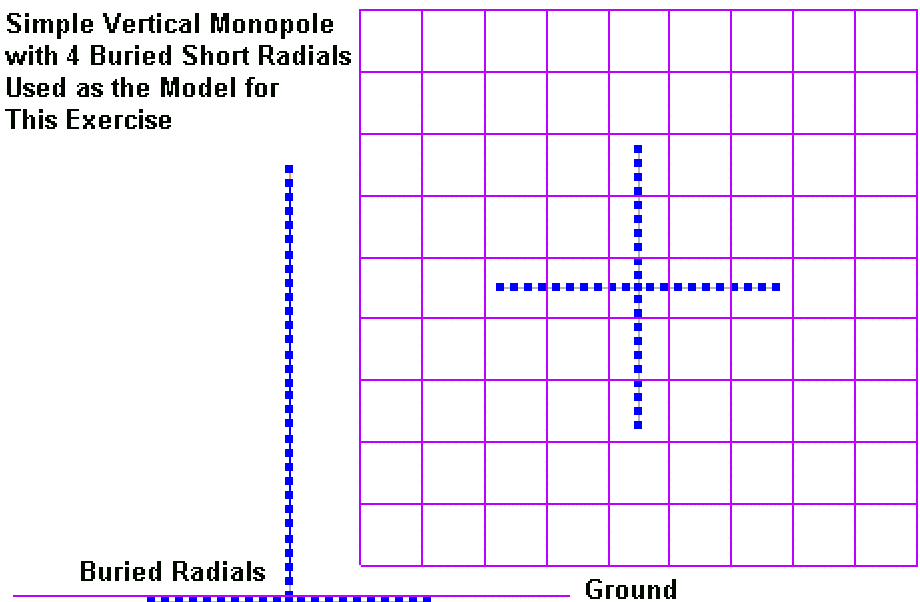

Fig. 85-1

If we run this model over average ground, the gain is -2.29 dBi at a TO angle of 27° elevation (63° theta). The feedpoint impedance is about 59.4 + j0.4 Ω. This is the typical data collection that many modelers are satisfied to collect, and for many types of modeling tasks, this information is sufficient to characterize the antenna.

Fig. 85-2 shows the theta (elevation) pattern that would normally accompany this omni-directional antenna. I shall omit the circular phi (azimuth) pattern that we might take at the TO angle.

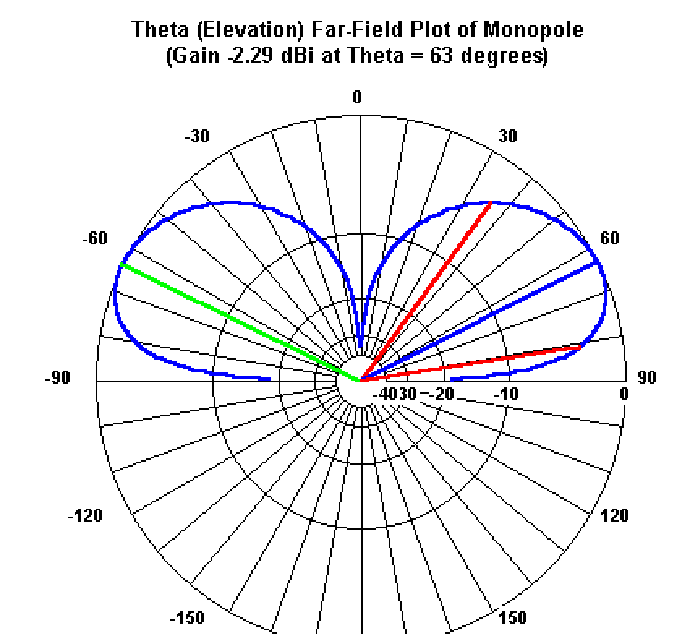

Fig. 85-2

However, many modelers are interested in the electrical fields from a given antenna. We may examine a portion of the data for the present model. The complete data set available from the NEC output report would be far too long to reproduce in these pages.

The 90° theta angle (0° elevation), of course, is not usable for anything, since results at the horizon are not usable. However, the other angles illustrate the sort of values that one will encounter in a typical scan of the e-fields when calling a standard far-field pattern. See model 85-1.

```
**** Electric Field: Phi Pattern ****
Z=2, Freq=7.05, File=vr4-rpl.NOU

              ---E (Theta)---       --- E (Phi) ---
  Phi       Magnitude     Phase    Magnitude     Phase
Degrees      Volts/m     Degrees    Volts/m     Degrees
   0.00   1.9180E-004    -19.95   1.6350E-022    119.22
   1.00   1.9180E-004    -19.95   5.1436E-012    134.30
   2.00   1.9180E-004    -19.95   1.0262E-011    134.30
   3.00   1.9180E-004    -19.95   1.5331E-011    134.30
   4.00   1.9180E-004    -19.95   2.0325E-011    134.30
   5.00   1.9180E-004    -19.95   2.5219E-011    134.30
   6.00   1.9180E-004    -19.95   2.9991E-011    134.30
   7.00   1.9180E-004    -19.95   3.4617E-011    134.30
   8.00   1.9180E-004    -19.95   3.9074E-011    134.30
   9.00   1.9180E-004    -19.95   4.3341E-011    134.30
  10.00   1.9180E-004    -19.95   4.7397E-011    134.30
```

In most instances, the values are useful only for comparative purposes. They do not provide any useful information directly about the e-field values at a given distance and a given theta (elevation) angle or height above ground.

One way to overcome this problem is to make an RP 1 ground-wave request. In this type of request, one sets a distance from the coordinate system origin using the (F5) position. Instead of specifying an initial theta angle in (F1), the user specifies a height above ground (Z) in meters. One may select for (F3) an increment for multiple readings. The number of theta values in (I2) will now become the number of heights for observation of the e-field, beginning at the value in (F1) at intervals determined by (F3). However, all values will lie along a cylinder extending from the surface upward at the distance set into (F5).

The following lines show a typical simple model using RP 1 at a distance of 1000 meters and a single height of 2 meters. See model 85-2.

```
CM 1/4-wl gp 4r
CE
GW 1,30,0.,0.,10.135,0.,0.,0.,.0254
GW 2,1,0.,0.,0.,0.,0.,-.1524,.0254
GW 3,10,0.,0.,-.1524,3.292,0.,-.1524,.003175
GW 4,10,0.,0.,-.1524,0.,3.292,-.1524,.003175
GW 5,10,0.,0.,-.1524,-3.292,0.,-.1524,.003175
GW 6,10,0.,0.,-.1524,0.,-3.292,-.1524,.003175
GE -1
FR 0,1,0,0,7.05
GN 2,0,0,0,13.,.005
EX 0,1,30,0,1.414214,0.
RP 1 1 361 1000 2 0 1.00000 1.00000 1000
EN
```

Note that only the RP line has changed relative to the initial model that made a far field request. However, we obtain what is essentially a limited data phi (azimuth) pattern output for the specified distance and height.

```
**** Electric Field: Phi Pattern ****
Z=2, Freq=7.05, File=vr4-rpl.NOU

             ---E (Theta)---      --- E (Phi) ---
  Phi       Magnitude      Phase     Magnitude      Phase
Degrees      Volts/m      Degrees     Volts/m      Degrees
   0.00   1.9180E-004    -19.95   1.6350E-022    119.22
   1.00   1.9180E-004    -19.95   5.1436E-012    134.30
   2.00   1.9180E-004    -19.95   1.0262E-011    134.30
   3.00   1.9180E-004    -19.95   1.5331E-011    134.30
   4.00   1.9180E-004    -19.95   2.0325E-011    134.30
   5.00   1.9180E-004    -19.95   2.5219E-011    134.30
   6.00   1.9180E-004    -19.95   2.9991E-011    134.30
   7.00   1.9180E-004    -19.95   3.4617E-011    134.30
   8.00   1.9180E-004    -19.95   3.9074E-011    134.30
   9.00   1.9180E-004    -19.95   4.3341E-011    134.30
  10.00   1.9180E-004    -19.95   4.7397E-011    134.30
```

The data must appear promising, but before we do anything with it, let's examine the EX line of the model. We specified a value of 1.414214 as the voltage magnitude (the peak value corresponding to 1 volt RMS). If we are interested in the power level that yields these values, we must also examine the power budget.

```
   - - - POWER BUDGET - - -

INPUT POWER    = 1.6842E-02 WATTS
RADIATED POWER= 1.6842E-02 WATTS
WIRE LOSS      = 0.0000E+00 WATTS
EFFICIENCY     = 100.00 PERCENT
```

The antenna input power is 0.016842 watts. This is not likely to be a power level that is useful for taking e-field readings. As well, the input power with a standard EX 0 voltage source will vary from model to model according to the source impedance, since P = (E^2/R), where E is an RMS value.

Suppose that we are interested in the e-field values at 1,000 meters using an antenna input power of 1 kW. To arrive at these values, we must adjust the source voltage to a value that will yield them. The required voltage multiplier will be the SQRT (desired power/modeled power), or in this case, SQRT (1000/0.016842). The multiplier is 243.6706, for a new voltage entry on the EX 0 line of 344.6024. If we revise the model, we arrive at the following power budget and sample e-field lines. See model 85-3.

```
    - - - POWER BUDGET - - -

 INPUT POWER   = 9.9999E+02 WATTS
 RADIATED POWER= 9.9999E+02 WATTS
 WIRE LOSS     = 0.0000E+00 WATTS
 EFFICIENCY    = 100.00 PERCENT
```

```
**** Electric Field: Phi Pattern ****
Z=2, Freq=7.05, File=vr4-rplk.NOU
```

	---E (Theta)---		--- E (Phi) ---	
Phi Degrees	Magnitude Volts/m	Phase Degrees	Magnitude Volts/m	Phase Degrees
0.00	4.6736E-002	-19.95	8.3783E-020	-55.87
1.00	4.6736E-002	-19.95	1.2533E-009	134.30
2.00	4.6736E-002	-19.95	2.5006E-009	134.30
3.00	4.6736E-002	-19.95	3.7356E-009	134.30
4.00	4.6736E-002	-19.95	4.9525E-009	134.30
5.00	4.6736E-002	-19.95	6.1452E-009	134.30
6.00	4.6736E-002	-19.95	7.3080E-009	134.30
7.00	4.6736E-002	-19.95	8.4352E-009	134.30
8.00	4.6736E-002	-19.95	9.5213E-009	134.30
9.00	4.6736E-002	-19.95	1.0561E-008	134.30
10.00	4.6736E-002	-19.95	1.1549E-008	134.30

The power budget confirms that the input power is now 1,000 watts. The e-field values now reflect the increased power, as well as the established distance of 1,000 meters at a height of 2 meters above ground. **Fig. 85-3** provides rectangular plots of the magnitude and phase of the vertical components of the fields.

The limitation of the RP 1 request is that it requires increments of height in meters. Hence, it does not give a ready angular read out of the e-fields at a distance.

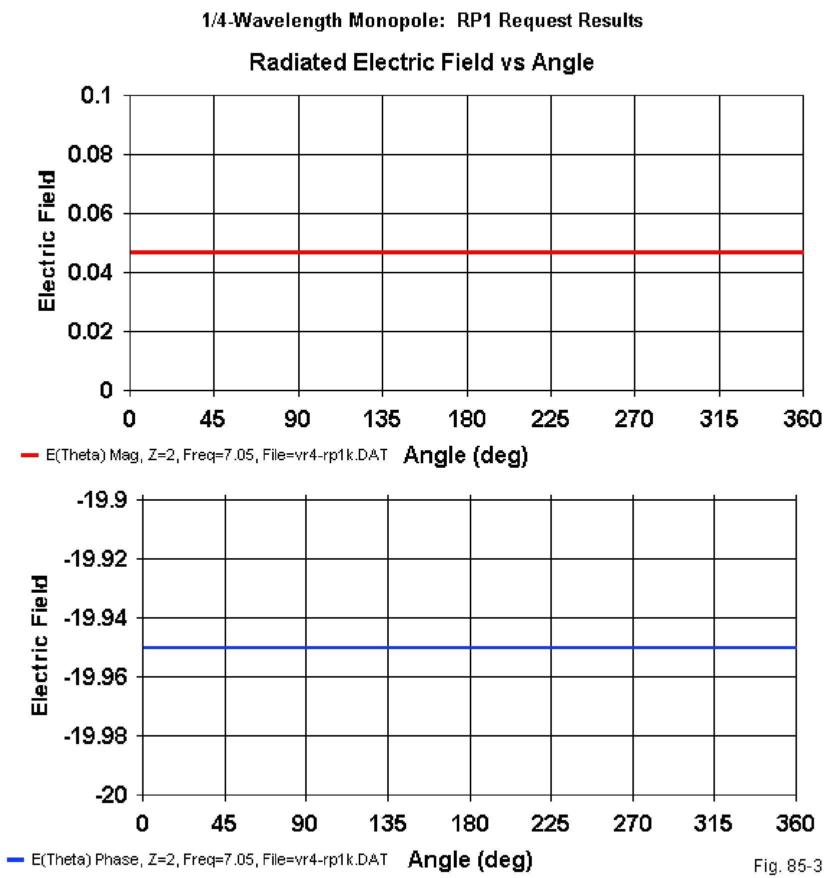

Fig. 85-3

There is also a way to overcome the height limitation: we may use the far-field request (RP 0). We insert a distance from the coordinate system origin into the (F5) position. Let's continue using the 1,000-meter distance we specified in the RP 1 request. However, we shall preserve the theta pattern request that we made in the initial model in order to obtain values at 1° intervals from the ground upward. The model will have the following appearance. See model 85-4.

```
CM 1/4-wl gp 4r
CE
GW 1,30,0.,0.,10.135,0.,0.,0.,.0254
GW 2,1,0.,0.,0.,0.,0.,-.1524,.0254
GW 3,10,0.,0.,-.1524,3.292,0.,-.1524,.003175
GW 4,10,0.,0.,-.1524,0.,3.292,-.1524,.003175
GW 5,10,0.,0.,-.1524,-3.292,0.,-.1524,.003175
GW 6,10,0.,0.,-.1524,0.,-3.292,-.1524,.003175
GE -1
FR 0,1,0,0,7.05
GN 2,0,0,0,13.,.005
EX 0,1,30,0,1.414214,0.
RP 0 181 1 1000 -90 0. 1.00000 1.00000 1000
EN
```

The only difference between this model and the one with which we started is that the RP 0 line has an extra number, the 1000-meter distance specification. This distance does not change the power gain pattern or value set, as evidenced by **Fig. 854**, a rectangular version of the pattern shown in **Fig. 85-2**.

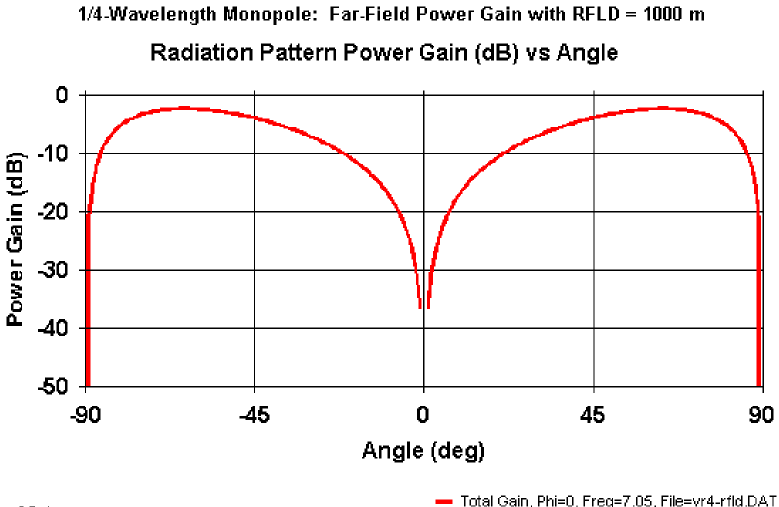

Fig. 85-4

The relevant data that we obtain from the tabular files has this appearance.

```
    - - - POWER BUDGET - - -

 INPUT POWER    = 1.6842E-02 WATTS
 RADIATED POWER= 1.6842E-02 WATTS
 WIRE LOSS      = 0.0000E+00 WATTS
 EFFICIENCY     = 100.00 PERCENT

**** Electric Field: Theta Pattern ****
Phi=0, Freq=7.05, File=vr4-rfld.NOU
```

	---E (Theta)---		--- E (Phi) ---	
Theta Degrees	Magnitude Volts/m	Phase Degrees	Magnitude Volts/m	Phase Degrees
-90.00	7.1434E-011	246.54	2.6078E-027	80.44
-89.00	9.5624E-005	248.00	3.6393E-021	80.08
-88.00	1.7909E-004	249.28	7.1385E-021	78.92
-87.00	2.5231E-004	250.41	1.0497E-020	78.44
-86.00	3.1683E-004	251.40	1.4097E-020	78.99
-85.00	3.7390E-004	252.30	1.7780E-020	79.38
-84.00	4.2453E-004	253.10	2.1636E-020	79.31
-83.00	4.6955E-004	253.82	2.4428E-020	78.34
-82.00	5.0965E-004	254.47	2.8494E-020	79.65
-81.00	5.4540E-004	255.07	3.1561E-020	79.16
-80.00	5.7729E-004	255.61	3.5149E-020	79.28

Once more, the data appears ok, but before we adopt it, let's re-examine the model on which we based it. Note that the model uses the same initial voltage source magnitude: 1.414214. Since the power input has not changed from the initial model (0.016842 w), we may use the same voltage adjustment ratio and replace the original source voltage with 344.6024.

```
   - - - POWER BUDGET - - -

 INPUT POWER   = 9.9999E+02 WATTS
 RADIATED POWER= 9.9999E+02 WATTS
 WIRE LOSS     = 0.0000E+00 WATTS
 EFFICIENCY    = 100.00 PERCENT

**** Electric Field: Theta Pattern ****
Phi=0, Freq=7.05, File=vr4-rfldlk.NOU
```

	---E (Theta)---		--- E (Phi) ---	
Theta	Magnitude	Phase	Magnitude	Phase
Degrees	Volts/m	Degrees	Volts/m	Degrees
-90.00	1.7406E-008	246.54	3.5717E-025	335.99
-89.00	2.3301E-002	248.00	4.9539E-019	337.96
-88.00	4.3638E-002	249.28	9.9617E-019	336.98
-87.00	6.1479E-002	250.41	1.4985E-018	336.03
-86.00	7.7202E-002	251.40	2.0201E-018	334.85
-85.00	9.1108E-002	252.30	2.5282E-018	336.04
-84.00	1.0345E-001	253.10	2.8632E-018	337.87
-83.00	1.1442E-001	253.82	3.4424E-018	335.74
-82.00	1.2419E-001	254.47	3.7840E-018	338.19
-81.00	1.3290E-001	255.07	4.2623E-018	336.94
-80.00	1.4067E-001	255.61	4.8567E-018	335.49

If we make the change, we obtain a somewhat different tabular set of values. See model 85-5.

The power budget confirms that we have an input power of 1,000 w. The following table then provides the key values of the electrical field at a distance of 1,000 meters for each increase in elevation of 1°. Given that we have a vertical monopole, the e-theta values are the most significant ones. The lowest usable value–89° or 1° above the horizon–is lower than the 2-meter height value given by the RP 1 request, even though the actual height at 1,000 m is close to 17.5 meters. However, the far-field output does not include the surface wave component. Notice that in the RP 1 data, the e-phi values are several orders of magnitude higher than those in the RP 0 data, even though both levels are operationally insignificant.

Remember that the reported values for the e-field are in peak volts. Multiply by 0.707 to obtain RMS values. (EZNEC provides all current and voltage output values in RMS. Version 2 of the NEC-Win software packages will provide a switch so that the user will have the option on inputting and outputting either peak or RMS values.)

The distance of 1,000 m or 1 km is one of the standards used in common engineering exercises involving antennas. An alternative to the km is the mile. However, the RP 0 and RP 1 lines require inputs as meters, so 1 mile = 1609.344 m. (Again, EZNEC provides flexibility of input and output units for the RP 1 request. It does not allow access to the RP 0 request to set a distance. However, it will provide tabular outputs in terms of 1 kW / km and 1 kW / mile.)

Although the 1-mile and 1-km distances are most commonly used, advanced modelers may have occasion to select other distances. As well, it may on some occasions be useful to compare the e-fields using different power levels. Consider the following model (model 85-6).

```
CM 1/4-wl gp 4r
CE
GW 1,30,0.,0.,10.135,0.,0.,0.,.0254
GW 2,1,0.,0.,0.,0.,0.,-.1524,.0254
GW 3,10,0.,0.,-.1524,3.292,0.,-.1524,.003175
GW 4,10,0.,0.,-.1524,0.,3.292,-.1524,.003175
GW 5,10,0.,0.,-.1524,-3.292,0.,-.1524,.003175
GW 6,10,0.,0.,-.1524,0.,-3.292,-.1524,.003175
GE -1
FR 0,1,0,0,7.05
GN 2,0,0,0,13.,.005
EX 0 1 30 0 24.36700  0.00000
RP 0 181 1 1000 -90 0. 1.00000 1.00000 1000
EN
```

If we compare this model to the one using 1000 w, we can see that the only difference is in the EX 0 line. The voltage magnitude is now 24.367 v (pk). To arrive at this value, I used the same calculation scheme, but set the desired power at 5 w instead of 1000 w. The adjustment factor was 17.2301. At 5 w, we obtain the following output data.

```
     - - - POWER BUDGET - - -

 INPUT POWER   = 4.9999E+00 WATTS
 RADIATED POWER= 4.9999E+00 WATTS
 WIRE LOSS     = 0.0000E+00 WATTS
 EFFICIENCY    = 100.00 PERCENT

**** Electric Field: Theta Pattern ****
Phi=0, Freq=7.05, File=vr4-rfld5w.NOU

                ---E (Theta)---      --- E (Phi) ---
 Theta      Magnitude      Phase     Magnitude      Phase
Degrees      Volts/m      Degrees     Volts/m      Degrees
 -90.00   1.2308E-009    246.54   9.7188E-026    325.03
 -89.00   1.6476E-003    248.00   1.3963E-019    324.60
 -88.00   3.0856E-003    249.28   2.7620E-019    324.84
 -87.00   4.3472E-003    250.41   4.1454E-019    324.53
 -86.00   5.4590E-003    251.40   5.5021E-019    324.48
 -85.00   6.4423E-003    252.30   6.7638E-019    325.11
 -84.00   7.3146E-003    253.10   8.0686E-019    325.08
 -83.00   8.0903E-003    253.82   9.3937E-019    324.72
 -82.00   8.7813E-003    254.47   1.0841E-018    323.95
 -81.00   9.3973E-003    255.07   1.1981E-018    324.34
 -80.00   9.9467E-003    255.61   1.3289E-018    324.25
```

The power budget confirms the 5-w input power level. The sample theta pattern lines provide a direct comparison of those for the 1-kw power level. With this simple exercise, one can compare the e-fields at selected distance between what amateur radio operators refer to as QRP and QRO. The 200-times power differential boils down to a 14.14-times difference in e-field strength over the specified distance.

(Since P = (E^2/R) and R has not changed, we would expect the square of the e-field difference to equal 200–and it does.) Such exercises are interesting ways to expand our understanding of the consequences of selecting different power levels relative to the strength of field at a receiving site. However, all such calculations done within modeling software omit the effects of propagation phenomena.

Too few modelers make use of the F5 entry position in the RP 0 pattern request line. By a simple double run, one may derive far-field e-field reports for any distance (even non-sensible ones) using any desired power level. Sometimes, that is very useful information indeed.

86. NEC-2 Manual Sample Files

The NEC-2 User Manual contains a series of examples designed to familiarize the NEC-2 user with many of the facets of the program outputs. Unfortunately, many NEC-2 users restrict themselves to the subset of outputs provided by entry-level programs, such as far-fields, near-fields, segment currents, etc. As well, many users employ only voltage sources (or indirectly provided current sources).

NEC-2 offers a command structure that is considerably more sophisticated than entry-level program's display. One way to approach the refinements that are possible is to work one's way through the sample models. The pages of sample output files generally strike users as unfathomable. However, if one runs the model for oneself, the output file generated by one's own core tends to make more sense and become infinitely more interesting. For example, the user can make small but significant variations in the initial sample and see what happens to the output data as a result of these changes. Suddenly, relatively opaque manual pages become transparent vehicles of illuminating data.

To ease the process of testing the examples from the NEC-2 User's Manual, I have transcribed them into this text. To use a file, simply block copy the model file text and insert it as an ASCII file to the input of your core. If you encounter any stray codes from this version, you may run the models through Notepad, cleanse them, and then save them in .txt format, but with a .NEC extension–or whatever the proper input file extension may be for your program.

Alternatively, you may use the files in the collection attached to this volume. The NEC-2 examples files use a slightly divergent coding system to ensure that you do not confuse similar NEC-2 and NEC-4 examples. Although some are identical, there are a number of new commands in NEC-4 as well as a few revised commands. Therefore, the models for NEC-2 are coded as 86-2-ex#.nec, where # is the example number.

Virtually all of the examples contain codes that the common entry-level programs may not recognize. Therefore, it is best to use them with full-featured programs or with cores having input sections that recognize all of the NEC command structure.

In the NEC User's Manual, Examples 1-4 are combined into one input file, as are Examples 7 and 8. I have separated them here as a convenience. However, by referring to the manual for the NX (Next Structure) command, you may recombine the files into their original format.

The introductions to each file come from the NEC-2 User's Manual, pp. 95-153. Quotation marks ("..") indicate material from the Manual. There are occasional references to discussions in other sections of the Manual. I have omitted here the referenced material for brevity.

Example 1

"Examples 1 through 4 are simple cases intended to illustrate the basic formats. Example 1 includes a calculation of near-electric-field along the wire. When the field is computed at the center of a segment without an applied field or loading, the Z-component of electric field is small since the solution procedure enforces the boundary condition at these points. This is a check that the program is operating correctly. The values would be still smaller if the field points were more precisely at the segment centers. The radial, or X, components of the near-field can also be compared with the charge densities at the segment centers (rho = 2 PI alpha epsilon$_{o}$ E$_{x}$). If the fields were computed along the wire axis, the radial field would be set to zero. For a non-planar structure, however, computation along the axis is the only way to reproduce the conditions of the current solution and obtain small fields at the match points."

```
CE EXAMPLE 1. CENTER FED LINEAR ANTENNA
GW 0 7 0. 0. -.25 0. 0. .25 .001
GE
EX 0 0 4 0 1.
XQ
LD 0 0 4 4 10. 3.000E-09 5.300E-11
PQ
NE 0 1 1 15 .001 0. 0. 0. 0. .01786
EN
```

Example 2

"In example 2 the wire has an even number of segments so that a charge discontinuity voltage source can be used at the center. The symbol "*" in the table of antenna input parameters is a reminder that this type of source has been used. Three frequencies are run for this case and the EX card option is used to collect and normalize the input impedances. At the end of example 2 the wire is given the conductivity of aluminum. This has a significant effect since the wire is relatively thin."

```
CM EXAMPLE 2. CENTER FED LINEAR ANTENNA.
CM CURRENT SLOPE DISCONTINUITY SOURCE.
CM 1. THIN PERFECTLY CONDUCTING WIRE
CE 2. THIN ALUMINUM WIRE
GW 0 8 0. 0. -.25 0. 0. .25 .00001
GE
FR 0 3 0 0 200. 50.
EX 5 0 5 1 1. 0. 50.
XQ
LD 5 0 0 0 3.720E+07
FR 0 1 0 0 300.
EX 5 0 5 0 1.
XQ
EN
```

Example 3

"Example 3 is a vertical dipole over ground. Since the wire is thick, the extended thin-wire approximation has been used. Computation of the average power gain is requested on the RP cards. Over a perfectly conducting ground the average power gain should be 2. The computed result differs by about 1.5%, probably due to the 10-degree steps used in integrating the radiated power. For a more complex structure, the average gain can provide a check on the accuracy of the computed input impedance over a perfect ground where it should equal 2 or in free space where it should equal 1. Example 3 also includes a finitely conducting ground where the average gain of 0.72 indicates that only 36% of the power leaving the antenna is going into the space wave. The formats for normalized gain and the combined space-wave and ground-wave fields are illustrated. At the end of example 3, the wire is excited with an incident wave at 10-degree angles and the PT card option is used to print receiving antenna patterns."

```
CM EXAMPLE 3. VERTICAL HALF WAVELENGTH ANTENNA OVER GROUND
CM 1. PERFECT GROUND
CM 2. IMPERFECT GROUND INCLUDING GROUND WAVE AND RECEIVING
CE PATTERN CALCULATIONS
GW 0 9 0. 0. 2. 0. 0. 7. .3
GE 1
EK
FR 0 1 0 0 30.
EX 0 0 5 0 1.
GN 1
RP 0 10 2 1301 0. 0. 10. 90.
GN 0 0 0 0 6. 1.000E-03
RP 0 10 2 1301 0. 0. 10. 90.
RP 1 10 1 0 1. 0. 2. 0. 1.000E+05
EX 1 10 1 0 0. 0. 0. 10.
PT 2 0 5 5
XQ
EN
```

Example 4

"Example 4 includes both patches and wires. Although the structure is over a perfect ground, the average power gain is 1.8. This indicates that the input impedance is inaccurate, probably due to the crude patch model used for the box. Since there is no ohmic loss, a more accurate input resistance can be obtained as

Radiated power = 1/2 (avg. gain) x (computed input power) = 1.016 (10^-3) W

Radiation resistance = 2 (radiated power)/|I source|^2 = 162.6 ohms.

"Since the input power used in computing the gains in the radiation pattern table is too large by 0.46 dB, the gains can be corrected by adding this factor."

```
CE EXAMPLE 4. T ANTENNA ON A BOX OVER PERFECT GROUND
SP 0 0 .1 .05 .05 0. 0. .01
SP 0 0 .05 .1 .05 0. 90. .01
GX 0 110
SP 0 0 0. 0. .1 90. 0. .04
GW 1 4 0. 0. .1 0. 0. .3 .001
GW 2 2 0. 0. .3 .15 0. .3 .001
GW 3 2 0. 0. .3 -.15 0. .3 .001
GE 1
GN 1
EX 0 1 1 0 1.
RP 0 10 4 1001 0. 0. 10. 30.
EN
```

Example 5

"Example 5 is a practical log-periodic antenna with 12 elements. Input data for the transmission line sections is printed in the table "Network Data." The table "Structure Excitation Data at Network Connection Points" contains the voltage, current, impedance, admittance, and power in each segment to which transmission lines or networks connect. This segment current will differ from the current into the connected transmission line if there are other transmission lines, network ports, or a voltage source providing alternate current paths. Thus, the current printed here for segment 3 differs from that in the table antenna "Input Parameters." The latter is the current through the voltage source and includes the current into the segment and into the transmission line. Power listed in the network-connection table is the power being fed into the segment. A negative power indicates that the structure is feeding power into the network or transmission line."

"With 78 segments, file storage must be used for the interaction matrix. The line after data card number 14 shows how the matrix has been divided into blocks for transfer between core and the files. The line "CP TIME TAKEN FOR FACTORIZATION," gives the amount of central processor time used to factor the matrix excluding time spent transferring data between core and the files. Hence it is less than the total time for factoring printed below."

"The EX card option has been used to print the relative asymmetry of the driving-point admittance matrix. The driving-point admittance matrix is the matrix of self and mutual admittances of segments connected to transmission lines, network ports, or voltage sources and should be symmetric."

```
CM EXAMPLE 5. 12 ELEMENT 10G PERIODIC ANTENNA IN FREE SPACE.
CM 78 SEGMENTS. SIGMA=D/L RECEIVING AND TRANS. PATTERNS
CM DIPOLE LENGTH TO DIAMETER RATIO=150.
CE TAU=0.93, SIGMA=0.70, BOOM IMPEDANCE=50. OHMS.
GW 1 5 0. -1. 0. 0. 1. 0. .00667
GW 2 5 -.7527 -1.0753 0. -.7527 1.0753 0. .00717
GW 3 5 -1.562 -1.1562 0. -1.562 1.1562 0. .00771
GW 4 5 -2.4323 -1.2432 0. -2.4323 1.2432 0. .00829
GW 5 5 -3.368 -1.3368 0. -3.368 1.3368 0. .00891
GW 6 7 -4.3742 -1.4374 0. -4.3742 1.4374 0. .00958
GW 7 7 -5.4562 -1.5456 0. -5.4562 1.5456 0. .0103
GW 8 7 -6.6195 -1.6619 0. -6.6195 1.6619 0. .01108
GW 9 7 -7.8705 -1.787 0. -7.8705 1.787 0. .01191
GW 10 7 -9.2156 -1.9215 0. -9.2156 1.9215 0. .01281
GW 11 9 -10.6619 -2.0662 0. -10.6619 2.0662 0. .01377
GW 12 9 -12.2171 -2.2217 0. -12.2171 2.2217 0. .01481
GE
FR 0 0 0 0 46.29
TL 1 3 2 3 -50.
TL 2 3 3 3 -50.
TL 3 3 4 3 -50.
TL 4 3 5 3 -50.
TL 5 3 6 4 -50.
TL 6 4 7 4 -50.
TL 7 4 8 4 -50.
TL 8 4 9 4 -50.
TL 9 4 10 4 -50.
TL 10 4 11 5 -50.
TL 11 5 12 5 -50.00 0 0 0 .02 0
EX 0 1 3 10 1.
RP 0 37 1 1110 90. 0. -5. 0.
EN
```

Example 6

"The geometry data for the cylinder with attached wires was discussed in section III-2 [of the Manual]. The wire on the end of the cylinder is excited first and a radiation pattern is computed. The CP card requests the coupling between the base segments of the two wires. Hence after the second wire has been excited, the table "ISOLATION DATA" is printed. The coupling printed is the maximum that would occur when the source and load are simultaneously matched to their antennas. The table includes the matched load impedance for the second segment and the corresponding input impedance at the first segment. The source impedance would be the conjugate of this input impedance for maximum coupling."

```
CE EXAMPLE 6.  CYLINDER WITH ATTACHED WIRES.
SP 0   0  10.0. 7.33330.  0. 38.4
SP 0   0  10.0. 0.  0. 0.  38.4
SP 0   0  10.0. -7.3333   0. 0.  38.4
GM 0   1  0.  0. 30.
SP 0   0  6.89  0.  11.   90.   0. 44.88
SP 0   0  6.89  0.  -11.  -90.  0. 44.88
GR 0   6
SP 0   0  0.  0. 11. 90.   0. 44.89
SP 0   0  0.  0. -11.  -90.  0.  44.89
GW 1   4  0.  0. 11. 0. 0.  23.   .1
GW 2   5  10. 0. 0.  27.6  0. 0.  .2
GS 0   0  .01
GE
FR 0   1  0   0  465.84
CP 1   1  2   1
EX 0   1  1   0  1.
RP 0   73 1 10000.  0. 5.  0.
EX 0   2  1   0  1.
XQ
EN
```

Example 7

"Examples 7 and 8 demonstrate the use of NEC for scattering. The columns labeled "gain" are, in this case, scattering cross sections in square wavelengths (rho/lambda^2)."

```
CM EXAMPLE 7. SAMPLE PROBLEMS FOR NEC - SCATTERING BY A WIRE.
CM 1. STRAIGHT WIRE - FREE SPACE
CM 2. STRAIGHT WIRE - PERFECT GROUND
CM 3. STRAIGHT WIRE - FINITELY CONDUCTING GROUND
CE (SIG.=1.E-4 MHOS/M., EPS.=6.)
GW 0 15 -55. 0. 10. 55. 0. 10. .01
GE 1
FR 0 1 0 0 3.
EX 1 2 1 0 0.
RP 0 2 1 1000 0. 0. 45. 0.
GN 1
EX 1 1 1 0 45. 0. 0.
RP 0 19 1 1000 90. 0. -10. 0.
GN 0 0 0 0 6. 1.000E-04
RP 0 19 1 1000 90. 0. -10. 0.
EN
```

Example 8

"Example 8 is a stick model of an aircraft as shown in [NEC-2 Manual] figure 19."

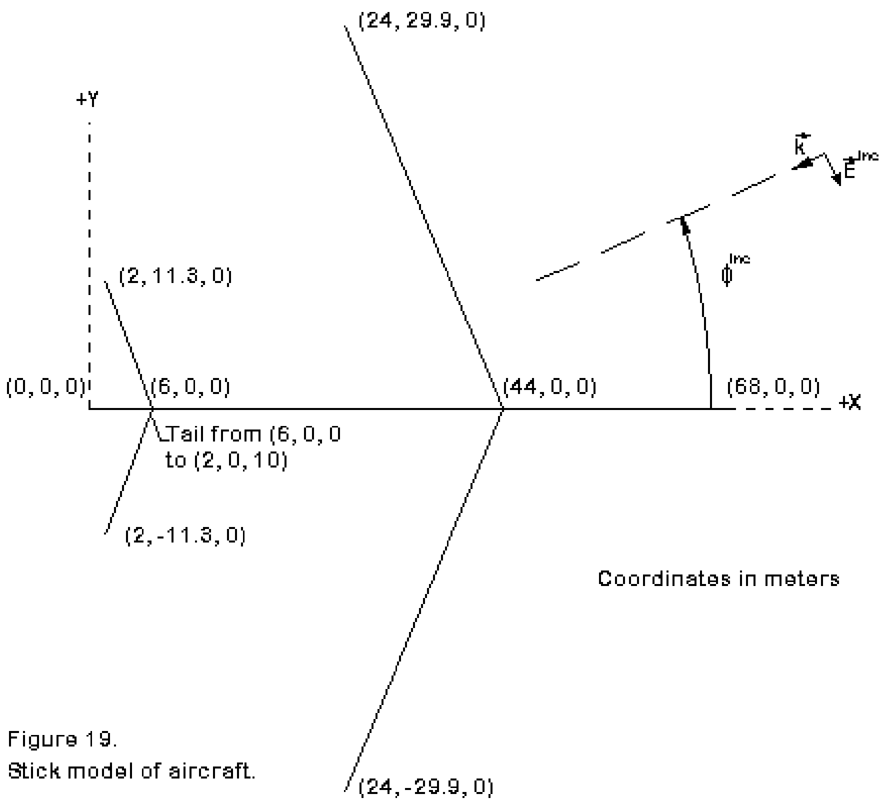

Figure 19.
Stick model of aircraft.

```
CM EXAMPLE 8. SAMPLE PROBLEM FOR NEC
CE STICK MODEL OF AIRCRAFT - FREE SPACE
GW 1 1 0. 0. 0. 6. 0. 0. 1.
GW 2 6 6. 0. 0. 44. 0. 0. 1.
GW 3 4 44. 0. 0. 68. 0. 0. 1.
GW 4 6 44. 0. 0. 24. 29.9 0. 1.
GW 5 6 44. 0. 0. 24. -29.9 0. 1.
GW 6 2 6. 0. 0. 2. 11.3 0. 1.
GW 7 2 6. 0. 0. 2. -11.3 0. 1.
GW 8 2 6. 0. 0. 2. 0. 10. 1.
GE
FR 0 1 0 0 3.
EX 1 1 1 0 0. 0. 0.
RP 0 1 1 1000 0. 0. 0.
EX 1 1 1 0 90. 30. -90.
RP 0 1 1 1000 90. 30.
EN
```

Example 9

"Example 9 shows scattering by a sphere with ka of 2.9 (ka = circumference/ wavelength). Bistatic scattering patterns are computed in the E and H planes, followed by near E and H field. The near fields within the sphere should be the negative of the incident field to produce zero total field. This condition is approximately satisfied in the example."

"If the frequency is changed to ka = 2.744, however, large internal fields will exist in the TM_{101} mode of the spherical cavity which is resonant at this ka. Such internal resonances may occur in any closed structure and result in severe errors. The errors may be avoided by placing wires inside the sphere to destroy the resonance condition at a given frequency. Since the magnetic field integral equation enforces zero tangential magnetic field on the inside of the surface, the surface acts as a perfect magnetic conductor on the inside. Hence, the resonant fields are the dual of those that would exist in a perfect electric conductor. Unfortunately, while the correct magnetic currents for the internal fields would not radiate externally, the electric currents radiate strongly."

```
CM EXAMPLE 9. BISTATIC SCATTERING BY A SPHERE.
CM PATCH DATA ARE INPUT FOR A SPHERE OF 1. M. RADIUS
CM THE SPHERE IS THEN SCALED SO THAT KA=FREQUENCY IN MHZ.
CM THE PATCH MODEL MAY BE USED FOR KA LESS THAN ABOUT 3.
CE FOR THIS RUN *-* KA=2.9 ***
SP 0  0 .13795 .13795   .98079   78.75 45..11957
SP 0  0 .51328 .21261   .83147   56.25 22.5  .17025
SP 0  0 .21261 .51328   .83147   56.25 67.5  .17025
SP 0  0 .80314 .21520   .55557   33.75 15..16987
SP 0  0 .58794 .58794   .55557   33.75 45..16987
SP 0  0 .21520 .80314   .55557   33.75 75..16987
SP 0  0 .96194 .19134   .19509   11.25 11.25 .15028
SP 0  0 .81549 .54490   .19509   11.25 33.75 .15028
SP 0  0 .54490 .81549   .19509   11.25 56.25 .15028
SP 0  0 .19134 .96194   .19509   11.25 78.75 .15028
GX 0 111
GS 0 0 47.71465
GE
FR 0  1 0   0  2.9
EX 1  1 1   0  90.0. 0.
RP 0  19 1 100090.0. -10.  0.
RP 0  1  19 1000  90.   0. 0. 10.
NE 0  1  1   11 0.  0. 0.  0. 0.  5.
NE 0  1  11  1  0.  0. 0.  0. 5.  0.
NE 0  11 1   1  0.  0. 0.  5. 0.  0.
NH 0  1  1   11 0.  0. 0.  0. 0.  5.
NH 0  1  11  1  0.  0. 0.  0. 5.  0.
NH 0  11 1   1  0.  0. 0.  5. 0.  0.
EN
```

Example 10

"Example 10 is a monopole antenna on a sparse radial wire ground screen using the Sommerfeld/Norton ground method. Part of the interpolation grid from SOMNEC is reproduced so that the user can check that his code is operating correctly."

"The NGF has been used to take advantage of the symmetry of the ground screen before adding the monopole on the axis of rotation. The addition of the monopole results in 12 new unknowns. This includes the six segments in the monopole and segments at the junction of the six radial wires. The basis functions for these junction segments are modified and have become new unknowns. The currents represented by these new unknowns are printed in their normal locations in the table of currents."

"The NGF can be tested on any of the other examples in this section by splitting the structure at some point. The results should be unchanged, although small differences may occur on computers with less than a 60-bit word length."

Note: Depending on the core or program used to test this example, you may be able to (and wish to) give the .WGF file a unique name, especially useful if you have other NGF files within the same directory/folder.

```
CM EXAMPLE 10. Green's Function for Radial-Wire Screen over
Finite Ground
CM Screen Radius = 30 m (1. wavelength radius)
CE Screen height = .01 m  6 radial wires
GW 0 12 0. 0. .01 30. 0. .01 .003
GR 0 6
GE 1
FR 0 1 0 0 10.
GN 2 0 0 0 4. .001
WG
NX
CE Monopole on radial wire ground screen from the NGF file.
GF
GW 1 6 0. 0. 0.01 0. 0. 7.51 .003
GE
EX 0 1 1 0 1.
RP 0 19 2 1001 0. 0. 5. 90.
EN
```

These model files are provided to encourage newer users of raw cores or of programs above the entry level to familiarize themselves with the complete scope of what NEC can do. As well, since many of the example narratives point to limiting factors, the user can familiarize himself or herself with NEC limitations and correctives or work-arounds.

87. NEC-4 Manual Sample Files

In the preceding episode, we presented the examples models that occur in the 2-decade-old NEC-2 User's Manual. This month, we shall meet the example models that appear in the 1992 NEC-4 User's Manual (pp. 100-181). A number of the models are identical to those in the earlier manual, while some others vary only to the degree required by revisions in some few of the command line structures. However, the NEC-4 Manual adds two new models covering features unique to NEC-4 (relative to NEC-2).

To ease the process of testing the examples from the NEC-4 User's Manual, I have transcribed them into this text. To use a file, simply block copy the model file text and insert it as an ASCII file to the input of your core. If you encounter any stray codes from this HTML version, you may run the models through Notepad, cleanse them, and then save them in .txt format, but with a .NEC extension–or whatever the proper input file extension may be for your program.

Alternatively, you may use the files in the collection attached to this volume. The NEC-4 examples files use a slightly divergent coding system to ensure that you do not confuse similar NEC-2 and NEC-4 examples. Although some are identical, there are a number of new commands in NEC-4 as well as a few revised commands. Therefore, the models for NEC-4 are coded as 86-4-ex#.nec, where # is the example number.

In the NEC User's Manual, Examples 1-4 are combined into one input file, as are Examples 7 and 8. I have separated them here as a convenience. However, by referring to the manual for the NX (Next Structure) command, you may recombine the files into their original format.

The introductions to each file come from the NEC-4 User's Manual, pp. 100-181. Quotation marks ("..") indicate material from the Manual. There are occasional references to discussions in other sections of the Manual. I have omitted here the referenced material for brevity.

Example 1

"Examples I through 4 are simple cases intended to illustrate the basic formats. In Example 1, a A/2 dipole is excited at its center. The XQ command requests only the calculation of current. After "ANTENNA INPUT PARAMETERS", a table shows the value of current at the center of each segment. Next, the antenna is loaded at its center with a series R-L-C circuit. Since the load coincides with the source segment, the effect on input impedance is simply to add the load impedance in series. If the load had been on another segment, the effect on input impedance would have been more complex."

"The PQ command requests a listing of the linear charge density at the center of each segment. In addition, the charge density is printed at the free ends of segments 1 and 7, with "E" following the segment number to indicate a free wire end. The values obtained for charge density at wire ends will be very dependent on the segment lengths. As more segments are added to reduce the segment lengths, the charge densities at the ends will increase, approaching the singular behavior expected at an edge. However, the values printed give some indication of the charge in the vicinity of the end."

"The NE commands request computation of near electric fields, first along the wire axis and then along the wire surface. Ideally, the *z* component of electric field would be zero along the wire axis and on the surface, except over the source region. On the wire axis the field is very small at the centers of segments away from the source, since these values are enforced in the moment-method solution. When the field is evaluated along the wire surface, the *z* component is small, but considerably larger than on the axis. Evaluating the *z* component of field on the wire surface is the worst case for the thin-wire approximation in NEC-4. This calculation illustrates a difference between NEC-4 and NEC-3. In NEC-3, the solution was obtained by matching the boundary condition on the wire surface, with the current treated as a filament on the axis. Hence NEC-3 would give very small tangential fields on the surface at the match points. When the near field is requested at a point on the wire axis in NEC-3, it is actually computed on the wire surface. The radial electric field (E_x) computed on the wire surface can be compared with the charge densities at the segment centers. For charge density rho and wire radius a the field is E_x = rho/2 PI alpha epsilon$_0$."

```
CE EXAMPLE 1. CENTER FED LINEAR ANTENNA
GW 0 7 0. 0. -.25 0. 0. .25 .001
GE
EX 0 0 4 0 1.
XQ
LD 0 0 4 4 10. 3.000E-09 5.300E-11
PQ
NE 0 1 1 15 0. 0. 0. 0. 0. .01786
NE 0 1 1 15 .001 0. 0. 0. 0. .01786
EN
```

Example 2

“In Example 2 the wire has an even number of segments, so a bicone voltage source model has been used to excite the wire at its center. The symbol ‘*’ in the table of antenna input parameters is, a reminder that this type of source has been used. The wire radius is very small for this problem, since the bicone source is only accurate for thin wires and small radius to segment-length ratios. A safer way to excite the center of this wire would be to use applied-field voltage sources on segments 4 and 5, each with half of the total voltage.”

“Three frequencies are run in Example 2, and the option on the EX command is used to collect and normalize the input impedances. At the end of Example 2, the wire is given the conductivity of aluminum. This has a significant effect, since the wire is relatively thin.”

```
CM EXAMPLE 2. CENTER FED LINEAR ANTENNA.
CM CURRENT SLOPE DISCONTINUITY SOURCE.
CM 1. THIN PERFECTLY CONDUCTING WIRE
CE 2. THIN ALUMINUM WIRE
GW 0 8 0. 0. -.25 0. 0. .25 .00001
GE
FR 0 3 0 0 200. 50.
EX 5 0 5 1 1. 0. 50.
XQ
LD 5 0 0 0 3.720E+07
FR 0 1 0 0 300.
```

```
EX 5 0 5 0 1.
XQ
EN
```

Example 3

“Example 3 is a vertical dipole over ground. The average power gain has been computed using the option on the RP command. For the first result, with perfectly conducting ground, the average gain is close to the ideal value of 2. For a more complex structure, the average gain can provide a check on the accuracy of the computed input impedance. The value of average gain should be 1.0 for a model in free space and 2.0 over perfectly conducting ground. Acceptable differences from the correct value may range from a few percent for a simple model to ten percent or more for large, complex models.”

“Example 3 also includes a solution for finitely conducting ground using the reflection coefficient approximation. With a finitely conducting ground the average gain cannot be used as a check on solution accuracy, but shows the radiation efficiency of the antenna, taking into account ground loss. Since the average gain has dropped from 2.0 for perfectly conducting ground to 0.72, the radiation efficiency is 36 percent.”

```
CM EXAMPLE 3. VERTICAL HALF WAVELENGTH ANTENNA OVER GROUND
CM 1. PERFECT GROUND
CM 2. IMPERFECT GROUND INCLUDING GROUND WAVE AND RECEIVING CE
PATTERN CALCULATIONS
GW 0 9 0. 0. 2. 0. 0. 7. .3
GE 1
FR 0 1 0 0 30.
EX 0 0 5 0 1.
GN 1
RP 0 10 2 1301 0. 0. 10. 90.
GN 0 0 0 0 6. 1.000E-03
RP 0 10 2 1301 0. 0. 10. 90.
RP 1 10 1 0 1. 0. 2. 0. 1.000E+05
EX 1 10 1 0 0. 0. 0. 10.
PT 2 0 5 5
```

```
XQ
EN
```

Example 4

"Example 4 is a simple model to demonstrate the connection of a wire to a surface patch. Although the structure is over a perfectly conducting ground, a value of 1.8 is obtained for average gain. This result indicates that the input impedance is inaccurate, probably due to the crude patch model used for the box. In a case such as this, the average gain can be used to compute corrected values for the radiated power, input resistance and antenna gain. The total radiated power from integrating the radiated field, 9.623(10-^{4}) watts, is printed after the average gain. In earlier versions of NEC, this value must be obtained by multiplying the average gain by the total input power. The radiation resistance can then be computed as

$$\text{Radiation resistance} = 2\ (\text{radiated power})/|\text{I source}|^2 = 167.8 \text{ ohms},$$

where I source is the source current, and the factor of 2 is necessary because values printed by NEC for current, voltage and field are peak rather than rms. Since the value of input power used in computing gains for the radiation pattern table is too large by 0.46 dB (10 $\log_{10}$[2/1.8]), the gains can be corrected by adding this amount."

```
CE EXAMPLE 4. T ANTENNA ON A BOX OVER PERFECT GROUND
SP 0 0 .1 .05 .05 0. 0. .01
SP 0 0 .05 .1 .05 0. 90. .01
GX 0 110
SP 0 0 0. 0. .1 90. 0. .04
GW 1 4 0. 0. .1 0. 0. .3 .001
GW 2 2 0. 0. .3 .15 0. .3 .001
GW 3 2 0. 0. .3 -.15 0. .3 .001
GE 1
GN 1
EX 0 1 1 0 1.
RP 0 10 4 1001 0. 0. 10. 30.
EN
```

Example 5

“Example 5 is a practical log-periodic antenna with 12 elements. Input data for the transmission line sections is printed in the table “NETWORK DATA.” The table “STRUCTURE EXCITATION DATA AT NETWORK CONNECTION POINTS” contains the voltage, current, impedance, admittance and power at each segment to which the transmission lines or networks connect. The currents printed in this table are the currents in the segments at the connection points, and will differ from the current into the connected transmission line if there are other transmission lines, network ports or a voltage source providing alternate current paths. Thus, the current printed for segment 3 differs from that in the table “INPUT PARAMETERS.” The latter is the current through the voltage source and includes the current into the segment and into the transmission line. Power listed in the network-connection table is the power being fed into the segment. A negative power indicates that the structure is feeding power into the network or transmission line.”

“This example was run with the parameter MAXMAT set to 64 to illustrate the output format when file storage must be used for the matrix. The line after the listing of input line 14 shows how the matrix has been divided into blocks for transfer between memory and file storage. The line “CP TIME TAKEN FOR FACTORIZATION” shows the amount of central processor time used to factor the matrix, excluding I/0 time. This will be less than the total factoring time printed below in the output.”

```
CM 12 ELEMENT 10G PERIODIC ANTENNA IN FREE SPACE.
CM 78 SEGMENTS. SIGMA=D/L RECEIVING AND TRANS. PATTERNS
CM DIPOLE LENGTH TO DIAMETER RATIO=150.
CE TAU=0.93, SIGMA=0.70, BOOM IMPEDANCE=50. OHMS.
GW 1 5 0. -1. 0. 0. 1. 0. .00667
GW 2 5 -.7527 -1.0753 0. -.7527 1.0753 0. .00717
GW 3 5 -1.562 -1.1562 0. -1.562 1.1562 0. .00771
GW 4 5 -2.4323 -1.2432 0. -2.4323 1.2432 0. .00829
GW 5 5 -3.368 -1.3368 0. -3.368 1.3368 0. .00891
GW 6 7 -4.3742 -1.4374 0. -4.3742 1.4374 0. .00958
GW 7 7 -5.4562 -1.5456 0. -5.4562 1.5456 0. .0103
GW 8 7 -6.6195 -1.6619 0. -6.6195 1.6619 0. .01108
GW 9 7 -7.8705 -1.787 0. -7.8705 1.787 0. .01191
```

```
GW 10 7 -9.2156 -1.9215 0. -9.2156 1.9215 0. .01281
GW 11 9 -10.6619 -2.0662 0. -10.6619 2.0662 0. .01377
GW 12 9 -12.2171 -2.2217 0. -12.2171 2.2217 0. .01481
GE
FR 0 0 0 0 46.29
TL 1 3 2 3 -50.
TL 2 3 3 3 -50.
TL 3 3 4 3 -50.
TL 4 3 5 3 -50.
TL 5 3 6 4 -50.
TL 6 4 7 4 -50.
TL 7 4 8 4 -50.
TL 8 4 9 4 -50.
TL 9 4 10 4 -50.
TL 10 4 11 5 -50.
TL 11 5 12 5 -50.00 0 0 0 .02 0
EX 0 1 3 10 1.
RP 0 37 1 1110 90. 0. -5. 0.
EN
```

Example 6

"The structure data for the cylinder with attached wires was discussed in section 3.4 [of the Manual]. In this example, the wire on the end of the cylinder is excited first, and a radiation pattern is computed. The CP command requests the coupling between the base segments of the two wires. The coupling printed is the maximum that would occur when the source and load are simultaneously matched to their antennas. The table includes the matched load impedance for the second segment and the corresponding input impedance at the first segment. The source impedance would be the conjugate of this input impedance for maximum coupling."

```
CE CYLINDER WITH ATTACHED WIRES.
SP 0   0  10.0. 7.33330.  0. 38.4
SP 0   0  10.0. 0.  0. 0.  38.4
SP 0   0  10.0. -7.3333   0. 0.  38.4
GM 0   1  0.  0. 30.
SP 0   0  6.89  0.  11.   90.   0. 44.88
```

```
SP 0   0  6.89  0. -11.  -90.  0. 44.88
GR 0   6
SP 0   0  0.  0. 11. 90.   0. 44.89
SP 0   0  0.  0. -11.  -90.  0.  44.89
GW 1   4  0.  0. 11. 0. 0.  23.    .1
GW 2   5  10. 0.  0.  27.6  0.  0.  .2
GS 0   0  .01
GE
FR 0   1  0   0  465.84
CP 1   1  2   1
EX 0   1  1   0  1.
RP 0   73 1 10000.  0. 5.  0.
EX 0   2  1   0  1.
XQ
EN
```

Example 7

"Examples 7 and 8 demonstrate the use of NEC for scattering calculations. The normalized cross sections (rho/lambda^2) for bistatic scattering are printed in the radiation-pattern tables."

```
CM SAMPLE PROBLEMS FOR NEC - SCATTERING BY A WIRE.
CM 1. STRAIGHT WIRE - FREE SPACE
CM 2. STRAIGHT WIRE - PERFECT GROUND
CM 3. STRAIGHT WIRE - FINITELY CONDUCTING GROUND
CE (SIG.=1.E-4 MHOS/M., EPS.=6.)
GW 0 15 -55. 0. 10. 55. 0. 10. .01
GE 1
FR 0 1 0 0 3.
EX 1 2 1 0 0.
RP 0 2 1 1000 0. 0. 45. 0.
GN 1
EX 1 1 1 0 45. 0. 0.
RP 0 19 1 1000 90. 0. -10. 0.
GN 0 0 0 0 6. 1.000E-04
RP 0 19 1 1000 90. 0. -10. 0.
EN
```

Example 8

"Example 8 is a stick-model of an aircraft, as shown in [NEC-4 Manual] figure 21."

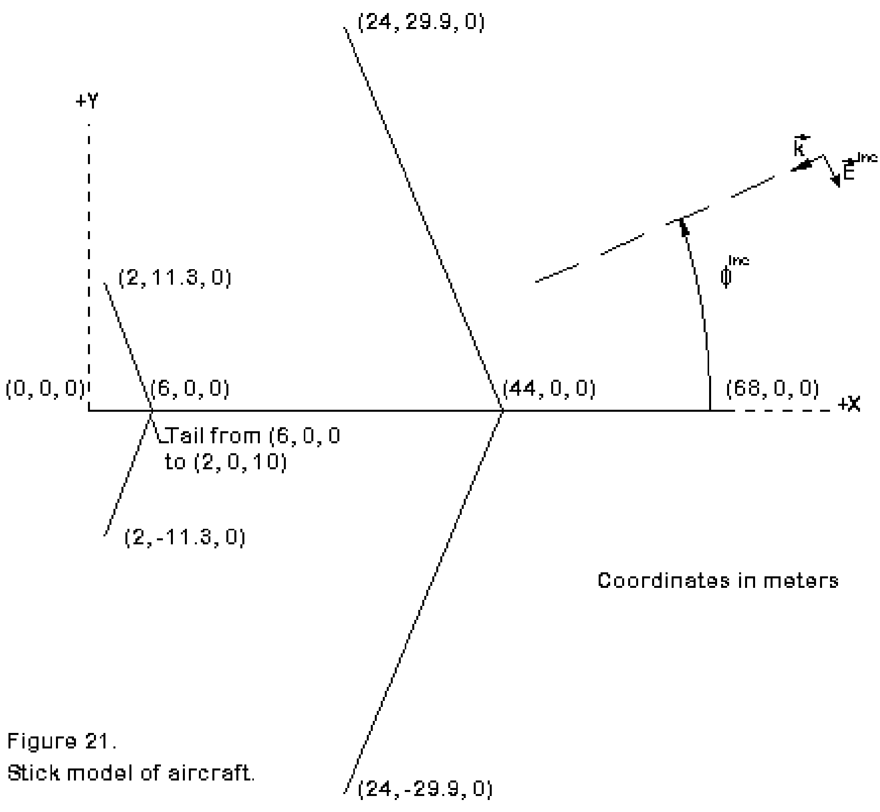

Figure 21.
Stick model of aircraft.

```
CM SAMPLE PROBLEM FOR NEC
CE STICK MODEL OF AIRCRAFT - FREE SPACE
GW 1 1 0. 0. 0. 6. 0. 0. 1.
GW 2 6 6. 0. 0. 44. 0. 0. 1.
GW 3 4 44. 0. 0. 68. 0. 0. 1.
GW 4 6 44. 0. 0. 24. 29.9 0. 1.
GW 5 6 44. 0. 0. 24. -29.9 0. 1.
GW 6 2 6. 0. 0. 2. 11.3 0. 1.
GW 7 2 6. 0. 0. 2. -11.3 0. 1.
GW 8 2 6. 0. 0. 2. 0. 10. 1.
GE
FR 0 1 0 0 3.
EX 1 1 1 0 0. 0. 0.
RP 0 1 1 1000 0. 0. 0.
EX 1 1 1 0 90. 30. -90.
RP 0 1 1 1000 90. 30.
EN
```

Example 9

"Example 9 shows the calculation of scattering by a sphere with ka of 2.9 (ka = 2 PI alpha/lambda = circumference/lambda.) Bistatic scattering patterns are computed in the E and H planes. Then near electric and magnetic fields are computed, starting at the center of the sphere and going out along the z, y and x axes. The fields within the sphere should be the negative of the incident field to produce zero total field. This condition is approximately satisfied in the example."

"If the frequency is changed so that the internal cavity of the sphere becomes resonant (ka = 2.744 for the TM_{101} mode) large fields will be found inside the sphere. Such internal resonances may occur in any closed structure, and will result in large errors in the computed currents and radiated fields. Since the magnetic-field integral equation used in NEC enforces the boundary condition of zero tangential magnetic field on the inside of the surface, the surface acts as a perfect magnetic conductor on the inside. Hence, the resonant fields that are seen will be the dual of those that would exist in a perfect electric-conducting sphere. Unfortunately, while the correct magnetic currents for the internal fields would not radiate externally, the electric currents in the NEC solution radiate strongly."

"A number of ways have been developed for avoiding internal resonances, one being to solve combined electric and magnetic field integral equations. The only solution to the problem in NEC is to place wires inside the sphere to destroy the resonance condition at a given frequency. Three orthogonal dipoles might be placed at the center of a sphere. If the wires are perfectly conducting the resonance would be shifted to a different frequency. However, if lossy wires are used, resonances could be reduced at all frequencies."

```
CM BISTATIC SCATTERING BY A SPHERE.
CM PATCH DATA ARE INPUT FOR A SPHERE OF 1. M. RADIUS
CM THE SPHERE IS THEN SCALED SO THAT KA=FREQUENCY IN MHZ.
CM THE PATCH MODEL MAY BE USED FOR KA LESS THAN ABOUT 3.
CE FOR THIS RUN *-* KA=2.9 ***
SP 0  0 .13795 .13795   .98079   78.75 45..11957
SP 0  0 .51328 .21261   .83147   56.25 22.5  .17025
SP 0  0 .21261 .51328   .83147   56.25 67.5  .17025
SP 0  0 .80314 .21520   .55557   33.75 15..16987
SP 0  0 .58794 .58794   .55557   33.75 45..16987
SP 0  0 .21520 .80314   .55557   33.75 75..16987
SP 0  0 .96194 .19134   .19509   11.25 11.25 .15028
SP 0  0 .81549 .54490   .19509   11.25 33.75 .15028
SP 0  0 .54490 .81549   .19509   11.25 56.25 .15028
SP 0  0 .19134 .96194   .19509   11.25 78.75 .15028
GX 0 111
GS 0 0 47.71465
GE
FR 0  1 0   0  2.9
EX 1  1 1   0  90.0. 0.
RP 0  19 1 100090.0. -10.  0.
RP 0  1  19 1000  90.   0. 0.  10.
NE 0  1  1   11 0.  0. 0.  0. 0.  5.
NE 0  1  11  1  0.  0. 0.  0. 5.  0.
NE 0  11 1   1  0.  0. 0.  5. 0.  0.
NH 0  1  1   11 0.  0. 0.  0. 0.  5.
NH 0  1  11  1  0.  0. 0.  0. 5.  0.
NH 0  11 1   1  0.  0. 0.  5. 0.  0.
EN
```

Example 10

"In Example 10, a horizontal dipole antenna 16 m long is modeled near the surface of a ground using the Sommerfeld solution. A file of Sommerfeld-integral values was generated by running the SOMNTX program for the ground parameters epsilon_g = 10, rho = 0.01 S/m and 5 MHz. The file from SOMNTX was given the name SOMEX10.NEC"

In the first data set the wire is modeled in free space and then at a height of 0.01 m over the ground. The input impedance is considerably closer to resonance when the wire is over ground, but the average gain of 1.59E-2 shows that only 0.795 percent of the input power is being radiated into the upper half space, with the rest absorbed by the ground."

"In the second data set, the dipole is modeled in an infinite medium with the same ground parameters, and then buried 0.01 m below the ground surface. When the wire is in a conducting medium the segment coordinates and segment lengths in the table "CURRENTS AND LOCATION" are normalized by the quantity $|\text{lambda}_g|$ = $\text{lambda}_g|\text{epsilon}_g$ - *j*rho/omega $\text{epsilon}_0^{1/2}$ where lambda_0 is the wavelength in free space. The normalized segment lengths should satisfy the criteria for solution accuracy as discussed in section 2.1."

"In computing the radiated field in the infinite medium, a factor of $e\text{-}^{jkR}$/R is omitted, as is always done when the distance R is not specified on the RP command. Since the actual field has an exponential decay when k is complex, the radiated field, defined as the component of field falling off as 1/R, is zero in a lossy medium. By omitting the exponential, NEC obtains a non-zero value that indicates the relative strength of field in any direction at a finite distance, but it should not be considered radiated field. Likewise, the average gain and radiated power cannot be interpreted in their usual senses. All power is absorbed in the medium and not radiated. While the interpretation of these values is open to question, the computed values seem more useful than printing zero. When the field is computed in a lossy medium with a ground interface, zero will be printed for the radiated field and gain, since then it is not possible to remove the exponential attenuation."

"With the dipole buried 0.01 m below the ground surface, the average gain is slightly larger than when the wire was above ground. This difference is probably due to the change in current distribution when the wire is in the ground. The attenuation through 0.01 m of this ground is negligible."

"In the final case, two dipoles are modeled, with one above the ground surface by 0.01 m and the other buried by the same distance. Both dipoles are driven by 1 volt sources, but opposing currents are set up in a transmission-line mode. The input resistance of the upper dipole is negative, indicating that it is absorbing power from the buried wire. The average gain and radiated power are smaller than for a single wire above or below ground, probably as a result of the large fields generated in the ground with this two-wire configuration."

```
CM Horizontal 16 m dipole
CM 1. Dipole in free space
CM 2. Dipole above ground - Ground: E = 10., SIG 0.01 S/M,5 MHz
CE Sommerfeld gound option
GW 1  11 -8. 0. 0.01  8.  0. 0.01  .001
GE -1
FR 0   1  0   0  5.
EX 0   1  6   0  1.
RP 0   10 2   1000  0. 0. 10.   90.
RP 0   10 10  1002  0. 0. 10.   10.
GN 2   0  0   0  10. 0.01  SOMEX10.NEC
RP 0   10 2   1000  0. 0. 10.   90.
RP 0   10 10  1002  0. 0. 10.   10.
NX
CM Horizontal 16 m dipole
CM 1. Dipole in an infinite lossy medium
CM 2. Dipole below the ground surface
CE Sommerfeld gound option - E = 10., SIG = 0.01 S/M, 5 MHz
GW 1  11 -8. 0. -0.01 8.  0. -0.01 .001
GE -1
FR 0   1  0   0  5.
EX 0   1  6   0  1.
UM 0   0  0   0  10. 0.01
RP 0   10 2   1000  0. 0. 10.   90.
```

```
RP 0   10 10  1002  0. 0.  10.   10.
CM NOTE: The above calculation of average gain in a lossy
medium cannot
CM be interpreted in the usual sense. A factor of EXP(-jkR)/R
CM has been omitted from the field so that a non-zero value can
CM be  obtained for R -> infinity with complex k. However, by
the
CM usual definition, the far-field gain is zero in a lossy
medium.
CM Set upper medium to free space, then use Sommerfeld ground.
GN 2   0  0   0  10. 0.01 SOMEXIO.NEC
RP 0   10 2   1000  0.  0. 10. 90.
RP 0   10 10  1002  0.  0. 10. 10.
NX
CM TWO HORIZONTAL 16 M DIPOLE ANTENNAS ABOVE AND BELOW GROUND
CE SOMMERFELD GOUND OPTION - E = 10., SIG = 0.01 S/M, 5 MHz
GW 1   11 -8. 0.  0.01  8.  0. 0.01   .001
GW 2   11 -8. 0.  -0.01 8.  0. -0.01 .001
GE -1
FR 0   1  0   0  5.
EX 0   1  6   0  1.
EX 0   2  6   0  1.
GN 2   0  0   0  10. 0.01 SOMEXIO.NEC
RP 0   10 2   1000  0. 0.  10.   90.
RP 0   10 10  1002  0. 0.  10.   10.
EN
```

Example 11

“In example 11, a 15 m monopole is modeled on a ground stake 2 m deep. Separate GW commands are used to define the monopole and ground stake to ensure that the junction will occur exactly at the interface. The average gain computation shows that the radiation efficiency of this antenna over ground is 16 percent. NE and NH commands are used to compute the electric and magnetic fields at a distance of 5000 m with the surface wave included. When the Sommerfeld ground option is in use, the near magnetic field is computed from a finite-difference evaluation of Ä x E. [The actual symbol is an inverted delta, not available in this transcription.] The increment for evaluating differences is ±10-3 λ_0. Hence, if the near magnetic field had been evaluated at a height of less than 0.06 ra in this example an incorrect value would have been obtained due to the negative increment in z falling on the wrong side of the interface."

"If the lower medium had a conductivity of zero, the average gain could be computed over both upper and lower half spaces (0° = 0 = 180°) and should have a value of 1.0. This can serve as a necessary, but not sufficient, check on the solution accuracy for a dielectric ground. In integrating the power in a dielectric ground, it may be necessary to use increments in theta of a degree or less to accurately sample the field near the totally reflecting or critical angle in the ground (theta = 180° - $\sin^{-1}$ $\text{epsilon}^{-1/2}$ = 162° for $\text{epsilon}_{\text{tau}}$ = 10, rho = 0.) The steepness of this near discontinuity increases with increasing height of the antenna above the ground."

```
CM 15 m monopole antenna on a ground stake 2 m deep.
CE Ground: E = 10., SIG = 0.01 S/m, 5 Mz.
GW 1  8  0.  0. -2.0. 0.  0.  0.01
GW 2  10 0.  0. 0.  0. 0.  15.0.01
GE -1
FR 0  1  0   0  5.
GN 2  0  0   0  10.  0.01 SOMEX10.NEC
EX 0  2  1   0  1.
RP       0   19 2   1002 0.   0.  5. 90.
NE 0  1  1   21 5000. 0.  0.1    0. 0.  10.
NH 0  1  1   21 5000. 0.  0.1    0. 0.  10.
EN
```

Example 12

"The monopole antenna from Example 11 is now modeled on a ground screen of six radial wires, with a screen radius of 12 meters. The Numerical Green's Function option was used to take advantage of the rotational symmetry of the ground screen. The monopole is added on the axis of rotation in the second part of the run."

"The screen was buried 5 cm below the surface of the ground. Since a segment cannot penetrate the interface, the junction of the monopole and the radial wires was located on the interface at the origin. The inner segment of each radial wire descends at an angle to the 5 cm depth, and the remainder of the radial is horizontal. The inner segment was chosen to have approximately the same length as the horizontal segments. The complete ground screen is generated with a GR command to set the code to use symmetry in the solution."

"The monopole is added to the NGF solution in the second part of the run. The summary of segment data includes all segments from the NGF file and those added for the monopole. After the summary of segment data, a line shows the number of new unknowns in the NGF solution. This number includes the new segments plus one new unknown for each segment from the NGF file that connects to a new segment. Segments in the NGF file that connect to new segments contribute new unknowns since they need new basis functions due to the changed junction condition. Since there are 10 segments in the monopole and six radials each connecting to the base of the monopole, the number of new unknowns is 16. The code must also recompute the field from the second ring of segments from the center of the screen, since the basis functions for the first segments extend onto the second segments. This additional integration can significantly reduce the advantage of using the NGF to take advantage of symmetry when many NGF segments connect to new segments."

"The computed results include a radiation pattern and average gain. From the average gain, it is seen that the radiation efficiency has increased to 29 percent from the 16 percent obtained with a ground stake. A better ground screen would increase the efficiency still further. The NEC-GS program is much more efficient than NEC-4 [11] for modeling monopoles on large radial-wire ground screens. However, at the present time there is no version of NEC-GS using the NEC-4 solution algorithms."

```
CM 6-Wire Radial-Wire Ground Screen.
CE An NGF file is written to take advantage of symnetry of the
screen.
GW 1  14 12.   0. -.05  0.8   0. -.05  .01
GW 1  1 0.8 0. -.05  0.  0. 0.  .01
GR 0  6
GE
FR 0  1  0   0  5.
GN 2  0  0   0  10. .01  SOMEX10.NEC
```

```
WG
NX
CE 15 m Monopole added to the ground screen from the NGF file.
GF
GW 2  10 0.  0. 0.  0. 0. 15. .01
GE
EX 0  2  1   0  1.
RP 0  19 2   1001  0. 0.  5. 90.
EN
```

These model files are provided to encourage newer users of NEC-4 to familiarize themselves with the complete scope of what NEC can do. As well, since many of the example narratives point to limiting factors, the user can familiarize himself or herself with NEC limitations and correctives or work-arounds.

88. EX and PT Commands

Most newer NEC antenna modelers and even experienced antenna designers have little occasion to use any other form of excitation than EX 0, the voltage source. Some software packages simulate a current source by placing–either overtly or covertly–a voltage source and a network (NT) between the actual excitation segment and the segment that the modeler wishes to call the source. Other packages allow split sources by exciting two adjacent segments in series and calculating the resulting source impedance for the user.

A typical model in .NEC format would look like the following simple 6-element Yagi in free-space (model 88-1). (The LD5 line assigns the aluminum material loss to the entire set of model segments. The last entry in the line is a permeability value of 1, indicating that this model is set up in NEC-4.) The dimensions are in meters.

```
CM 6-el 2M Yagi
CE
GW 1 21 -.514604 0. 0. .514604 0. 0. .0024
GW 2 21 -.5075174 .257302 0. .5075174 .257302 0. .0024
GW 3 21 -.4746752 .3637788 0. .4746752 .3637788 0. .0024
GW 4 21 -.461137 .6585204 0. .461137 .6585204 0. .0024
GW 5 21 -.461137 .9469628 0. .461137 .9469628 0. .0024
GW 6 21 -.443992 1.377137 0. .443992 1.377137 0. .0024
GE 0
LD 5 0 0 0 2.5E+07 1.
FR 0 1 0 0 146. 0
GN -1
EX 0 2 11 0 1 0.
RP 0 1 361 1000 90. 0. 1.00000 1.00000 0.
EN
```

From a model such as this one, perhaps the most used output is the E-plane pattern, in this case, a Phi or Azimuth pattern, according to the names assigned by the software. **Fig. 88-1** shows a sample for the present model, along with the data for the pattern. Not shown is the other most desired piece of information, the source impedance: 50.0 + j9.5 Ω at 146 MHz for this model.

E-Plane Pattern of a 6-Element 146-MHz Yagi with Data

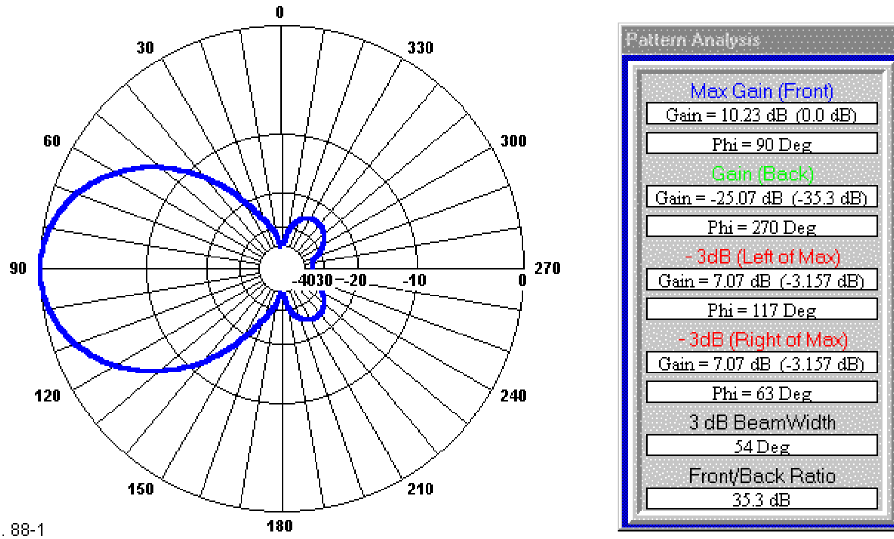

Fig. 88-1

Plane-Wave Excitation

There are occasions when a modeler may seek other information from the model, information that may emerge from the use of plane wave excitation. The EX command has three significant options for the modeler:

EX 1: incident plane wave, linear polarization
EX 2: incident plane wave, right hand (thumb along the incident vector) elliptic polarization
EX 3: incident plane wave, left hand (thumb along the incident vector) elliptic polarization

Both of the elliptical polarization options are useful when simulating signal sources from helical and similar antennas. Linear polarization simulates line-of-sight signal sources. These notes do not pretend to provide a compendium of uses for the various signal sources. Instead, they are designed to introduce the rudiments of using incident plane-wave sources, as well as a few tips on making incident plane-wave models do what the modeler wants them to do in terms of data output.

For anyone not acquainted with incident plane-wave excitation, the first item to understand is that these sources do not excite a specific wire segment on the model. Instead, they simulate an external signal source that excites the entire antenna structure. The entry-line structure for them has a number of interesting properties that differ from the line structure of a simple voltage source.

```
Com  I1   I2     I3     I4   F1         F2         F3          F4    F5   F6    F7
ID   Type # Thta # Phi  Not  Th angle   Ph angle   Eta         Theta Phi  Axis  El. field
          angles angles used to vector  to vector  pol. angle  step  step ratio V/m
EX   1    1      8      0    90         0          90          0     45   0     0
```

The sample entry is for a linear plane wave. Hence, F6 is 0 by non-relevance. F7 also has a 0, but that value indicates a default value of 1 V/m. In some problems designed to ferret out coupling potentials among wires, you may use a specific value that closely approximates the value from the source signal at the structure being examined in model form.

Most of the remaining entries define incident plane waves as a calculation loop within NEC (with some properties resembling the loop operation of frequency sweeps using the FR command). In the sample, for the sake of clarity, there is only one theta angle: 90°. This angle is parallel to the plane of the antenna elements. The sample specifies 8 phi-angle (azimuth-angle) steps at 45° increments, thus providing samples evenly spaced in the element plane.

The F3 entry, called Eta, under linear polarization is easy to memorize. With a value of 0, the polarization is in the +/-Z direction–vertically polarized for antennas over ground. If F3 is 90, the polarization is in the X-Y plane–horizontally polarized for antennas over ground. The sample in free space uses horizontal polarization for simplicity, but there is no restriction against checking results when cross-polarized or with the polarization set to intermediate angles. When using EX 2 or EX 3, elliptical polarization, the entry changes its meaning and defines the major ellipse axis. (Remember that true circular polarization is simply a special case of elliptical polarization having equal axes.)

[*Special Note for NEC-2 Users*: The structure of the NEC-2 plane-wave excitation entry is slightly different than the NEC 4 entry. It has the following structure:

Com ID	I1 Type	I2 # Thta angles	I3 # Phi angles	I4 Not used	F1 Th angle to vector	F2 Ph angle to vector	F3 Eta pol. angle	F4 Theta step	F5 Phi step	F6 Axis ratio
EX	1	1	8	0	90	0	90	0	45	0

Note that the NEC-2 version lacks the F7 floating point entry for the electrical field strength, and the default value of 1 V/m always applies. Only 1 incident plane wave is allowed at a time (that is, before a succeeding execution step). If excitation types are mixed before a succeeding execution step, then the program will use only the last excitation type encountered.]

Let's replace the lines of our original model from EX onward with the following (NEC-4) lines (model 88-2).

```
EX 1 1 8 0 90 0 90 0 45 0 0
RP 0 1 361 0000 90. 0. 1.00000 1.00000 0.
EN
```

The EX entry is the one used in the sample. The RP 0 request calls for far field patterns, and the EX 1 loop will produce 8 of them, each one with a plane wave source spaced 45° from the preceding one. Although unnecessary for linear polarization, the RP 0 request varies the XNDA entry. In the original model, the request used 1000 for XNDA, indicating that the output report would be printed in terms of the vertical, horizontal, and total gain. The replacement entry beginning with 0 prints the output in terms of major axis, minor axis, and total gain. This option is significant for elliptical plane waves. For a total-gain-only output desire, the initial digit is not important, but it can become important as one explores the components of the total gain report value.

Receive Patterns

Plane-wave excitation is particularly important to the modeling of structures that do not themselves have energy sources, but which receive radiation from external sources. In some cases, they may re-radiate the energy, such as the case of a cell phone tower that is the right size and too close to a broadcasting tower. At a minimum, such a tower may change the pattern of the broadcast signal from its original shape that was certified to the licensing agency. In other cases, we may be interested in the scattering radiation from an object–a boat, aircraft, or other vehicle, for instance–illuminated by a radar or other signal. The number of potentially interesting and important cases that call for plane-wave excitation is as unending as the growing list of our concerns for the effects of radiation on animal, vegetable, and mineral objects around us.

Under these conditions, we are interested in structures as receiving devices, meaning recipients of energy. For our sample, we shall use the 6-element Yagi antenna as a receiving antenna. The question that next arises is how to derive useful data from the structure. For that purpose, NEC has an interesting command: PT. The PT command has a number of options.

PT -2: All current printed. This also occurs if PT is omitted altogether.
PT -1: Suppress printing of all wire-segment currents.
PT 0: Current printed for specified segments only.
PT 1: Currents printed in a format designed for a receiving pattern.
PT 2: Currents printed in a format designed for a receiving pattern, plus a normalized value for the last segment's current.
PT 3: Only the normalized current is printed.

The PT -1 option is useful when we only need 1 set of current data, but modeling circumstances would normally yield multiple sets of current tables. For example, a frequency sweep for which we need a collection of both theta and phi patterns would require a repetition of the FR command above each RP 0 request. Hence, the FR loop would repeat and normally yield two sets of the current data. Inserting a PT -1 command after the second FR command will suppress the printing of the second set of current data. PT 0 is useful in large models to isolate the current data on specific portions of a model.

However, our present interest lies in the PT entries followed by positive integers. The general format is as follows.

```
Com   I1     I2      I3         I4
ID    Type   Tag #   1st Seg    Last Seg
PT    2      2       1          11
```

The I2 through I4 entries are necessary only for PT 0 through PT 3. In this instance, the sample request asks both for the data on Tag 2, Segments 1-11, and for the normalized value of the data on segment 11. To make sense of this entry, refer to the initial model. Tag 2 represents the Yagi driver, and segment 11 is the segment connected to the feedline–a source segment in the transmitting mode and the focal segment in the receiving mode. A single value of normalized current level would not be of much use. In fact, a very normal use of the PT 1 through PT 3 commands is in conjunction with an EX 1 command. Let's combine these lines into a different set of concluding lines for our initial model (model 88-3).

```
PT 2 2 1 11
EX 1 1 37 0 90 0 90 0 10 0 0
XQ
EN
```

The EX 1 line specifies a loop of 37 excitations, each 10° apart on the phi coordinates, and all at a theta angle of 90° throughout. We might have selected any portion of the coordinate system sphere by specifying both phi and theta increments and steps. In that case, theta changes would occur before phi changes. However, for illustrative simplicity, theta remains constant in this introduction. Note that without a self-executing command to follow the EX 1 line, we need to insert XQ to execute the calculation of the specified currents.

The output file for the PT 2 request has two parts. The first is a list of all currents on the specified segments in terms of relative magnitude and phase angle, given the excitation level of 1 V/m. A PT 1 entry using the same form would produce this first data set. The data table has the following appearance–carried only through the first two excitation coordinates.

```
                - - - RECEIVING PATTERN PARAMETERS - - -
                          ETA=  90.00 DEGREES
                             TYPE -LINEAR
                          AXIAL RATIO= 0.000

  THETA       PHI          -  CURRENT  -          SEG
  (DEG)      (DEG)       MAGNITUDE     PHASE      NO.

   90.00       0.00     1.3360E-26     14.58        22
   90.00       0.00     3.2918E-26     15.61        23
   90.00       0.00     4.9538E-26     16.58        24
   90.00       0.00     6.4222E-26     17.45        25
   90.00       0.00     7.6951E-26     18.24        26
   90.00       0.00     8.7620E-26     18.95        27
   90.00       0.00     9.6115E-26     19.61        28
   90.00       0.00     1.0234E-25     20.21        29
   90.00       0.00     1.0625E-25     20.75        30
   90.00       0.00     1.0782E-25     21.25        31
   90.00       0.00     1.0708E-25     21.70        32
   90.00      10.00     6.9810E-05   -125.22        22
   90.00      10.00     1.7385E-04   -122.98        23
   90.00      10.00     2.6449E-04   -120.90        24
   90.00      10.00     3.4657E-04   -119.02        25
   90.00      10.00     4.1959E-04   -117.32        26
   90.00      10.00     4.8257E-04   -115.76        27
   90.00      10.00     5.3448E-04   -114.32        28
   90.00      10.00     5.7442E-04   -112.97        29
   90.00      10.00     6.0169E-04   -111.71        30
   90.00      10.00     6.1584E-04   -110.51        31
   90.00      10.00     6.1671E-04   -109.36        32
```

We can plot the data for any of the selected segments around the complete phi circle. In fact, we used 37 steps in the model in order to be able to have a graph that started and finished at the same level. If we plot the data for Segment 32 (the absolute segment number for segment 11 on tag 2), we obtain the traces in **Fig. 88-2**. The magnitude and the phase angle have separate plots, since plotting them with a single Y-axis would have given us a virtually flat line for the small changes in magnitude.

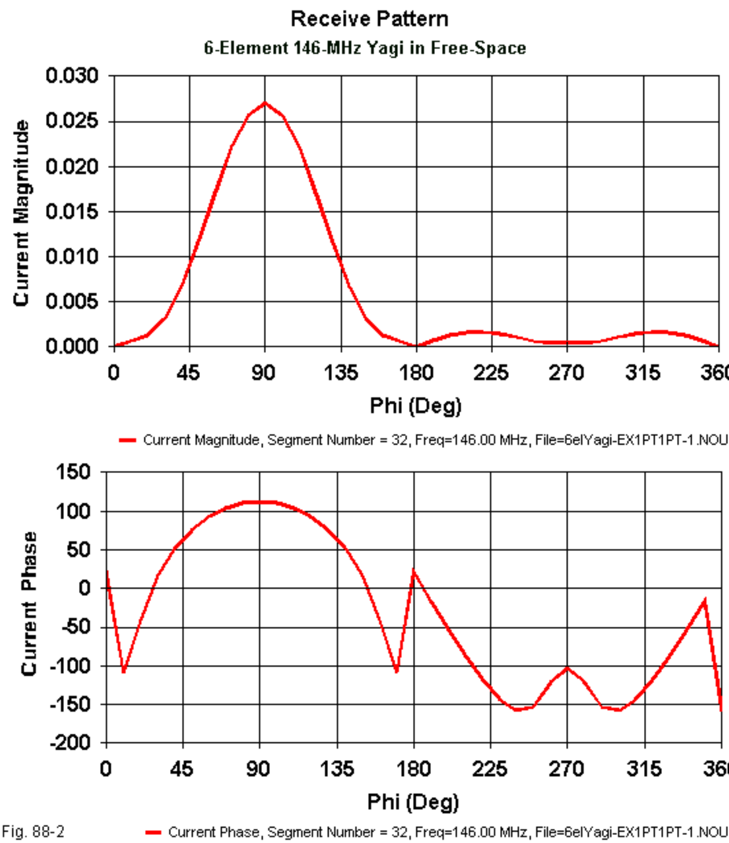

Fig. 88-2

The graph for phase, of course, does not give us the perfect match between 0° and 360°. The result stems from two facts. First, the 0/360° point is in a region where the phase angle is changing very rapidly. So too is the magnitude, but it is in both cases too close to zero to show any variation between the graph-line ends. Second, NEC is subject to a number of occurrences of rounding in the course of its calculations. Hence, what it calls 360 degrees may be fractionally off. In most cases, this variation makes no difference, even visually, to a result. However, in this case, the combination of circumstances yields a visually divergent set of graph-line ends. The reported data for the two points is as follows.

Angle	Magnitude	Phase Angle
0 deg.	1.34E-26	14.58 deg
360	8.39E-14	158.30

With a initial electrical field magnitude of 1 V/m, values below 1E-10 are subject to seemingly wide variations in magnitude and phase angle. However, the actual voltage levels are too low to be significant, whichever level and angle one selects.

The second set of data produced by the PT 2 entry (and the only data produced by a PT 3 entry) includes the normalized values for Tag 2, Segment 11, or absolute segment 32. There will be 37 entries on this list.

As we did for the raw magnitude information, we can plot the normalized data as well. As a first move, let's look at a plot of the feedline segment relative magnitude of current normalized to a maximum value of 1.0. **Fig. 88-3** shows us the plot.

```
 - - - NORMALIZED RECEIVING PATTERN - - -
    NORMALIZATION FACTOR= 2.6983E-02
           ETA=  90.00 DEGREES
              TYPE -LINEAR
           AXIAL RATIO= 0.000
           SEGMENT NO.=   32

THETA      PHI        -  PATTERN  -
(DEG)     (DEG)         DB        MAGNITUDE

 90.00      0.00    -999.99     3.9686E-24
 90.00     10.00     -32.82     2.2856E-02
 90.00     20.00     -26.60     4.6774E-02
 90.00     30.00     -18.80     1.1475E-01
 90.00     40.00     -12.15     2.4691E-01
 90.00     50.00      -7.32     4.3037E-01
 90.00     60.00      -3.94     6.3530E-01
 90.00     70.00      -1.70     8.2236E-01
 90.00     80.00      -0.42     9.5310E-01
 90.00     90.00       0.00     1.0000E+00
 90.00    100.00      -0.42     9.5310E-01
 90.00    110.00      -1.70     8.2236E-01
 90.00    120.00      -3.94     6.3530E-01
 90.00    130.00      -7.32     4.3037E-01
 90.00    140.00     -12.15     2.4691E-01
 90.00    150.00     -18.80     1.1475E-01
 90.00    160.00     -26.60     4.6774E-02
 90.00    170.00     -32.82     2.2856E-02
 90.00    180.00    -236.16     1.5553E-12
 90.00    190.00     -31.35     2.7077E-02
 90.00    200.00     -26.29     4.8478E-02
 90.00    210.00     -24.51     5.9467E-02
 90.00    220.00     -24.35     6.0584E-02
 90.00    230.00     -25.47     5.3265E-02
 90.00    240.00     -28.13     3.9206E-02
 90.00    250.00     -32.55     2.3572E-02
 90.00    260.00     -35.65     1.6502E-02
 90.00    270.00     -35.30     1.7187E-02
 90.00    280.00     -35.65     1.6502E-02
 90.00    290.00     -32.55     2.3572E-02
 90.00    300.00     -28.13     3.9206E-02
 90.00    310.00     -25.47     5.3265E-02
 90.00    320.00     -24.35     6.0584E-02
 90.00    330.00     -24.51     5.9467E-02
 90.00    340.00     -26.29     4.8478E-02
 90.00    350.00     -31.35     2.7077E-02
 90.00    360.00    -230.14     3.1105E-12
```

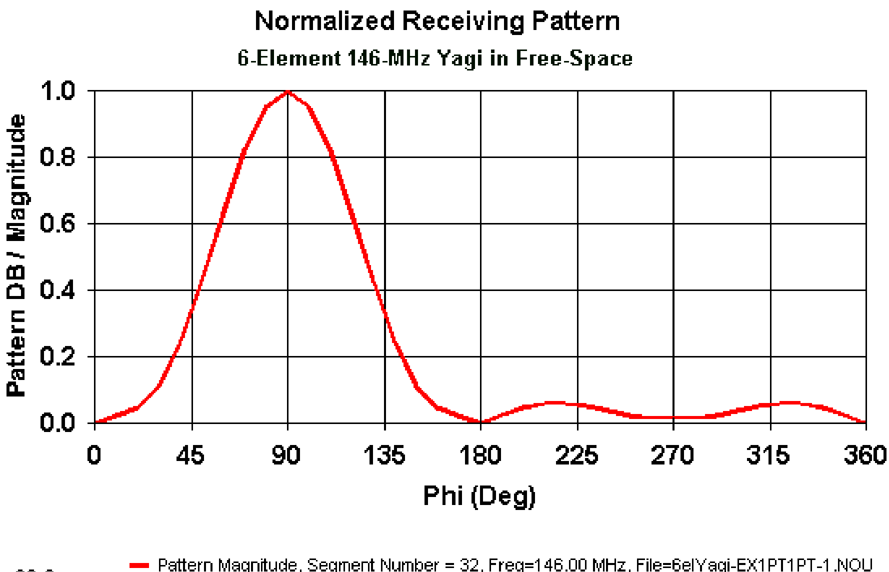

Fig. 88-3

The resulting graph is virtually identical to the upper portion of **Fig. 88-2**, with the exception that the new graph fills the space from bottom to top. This type of graphical and tabular information may be very useful in some cases, but it seems to lack much informative power for our simple example.

Therefore, let's give our illustrative model a question for which the data may be able to yield an answer. Does the pattern shape change between transmit and receive, or is the basic antenna essentially reciprocal, that is, does it have the same pattern regardless of whether it is transmitting or receiving? Note that this question excludes any factors applying to propagation phenomena between transmitting and receiving antennas.

First, we need to convert the polar plot of **Fig. 88-1** into a rectangular plot–only because my software presently only has rectangular plot facilities for receive patterns. The data on such a plot will still be in dB. In fact, let's set the plot limits (Y-axis) at +10 dB and -40 dB to allow the overall pattern variations show themselves with some clarity. The maximum gain of the Yagi is 10.23 dBi, so the peak value will not over-extend the top line by any significant amount.

Second, let's plot the normalized receiving data over a similar 50-dB span: from 0 dB down to -50 dB. While we set this up, let's also note that the normalized receiving plot data uses a 10° increment, while the radiation plot uses a 1° increment. The difference is due to further limitations of the rectangular plot facility in the software that I used.

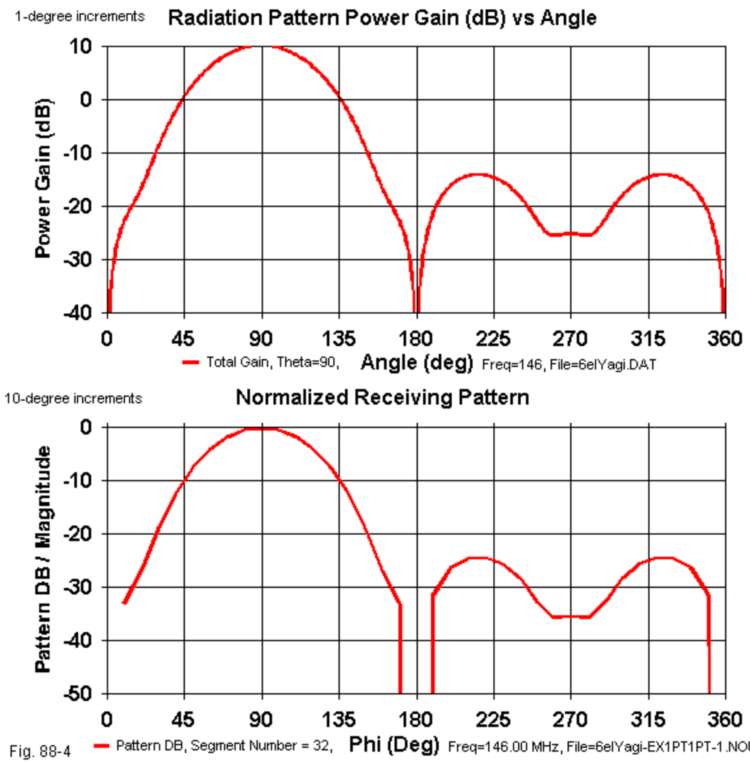

Fig. 88-4

Fig. 88-4 shows the two plots, and their agreement is clearly evident within the limits of the different increments used in this simple demonstration. There is no evidence that the transmitting and receiving plots are any different. Of course, one might expand at least the tabular receiving results to a full 360 degrees using 1° increments and then compare that table with the values in the transmit version radiation table. That, as they say in all of those math texts, is an exercise I am content to leave to the reader.

Combining Modeling Goals in a Single Model

In this exercise, we have looked at two different types of projects involving linear incident plane-wave excitation. The first involved generating patterns–which tend to be of little use here, but in some cases might be useful as re-transmission or scattering patterns–and the second developed tabular data and rectangular plots of received patterns. Each called for a different increment in the phi circle. For patterns, we do not need either the full current set or the restricted set called out by the PT 2 command. For the receive rectangular plots, we need only the current data shown.

The easiest way to achieve these ends is to separate them within the model with the XQ command for the currents and a new EX 1 line before the RP 0 command. See model 88-4.

```
CM 6-el 2M Yagi
CE
GW 1 21 -.514604 0. 0. .514604 0. 0. .0024
GW 2 21 -.5075174 .257302 0. .5075174 .257302 0. .0024
GW 3 21 -.4746752 .3637788 0. .4746752 .3637788 0. .0024
GW 4 21 -.461137 .6585204 0. .461137 .6585204 0. .0024
GW 5 21 -.461137 .9469628 0. .461137 .9469628 0. .0024
GW 6 21 -.443992 1.377137 0. .443992 1.377137 0. .0024
GE 0
LD 5 0 0 0 2.5E+07 1.
FR 0 1 0 0 146. 0
GN -1
PT 2 2 1 11
EX 1 1 37 0 90 0 90 0 10 0 0
XQ
```

```
EX 1 1 8 0 90 0 90 0 45 0 0
PT -1
RP 0 1 361 0000 90. 0. 1.00000 1.00000 0.
EN
```

The techniques shown in the sample model are also useful in other models, even when we wish to use the same EX 1 line but for both theta and phi patterns. We would lose all but the last of the second set of patterns if we do not repeat the EX 1 line, and we can omit the repetitious data with the PT -1 command.

If we want to frequency sweep both sets of results, we must also include a second FR line, and both should reflect the desired sweep. The following lines that revise the end of the model illustrate the principle with a 2-step sweep. Had we omitted the second FR entry, we would obtain far-field plots only for 147 MHz, the last frequency in the FR loop. See model 88-5.

```
FR 0 2 0 0 146. 1
GN -1
PT 2 2 1 11
EX 1 1 37 0 90 0 90 0 10 0 0
XQ
FR 0 2 0 0 146. 1
EX 1 1 8 0 90 0 90 0 45 0 0
PT -1
RP 0 1 361 0000 90. 0. 1.00000 1.00000 0.
EN
```

These notes are not designed to be comprehensive in the treatment of either the EX command or the PT command. However, they do illustrate how the two commands work together to yield receive data and patterns. That is enough to get you started. Undoubtedly task specifications will let you modify the elements of this simple example so that you can obtain the desired results for most modeling efforts that require plane wave excitation and/or receive patterns.

89. Archimedes & Log Spirals for the NEC-4 GH Command

The GH command in NEC-4 permits two kinds of spirals having different initial and terminal radii: Archimedes and log spirals. The user makes his or her selection by a simple choice in the last floating point decimal entry, F7. The following notes are for those who have never encountered spirals of different type or who may have cut the class in which they were introduced. To see what sort of coordinates NEC will produce for each type of spiral requires only that we have a hand calculator with a y^x (y to the x-power) key in addition to the other usual keys. A spreadsheet will be handier in the long run, especially for log spiral calculations.

In columns 61 and 62, we examined the basic formation of helices with regular structures in both the NEC-2 and the NEC-4 versions of the GH command. NEC-2 permitted regular spirals of a single sort, along with the potential for oval turns in which the radius along the X-axis differed from the radius along the Y-axis. NEC-4 reduced the options to circular turns, but offered a choice between spiral types. NEC-4 is able to create flat spirals by setting the height to zero. However, many implementations of the NEC-2 GH command, which was an unofficial addition to the command set, do not allow truly flat spirals.

A typical but simple helical antenna over perfect ground might result in the following model. Note that NEC builds a helix under a single tag #, with all individual segments using the same tag number, whatever the number of segments. As well, NEC builds the helix from Z=0 upward to some positive value of Z. If the modeler desires a different orientation or a wholly different position, the GM command is available to move or rotate the structure–or both. See model 89-1.

```
CM General Helix over Perfect Ground
CE
GH 1 100 5 1 1 2 .001 .001 0
GE 1 -1 0
GN 1
EX 0 1 1 0 1 0
FR 0 1 0 0 299.7925 1
RP 0 181 1 1000 -90 90 1.00000 1.00000
RP 0 181 1 1000 -90 0 1.00000 1.00000
EN
```

The GH line has the following structure.

	I1	I2	F1	F2	F3	F4	F5	F6	F7
GH	1	100	5	1	1	2	.001	.001	0
Cmd	Tag #	# of Segs	No of Turns	Length	Initial Radius	Final Radius	Initial Wire Rad	Final Wire Rad	Spiral Type

Most of the command entries are self-explanatory with the brief notations. However, F1, the number of turns, is a bit special. The number of turns need not be an integer, but may be fractional. As well, if the value for F1 is positive, the helix is right-handed, and if negative, the helix is left-handed. (In NEC-2, the left vs. right option is implemented in F2, the total length of the helix.) If the initial and final helix radii and wire radii are the same, then the entry in F7 makes no difference. However, if F3 and F4 are different, then the spiral-type entry makes a considerable difference in the resulting helix. Here is a table of values for the start-end radii of each turn in terms of coordinates (where Y=0 in all cases) for the sample model shown earlier.

Turn--Seg Numbers		Archimedes X	Z	Log X	Z
1	1	0.0	0.0	0.0	0.0
1-2	20-21	1.2	0.2	1.14869	0.14869
2-3	40-41	1.4	0.4	1.31950	0.31950
3-4	60-61	1.6	0.6	1.51571	0.51571
4-5	80-81	1.8	0.8	1.74110	0.74110
5	100	2.0	1.0	2.0	1.0

Note that the rise in value along the Z-axis is exactly proportional to the increase in radius. Of course, the two spirals do not have the same electrical properties as radiators. However, the purpose of our model and its two variations is not to establish a working antenna, but to sample the two types of available spirals.

The simpler spiral is the Archimedes, with its arithmetically regular structure. In an Archimedes spiral, the radius (R) at any wire junction is given by a simple equation:

R = Ri + (a * theta)

R is the radius under consideration, Ri is the initial radius, a is a constant, and theta is an angle.

Because the change of radius is uniform, we can formulate values for a and theta in a variety of ways, so long as the product of the two yields a progression of values that steps by an increment of 0.01 per segment. (In the model, the units are meters, but the same considerations apply to any system of units.) Theoretically, we should devise a single value for the constant a and vary the value of theta in radians to continuously increase from zero through 5 * 2 * pi or 31.415927. However, our interest in the spiral is only to check the coordinates that the NEC core will assign to wire junctions. So we can change procedures without loss. Every turn has 20 segments in the model, so every radius will occur in increments of 0.05 (turn) of a complete circle. The entire helix will reach a value of 1.0 (turn) at the start of each new turn. The radius will increase by 0.01 per segment or 0.2 per turn (a). At the start of turn 3 (end 1 of segment 41), the angle will have increased through 2.0 cycles (turns) or 40 segments. Theta is 40 * 0.05 = 2.0, and a*theta is 2.0 * 0.2 = 0.4. Added to the initial radius, 1.0, the new radius is 1.4, and the new Z value is 0.4. (In this simple example, I have set the total height to equal the total increase in radius. The change in height, however, will always be proportional to the change in radius.)

We can short-circuit the complexities even further once we know how much the radius and height change for each segment. With 100 segments and a total radius increase of 1.0, along with a total height of 1.0, each segment will increase the radius and the height by 0.01 of the total. Hence, 40 segments times 0.01 = 0.4. Since the height begins at zero, the new height is 0.4. Since the radius begins at 1.0, the new height is 1.0 + 0.4 or 1.4. If all that we ever use are Archimedes spirals, then the simplified method of checking coordinates will suffice.

For those who have lost–or never had–an introduction to log spirals–the basic formulation may seem deceptively simple:

R = Ri*a^theta

R is the radius under consideration, Ri is the initial radius, a is a constant, and theta is an angle. The constant, a, is not the same constant as it is for an Archimedes spiral with its regular or uniform variation along the length of the helix. **Fig. 89-1** compares the appearance of both types of spirals. Both spirals have the same initial and end radii and the same overall length from bottom to top. The uniformity of the increase of the Archimedes spiral is readily apparent both in the top view (or the bottom, depending on your position) and in the side view. In contrast, the log spiral not only increases in diameter as we move upward, but the rate of radius increase and the rate of height increase also go up along the progression from bottom to top.

As a side note, we shall maintain a GH-orientation in all that follows. GH helices initially form from the plane of the X and Y coordinates, that is, from Z=0. In addition, GH helices in NEC-4 have radii centered at X=0 and at Y=0. The GM command is available in NEC to allow the modeler to move the helix or to turn it to any angle possible within the Cartesian coordinate system, so we shall make a like assumption. Hence, all spirals that will appear in these notes will begin with their initial or minimum radius at the bottom and the maximum radius at the top, and the spiral length will be measured from Z=0 upward.

A modeling caution to observe is that both types of spiral increase the length of segments as they move upwards toward a larger radius. The increase from one segment to the next is normally quite small for helices with at least 20 segments per turn. In many cases it is more critical to keep the segments aligned from turn-to-turn, especially if the spiral is tight.

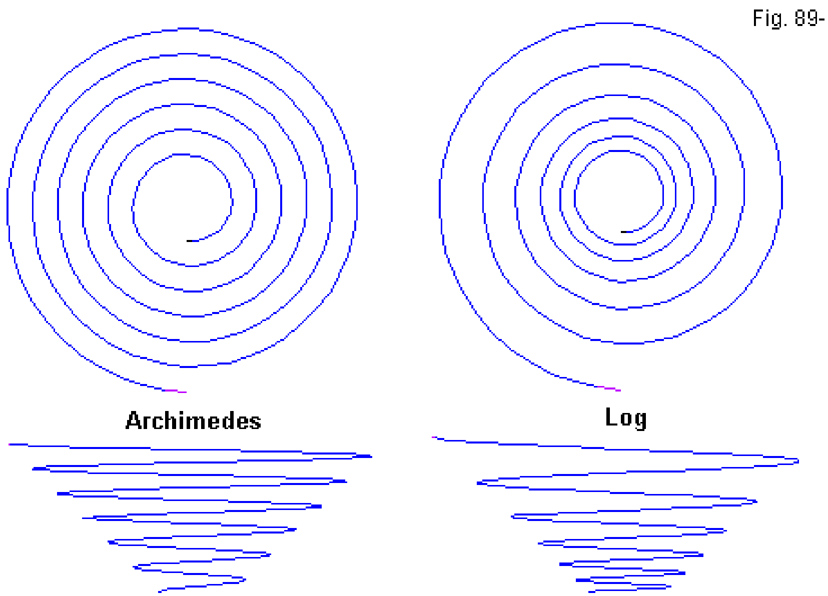

A Comparison of Archimedes and Log Spirals

Fig. 89-2 shows a well-aligned spiral with an even number of segments along side a less-well aligned spiral. In all spirals, performing an average gain test (AGT) will reveal whether segment misalignment introduces any significant degree of model inadequacy. The very close spacing of turns in the sample model results in rather inadequate models over perfect ground, with the bulk of the poor AGT values resulting from placing the source (EX) on the segment adjacent to ground. It fails to have segments on each side of the source segment that are as equal in length to the source segment as possible, and the segment meets the perfect ground at an oblique angle rather than vertically. Nevertheless, these faults do not affect our calculation of the running dimensions of a spiral of either the log or Archimedes sort. To check the effects of the spiral itself, without the effects of the source position, place the source on a segment other than the first segment.

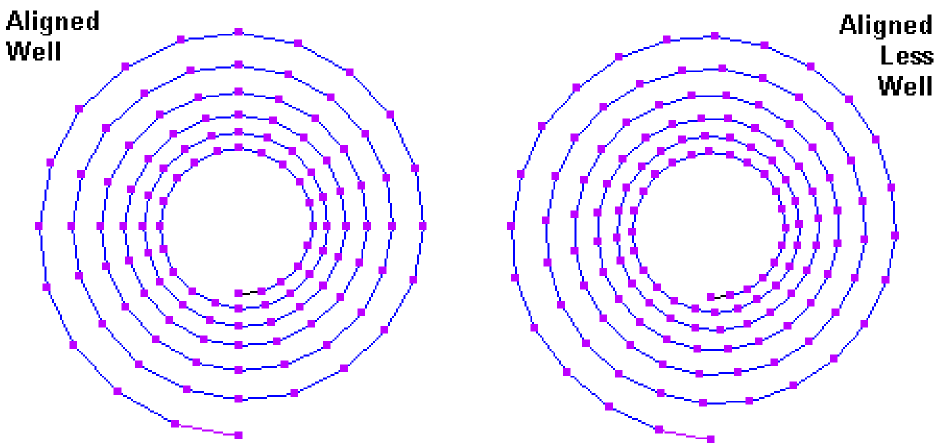

Segment Alignment Within Spirals

Fig. 89-2

The calculation of both a and theta in the equations for the radius at any point along a log spiral is intrinsically interesting, especially if we adapt it to models of such spirals formed from straight wires under the NEC-4 GH command. The procedure to follow is independent of the system used within the core itself. Any system of calculations that yields values for a and theta should yield radius values or their equivalent in X and Y coordinates that are numerically precise relative to those produced by the core. To obtain a complete report on the spiral, we need to be prepared to enter the following information (all within the same units of measure, of course).

Rmax–the maximum radius of the spiral.
Rmin=Ri–the initial or minimum radius of the spiral.
s–the number of segments per turn of the helix.
t–the total number of turns in the helix.

Lt–the total length of the spiral.
theta–the segment of interest, using end 2 of the segment.

Since end 1 of the first segment is at a helix length of zero, and the radius at zero length is Rmin, extended along the +X direction. Therefore, all further segment references apply to end 2 of the segment. Hence, the last segment calculated will yield the final radius and the final height of the spiral.

To obtain a progression of radii, we need to obtain values for both a and theta. Finding theta is the easier task, since we have already entered it as the total number of segments in the spiral. However, we may also define theta' as the increment or step around the circle taken by each segment. Because we are working with increments of the circle defined by the segments, we may bypass degrees and radians and take theta' in terms of the amount of the circle intersected by the ends of any given segment.

theta' = 1/s

This is one step in the process of finding the value of a from the data that we are ready to enter. The next step requires that we find the ratio of maximum to minimum radius, Rr.

Rr = Rmax/Rmin

We also need the ratio of the segments per turn (s) to the total number of turns (t) to define an intermediate term, n.

n = s/t

Now let m be a function of Rr and n.

m = Rr^n

Then a becomes a function of m and theta'. We use the square of theta' as the exponent for m to arrive at a, which is also the radius increment for the first segment of the series forming the spiral.

a = m^(theta'^2)

The composite form of the equation sequence is

a = ((Rmax/Rmin)^(s/t))^((1/s)^2)

I have used spreadsheet notation because progressive superscripts are almost impossible to read and because the form allows direct transfer to a spreadsheet of your choice. Having values for all of the needed terms, Ri (or Rmin), a, and theta, we may calculate the new radius anywhere along the spiral. All that we need to do is to enter theta, the segment number in which we are interested.

R = Ri*a^theta

As well we can easily determine at what turn (or fraction of a turn) the segment occurs.

turns = theta'*theta

For any spiral length, we can determine the length up to segment theta (Lth) by beginning with the total length of the spiral, Lt, which we entered initially. Theoretically, the spiral rises in height in exact proportion to the increase in the radius.

R-Rmin/Rmax-Rmin = L-Lmin/Lmax-Lmin

R is the radius at any segment, theta, and L is the spiral length up to that same segment. Lmax is the total length, Lt. Since Lmin is zero in the GH formation of a spiral, then Lth, the length at segment theta, is readily determined.

Lth = ((R-Rmin)*Lt)/(Rmax-Rmin)

The calculations given for the radius in these notes result in values that exactly coincide with those generated by the NEC-4D core that I use. However, the values produced by that core for the length of the spiral up to end 2 of any segment sometimes show a slight variance, suggesting that the core uses another approach to length determination (or the Z coordinate). The variance is greatest in the first turn of the spiral and appears in the third significant digit. Beyond that point, the variance appears in the fourth significant digit. There are certain ratios of Rmax to Rmin where no variance appears at all. Functionally, the differences do not make a difference, but the numerical variance needs to be noted.

Finally, we can easily calculate the end-2 coordinates of the segment that we have entered as theta. First define the angle (A) of the specified segment in radians.

A = 2*pi*theta*theta' = (2*pi*theta)/s

Then the X, Y, and Z coordinates follow.

X = R cosA
Y = R sinA
Z = Lth

If it were not easy to place this progression of straightforward calculations into a spreadsheet page, the exercise would perhaps have only academic interest as a means to checking some particular set of coordinates of a modeled log spiral formed by the GH command. **Fig. 89-3** shows a typical spreadsheet from my collection. I normally keep two working columns of data for entry and calculation, where a label indicates the entered data. I could lock the column marked sample, since I do not vary it. Instead, I use it for reference, that is, to remind myself of the calculation procedures and what data that I need to enter for a spiral under analysis. I also retain the Sample model on file to refresh myself from time to time. Those who deal daily with spirals can, of course, omit these memory aids.

Log Spirals for NEC-4 GH Command							Fig. 89-3
				Sample		Work 1	
Radius							
R = Ri a^theta			Rmax	3	Enter	4	Rmax
			Rmin=Ri	1	Enter	3	Rmin=Ri
Rr = Ratio	Rr = Rmax/Rmin		Rr	3		1.333333	Rr
s=segs/turn			Segs/Turn	20	Enter	50	Segs/Turn
t=no turns			No Turns	6	Enter	6	No Turns
n=s/t			n	3.333333		8.333333	n
m=Rr^n			m	38.94074		10.99401	m
theta' = angular increment				0.05		0.02	
a = m^(theta'^2)			a	1.009197		1.000959	a
theta	No segs (end 2)		theta	100	Enter	72	theta
turns	theta' * theta (no. of segments)			5		1.44	
R	R = Ri a^theta		R	2.49805		3.214449	R
Length (or Height)		(Presumes that helix starts at Z=0)					
Lt = total length			Lt	1	Enter	4	Lt
Lth = length at theta			Lth	0.749025		0.857796	Lth
	Lth=((R-Rmin)*Lt)/(Rmax-Rmin)						
Coordinates		(Presumes that helix is centered on X=0 and Y=0)					
A = angle at selected segment number							
	A = 2*PI*theta*theta'			31.41593		9.047787	
X = R*cosA			X	2.49805		-2.98872	X
Y = R*sinA			Y	5.8E-15		1.183318	Y
Z = Lth (above Z=0)			Z	0.749025		0.857796	Z

The following two lines are the GH entries for the Sample and the Work spirals in **Fig. 89-3**. The remaining model lines are identical to those in the initial example.

```
Sample:  GH 1 120 6 1 1 3 .001 .001 0
Work:    GH 1 300 6 4 3 4 .001 .001 0
```

The added utility of the spreadsheet is for modelers who wish to model a spiral but who have only the GH entry of NEC-2 with which to work. Most helix-makers attached to NEC-2 programs only create uniform helices in which the radius at the top and the bottom are the same. However, one might expand the spreadsheet to create a list of wires and coordinates for each value of theta, that is, for each segment comprising a spiral of any size whatsoever. Since the equations for creating an Archimedes spiral are so straightforward, I did not include them in this spreadsheet, but if the modeler is interested in both Archimedes and log spirals, the additions are simple enough to make. With judicious spreadsheet planning, one might even create columns for either direct or indirect transfer to a NEC file as a set of wire coordinates. Of course, such a construct would consist of a separate 1-segment wire for each new straight-wire section of the spiral. (In contrast, the GH entry produces a new wire segment for each spiral section, all under a single tag number.) However, the end result would not differ in appearance from the helices created by existing uniform-radius helix makers associated with commercial implementations of NEC–except, of course, for the coordinates that transform a helix into a spiral.

The spreadsheet table of wires might have the following appearance, with variations customized to the input system of the version of NEC being used.

		Transfer Data						Reference Radius	
		End 1			End 2				
Cmd	Wire#	X	Y	Z	X	Y	Z	End 1	End 2
GW	1	1.0000	0.0000	0.0000	0.9598	0.3119	0.0046	1.0000	1.0092
GW	2	0.9598	0.3119	0.0046	0.8240	0.5986	0.0092	1.0092	1.0185
GW	3	0.8240	0.5986	0.0092	0.6042	0.8315	0.0139	1.0185	1.0278
GW	4	0.6042	0.8315	0.0139	0.3205	0.9865	0.0187	1.0278	1.0373
GW	5	0.3205	0.9865	0.0187	0.0000	1.0468	0.0234	1.0373	1.0468
etc. . . .									

Transfer of the spreadsheet data will depend upon the input system of the NEC implementation. A standard ASCII input system will require entry of the command name (GW) as well as the wire number, the number of segments for each wire (1), the End-1 and End-2 coordinates, and a wire radius. You can place these on the spreadsheet list and transfer complete lines of entry without need for later "touch-up." Other systems may not need either the command name or the wire number, although almost all will need the number of segments and a wire radius or diameter. In some systems, you can add these later with block operations.

Most spreadsheets separate data columns with Tabs. Some NEC implementations will accept Tabs; others will not. If you need to get rid of the Tabs, you can transfer the blocked data to a word processor. Often, the "unformatted text" or similar option will prevent the inclusion of the spreadsheet cell outlines while preserving the Tabs. Whether the word processor retains the Tabs or replaces them with multiple Spaces, you may use the global replace function to convert either one to a single space between entries on a line. (Using the same number of digits per entry, even if zeroes, simplifies the replacement procedure.) If some of these steps sound involved, compare the process to hand entering dozens of individual numbers without error. The bottom line is that it is possible to create wire lists that form either Archimedes or log spirals (flat or extended) in NEC implementations that lack the NEC-4 GH command.

Since each application is likely to differ in needs, I shall leave further extensions of the spreadsheet calculations to you. If these notes have acquainted you with the differences between an Archimedes and a log spiral in both visual and calculation terms, they have served their purpose. The NEC-4 GH entry offers considerable flexibility in creating helical shapes. Having a choice of spiral types is an advantage over the usual NEC-2 GH entry offerings, although the NEC-4 entry did give up the ability to create directly oval helices in the process.

90. An Orientation to NEC Near Fields Part 1. NEC-2 Input Basics & Simple Outputs

Beginning modelers tend to focus on the far-field properties of antennas and to overlook near-field data. There are both good and bad reasons for this situation. First, not every entry-level program makes the near-field data available. Second, reading and using the inherent NEC-2 data output can be daunting in the absence of an adequate orientation to that data. Third, compromises in some programs relative to the Cartesian coordinate system and the inherent NEC output angle system can generate some confusion. Fourth, little effort has gone into making the near-field interface more user friendly. Fifth, outside of one piece of data, not inherent to the NEC-2 core, the remainder of the near field data is relatively foreign and therefore useless to the beginning modeler. These are not the only reasons we might give for the disuse into which near field data falls among relatively new modelers, but the list is long enough for an introduction to a partial corrective for the situation.

Most practical applications of antennas tend to follow compass headings and elevation angles. We record heading in a clockwise fashion around a compass rose to derive azimuth bearings. Similarly, we count degrees upward from the horizon to arrive at elevation angles. However, NEC employs a true Cartesian system of coordinates that defines points by reference to X-, Y-, and Z-axes. When we translate the coordinates to headings and angles, we count in a counterclockwise direction in which 0° lies along the X-axis of the coordinate graph. Hence, +Y is at 90°, -X at 180°, and -Y at 270°. NEC does not inherently use an elevation system that counts from the ground up, but instead uses theta angles measured from the zenith downward. **Fig. 90-1** shows the correct system. Note that since a standard theta angle would run from the zenith downward, it would be correct to count both horizon points as 90°. The continuous count for a 360° theta circle is only one of several schemes used.

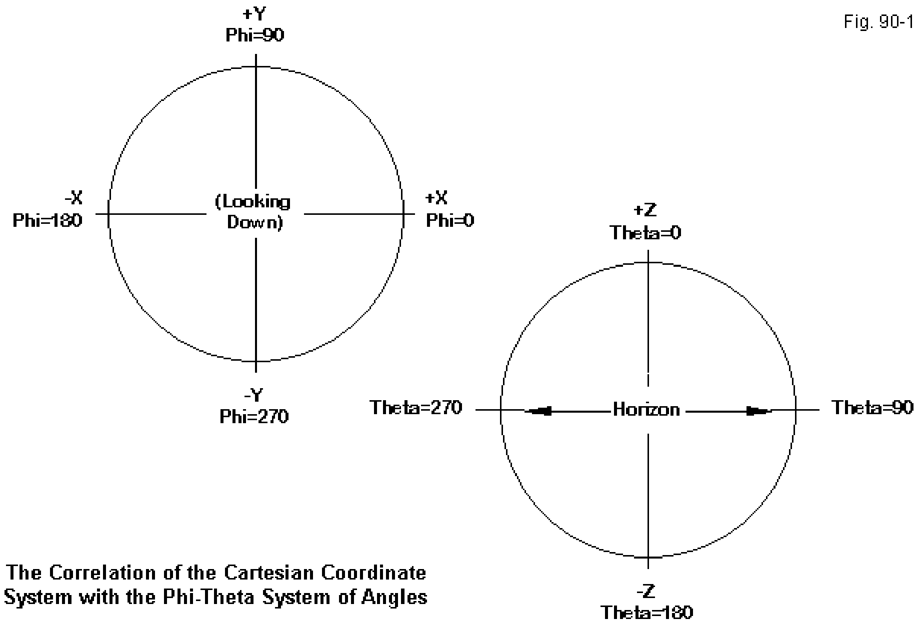

Fig. 90-1 uses two separate circles to sort out the elements of the coordinate and angle systems. It is difficult to adequately present the 3-dimensional system on a flat or 2-dimension surface. However, **Fig. 90-2** provides an often-used 3-diminsional conventionalization.

My reason for not using the type of sketch shown in **Fig. 90-2** is that it takes an expert graphic artist to select just the correct angles for the three axes in order to portray the observation point at a position that is intuitively correct to the reader. Lacking the services of such a skilled artisan, I shall rely on the simpler 2-circle sketch to portray positions.

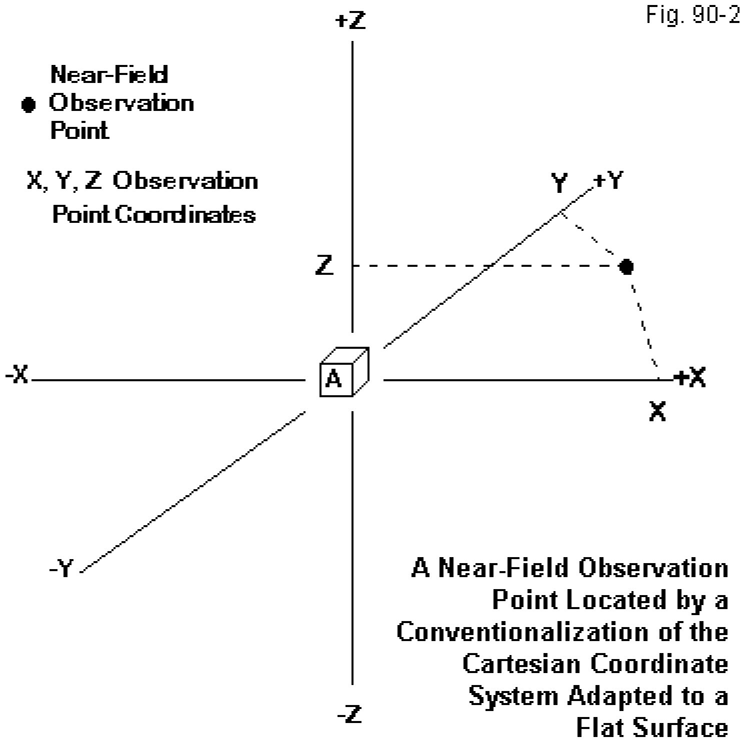

One of the reasons that NEC users sometimes never get clear on how to manipulate the inputs for near fields is that entry-level programs try as best they can to accommodate the user's likely orientation toward azimuth (compass rose) headings and elevation angles. The conversion to elevation angles is simple enough, since the elevation angle = 90 (degrees) - theta (or theta = 90 - elevation). Azimuth is another matter. Some entry-level programs simply switch the outer ring number without altering the phi pattern and call the result an azimuth pattern. Other programs use a phi pattern, but label it as an azimuth pattern. Still other programs simply use and label the patterns as phi patterns as they emerge from the NEC output file. Given the morass of potentially confusing orientations and the fact that near-field entries require a single clear and unambiguous orientation, let's take a problem and work through it.

Entry Using Cartesian or Rectangular Coordinates

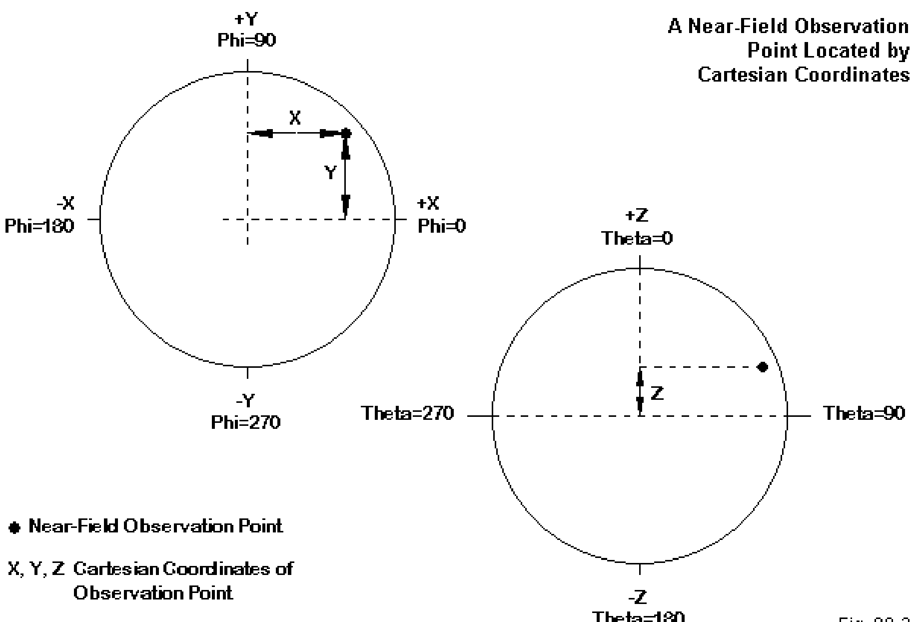

Fig. 90-3 shows one of the two ways of locating an observation position for a near-field request. Following Cartesian convention, the observation location is lo-

cated by values for X, Y, and Z. Now let's translate that into an actual model using these conventions. See model 90-1.

```
CM NE/NH test
CE
GW 1 11 0 0 .25 0 0 .75 .001
GE 1 0 0
GN 2 0 0 0 13.0000 0.0050
EX 0 1 6 00 1 0
FR 0 1 0 0 299.7925 1
NE 0 1 1 1 5 10 5 1.0 1.0 1.0
NH 0 1 1 1 5 10 5 1.0 1.0 1.0
EN
```

The NE and NH lines provide the near-field entry requests for electrical and magnetic field strengths. The preceding lines define a simple 2-mm-diameter vertical dipole that is 0.5-ë long, with its base 0.25-ë above average ground, as specified by the GN entry. The frequency is 299.7925 MHz. Since we are requesting only a pair of single-frequency near-field reports, they will self-execute.

Notice that the near field requests separate the electrical and magnetic field solution requests. Otherwise, they are identical in form. Let's expand the form so that we can separate the NEC-2 entries in this model. Since the NE and NH commands occur after the closure of the geometry section of the model, the dimensions must be in meters, regardless of the units used and scaled within the geometry section of the model.

Cmd	Cart/	No. of Points			Coordinate			Step Size		
	Spher	X	Y	Z	X	Y	Z	X	Y	Z
NE	0	1	1	1	5	10	5	1.0	1.0	1.0
NH	0	1	1	1	5	10	5	1.0	1.0	1.0

With respect to the entry of Cartesian or rectangular coordinates to specify the NE and NH requests, NEC-2 and NEC-4 use identical command entries.

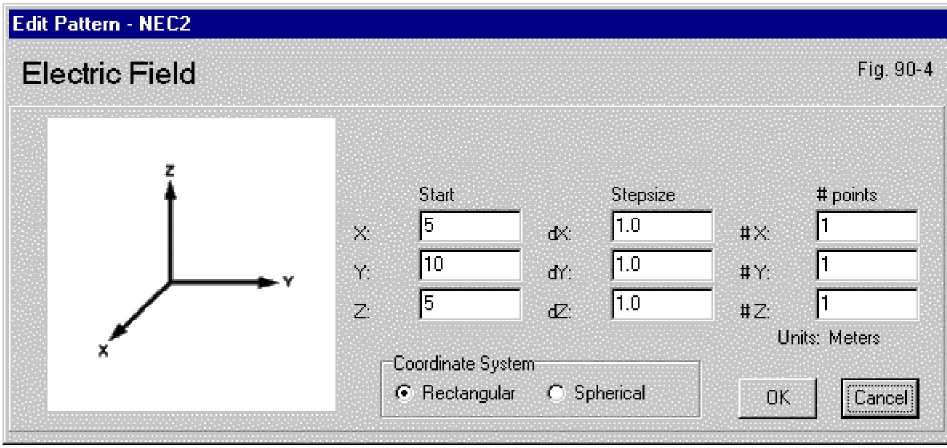

Fig. 90-4 shows a help screen used by NEC-Win Pro to form one of the near-field command entries. The use of "1" for the number of points in each of the three coordinate directions does not yield 3 observation points, but only a single point defined by the three coordinates. (We shall briefly examine multiple points before we quit.) One of the uses made of single-point near-field requests is to satisfy certain government regulations regarding the magnitudes of electrical and/or magnetic fields in the vicinity of antennas used by various services, including the amateur service. The output report–if within limits set by regulations–will satisfy the requirements of those regulations for a large variety of well-designed antenna models. We can glean the requisite data from the output table for the near-field request, as sampled below for this model.

```
**** NEAR ELECTRIC FIELDS ****
**** Frequency = 299.79, File: C:\ant\NE-NH\amod90-6.nec

        -  LOCATION  -                      -  EX  -              -  EY  -              -  EZ  -          - PEAK FLD -
     X          Y           Z          MAGNITUDE   PHASE     MAGNITUDE   PHASE     MAGNITUDE   PHASE      MAGNITUDE
   METERS     METERS      METERS        VOLTS/M   DEGREES     VOLTS/M   DEGREES     VOLTS/M   DEGREES      VOLTS/M
  5.000000  10.000000   5.000000     6.6689E-03    25.21    1.3338E-02    25.21   3.8323E-02  -149.78    4.1105E-02

**** NEAR MAGNETIC FIELDS ****
**** Frequency = 299.79, File: C:\ant\NE-NH\amod90-6.nec

        -  LOCATION  -                      -  HX  -              -  HY  -              -  HZ  -          - PEAK FLD -
     X          Y           Z          MAGNITUDE   PHASE     MAGNITUDE   PHASE     MAGNITUDE   PHASE      MAGNITUDE
   METERS     METERS      METERS         AMPS/M   DEGREES      AMPS/M   DEGREES      AMPS/M   DEGREES       AMPS/M
  5.000000  10.000000   5.000000     9.7519E-05  -150.52    4.8760E-05    29.48   5.0538E-11    18.32    1.0903E-04
```

For the simple purpose of the presumed near-field requests, we are interested in 2 parts of the output report. First, the observation location coordinates appear in the report and serve as a check on the accuracy of our input. In more extensive reports, the coordinate locations would define separate observation points within the range of our request.

Second, the last entry in each line lists the peak field magnitude in volts/meter for the electric field and in amperes/meter for the magnetic field. Since this report emerges directly from the NEC output file, the values are in peak volts/meter. Compare those lines with the following ones from an identical EZNEC model.

```
          --------------- NEAR-FIELD PATTERN DATA ---------------

 Frequency = 299.793 MHz
 Power = 0.0046119 watts
 Max field = 0.0290653 V/m RMS
  at X,Y,Z = 5, 10, 5 m

 Electric (E) Field (V/m RMS)

 X (m)      Y (m)      Z (m)       Ex Mag     Ey Mag     Ez Mag     Etot
 5          10         5          .00471558  .00943117  0.0270987  0.0290653


 Frequency = 299.793 MHz
 Power = 0.0046119 watts
 Max field = 7.84369E-05 A/m RMS
  at X,Y,Z = 5, 10, 5 m

 Magnetic (H) Field (A/m RMS)

 X (m)      Y (m)      Z (m)       Hx Mag     Hy Mag     Hz Mag     Htot
 5          10         5          7.0156E-5  3.5078E-5  0          7.8437E-5
```

The “Etot” and “Htot” columns correspond to the “Peak Field” columns in the first report, but the values under those columns differ radically. Actually, they differ not at all once we realize that the peak voltage/meter (and current/meter) of the

NEC output report have been converted into RMS values in the EZNEC report. The SQRT(2) or 1.4142 times the RMS values will yield values very close to those of the NEC-Win Pro output, allowing for the slight differences in actual numbers that results from using different FORTRAN compilers.

We shall note in passing that the original NEC-2 core did not yield a total or peak magnitude column. However, many implementations of NEC-2 have added that calculation because it is fundamentally useful, even to casual modelers.

Although these calculations yield values called near-field reports, they differ from those shown in most basic texts under near-field calculations. In most texts, near-field equations extract from the total field equations those terms most relevant to strict near-field phenomenon calculation. The result is a simpler set of equations to manipulate. Since NEC must ultimately deal with the total field, including all components, the near-field reports are for the total solution, including surface-wave components.

Entry Using Spherical Coordinates

Let's now enter the same problem using the spherical coordinate entry option. The rudiments of this option appear in **Fig. 90-5**. The key ingredients of the alternative entry system are the radius-line from the coordinate center to the observation location, the phi angle pf the observation point, and the theta angle of that point. If we wish to use the same observation position, we shall have to do some calculating. I shall show all results to the display limits of my hand calculator, since I wish the output report to coincide as precisely as possible with the first model. You may round numbers as your task dictates or permits.

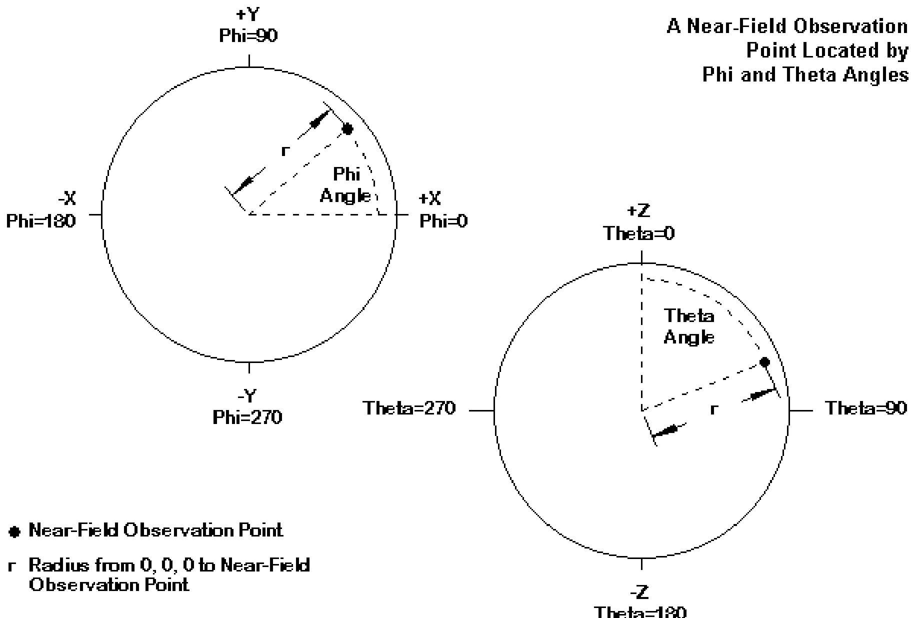

Fig. 90-5

1. Beginning with the original X, Y, and Z coordinates, we can calculate the radius in standard vector form, Hence, the radius r = SQRT(X^2 + Y^2 + Z^2). For X=5, Y=10, and Z=5, r=12.247449.

2. The phi angle is a function of the X and Y coordinate, such that Y/X = tan(phi). Hence, phi = arctan(Y/X) or 63.434949 degrees–and NEC wants the angle in degrees.

3. The theta angle is a function of the radius R and the Z coordinate. It tends to be easier to start with an elevation angle, such that el=arcsin(Z/r) degrees, and theta=90-el degrees, that is 65.905157 degrees.

See model 90-2.

```
CM NE/NH test
CE
GW 1 11 0 0 .25 0 0 .75 .001
GE 1 0 0
GN 2 0 0 0 13.0000 0.0050
EX 0 1 6 00 1 0
FR 0 1 0 0 299.7925 1
NE 1 1 1 1 12.247449 63.434949 65.905157 1.0 1.0 1.0
NH 1 1 1 1 12.247449 63.434949 65.905157 1.0 1.0 1.0
EN
```

The sample model uses the same antenna and varies only the NE and NH requests to coincide with the coordinate system for entry. The following lines expand the entries with notations for the meaning of each entry in each line.

Cmd	Cart/	No. of Points			Coordinate			Step Size		
	Spher	r	phi	theta	r (radius)	phi angle	theta angle	r	phi	theta
NE	1	1	1	1	12.247449	63.434949	65.905157	1.0	1.0	1.0
NH	1	1	1	1	12.247449	63.434949	65.905157	1.0	1.0	1.0

For each sequence of r, phi, and theta, phi precedes theta in the entry. This order applies to NEC-2. However, NEC-4 reverses the phi and theta positions so that the order is r, theta, phi. For now, we shall restrict ourselves to NEC-2.

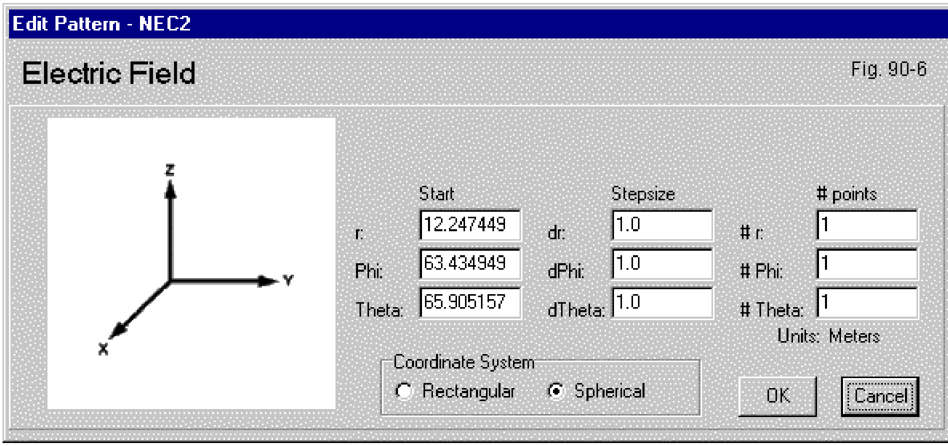

Fig. 90-6 presents the entry set-up screen for the present model to correspond with the earlier model using Cartesian coordinates. Both screens request data inputs that track exactly what will appear in the entry line. However, there is an alternative way to request the input data that some users find more convenient if their request involves more than one point along an axis or other line. Instead of requesting the starting values, the increment, and the number of points, the system requests the start values, the stop values, and the number of points. EZNEC uses such as system, as shown in **Fig. 90-7**, and then internally converts the request to the form required by the core.

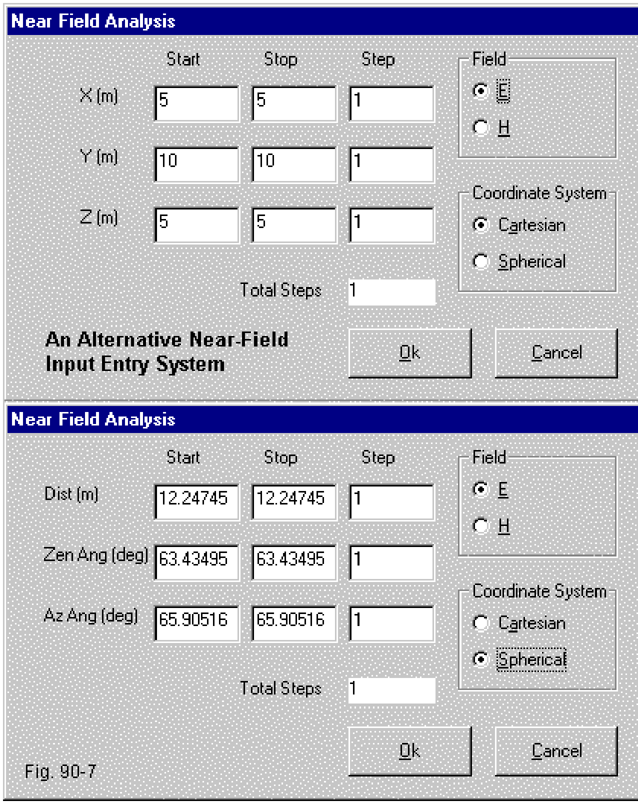

Fig. 90-7

To see if we have done our set-up calculations correctly, let's examine the output report for this new model in NEC-Win Pro format.

```
**** NEAR ELECTRIC FIELDS ****
**** Frequency = 299.79, File: C:\ant\NE-NH\amod90-6.nec

        -  LOCATION  -                  -  EX  -             -  EY  -             -  EZ  -          - PEAK FLD -
     X          Y           Z       MAGNITUDE   PHASE    MAGNITUDE   PHASE    MAGNITUDE   PHASE     MAGNITUDE
   METERS     METERS      METERS     VOLTS/M   DEGREES    VOLTS/M   DEGREES    VOLTS/M   DEGREES     VOLTS/M
  5.000000  10.000000   5.000000   6.6689E-03    25.21  1.3338E-02    25.21  3.8323E-02  -149.78   4.1105E-02

**** NEAR MAGNETIC FIELDS ****
**** Frequency = 299.79, File: C:\ant\NE-NH\amod90-6.nec

        -  LOCATION  -                  -  HX  -             -  HY  -             -  HZ  -          - PEAK FLD -
     X          Y           Z       MAGNITUDE   PHASE    MAGNITUDE   PHASE    MAGNITUDE   PHASE     MAGNITUDE
   METERS     METERS      METERS      AMPS/M   DEGREES     AMPS/M   DEGREES     AMPS/M   DEGREES      AMPS/M
  5.000000  10.000000   5.000000   9.7519E-05  -150.52  4.8760E-05    29.48  5.0538E-11    18.32   1.0903E-04
```

The first thing to notice is that the “Peak Field” magnitude reports are identical to those produced using the Cartesian coordinate system for entry. The result is expected the moment that we also examine the observation location data at the left end of each line. The values for X, Y, and Z are identical to those in the Cartesian output report. That is the second notable feature of near-field reports: regardless of which input system we use, the output report is always in terms of Cartesian coordinates for the distinct observation points.

For single-point reports, it makes no difference which input system we use, and so the best advice is to choose the simplest based on the data available. Suppose that we are calculating the field intensity of an antenna at a certain height above ground with an observer some specified distance away in a clear field. In such a case, we can often simplify the problem by placing the line from the antenna support along a model geometry axis for either an X or a Y entry on the Cartesian system. The height of the antenna above ground becomes a simplified Z-axis entry. We do not have to pre-calculate the angular distance from the antenna down to the observer. Hence, for many simple cases, the Cartesian entry system is the easier to use.

However, let’s attend to the limitations of the model. It presumes that the antenna is oriented correctly relative to the observation point. For a vertical dipole in a clear field, the presumption may hold. However, if the antenna is directional in any way, the presumption may not hold unless the orientation is modeled into the geometry. Note also that the hypothetical case presumes a clear field with no absorbing, refracting, or reflecting objects within a relevant distance from either the antenna or the observation point. In the situations of real antennas, we rarely encounter this ideal condition. A fully adequate model would require us to model reasonable approximations of all such objects along with the antenna itself.

Which Input System?

It would be easy to summarize the cases for the use of each input system in a couple of lines.

Use the Cartesian coordinate input system wherever you require a field of observation points spaced apart by equal or otherwise specified increments of distance.

Use the spherical coordinate input system whenever you need a field of observation point separated by equal angular increments or when you need a set of observation points along equal increments in the direction of the radius line.

```
CM NE/NH test
CE
GW 1 11 0 0 .25 0 0 .75 .001
GE 1 0 0
GN 2 0 0 0 13.0000 0.0050
EX 0 1 6 00 1 0
FR 0 1 0 0 299.7925 1
NE 0 3 3 3 5 10 5 1.0 1.0 1.0
EN
```

The initial test model uses Cartesian coordinates for the electric field only to illustrate the “box” effect produced by their use in multiple steps. **Fig. 90-8** shows to entry formation screen to clarify what the model requests. See model 90-3.

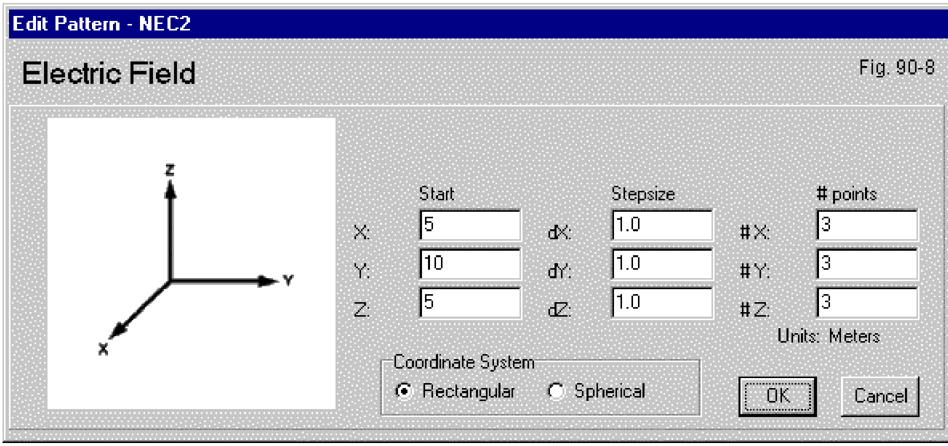

For each axis, the NE requests wants 3 steps at the indicated increment of 1.0-meter each. Hence, the output report will yield 27 lines. For some purposes, this type of report, as illustrated by the following lines, may be just what a task dictates. However, we may need only a few of the values produced out of the entire set of lines.

Note that NEC uses an order of precedence in the rate of change of each coordinate, with the X-coordinate changing value most rapidly, followed by the Y- and finally the Z-coordinate.

**** NEAR ELECTRIC FIELDS ****
**** Frequency = 299.79, File: C:\ant\NE-NH\amod90-4-3.nec

- LOCATION -			- EX -		- EY -		- EZ -		- PEAK FLD -
X	Y	Z	MAGNITUDE	PHASE	MAGNITUDE	PHASE	MAGNITUDE	PHASE	MAGNITUDE
METERS	METERS	METERS	VOLTS/M	DEGREES	VOLTS/M	DEGREES	VOLTS/M	DEGREES	VOLTS/M
5.000000	10.000000	5.000000	6.6689E-03	25.21	1.3338E-02	25.21	3.8323E-02	-149.78	4.1105E-02
6.000000	10.000000	5.000000	7.4387E-03	-136.47	1.2398E-02	-136.47	3.8370E-02	48.47	4.0987E-02
7.000000	10.000000	5.000000	7.9924E-03	40.01	1.1418E-02	40.01	3.8327E-02	-135.21	4.0767E-02
5.000000	11.000000	5.000000	5.8165E-03	81.69	1.2796E-02	81.69	3.8346E-02	-93.49	4.0826E-02
6.000000	11.000000	5.000000	6.5235E-03	-69.28	1.1960E-02	-69.28	3.8250E-02	115.36	4.0590E-02
7.000000	11.000000	5.000000	7.0459E-03	118.42	1.1072E-02	118.42	3.8054E-02	-57.17	4.0243E-02
5.000000	12.000000	5.000000	5.0622E-03	131.45	1.2149E-02	131.45	3.8072E-02	-44.11	4.0272E-02
6.000000	12.000000	5.000000	5.7020E-03	-10.04	1.1404E-02	-10.04	3.7853E-02	174.19	3.9932E-02
7.000000	12.000000	5.000000	6.1871E-03	-172.23	1.0607E-02	-172.23	3.7536E-02	11.75	3.9485E-02
5.000000	10.000000	6.000000	6.4090E-03	-114.92	1.2818E-02	-114.92	3.1057E-02	68.49	3.4195E-02
6.000000	10.000000	6.000000	7.1580E-03	86.85	1.1930E-02	86.85	3.1200E-02	-89.38	3.4151E-02
7.000000	10.000000	6.000000	7.7435E-03	-92.96	1.1062E-02	-92.96	3.1394E-02	91.08	3.4164E-02
5.000000	11.000000	6.000000	5.6244E-03	-52.12	1.2374E-02	-52.12	3.1349E-02	131.88	3.4158E-02
6.000000	11.000000	6.000000	6.3577E-03	159.88	1.1656E-02	159.88	3.1508E-02	-15.99	3.4180E-02
7.000000	11.000000	6.000000	6.9433E-03	-9.14	1.0911E-02	-9.14	3.1666E-02	175.05	3.4194E-02
5.000000	12.000000	6.000000	4.9841E-03	3.65	1.1962E-02	3.65	3.1656E-02	-172.16	3.4194E-02
6.000000	12.000000	6.000000	5.6705E-03	-135.22	1.1341E-02	-135.22	3.1757E-02	48.97	3.4184E-02
7.000000	12.000000	6.000000	6.2275E-03	65.52	1.0676E-02	65.52	3.1831E-02	-110.35	3.4136E-02
5.000000	10.000000	7.000000	6.4443E-03	85.40	1.2889E-02	85.40	2.6446E-02	-93.43	3.0116E-02
6.000000	10.000000	7.000000	7.0583E-03	-68.31	1.1764E-02	-68.31	2.6269E-02	113.41	2.9633E-02
7.000000	10.000000	7.000000	7.5220E-03	116.39	1.0746E-02	116.39	2.6219E-02	-61.32	2.9313E-02
5.000000	11.000000	7.000000	5.4786E-03	156.26	1.2053E-02	156.26	2.6218E-02	-21.57	2.9368E-02
6.000000	11.000000	7.000000	6.1422E-03	11.69	1.1261E-02	11.69	2.6247E-02	-165.72	2.9209E-02
7.000000	11.000000	7.000000	6.6806E-03	-153.71	1.0498E-02	-153.71	2.6351E-02	29.27	2.9135E-02
5.000000	12.000000	7.000000	4.7962E-03	-141.18	1.1511E-02	-141.18	2.6341E-02	41.76	2.9138E-02
6.000000	12.000000	7.000000	5.4556E-03	82.77	1.0911E-02	82.77	2.6459E-02	-94.04	2.9129E-02
7.000000	12.000000	7.000000	6.0079E-03	-73.40	1.0299E-02	-73.40	2.6614E-02	109.99	2.9156E-02

Suppose that we wish only a line of reading along the axis of the radius line. For this type of task, the spherical coordinate system is usually the most apt, as illustrated by the following revision to our basic spherical-coordinate model.

```
CM NE/NH test
CE
GW 1 11 0 0 .25 0 0 .75 .001
GE 1 0 0
GN 2 0 0 0 13.0000 0.0050
EX 0 1 6 00 1 0
FR 0 1 0 0 299.7925 1
NE 1 4 1 1 12.247449 63.434949 65.905157 1.0 1.0 1.0
EN
```

Once more, I have restricted the model to only an NE entry for simplicity. **Fig. 90-9** shows the NE entry screen to clarify the maneuver of requesting 4 points along the radius line.

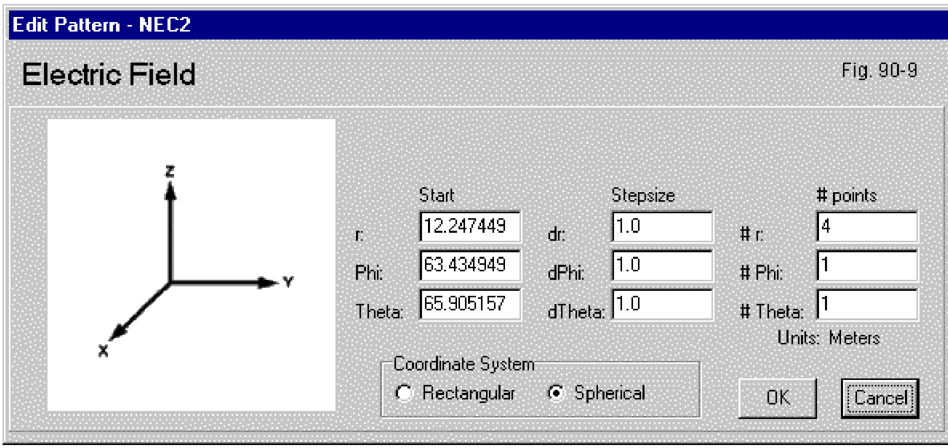

The model requests 4 observation points, spaced 1 meter apart along the radius line. The core returns the following report.

```
**** NEAR ELECTRIC FIELDS ****
**** Frequency = 299.79, File: C:\ant\NE-NH\amod90-6-3.nec
```

- LOCATION -			- EX -		- EY -		- EZ -		- PEAK FLD -
X METERS	Y METERS	Z METERS	MAGNITUDE VOLTS/M	PHASE DEGREES	MAGNITUDE VOLTS/M	PHASE DEGREES	MAGNITUDE VOLTS/M	PHASE DEGREES	MAGNITUDE VOLTS/M
5.000000	10.000000	5.000000	6.6689E-03	25.21	1.3338E-02	25.21	3.8323E-02	-149.78	4.1105E-02
5.408248	10.816497	5.408249	6.2225E-03	25.84	1.2445E-02	25.84	3.5339E-02	-149.52	3.7965E-02
5.816497	11.632993	5.816497	5.8311E-03	26.38	1.1662E-02	26.38	3.2787E-02	-149.30	3.5273E-02
6.224745	12.449490	6.224745	5.4853E-03	26.85	1.0971E-02	26.85	3.0581E-02	-149.11	3.2939E-02

For our limited purposes, the most notable part of the output report is the set of coordinates. If we take a vector sum of the coordinates for each observation point, we shall find that each differs by exactly 1.0 meter from the preceding or following point.

The End of the Beginning. . .

The exercises in this episode have tried to develop a bit of comfort with the alternative near-field input systems available in NEC-2. We looked mostly at single observation point situations to make the input systems clear, and we essentially examined only one part of the output data.

I have not tried to replicate the mathematical background of near fields as calculated by NEC, since the theory portions of the manuals do a far better job than I can in these columns. Instead, my task has been to orient the modeler toward using the NE and NH inputs to obtain the information needed for observation points of choice. Nevertheless, we have left some questions open. How does the data within each report line integrate? How does the NEC-4 input system differ from the NEC-2 system? Finally, how does the new request command, called LE and LH, differ from the present set of request commands that we have so far surveyed? Those are enough questions to occupy another entire episode.

91. An Orientation to NEC Near Fields Part 2. Some Refinements and NEC-4 Additions

The preceding episode had a simple goal: to orient you to the specifications of a location for a near-field reading using either Cartesian or spherical coordinates. The reading can be for either the electric or the magnetic field. In the process, we also explored the basics of setting up the reading or observation location at multiple points. As indicated in **Fig. 91-1**, we learned that if we need multiple observation points at linear intervals, the Cartesian coordinate system of entry may be more useful. If we need observation points at equal-angle increments, then spherical coordinates may prove simpler.

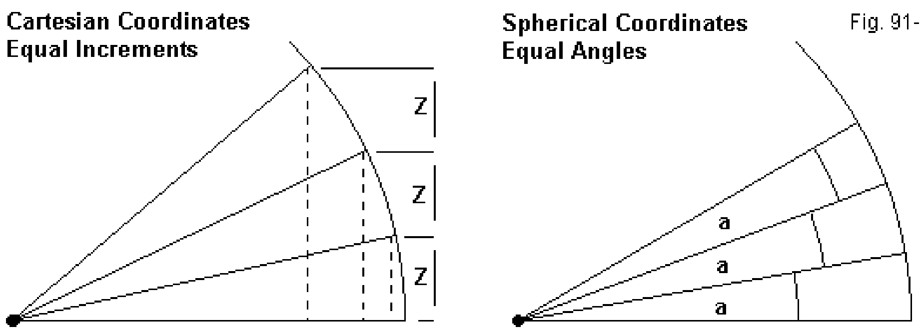

Fig. 91-1

Once we have become oriented to obtaining near-field readings, we are in a better position to appreciate some refinements in the command and its output. We hinted at a number of these items, but the time has come to set them forth explicitly.

1. *Near-Field Execution*: When we request a far-field radiation pattern (RP0), NEC automatically executes the request. If we need a frequency sweep for a single RP0 request, the RP0 automatically executes it. However, if we make multiple RP0 requests and wish the same frequency sweep for each pattern, then we must repeat the FR command specifications prior to each RP0 entry.

Near-field requests operate differently. As we saw in the preceding episode, when we request a single frequency, the NE and NH commands will self-execute, similarly to the RP0 request. The following model provides us with a concrete example of this situation. You may extract and run the model. Then check the output tables to ensure that results for both the NE and NH command appear. See model 91-1.

```
CM NE/NH test
CM 1-step, Cartesian coordinates
CM 1 Frequency
CE
GW 1 11 0 0 .25 0 0 .75 .001
GE 1 0 0
GN 2 0 0 0 13.0000 0.0050
EX 0 1 6 00 1 0
FR 0 1 0 0 299.7925 1
NE 0 1 1 1 5 10 5 1.0 1.0 1.0
NH 0 1 1 1 5 10 5 1.0 1.0 1.0
EN
```

Let's modify only the FR command to set up a 2-step frequency sweep. As the extract from the model shows, we retain the NE and the NH commands, but ask for a 2-step sweep. If you run the model, no near-field outputs will appear. See model 91-1a.

```
FR 0 2 0 0 295 10
NE 0 1 1 1 5 10 5 1.0 1.0 1.0
NH 0 1 1 1 5 10 5 1.0 1.0 1.0
EN
```

When we request multiple frequencies, each NE or NH command must have a request for execution (normally XQ) somewhere after each request. So the following model puts the requests in place. See model 91-1b.

```
FR 0 2 0 0 295 10
NE 0 1 1 1 5 10 5 1.0 1.0 1.0
XQ
```

```
NH 0 1 1 1 5 10 5 1.0 1.0 1.0
XQ
EN
```

However, we are still deficient, since the output will show near electric field readings for both frequencies, but near magnetic fields only for the higher frequency. What we forgot was that the FR command forms a loop relative to the most immediately following execution command (such as XQ or RP). Subsequent execution requests make use only of the highest or final frequency in the sweep. In order to obtain data for both frequencies for both near-field requests, we must repeat the FR loop, as in the final model of this series. See model 91-1c.

```
FR 0 2 0 0 295 10
NE 0 1 1 1 5 10 5 1.0 1.0 1.0
XQ
FR 0 2 0 0 295 10
NH 0 1 1 1 5 10 5 1.0 1.0 1.0
XQ
EN
```

Now the output report will show a pair of entries each for the near electric and magnetic fields.

2. *The Peak Field Value Reading*: Because many beginning modelers are interested only on the peak field value reading from a given set of near-field requests, we called attention to that entry in the near-field output tables in the preceding episode. We also noted in passing that the value is not the simple vector sum of the values specified in the X, Y, and Z columns. Let's pause a moment to see what that remark meant. We may begin with the single entry tables for our basic model at the beginning of this episode.

```
**** NEAR ELECTRIC FIELDS ****
**** Frequency = 299.79, File: C:\ant\NE-NH\91-1.nec

          -  LOCATION  -                 -  EX  -             -  EY  -             -  EZ  -         - PEAK FLD -
    X          Y          Z        MAGNITUDE   PHASE    MAGNITUDE   PHASE    MAGNITUDE   PHASE     MAGNITUDE
  METERS     METERS     METERS      VOLTS/M   DEGREES    VOLTS/M   DEGREES    VOLTS/M   DEGREES     VOLTS/M
 5.000000  10.000000   5.000000   6.6689E-03    25.21   1.3338E-02    25.21   3.8323E-02  -149.78   4.1105E-02

**** NEAR MAGNETIC FIELDS ****
**** Frequency = 299.79, File: C:\ant\NE-NH\91-1.nec

          -  LOCATION  -                 -  HX  -             -  HY  -             -  HZ  -         - PEAK FLD -
    X          Y          Z        MAGNITUDE   PHASE    MAGNITUDE   PHASE    MAGNITUDE   PHASE     MAGNITUDE
  METERS     METERS     METERS       AMPS/M   DEGREES     AMPS/M   DEGREES     AMPS/M   DEGREES      AMPS/M
 5.000000  10.000000   5.000000   9.7519E-05  -150.52   4.8760E-05    29.48   5.0537E-11    18.32   1.0903E-04
```

If we create vector sums for EX, EY, and EZ, and then for HX, HY, and HZ, we arrive at two values: 4.1122E-2 V/m for the electric field and 1.0903E-4 A/m for the magnetic field. The fact that the square root of the sum of the squares of the magnitudes appears to give a precise result for the magnetic near field often leads us to believe that something must be wrong with the core when it calculates the value for the other field.

What is wrong is our geometric interpretation of what is essentially a temporal calculation. If the phase angles were identical or if one component dominates, then the simple vector sum would be a good approximation of the peak voltage or current. Otherwise, the peak value will be equal to or less than the result of the geometric calculation. The phase differences among the component values tell us that each reaches its magnitude at a different time during a cycle, and so the calculation of a peak value must take that fact into account.

The actual calculation of the peak value is a multi-step procedure found in the NEC routine called NFPAT. It proceeds approximately as follows:

For either NE or NH, for a given field point defined by X, Y, and Z, let

–EXM, EYM, EZM = magnitude of EX, EY, EZ (given in peak volts/m or peak amps/m)

–EXP, EYP, EZP = phase angle of EX, EY, EZ (degrees or radians)

"E" is a stand-in for either the voltage or the current. There is no difference in the calculation procedures. Next, let's calculate some intermediate terms involving the phase angles, finally arriving at a term called "TP."

$$CP = EXM^2 \cdot \cos(2\,EXP) + EYM^2 \cdot \cos(2\,EYP) + EZM^2 \cdot \cos(2\,EZP)$$

$$SP = EXM^2 \cdot \sin(2\,EXP) + EYM^2 \cdot \sin(2\,EYP) + EZM^2 \cdot \sin(2\,EZP)$$

$$TP = CP^2 + SP^2$$

Now we may include TP in the final calculation involving the squares of the component magnitudes.

$$E_{peak} = \sqrt{0.5\left(EXM^2 + EYM^2 + EZM^2 + \sqrt{TP}\right)}$$

The resulting peak voltage or current reading (called "Epeak") in V/m or A/m is also in peak units.

3. *NEC-2 vs. NEC-4 Spherical Coordinate Entries*: When entering rectangular coordinates (NE0/NH0), there is no difference between the NEC-2 and NEC-4 entries. However, there is an important difference between the two cores when entering spherical coordinates. The two cores swap places between the phi and theta entries. Consider the following model in NEC-2 format. See model 91-2-nec2.

```
CM NE/NH test
CE
GW 1 11 0 0 .25 0 0 .75 .001
GE 1 0 0
GN 2 0 0 0 13.0000 0.0050
EX 0 1 6 00 1 0
FR 0 1 0 0 299.7925 1
NE 1 1 1 1 12.247449 63.434949 65.905157 1.0 1.0 1.0
NH 1 1 1 1 12.247449 63.434949 65.905157 1.0 1.0 1.0
EN
```

The format for the NE and the NH lines is as follows:

	I1	I2	I3	I4	F1	F2	F3	F4	F5	F6
Cmd	Cart/	No. of Points			Coordinate			Step Size		
	Spher	r	phi	theta	r (radius)	phi angle	theta angle	r	phi	theta
NE	1	1	1	1	12.247449	63.434949	65.905157	1.0	1.0	1.0
NH	1	1	1	1	12.247449	63.434949	65.905157	1.0	1.0	1.0

To achieve the same goal in NEC-4, we must use the following model (91-2-nec4).

```
CM NE/NH test
CE
GW 1 11 0 0 .25 0 0 .75 .001
GE 1 0 0
GN 2 0 0 0 13.0000 0.0050
EX 0 1 6 00 1 0
FR 0 1 0 0 299.7925 1
NE 1 1 1 1 12.247449 65.905157 63.434949 1.0 1.0 1.0
NH 1 1 1 1 12.247449 65.905157 63.434949 1.0 1.0 1.0
EN
```

The terms of the NE and NH lines have changed position with respect to phi and theta.

	I1	I2	I3	I4	F1	F2	F3	F4	F5	F6
Cmd	Cart/	No. of Points			Coordinate			Step Size		
	Spher	r	phi	theta	r (radius)	theta angle	phi angle	r	phi	theta
NE	1	1	1	1	12.247449	65.905157	63.434949	1.0	1.0	1.0
NH	1	1	1	1	12.247449	65.905157	63.434949	1.0	1.0	1.0

In programs like GNEC and NEC-Win Pro, the assist screens will appear identical, as in **Fig. 2**. However, each screen will create the required NE or NH entry correctly for the core in use. Since there is nothing in the NE or NH entries to create an error in the core run, NEC will not warn you if you accidentally mis-enter the phi and theta angles when creating the line without assistance. The results will simply be wrong. You may block copy the two versions of the model and run them on the same core to examine the disparity of the results.

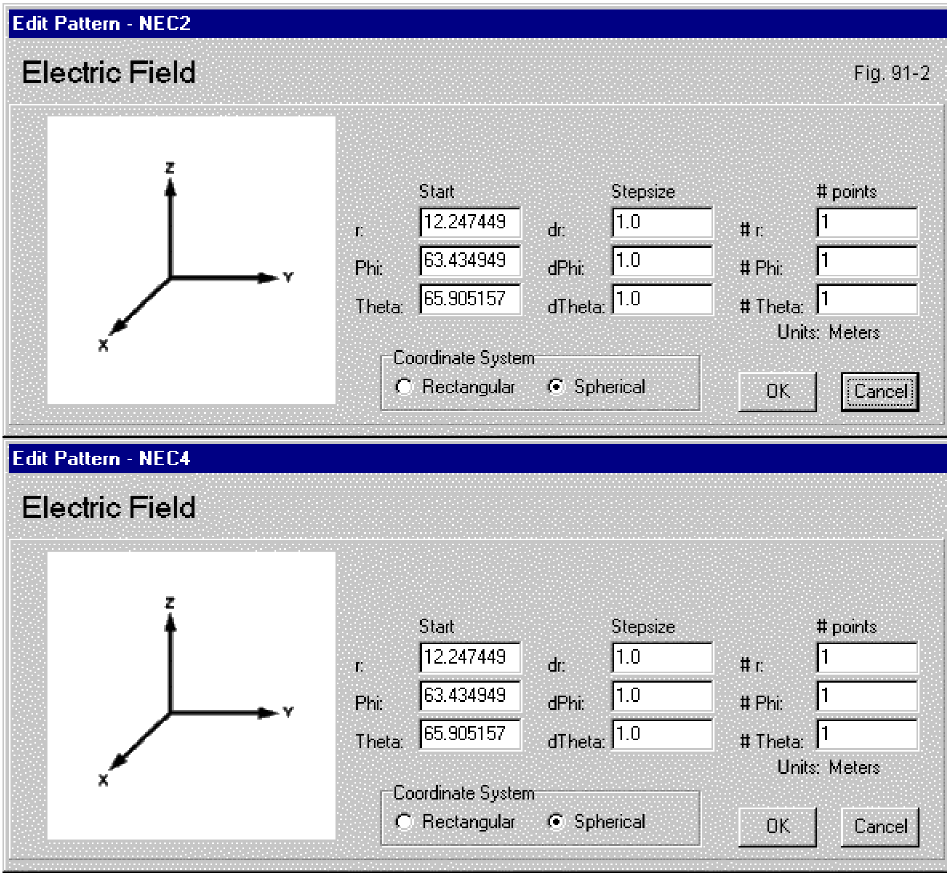

Fig. 91-2

4. *The Antenna Structure and the Ground*: The safest procedure to obtain controlled results is to ensure that no selected field point falls within the wires of the antenna, that is, along the segment line or within its radius. If a field point does fall

within these confines, NEC will move it an amount equivalent to the wire radius outside the wire in a direction normal to the plane for a reading and along the vector from the source segment to the observation point. Because the results may not include that segment's contribution to the H field or to the radial component of the E field, it is always wise to pre-plan the observation points so that they all fall outside the wire segments of the model.

The preferred ground calculation system for near-field analysis is the Sommerfeld-Norton (SN) system. However, there are restrictions. To minimize errors that tend to appear at very low frequencies, no observation point should be exactly at ground level. In fact, the minimum distance above ground in NEC-2 should be 0.001 ë. The reflection coefficient approximation (RCA) system, sometimes called the "fast" ground calculation system, may produce errors in the magnetic field calculations for observation points at some distance from the source. The RCA system does not include surface-wave contributions for this calculation and so may underestimate the field strength.

As noted in the previous episode, NEC differs from textbook treatments of near field calculations. Most texts introduce near-field calculations by extracting from a total field equation those elements that are most influential relative to the near field strength and then ignoring the remaining elements. NEC includes the near field and the total field elements and so will take into account influences by the near field and the ground-wave factors.

NE/NH and LE/LH

NEC-4 introduced a new pair of near-field commands to the pair that it inherited from NEC-2. So you have a choice between using the pair that best suits the requirement of the modeling task. (Of course, you have no requirement to use either NE and NH or LE and LH in pairs, and you may use both within the same model.) NE and NH are general abbreviations for near-electric and near-magnetic fields. LE and LH indicate near-electric and near-magnetic fields along a line. The differences between the two systems of calculating near fields may prove useful, not only in understanding the new NEC-4 commands, but as well in better appreciating the terms of the NE and NH output reports.

The NE/NH command set calculates its observation positions based upon either Cartesian or spherical coordinates, but it always reports its results in terms of field strength in Cartesian coordinates. However, it does not initially yield a single field strength value for the X, Y, and Z coordinate marking the observation position. Instead, it yields 3 values, each of which apply to that position in a plane parallel to the indicated axis. The components of the peak field strength are individual field strengths related to the axes of the coordinate system itself. See the left side of **Fig. 91-3** for a rough representation.

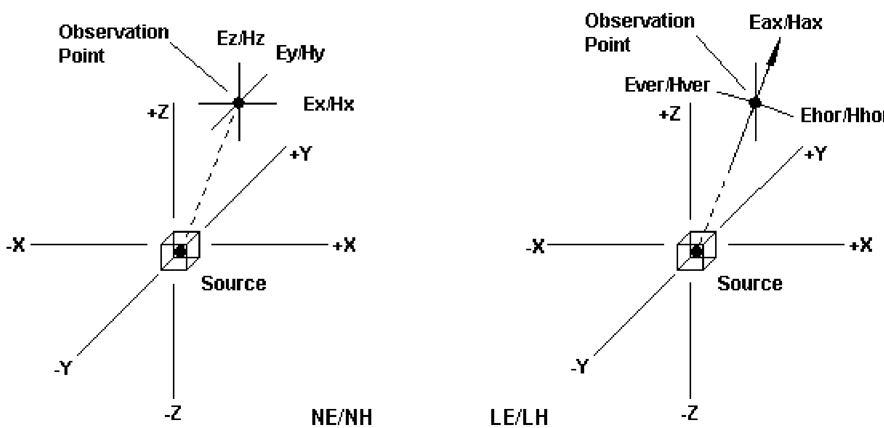

Fig. 91-3

On the right in **Fig. 3** is a similar situation. An observation point has a bearing from the source that is identical to the one on the left. However, the LE and LH command pair request output data along a defined line, in this case, running from the source to the final observation point. The data returned by the request provides electric or magnetic field strength using the axial direction of the line as the primary field component. Also provided are two transverse components, one horizontal and the other vertical. If we define the axial vector as a-cap, and we may let h-cap and v-cap be the horizontal and vertical transverse components, respectively, as roughly represented on the right side of **Fig. 3**. The actual vectors use the following equations:

$$\hat{a} \qquad \hat{h} = \hat{z} \times \hat{a} / |\hat{z} \times \hat{a}| \qquad \hat{v} = \hat{a} \times \hat{h}$$

The key entry data for both the LE and LH command are the number of points along the line to use for field strength reports and the starting and ending coordinates of the line. Hence, the pair of commands has the following structure.

CMD	I1	I2	I3	I4	F1	F2	F3	F4	F5	F6
	RSET	NPTS	0	0	X1	Y1	Z1	X2	Y2	Z2
LE	0	16	0	0	0	0	0	0	1.5	.5
LH	0	16	0	0	0	0	0	0	1.5	.5

Both of the sample lines request a report using 16 points along a line defined by 0, 0, 0 at end 1 and by 0, 1.5, and 0.5 at end 2. The command uses the same execution rules as the NE/NH pair. It will self-execute if there is only one frequency requested. However, for multiple frequencies in the FR command, it requires either a following RP or XQ command to execute. As well, if there are multiple requests as well as multiple frequencies, then the FR command requires repetition before each LE or LH command to ensure that data is available for all requests at all frequencies. As well LE and LH are subject to the same ground and boundary conditions as NE and NH.

It is possible to set up NE/NH models so that they cover the same observation points as corresponding LE/LH models. Consider the following conventional near-field model. It uses spherical coordinates and is set up for NEC-4. See model 91-3.

```
CM NE/NH test
CE
GW 1 11 0 0 -.5 0 0 .5 .001
GE 0 0 0
GN -1
EX 0 1 6 00 1 0
FR 0 1 0 0 299.7925 1
NE 1 16 1 1 0 71.565051 90 .10540932 0 0
```

```
NH 1 16 1 1 0 71.565051 90 .10540932 0 0
EN
```

The model requests 16 observation points along a line defined by a phi angle of 90° and a theta angle of 71.565°. The selection is not accidental, since the line formed has regularly spaced observation points that terminate at round numbers. The electric field report from NEC-4 is as follows.

** NEAR ELECTRIC FIELDS **

**** Frequency = 299.79, File: C:\ant\NE-NH\91-3.nec

- LOCATION -			- EX -		- EY -		- EZ -		- PEAK FLD -
X METERS	Y METERS	Z METERS	MAGNITUDE VOLTS/M	PHASE DEGREES	MAGNITUDE VOLTS/M	PHASE DEGREES	MAGNITUDE VOLTS/M	PHASE DEGREES	MAGNITUDE VOLTS/M
0.000000	0.000000	0.000000	0.0000E+00	0.00	0.0000E+00	0.00	1.1000E+01	-180.00	1.1000E+01
0.000000	0.100000	0.033333	3.3698E-09	-3.88	2.7694E-01	-3.88	8.1373E-01	147.90	8.5038E-01
0.000000	0.200000	0.066667	1.0570E-09	-4.90	8.6864E-02	-4.90	3.9996E-01	101.89	4.0078E-01
0.000000	0.300000	0.100000	2.9706E-10	20.67	2.4413E-02	20.67	3.0347E-01	58.81	3.0408E-01
0.000000	0.400000	0.133333	2.9407E-10	79.32	2.4168E-02	79.32	2.5943E-01	21.14	2.5974E-01
0.000000	0.500000	0.166667	4.0556E-10	75.92	3.3330E-02	75.92	2.2690E-01	-14.38	2.2690E-01
0.000000	0.600000	0.200000	4.5147E-10	56.32	3.7103E-02	56.32	1.9972E-01	-49.58	1.9999E-01
0.000000	0.700000	0.233333	4.5907E-10	31.00	3.7728E-02	31.00	1.7694E-01	-85.08	1.7774E-01
0.000000	0.800000	0.266667	4.4839E-10	2.55	3.6850E-02	2.55	1.5796E-01	-120.99	1.5932E-01
0.000000	0.900001	0.300000	4.2974E-10	-27.93	3.5317E-02	-27.93	1.4217E-01	-157.27	1.4399E-01
0.000000	1.000001	0.333334	4.0824E-10	-59.84	3.3550E-02	-59.84	1.2897E-01	166.13	1.3114E-01
0.000000	1.100001	0.366667	3.8636E-10	-92.79	3.1752E-02	-92.79	1.1785E-01	129.29	1.2026E-01
0.000000	1.200001	0.400000	3.6526E-10	-126.55	3.0018E-02	-126.55	1.0840E-01	92.25	1.1097E-01
0.000000	1.300001	0.433334	3.4543E-10	-160.93	2.8389E-02	-160.93	1.0029E-01	55.07	1.0296E-01
0.000000	1.400001	0.466667	3.2706E-10	164.19	2.6879E-02	164.19	9.3273E-02	17.77	9.5988E-02
0.000000	1.500001	0.500000	3.1014E-10	128.92	2.5488E-02	128.92	8.7149E-02	-19.63	8.9880E-02

A corresponding LE/LH model set up for the same observation points has the following appearance. See model 91-3a-nec4.

```
CM LE/LH test
CE NEC-4 only
GW 1 11 0 0 -.5 0 0 .5 .001
GE 0 0 0
GN -1
EX 0 1 6 00 1 0
FR 0 1 0 0 299.7925 1
LE 0 16 0 0 0 0 0 0 1.5 .5
LH 0 16 0 0 0 0 0 0 1.5 .5
EN
```

It produces (on NEC-4 only) the following electric field report.

```
********************************** NEAR ELECTRIC FIELDS ALONG A LINE ***********************************
**** Frequency = 299.79, File: C:\ant\NE-NH\91-3a-nec4.nec

 Unit Vectors:      X        Y        Z
 Axial       =   0.00000  0.94868  0.31623
 Transverse1 =  -1.00000  0.00000
 Transverse2 =   0.00000 -0.31623  0.94868

          -  LOCATION  -                      - Axial -            - Transverse1 -        - Transverse2 -
       X           Y            Z          MAGNITUDE   PHASE     MAGNITUDE   PHASE      MAGNITUDE   PHASE
     METERS      METERS       METERS        VOLTS/M   DEGREES     VOLTS/M   DEGREES      VOLTS/M   DEGREES
      0.0000      0.0000      0.0000     3.4785E+00  -180.00   0.0000E+00     0.00   1.0436E+01  -180.00
      0.0000      0.1000      0.0333     1.2688E-01    69.64   0.0000E+00     0.00   8.5015E-01   150.69
      0.0000      0.2000      0.0667     1.2948E-01    64.35   0.0000E+00     0.00   3.8826E-01   105.77
      0.0000      0.3000      0.1000     1.1507E-01    51.67   0.0000E+00     0.00   2.8186E-01    59.78
      0.0000      0.4000      0.1333     9.6121E-02    32.83   0.0000E+00     0.00   2.4217E-01    19.60
      0.0000      0.5000      0.1667     7.8259E-02     9.45   0.0000E+00     0.00   2.1557E-01   -17.18
      0.0000      0.6000      0.2000     6.3321E-02   -17.26   0.0000E+00     0.00   1.9302E-01   -52.93
      0.0000      0.7000      0.2333     5.1490E-02   -46.44   0.0000E+00     0.00   1.7343E-01   -88.62
      0.0000      0.8000      0.2667     4.2284E-02   -77.42   0.0000E+00     0.00   1.5660E-01  -124.54
      0.0000      0.9000      0.3000     3.5128E-02  -109.74   0.0000E+00     0.00   1.4222E-01  -160.75
      0.0000      1.0000      0.3333     2.9527E-02  -143.07   0.0000E+00     0.00   1.2995E-01   162.77
      0.0000      1.1000      0.3667     2.5097E-02  -177.16   0.0000E+00     0.00   1.1945E-01   126.06
      0.0000      1.2000      0.4000     2.1553E-02   148.14   0.0000E+00     0.00   1.1039E-01    89.16
      0.0000      1.3000      0.4333     1.8685E-02   112.98   0.0000E+00     0.00   1.0254E-01    52.12
      0.0000      1.4000      0.4667     1.6337E-02    77.44   0.0000E+00     0.00   9.5684E-02    14.95
      0.0000      1.5000      0.5000     1.4395E-02    41.59   0.0000E+00     0.00   8.9652E-02   -22.32


 Line integral of E       = -1.45652E-01 3.06530E-02 Volts
 Cumulative line integral = -1.45652E-01 3.06530E-02 Volts
```

The coordinates of each observation point are the same. However, the electric field strength values are nowhere the same, due to the differences in the way in which each command calculates the field component values. The only condition that will yield the same values for both commands is a model in which the observation points extend along one of the axes.

Note that within the LE (and LH) report are supplemental data. At the top of the report, we find the axial, horizontal, and vertical vectors that define the components listed as axial, transverse 1, and transverse 2. For each line, the square root of the sum of the squares of the values is, of course, 1.0. You may use the arccosine of axial Z value to obtain the theta angle used in the NE/NH version of the model (71.656°). Given that we have a vertical dipole in free space, the zero-readout for the horizontal vector should not be surprising.

At the end of the report, we find the line integral of E, as well as a cumulative integral. We may add to this model additional LE and LH requests so that the end of one line is the beginning of the next. The next line may run in any direction and even return to the series starting point. Each subsequent LE or LH command, as appropriate, will show its own line integral and a new cumulative value. However, the lines must form a continuous string with no breaks; that is, the end-2 coordinates of one line must be the end-1 coordinates of the next line. In addition, the LE and LH commands must form a group with no intervening control commands.

These models will serve to both introduce the LE and LH commands within NEC-4 and to show some of the differences between them and the NE/NH commands that are common to both NEC-2 and NEC-4. By no means is this a complete treatment of near-field analysis. In fact, we have not mentioned such fundamental textbook matters as the limit of the near field and the relationship of that limit to the longest dimension of the antenna. These are matters for study outside of the context of the ways to obtain near-field strength calculations within NEC-2 and NEC-4.

Instead, our goal has been to orient you to the near-field commands in terms of locating observation points relative to the input options and the output data. In most cases, you will wish to set the voltage source (EX0) for a value that will provide a set input power in order to make the near-field strength data more relevant. We covered such adjustments in past episodes. Indeed, the more you delve into the wide array of available control commands within NEC, the more you realize how interrelated they are in terms of making the most of a modeling endeavor.

92. Calculating Circular Gain

In its RP0 or far-field output report, NEC provides a good bit of information. To illustrate, I have extracted a single line from a 180° theta (elevation) report.

- - - RADIATION PATTERNS - - -

- - ANGLES - -		- POWER GAINS -			- - - POLARIZATION - - -			- - - E(THETA) - - -		- - - E(PHI) - - -	
THETA DEGREES	PHI DEGREES	VERT. DB	HOR. DB	TOTAL DB	AXIAL RATIO	TILT DEG.	SENSE	MAGNITUDE VOLTS	PHASE DEGREES	MAGNITUDE VOLTS	PHASE DEGREES
0.00	90.00	10.39	3.84	11.261	0.46544	-3.89	RIGHT	1.00721E+00	-99.56	4.73544E-01	163.94

Most users rely upon the polar plot facilities built into their implementations of NEC for the relevant data and overlook the valuable information in the tabular report. However, the report is an extremely useful tool as well as a source of data. It will always be in basic NEC formulation using phi and theta angles, although some implementations of NEC convert or quasi-convert the angles to azimuth and elevation. A theta angle of zero degrees is the zenith directly overhead, while the phi angle of 90° indicates a heading along the Y-axis.

The next three entries are the ones most printed along with polar plots: the power gains in dBi for the total field, the horizontal component and the vertical component. Allowing for rounding, the component powers add up to the total field power level, however, not by direct addition of dB. Rather, we must first convert the values in decibels into dimensionless power gain, using the standard procedure of dividing the value in dB by 10 and taking the antilog (base 10) of the result. The horizontal gain is 10.94, while the vertical gain is 2.42, for a total of 13.36. The dimensionless power gain of the total field is 13.37, although this simple exercise must allow for rounding of the original double-precision calculation numbers.

The central columns are relevant to elliptically polarized antennas. Although very important to numerous application involving elliptical polarization, we shall pass over them in this exercise. Basic explanations of the terms “axial ratio” and “tilt angle” appear in many basic college antenna texts, for example, Balanis, *Antenna Theory: Analysis and Design*, 2nd Ed. (Wiley, 1997), pp. 64-73. Perhaps the most important function of this data within this exercise is to remind us that even circular helices yield elliptically rather than circularly polarized patterns, where a perfectly circularly polarized pattern would have an axial ratio of 1.0. Although ideally, a linearly polarized pattern would have an axial ratio of zero, NEC will classify a pattern as linear when the minor axis is many orders of magnitude smaller than the major axis so that a practical calculation of the value results in a zero value. Apparently, to avoid excessively large numbers, NEC inverts the classic or textbook definition of axial ratio to "minor axis over major axis." Considerable effort is presently underway in many quarters to improve the circularity of polarization of antennas for special applications, with the quadrifilar design receiving extensive design scrutiny.

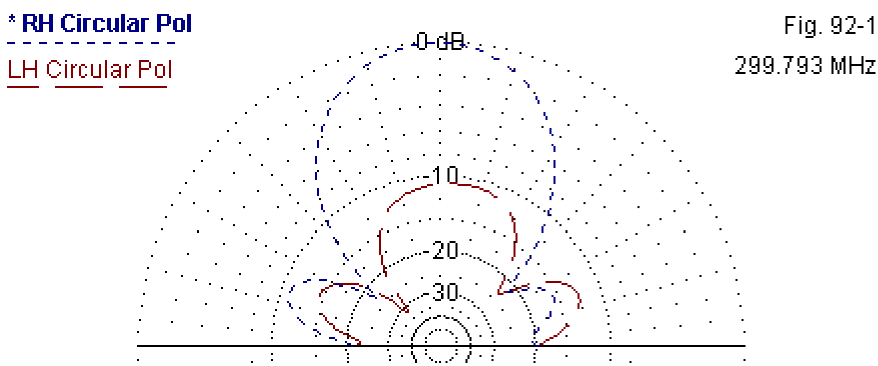

A Sample Pair of Circularly Polarized Patterns for a Helix over Perfect Ground

Relative to the central set of three columns, our interest is in the last entry, the sense. It tells us whether a circularly or elliptically polarized antenna has right-hand (clockwise) or left-hand counterclockwise) polarization. Since virtually no antenna will produce a pure circularly polarized signal that is only one or the other hand, the sense tells us which pattern will dominate–the left-hand or the right-hand pattern. Some newer modelers are often surprised that one can produce patterns for the respective circular polarizations, but **Fig. 92-1** shows in the EZNEC example that we certainly can.

In fact, the patterns are drawn for the model from which the RP 0 report line has been drawn. In NEC format, the model appears in the following lines. See model 92-1. The model uses the NEC-4 version of the GH command.

```
CM General Helix over Perfect Ground
CE
GH 1 100 5 .6959 .191 .191 .0005 .0005 0
GE 1 -1 0
GN 1
EX 0 1 1 0 1 0
FR 0 1 0 0 299.7925 1
RP 0 181 1 1000 -90 90 1.00000 1.00000
EN
```

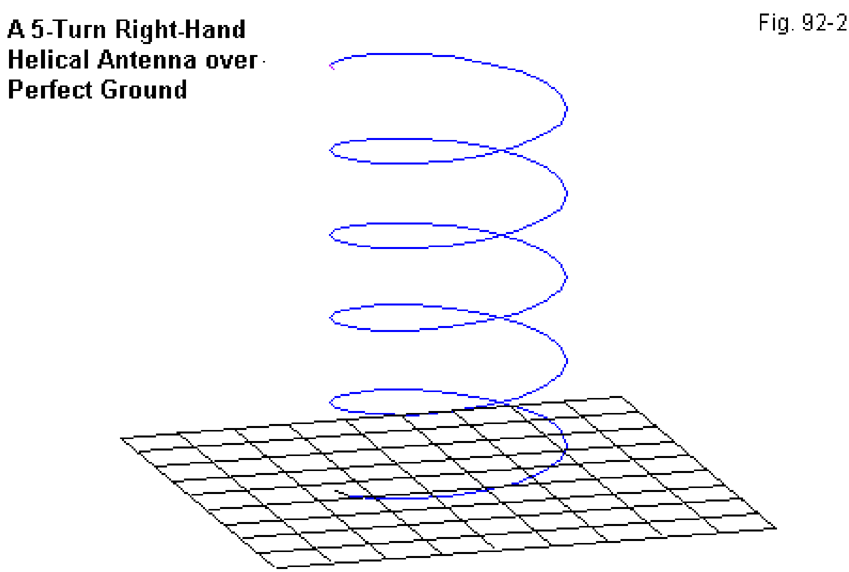

The third numeric entry on the GH line is positive (and records the number of turns in this NEC-4 version). Hence, the helix formed is a right-hand helix with a dominant right-hand polarization. **Fig. 92-2** shows the outlines of the helix over perfect ground to show the correspondence of the model and the patterns in **Fig 92-1**, where the right-hand pattern dominates. The RP 0 request in this model produces the report from which I drew the initial sample line. All other lines in the model are very standard.

Returning to our sample report line, the final columns provide the Etheta and Ephi field intensities. These values are simply proportional measures, since we have not specified in the request any specific distance from the coordinate system center. As a result, many modelers treat these entries as idle relative to the first order business of finding the total field gain of the antenna. The specific sample line is for the zenith angle overhead and the helix is pointed straight up. Hence, we might believe that the total field value is the maximum gain. However, because the pattern is a combination of left-hand and right-hand components, the actual maximum total-field gain heading is a degree off the zenith or 0-degree theta angle heading.

We can calculate the pattern values for both the left-hand and right-hand patterns using the previously ignored Etheta and Ephi data. Some implementations of NEC, such as EZNEC Pro, GNEC, NEC-Win Pro, and NEC-Win Plus, already perform these calculations. EZNEC Pro offers the patterns and a tabular form of the calculations as a pattern option. The Nittany-Scientific programs provide circular polarization data and patterns in its MultiPlot feature. If you are using a generic NEC core, you can also calculate the information and apply it to almost any polar plotting module to which you may have access.

In order to see how the calculation proceeds, let's repeat the relevant parts of our sample line.

```
 - - ANGLES - -  - POWER GAIN -  POLARIZATION    - - - E(THETA) - - -    - - - E(PHI) - - -
 THETA     PHI       TOTAL       SENSE          MAGNITUDE     PHASE      MAGNITUDE     PHASE
DEGREES  DEGREES      DB                        VOLTS         DEGREES    VOLTS         DEGREES

   0.00    90.00   11.261       RIGHT           1.00721E+00   -99.56     4.73544E-01   163.94
```

The procedure begins by taking the real and imaginary components of each value of E (theta and phi), which appear in terms of magnitude and phase angle in the sample line.

vetr = EthetaMag * cos(Ethetaphase); theta real
veti = EthetaMag * sin(Ethetaphase); theta imaginary
vepr = EphiMag * cos(Ephiphase); phi real
vepi = EphiMag * sin(Ephiphase); phi imaginary

Depending upon your calculating medium, you may have to convert the phase angles to radians to arrive at the correct values for the sines and cosines, for example in many spreadsheets. These initial values are simply intermediate steps. We next must re-combine the collection into units that reflect the polarization of the antenna.

velr = 0.5*(vetr + vepi); left real circular component
veli = 0.5*(veti - vepr); left imaginary circular component
verr = 0.5*(vetr - vepi); right real circular component
veri = 0.5*(veti + vepr); right imaginary circular component

Now we can combine the circular components into values of magnitude by standard "SQRT of SQRs" techniques.

elm = sqrt(velr*velr + veli*veli); left magnitude
erm = sqrt(verr*verr + veri*veri); right magnitude

What we now have are the magnitudes of the left-hand and the right-hand electrical fields in volts (peak). The move from these voltage magnitudes to pattern data in dBic (dBi circular) requires a few more steps. The following are the calculations required for the conversion.

a. *Power Gain*: Convert the Total Field Gain into a dimensionless gain measure:

PwrGn = antilog (base 10) (TtlFldGn/10)
Note: My spreadsheet does not return antilogs to base 10, but does return antilogs to base e. The spreadsheet formulation compensates for that limitation.

The @EXP function returns the antilog to the base *e*, and the multiplier is the standard log-ln conversion.

@EXP((TtlFldGn*2.3025851)/10)

b. *Voltage Gain Ratio vs. Power Gain Ratio*: Square the ratio of the right voltage magnitude (erm) to the left voltage magnitude (elm). This squared ratio is the ratio of the dimensionless power gains for right and left patterns.

RatSq = (erm/elm)^2

The next steps are predicated on the assumption that the sum of the two dimensionless circular power gains is the dimensionless total field power gain.

c. *Right Gain*: Right Gain and Left Gain are 2 unknowns subject to simultaneous equations. Selecting Right Gain first, we obtain the following.

GnRt = RatSq * PwrGn/(1 + RatSq)

d. *Right Gain dBi*: Conversion to dBi is standard.

GnRtdBi = 10 * log(GnRt)

e. *Left Gain*: Left Gain is simply the power gain minus the right gain (all dimensionless).

GnLf = PwrGn - GnRt

f. *Left Gain dBi*: Conversion to dBi is standard

GnLfdBi = 10 * log(GnLf)

For our single sample line of RP 0 reporting, we obtain the following values.

Theta	ERM	ELM	Sense	RatSq	PwrGn	GnRt	GnRtdBic	GnLf	GnLfdBic
0	.7393	.2697	right	7.516	13.369	11.799	10.718	1.570	1.959

A spreadsheet or other program can be set-up to handle as many entries as we might need to encompass a full pattern for the range of angle that we choose. In fact, let’s compare a fuller range of values for our sample helix and see what the RP 0 lines look like when sampled every 10° in a theta pattern from one horizon to the other.

GH5-08-1a - - - RADIATION PATTERNS - - -

- - ANGLES - -		- POWER GAINS -			- - - POLARIZATION - - -			- - - E(THETA) - - -		- - - E(PHI) - - -	
THETA DEGREES	PHI DEGREES	VERT. DB	HOR. DB	TOTAL DB	AXIAL RATIO	TILT DEG.	SENSE	MAGNITUDE VOLTS	PHASE DEGREES	MAGNITUDE VOLTS	PHASE DEGREES
-90.00	90.00	-9.36	-148.77	-9.357	0.00000	0.00	LINEAR	1.03655E-01	70.66	1.10934E-08	-51.70
-80.00	90.00	-7.05	-6.59	-3.801	0.40133	-47.10	RIGHT	1.35220E-01	83.37	1.42590E-01	-52.82
-70.00	90.00	-3.56	-3.67	-0.607	0.20487	-44.61	RIGHT	2.01953E-01	99.75	1.99439E-01	-57.10
-60.00	90.00	-2.80	-6.54	-1.269	0.06595	-32.93	LEFT	2.20486E-01	116.54	1.43387E-01	-71.72
-50.00	90.00	-5.07	-10.68	-4.018	0.35876	21.30	LEFT	1.69708E-01	157.82	8.90534E-02	-151.60
-40.00	90.00	-1.02	-2.59	1.275	0.56022	35.00	RIGHT	2.70616E-01	-135.73	2.25904E-01	164.19
-30.00	90.00	4.83	1.49	6.483	0.68079	1.68	RIGHT	5.30634E-01	-112.46	3.61516E-01	158.86
-20.00	90.00	8.19	3.33	9.421	0.56596	-4.79	RIGHT	7.81870E-01	-104.15	4.46826E-01	160.14
-10.00	90.00	9.89	3.99	10.887	0.50102	-4.55	RIGHT	9.50856E-01	-100.57	4.81993E-01	162.68
0.00	90.00	10.39	3.84	11.261	0.46544	-3.89	RIGHT	1.00721E+00	-99.56	4.73544E-01	163.94
10.00	90.00	9.83	2.93	10.635	0.44749	-3.71	RIGHT	9.43675E-01	-100.68	4.26509E-01	162.74
20.00	90.00	8.05	1.20	8.865	0.45047	-3.45	RIGHT	7.69033E-01	-104.32	3.49384E-01	159.62
30.00	90.00	4.56	-1.46	5.530	0.49995	0.19	RIGHT	5.14647E-01	-112.48	2.57304E-01	157.80
40.00	90.00	-1.65	-4.82	0.060	0.50176	27.07	RIGHT	2.51829E-01	-135.28	1.74695E-01	165.86
50.00	90.00	-6.13	-6.49	-3.297	0.35333	43.47	LEFT	1.50288E-01	152.44	1.44159E-01	-168.60
60.00	90.00	-3.18	-5.19	-1.059	0.74593	-18.59	LEFT	2.11052E-01	109.98	1.67502E-01	-149.83
70.00	90.00	-3.54	-5.01	-1.201	0.56213	-35.58	LEFT	2.02554E-01	94.54	1.70983E-01	-145.53
80.00	90.00	-6.46	-8.74	-4.441	0.42198	-34.22	LEFT	1.44683E-01	81.98	1.11320E-01	-145.85
90.00	90.00	-8.48	-151.11	-8.476	0.00000	0.00	LINEAR	1.14726E-01	73.72	8.47569E-09	-146.31

Notice that the pattern changes its sense along the selected sampling path. At the horizons, the Etheta values dominate to a degree that allows NEC to classify the pattern as linear. The left-hand and right-hand reversals may be less apparent until we perform the circular pattern calculations on them.

	Values Calculated by the Listed Equations					Reference	
Theta	ERM	ELM	Sense	GnRtdBic	GnLfdBic	R-H Gn	L-H Gn
-90	.0518	.0518	linear	-12.367	-12.367	-12.37	-12.37
-80	.1278	.1105	right	-4.529	-11.916	-4.53	-11.91
-70	.1675	.1105	right	-2.178	-5.786	-2.18	-5.79
-60	.1226	.1399	left	-4.891	-3.743	-4.89	-3.74
-50	.0578	.1226	left	-11.414	-4.891	-11.42	-4.89
-40	.2399	.0676	right	0.943	-10.056	0.94	-10.06
-30	.4460	.0847	right	6.329	-8.100	6.33	-8.10
-20	.6136	.1701	right	9.100	-2.045	9.10	-2.04
-10	.7153	.2378	right	10.432	0.866	10.43	0.87
0	.7393	.2697	right	10.718	1.959	10.72	1.96
10	.6841	.2611	right	10.044	1.679	10.04	1.68
20	.5585	.2116	right	8.283	-0.148	8.28	-0.15
30	.3860	.1287	right	5.072	-4.469	5.07	-4.47
40	.2057	.0682	right	-0.393	-9.977	-0.40	-9.98
50	.0635	.1329	left	-10.605	-4.190	-10.61	-4.19
60	.0274	.1885	left	-17.890	-1.150	-17.88	-1.15
70	.0506	.1805	left	-12.578	-1.529	-12.58	-1.53
80	.0486	.1196	left	-12.924	-5.105	-12.93	-5.10
90	.0574	.0574	linear	-11.486	-11.486	-11.49	-11.49

The higher gain in the Left-Hand Gain column for the entries sensed as left becomes much more apparent. Of course, the table–or any enlargement of it–becomes suitable for creating a polar or rectangular plot of the two circular components of the overall helix pattern. The reference columns are taken from the tabular output of EZNEC Pro, version 4, and serve to demonstrate that the calculation method shown here is consistent with techniques currently in use. Note that I do not say that the method is in fact the method used in EZNEC, since I did not reference that code when working out these calculations. Rather, the results of the calculations are consistent with those of EZNEC (and of the other programs mentioned early on in this exercise.)

As one final exercise, let's see what happens for a helix that is left-handed, as in the following example. See model 92-2. It uses NEC-4's version of the GH command and thus may not be transferable to NEC-2 without modification.

```
CM General Helix over Perfect Ground
CE
GH 1 100 -5 .6959 .191 .191 .0005 .0005 0
GE 1 -1 0
GN 1
EX 0 1 1 0 1 0
FR 0 1 0 0 299.7925 1
RP 0 181 1 1000 -90 90 1.00000 1.00000
EN
```

The only difference between this model and the one that we have previously used is the minus sign in the third entry of the GH or helix-forming line. The negative value for the number of turns creates a left handed helix, as shown in **Fig. 92-3**.

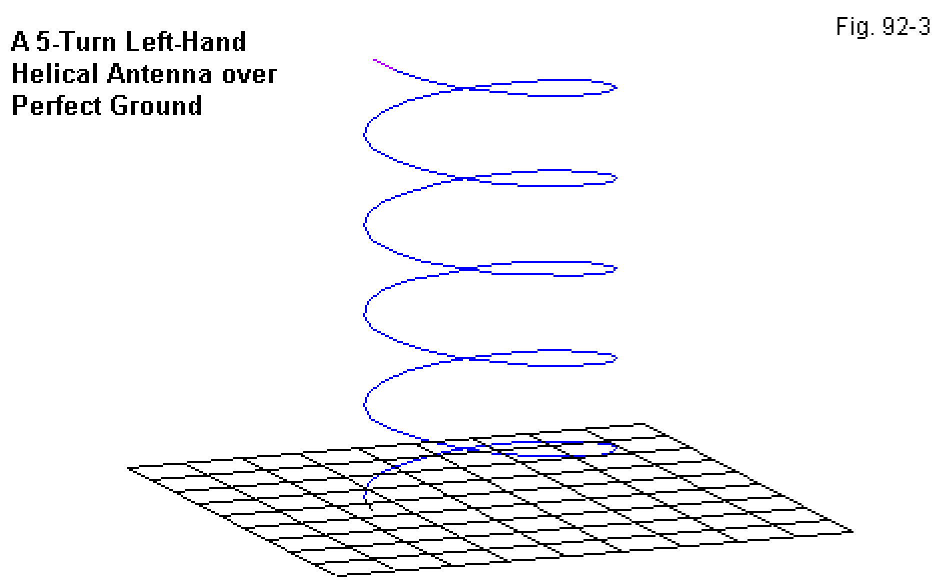

The sample RP 0 line that corresponds to the one for the previous example appears in the NEC output file.

- - - RADIATION PATTERNS - - -

- - ANGLES - -		- POWER GAINS -			- - - POLARIZATION - - -			- - - E(THETA) - - -		- - - E(PHI) - - -	
THETA DEGREES	PHI DEGREES	VERT. DB	HOR. DB	TOTAL DB	AXIAL RATIO	TILT DEG.	SENSE	MAGNITUDE VOLTS	PHASE DEGREES	MAGNITUDE VOLTS	PHASE DEGREES
0.00	90.00	10.39	3.84	11.261	0.46544	3.89	LEFT	1.00721E+00	80.44	4.73544E-01	163.94
Reference:	Corresponding line for the right-hand helix										
0.00	90.00	10.39	3.84	11.261	0.46544	-3.89	RIGHT	1.00721E+00	-99.56	4.73544E-01	163.94

Very little has changed, but the changes make a world of difference. Only the tilt angle and the Etheta phase angle have different numbers. However, those numbers alter the circular polarization calculations.

Theta	ERM	ELM	Sense	RatSq	PwrGn	GnRt	GnRtdBic	GnLf	GnLfdBic
0	.2697	.7393	left	0.133	13.369	1.570	1.959	11.799	10.718
Reference:	Corresponding line for the right-hand helix								
0	.7393	.2697	right	7.516	13.369	11.799	10.718	1.570	1.959

The values for the zenith angle show a flip-flop that is not true of the values for the entire pair of left- and right-hand patterns. **Fig. 92-4** shows some of the detail.

Below the zenith angle, the patterns for the left- and right-handed versions of the helix differ considerably–at least when examining them for fine detail. A comparison of the two model views in **Fig. 92-1** and **Fig. 92-3** will uncover the basic reason. The left-hand helix uses the same phi angle as the right-hand helix, but departs the ground plane at essentially a 90° angular difference to produce a true mirror image of the right-hand helix patterns. The left-hand patterns are a mirror image of the patterns we might obtain for the other helix by giving it a 90° phi-angle adjustment.

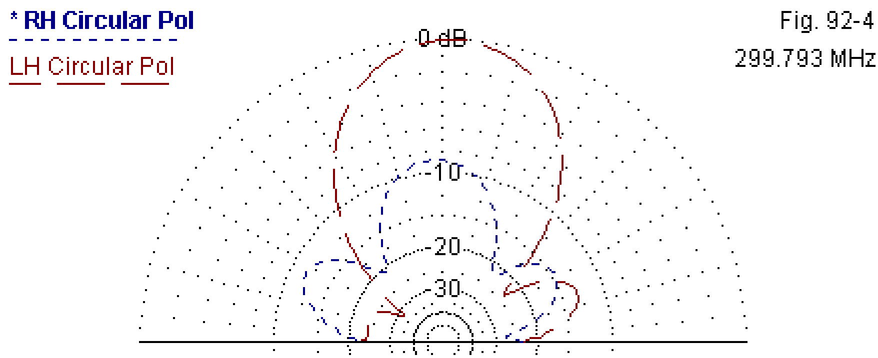

Sample Patterns of a Left-Hand Circularly Polarized Helix

This exercise has provided a procedure by which you can calculate your own circular power gain patterns, if you are using an implementation of NEC that does not include them. Since they involve only data within the RP 0 section of the output report, the calculations are equally applicable to NEC-2 and NEC-4, even though the sample models are from NEC-4. If you already have provision for obtaining circularly polarized power gain patterns in your implementation of NEC, then perhaps the exercise will provide some insight into at least one way to obtain them.

93. Convergence Revisited

In the very first column in this series, we examined the convergence test of model adequacy. The convergence test actually emerged from the development of MININEC, in contrast to NEC. However, the test generally carries over to NEC (-2 or -4) as one of two necessary but not sufficient conditions of model adequacy. The other test, of course, is the Average Gain Test (AGT), which has become a special function in some implementations of NEC, for example, in EZNEC, NEC2GO, and the NEC-Win/GNEC series of programs from Nittany Scientific. We examined the AGT test in three past columns, #20, #55, and #71.

Under limited conditions, the AGT allows the user to correct the reported gain for a model, and under even more restricted conditions, to correct the reported source resistance. The correctives are most accurate when the AGT value is not far off an ideal value (1.00 for free space and 2.00 over a perfect ground) and when the source impedance has a relatively low reactive component. In contrast, the convergence test gives the modeler information on the best level of segmentation to use in order to obtain the most accurate results.

In passing, I have had occasion to note that the convergence test works somewhat differently when using a NEC core than when using a MININEC core. This statement is not always true–at least not always true within the limits of the levels of segmentation that a modeler is likely to be willing to use. This seemingly small nuance suggests that we might spend a little time with a set of examples to illustrate what the qualification means in practical terms.

A Pair of Test Yagi Models

Let's explore two distinctly different Yagi models. The first will be an OWA 6-element Yagi, shown in the right in **Fig. 93-1**. OWA Yagis are optimized for wide-band performance with usable performance and impedance properties that extend for about a 7% bandwidth. Another type of Yagi is the narrow-band NBS design, sketched in outline on the left in **Fig. 93-1**. Jim Breakall used a similar design when he wrote "A Validative Comparison of NEC and MININEC Using NBS Experimental Yagi Antenna Results" for *The Applied Computational Electromagnetic Society Jour-*

nal, November, 1986. So it is fitting to resurrect this antenna–even with some modifications–in this re-visit of the convergence test.

Fig. 93-1

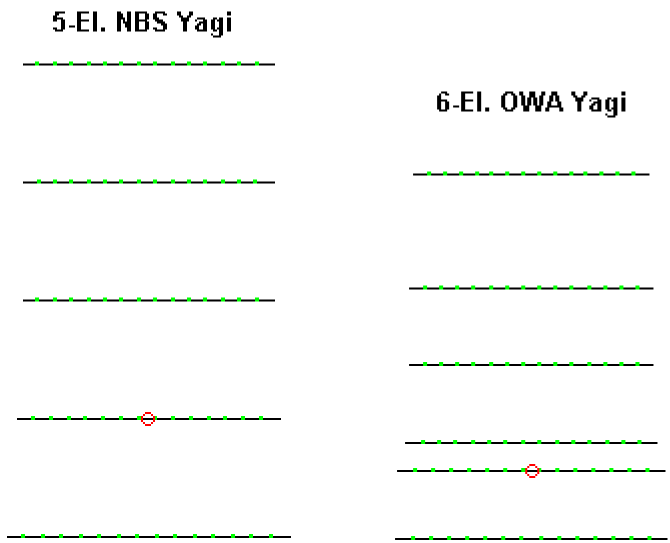

Comparative Sizes of 2 Test Yagis

For this test, I modeled both antennas at 299.7925 MHz, where 1 meter = 1 wavelength. The two antennas perform in significantly different ways. The shorter OWA Yagi has slightly lower gain, as one might expect from the boom-length. It uses a master and slave driver set (the fed driver and director 1) to increase the operating bandwidth. In conjunction with the second and third directors, the array has its maximum gain, maximum front-to-back ratio, and its SWR passband center all on or very close to the same frequency. **Fig. 93-2**, at the top, shows a 3-D pattern on the test frequency. See model 93-1.

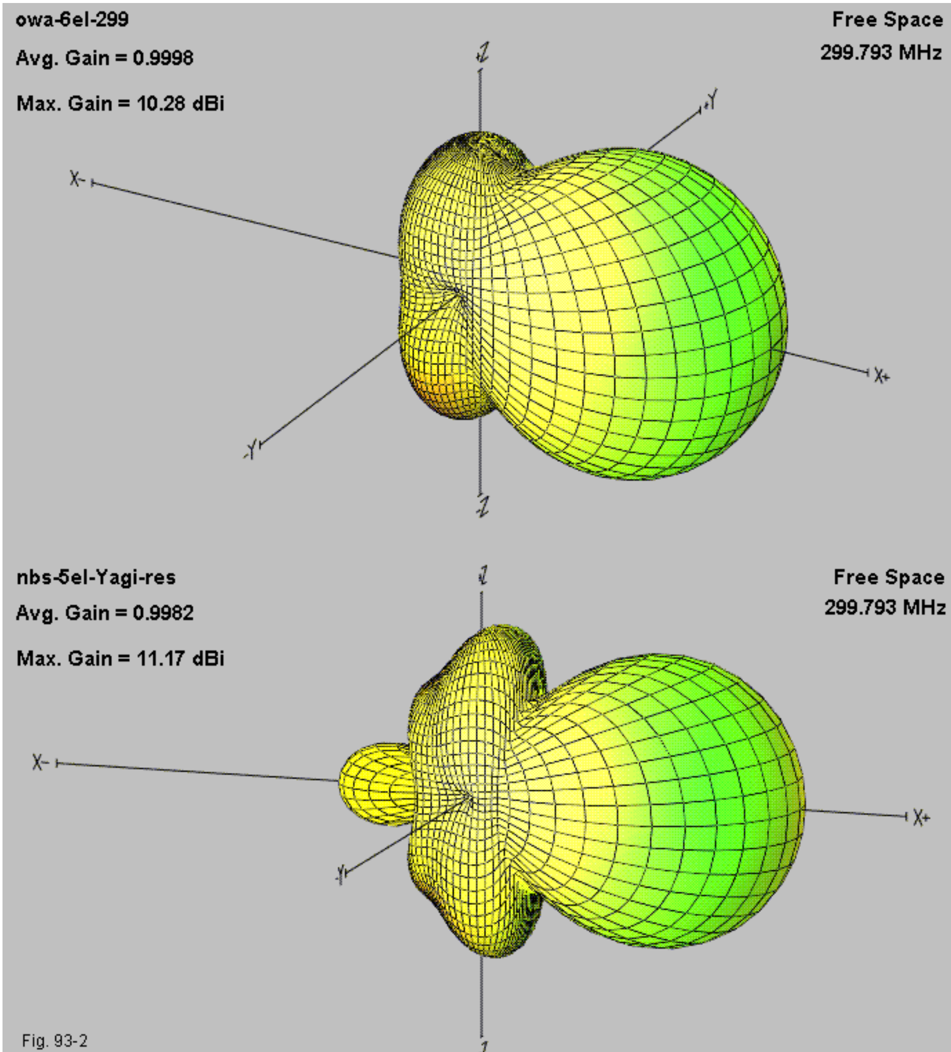

Fig. 93-2

The NBS Yagi uses fewer elements on a longer boom to achieve its higher forward gain. See model 93-2. In addition, it uses equal spacing between the successive elements. As a result, its pattern (**Fig. 93-2**, bottom), is less "well-behaved" than the OWA pattern. The array has a significant rear main lobe. (In this contest, "significant" means only highly noticeable. Whether the rear lobe is significant to any particular potential use of the array requires the introduction of task criteria outside the scope of this exercise.) In addition, the NBS Yagi shows very significant radiation in the region around 90° to the line along the main forward and rearward lobes. The magnitude of this band of radiation would not show up in a 2-diemensional E-plane pattern, since the dimples in the 3-D pattern are very deep. In an E-plane pattern, they would show up as very deep nulls with seemingly small secondary lobes both forward and aft of the null headings. However, the 3-D pattern shows to what degree the nulls are operationally illusory, since at all other headings that form the band around the pattern, the radiation is significant. In contrast, the OWA pattern shows no secondary forward lobes and only the standard H-plane pattern broadening at right angles to the plane of the elements.

The two modeled antennas have other differences, as well. The OWA Yagi is designed to directly match a 50-Ω feedline. However, the NBS antenna displays a low impedance. For this exercise, I shortened the driver from its NBS-specified 0.5-ë size. At the NBS length, the feedpoint impedance is highly inductively reactive. Shortening the driver does not significantly change other performance values, but it does allow one to derive a meaningful SWR curve referenced to the resonant feedpoint impedance: 17 Ω. **Fig. 93-3** overlays the 50-Ω OWA SWR curve and the 17-Ω NBS curve for comparison, using NEC-4 models of each. X-axis frequency increments are 2.5 MHz.

The OWA 2:1 SWR curve extends from just above 285 MHz to just above 306 MHz, for a 21-MHz passband: just about the advertised 7%, using the design frequency as the divisor. In contrast, the NBS Yagi has a 2:1 SWR curve that extends from about 293 MHz to 302 MHz for a 6-MHz or 2% passband. In both cases, and typical of Yagi design, the SWR rises more rapidly above the design frequency than below it.

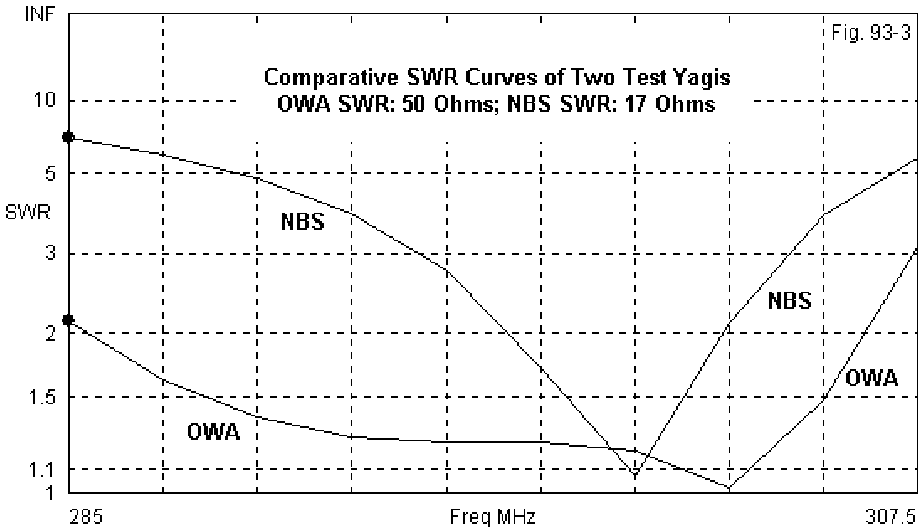

We may note as well that the NBS design requires considerably fatter elements to achieve its narrow operating bandwidth than the OWA needs for its wider passband. The OWA elements are 2.5 mm in diameter, while the NBS elements are 8.5 mm, a 3.4:1 ratio. It is possible to widen the OWA passband even further by optimizing the design for fatter elements, although a wider passband is unnecessary for our purposes here.

The data on these two interesting Yagi designs is useful as background, but the information seems distant from the subject of model convergence. That impression is not a true one. We shall have occasion to call attention to the antenna differences as we gradually get a better handle on convergence as applied to both NEC and MININEC.

The OWA Yagi and Convergence

To permit you to replicate the OWA Yagi and the convergence exercise, for which it is one test subject, the following table provides the relevant dimensions. Element lengths appear in two forms: as half-lengths for modeling +/- to one of the axes and as full lengths for reference. All dimensions are in meters except for the diameter and radius, which are in mm. The models using these dimensions prescribe perfect or lossless wire and are in free space.

Dimensions of the 6-Element OWA Yagi for 299.7925 MHz

Element	Half-Length	Full Length	Space from Reflector	Diameter/Radius
Reflector	0.250	0.500	----	2.5/1.25
Driver	0.247	0.494	0.125	2.5/1.25
Director 1	0.231	0.462	0.177	2.5/1.25
Director 2	0.225	0.450	0.321	2.5/1.25
Director 3	0.225	0.450	0.461	2.5/1.25
Director 4	0.216	0.432	0.671	2.5/1.25

The OWA Yagi does not show its lowest SWR value at the design frequency. The lowest value occurs close to the point where the SWR rises rapidly. Hence, design-frequency impedances values always show a small inductive reactance. Nevertheless, I designed the original model using 15 segments per element in NEC and 14 segments per element in MININEC. The different algorithms used by the two types of cores have different requirements for calculating currents and hence for source placement. NEC uses the center of each segment as its foundation. To place a source at a segment center and have it also be centered on the element requires an odd number of element segments. In contrast, MININEC calculates from pulses, which generally occur on segment junctions. To place a source on a pulse requires that we use an even number of segments on the element. Since all of the elements in the model have similar lengths, we adhere to the same number of segments per element throughout the model.

To observe the numerical trends in convergence within the broadband OWA model, I stepped each core through 7 levels of segmentation. I began the NEC models at 11 segments with increments of 4 segments per element and stopped at

35 segments. The MININEC version of the same model used the same increment, but ran from 10 through 34 segments per element.

For the test, I used NEC-4D (double precision) as found in version 4 of EZNEC. Actually, the use of a single or double precision core makes no differences to the progression. The practical performance of the antenna changes in no significant way through the progression. However, we shall be interested in the numerical trends. The reason that I mention the core and the program used for the runs is that the exact numbers you obtain depend in part on the FORTRAN compiler used with the core for running it on a standard PC. Hence you may find that your own NEC core (-2 or -4, single or double precision) may give a slightly different result. Nevertheless, the trends should remain true.

Since the test frequency is at the border between VHF and UHF, I selected Antenna Model (AM) for the MININEC runs. Only the MININEC frequency offset is at stake in these models, since they have no odd geometries to challenge other MININEC limitations. Therefore, your should obtain the same results using any version of MININEC that has been adequately corrected for the frequency offset that emerges as we increase the design frequency of a model. AM also calculates the AGT value, which will be useful in the comparisons.

OWA Yagi Convergence Tests: NEC-4D Results

# Segments per element	Gain dBi	Front-to-Back Ratio dB	Source Impedance R +/- jX Ohms	AGT	Ave. Seg. Length	Seg. Len. to Radius Ratio
11	10.26	32.17	51.83 + j9.43	0.992	0.0422	33.8:1
15	10.28	32.33	51.83 + j9.01	0.996	0.0311	24.8:1
19	10.29	32.24	51.93 + j8.65	0.998	0.0245	19.6:1
23	10.29	32.08	52.02 + j8.37	0.998	0.0202	16.2:1
27	10.29	31.91	52.10 + j8.14	0.999	0.0172	13.8:1
31	10.29	31.77	52.16 + j7.95	0.999	0.0150	12.0:1
35	10.29	31.64	52.21 + j7.79	0.999	0.0133	10.6:1

OWA Yagi Convergence Tests: MININEC (AM) Results

# Segments per element	Gain dBi	Front-to-Back Ratio dB	Source Impedance R +/- jX Ohms	AGT	Ave. Seg. Length	Seg. Len. to Radius Ratio
10	10.27	32.12	49.86 + j9.51	1.0005	0.0465	37.2:1
14	10.28	32.22	51.05 + j9.01	0.9998	0.0332	26.6:1
18	10.28	32.24	51.60 + j8.69	0.9996	0.0258	20.7:1
22	10.28	32.19	51.91 + j8.44	0.9995	0.0211	16.9:1
26	10.28	32.13	52.10 + j8.26	0.9994	0.0179	14.3:1
30	10.28	32.06	52.22 + j8.10	0.9994	0.0155	12.4:1
34	10.28	31.99	52.31 + j7.98	0.9994	0.0137	10.9:1

The tables of results for NEC-4D and for corrected MININEC appear above. They contain the usual information on free-space gain in dBi, the 180° front-to-back ratio in dB, and the reported source impedance in terms of resistance and reactance in Ω. In addition, the tables provide some supplementary information, namely, the AGT score, along with the length of an average segment and the ratio of this length to the element radius. We shall have occasion to explore all of these data along the way.

Perhaps the most notable feature of the NEC-4 and MININEC tables is how little they differ from each other. The gain value quickly levels off (by 19 segments per elements), while the front-to-back ratio shows a very slow descent as we increase the segment density. The source resistance climbs slowly, while the reactance decreases slowly. Any slowing of the rate of change from one segmentation level to the next is largely a function of the fact that as we increase the density in increments of 4 segments per element, each step in the progression is a smaller percentage of increase over the preceding step.

In a very real and practical sense, the models are fully converged by no later than 14/15 segments per element. In terms of a numerical progression, neither core shows full convergence, that is, no change from one step to the next. These results are quite unsurprising in view of the fact that the smallest ratio of segment length to wire radius is over 10:1. The models in no way stress or stretch the thin-wire algorithms at the hearts of the cores. Perhaps the only anomalous data between the two tables occurs in the AGT column. The MININEC values decrease with increasing segmentation, while the NEC values increase as the segmentation rises in density. However, the amount of change is truly insignificant. My only point in noting the reverse trends is to show that the AGT value need not parallel the convergence progression.

The goal of the OWA example is to show that there are cases in which the two different cores–NEC and MININEC– will show very close, if not coincident, convergence tracks. Two properties of the OWA having an impact on this parallelism are the broadband characteristics of the OWA and the use of relatively thin elements. The NBS Yagi differs from the OWA in both categories.

The NBS Yagi and Convergence

The NBS Yagi is a narrow-bandwidth array that uses relatively fat elements: 8.5 mm in diameter. The elements are about 3.4 times larger in diameter than the ones used in the OWA array. The parasitic beam itself is a highly usable design. With adjustment of the driver length, a gamma or beta match will allow the use of a 50-Ω coaxial cable as the feedline. More specifically, the following table lists the dimensions of the NBS array, using the same conventions as for the OWA Yagi. Element lengths appear in two forms: as half-lengths for modeling +/- to one of the axes and as full lengths for reference. All dimensions are in meters except for the diameter and radius, which are in mm. The models using these dimensions specify perfect or lossless wire and are in free space.

Dimensions of the 5-Element NBS Yagi for 299.7925 MHz

Element	Half-Length	Full Length	Space from Reflector	Diameter/Radius
Reflector	0.241	0.482	----	8.5/4.25
Driver	0.2225*	0.445*	0.200	8.5/4.25
Director 1	0.214	0.428	0.400	8.5/4.25
Director 2	0.212	0.424	0.600	8.5/4.25
Director 3	0.214	0.428	0.800	8.5/4.25

*The driver lengths shown is for the NEC-4 model. The driver of the MININEC model has a half length of 0.223 (full length 0.446) m to achieve resonance on the test frequency. Resonance for this exercise means a reactance of under +/-j1 Ohm at the test frequency.

The NBS Yagis longer boom yields almost a full dB of gain over the OWA Yagi, with 1 less element. The cost for this added gain is less control over the source impedance and a significantly narrower bandwidth. These attributes do not count for or against the NBS Yagi without review in the presence of the criteria of intended use.

I ran the NEC-4 and MININEC models through the same exercise that I used on the OWA Yagi. The NEC-4 models increased the segmentation density from 11 to 35 segments per element in 4-segment increments. The MININEC model used the same increment in moving from 10 to 34 segments per elements. The following table records the results.

NBS Yagi Convergence Tests: NEC-4D Results

# Segments per element	Gain dBi	Front-to-Back Ratio dB	Source Impedance R +/- jX Ohms	AGT	Ave. Seg. Length	Seg. Len. to Radius Ratio
11	11.20	13.72	17.10 - j1.15	0.997	0.0401	9.4:1
15	11.22	13.28	17.02 + j0.33	0.998	0.0294	6.9:1
19	11.22	13.10	17.00 + j0.96	0.999	0.0232	5.5:1
23	11.22	13.06	17.01 + j1.08	1.000	0.0192	4.5:1
27	11.22	13.10	17.03 + j0.94	1.000	0.0163	3.8:1
31	11.22	13.18	17.06 + j0.64	1.000	0.0142	3.4:1
35	11.22	13.29	17.08 + j0.28	1.000	0.0129	2.9:1

NBS Yagi Convergence Tests: MININEC (AM) Results

# Segments per element	Gain dBi	Front-to-Back Ratio dB	Source Impedance R +/- jX Ohms	AGT	Ave. Seg. Length	Seg. Len. to Radius Ratio
10	11.14	14.58	17.51 - j2.28	0.9980	0.0441	10.4:1
14	11.17	14.09	17.52 - j0.84	0.9982	0.0315	7.4:1
18	11.18	13.83	17.53 - j0.04	0.9984	0.0245	5.8:1
22	11.18	13.70	17.55 + j0.40	0.9985	0.0201	4.7:1
26	11.19	13.64	17.58 + j0.60	0.9987	0.0167	4.0:1
30	11.19	13.63	17.61 + j0.68	0.9988	0.0147	3.5:1
34	11.19	13.63	17.64 + j0.68	0.9988	0.0130	3.1:1

There is more divergence between the NEC-4 and MININEC trends with respect to the NBS Yagi than with respect to the OWA Yagi. However, the AGT values track each other very well relative to the two cores. As noted, the segment-length-to-radius ratio is much lower for the NBS model, and the antenna is narrow banded with regard to both performance and source impedance. The narrow-band characteristic of this antenna largely accounts for intrinsic differences in the gain and front-to-back readings, which are numerical (but not practically) more distant that the comparable OWA value pairs. It is likely a combination of the two characteristics that accounts for the half-Ω difference in the source resistance.

The characteristics are precisely what we need to show a convergence phenomenon in NEC, one that occurs often–but not so often as not to be disconcerting to someone who encounters it. The MININEC results are almost perfectly in accord with those for the thin-element wide-band Yagi. Like the preceding example, the MININEC model is practically converged at the 14 or 18 segment per element level. For the most finicky numerical analysis, we find virtually complete convergence between the 30 and 34 segment per element levels, with identical values of gain, front-to-back ratio, source reactance, and AGT. (However, the preceding example taught us that the AGT and convergence progressions need not coincide, so we may view the last element of convergence as accidental.) The source resistance difference between the two steps is 0.03 Ω.

The NEC-4 model is somewhat different. Convergence does not occur at the highest levels of segmentation. Rather, it occurs in the region between 19 and 27 segments per element. For almost all data, the increments of change from step-to-step within the region are equal to or smaller than the incremental steps outside the region. In addition, we find that many of the progressions of values actually change direction. The fact that NEC models often converge at a segmentation level below the maximum possible level (without violating the minimum segment-length-to-radius ratio) appears to be unique to NEC models–at least in the range of models that I have so far encountered. Normally, it will show up only at levels of segmentation density far beyond what may be practical for a given model and beyond what is necessary for results that meet every canon of practical need. But it remains a notable difference from the manner in which convergence tends to work with MININEC models.

Conclusion

The sample models that we have used in this exercise are the best of all possible models and the worst or all possible models. They are the best because they have allowed us to see some of the major factors that contribute to the differences in convergence testing in MININEC and in NEC models. At the same time, they are the worst of models because–for all practical and almost all theoretical purposes–we would never reach the level of segmentation density that shows a full converged NEC model of the NBS Yagi, let along full convergence of the MININEC version of the NBS model. (However, having the best of all models and the worst of all models will not convince me to title this episode “A Tale of Two Yagis.”)

Putting those concerns aside, there are differences in the manner in which NEC models converge relative to the way in which MININEC models converge. Although the matter may fall among the minor details of the differences between the two types of cores, the more that we understand these minor differences, the better use we may make of each of them.

94. GR: The “Generate Cylindrical Structure” Command

The GR command is a specialized rotational device that can use symmetry for rapid calculation of a replication of an initial structure. View the initial structure as vertical and offset from the center (X = 0, Y = 0) position. Invoking the GR command will then created rotated versions of the initial structure the number of times (NR) specified by the command with each new version rotated around the Z-axis by 360°/NR. The result is a cylindrical structure with the added property of running much faster than a similar structure produced by the GM command due to the use of symmetry. All of models in this exercise are run in NEC-Win Pro, a NEC-2-based program that makes available all of the commands.

Like the GX command, GR is deceptively simple, since it employs only the first two integer positions on the command line. It does not use any of the floating decimal positions. Due to its simplicity, the command carries with it a host of restrictions, some of which have led modelers to by-pass the command in favor of others. Like GX, GR is identical in both NEC-2 and NEC-4.

Cmd	I1 Tag No. Increment	I2 Total No. of Occurrences
GR	1	6

Like GX, the I1 entry should specify an increment such that each new occurrence of the initial structure takes on a previously unused tag number. In some commands, such as GM, you will specify the number of new structures beyond the initial structure. However, in GR, you specify the total number of structures, including the initial structure. Now let’s sample the restriction list.

1. Avoid using GR when segments lie on or cross (at other than junctions) the Z-axis to prevent the occurrence of overlapping segments.

2. Avoid adding a GW entry following GR or the symmetry function may be defeated (sometimes referred to as “destroyed”).

3. Use a following GM command only if the number of new structures is set to zero and if the command acts only the entire structure. Also avoid rotating the structure with GM around the X- or Y-axis when a ground is specified.

4. A following GX or GR entry will destroy the previously established symmetry.

5. Avoid non-symmetrical lumped loads. However, non-radiating networks and sources will not affect symmetry.

The GR command differs from the corresponding GX command in several important ways, even though both make use of symmetry during the core run. First, GX allows symmetry in all 3 planes–X, Y, and Z–and the modeler can select from 1 to 3 planes of symmetry for any model. See column #72 of this series for the rudiments of applying the GX command. In contrast, the GR command applies symmetry around the Z-axis only.

Second, the GX command applies symmetry once per option, although with multiple planes of symmetry, we may end up with up to 8 total objects. One is the original and the other 7 are replications created in a cube if we select the maximum level of symmetry available. The GR command uses symmetry rotationally relative to the original structure. Hence, in principle, there is no limit to the number of replications (one less than the total number of occurrences that we specify within the command itself). However, there are very practical limitations on the number of successful replications we may have. That number depends upon the X-Y dimensions of the original structure. Specifying too many occurrences will result in overlapping or inter-penetrating structures that yield a defective model.

Third, the reflections in the GX command are essentially linear across a specified plane of reflection. For the plane in question, we arrive at the same absolute values for the coordinates, but with the signs reversed. The GX command uses symmetry rotationally, separating each occurrence of the structure by an angular distance, but at the same distance from X=0 and Y-0 as the original structure.

We shall sample the formation of GR structures using the simplest possible structures. **Fig. 94-1** shows the structures that result from the sample models.

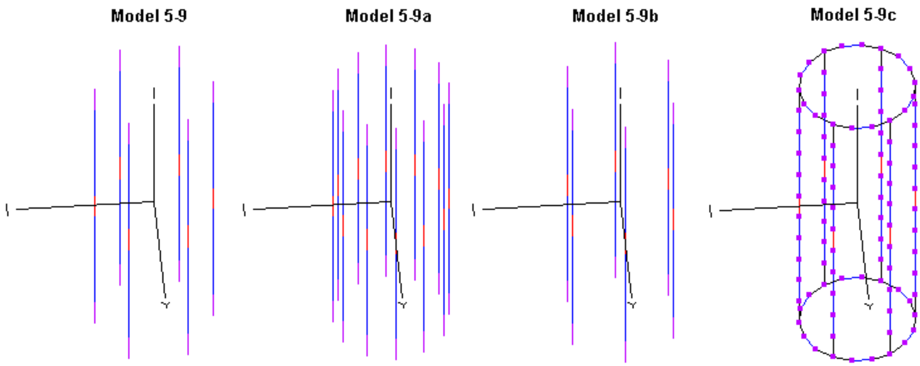

Fig. 94-1

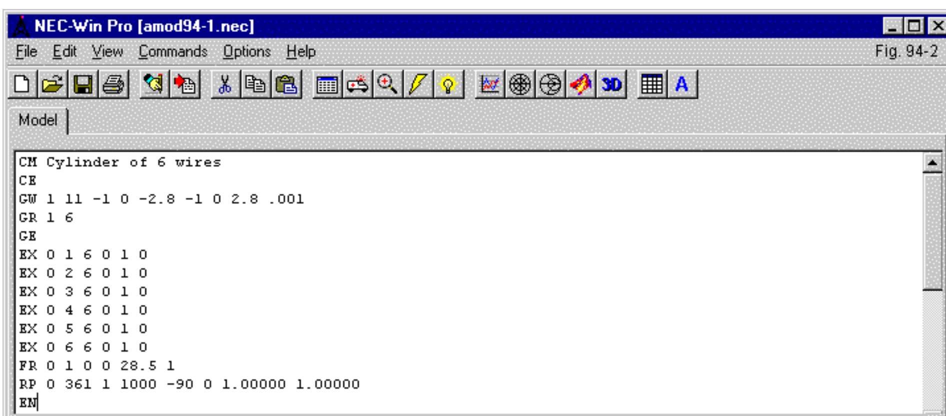


```
CM Cylinder of 6 wires
CE
GW 1 11 -1 0 -2.8 -1 0 2.8 .001
GR 1 6
GE
EX 0 1 6 0 1 0
EX 0 2 6 0 1 0
EX 0 3 6 0 1 0
EX 0 4 6 0 1 0
EX 0 5 6 0 1 0
EX 0 6 6 0 1 0
FR 0 1 0 0 28.5 1
RP 0 361 1 1000 -90 0 1.00000 1.00000
EN
```

Fig. 94-2

Despite the seeming complexity of some of the structures, formation is very straightforward. To create the set of 6 vertical dipoles in the left-most portion of **Fig. 94-1**, we need only 2 geometry commands (plus the obligatory GE command to terminate the geometry portion of the model). **Fig. 94-2** shows perhaps the simplest of GR models. See model 94-1.

GW1 sets up a vertical dipole in this free-space model. It extends equally above and below the Z = 0 level. As well, the dipole is displaced 1 m along the X-axis. However, a starting structure may begin with any values of X and Y so long as they are not both zero. Since we have only one tag number, we need increment it only by 1 in the GR line. Then we specify 6 total structures to form the cylinder at the left in **Fig. 94-1**.

```
                              - - - STRUCTURE SPECIFICATION - - -

                                  COORDINATES MUST BE INPUT IN
                                  METERS OR BE SCALED TO METERS
                                  BEFORE STRUCTURE INPUT IS ENDED
  WIRE                                                                               NO. OF    FIRST  LAST     TAG
  NO.       X1         Y1         Z1          X2         Y2         Z2      RADIUS   SEG.      SEG.   SEG.     NO.
     1  -1.00000    0.00000   -2.80000    -1.00000    0.00000    2.80000    0.00100     11         1    11       1
      STRUCTURE ROTATED ABOUT Z-AXIS  6 TIMES.  LABELS INCREMENTED BY    1

   TOTAL SEGMENTS USED=    66     NO. SEG. IN A SYMMETRIC CELL=   11     SYMMETRY FLAG= -1
 STRUCTURE HAS    6 FOLD ROTATIONAL SYMMETRY
```

The sample structure specification portion of the output file for the model shows how the core sets up the GR command. The segmentation data provides a full set of the 66 segments within the overall cylinder of wires. Note that in the original model, there is an EX0 entry for each wire. In the source impedance report, the actual value is not especially meaningful to any real antenna structure. However, observing that all the values are the same is good modeler evidence that the geometry has a correct set-up.

We may easily change the number of wires in the model by altering only the GR line of the model. Examine the GR line for the model in **Fig. 94-3** and see model 93-2. The new version of the model produces the structure in **Fig. 94-1** just left of center. The command automatically recalculates the proper angular displacement for the 12-wire cylinder. Note also in the model that there are now 12 EX0 entries to make this model comparable to the first one. One caution to observe when increasing the number of occurrences of the initial structure is not to add so many that the individual wires are too close together. Although not a problem with our standard 0.001-m radius wire, inaccuracies may result if the individual wire radii are too large for the spacing between them.

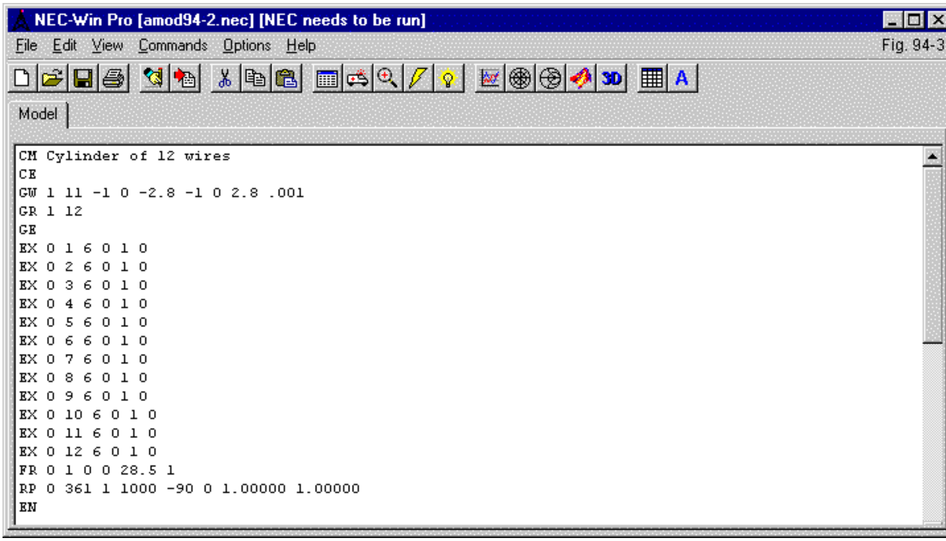
NEC-Win Pro [amod94-2.nec] [NEC needs to be run]
File Edit View Commands Options Help
Fig. 94-3
Model
CM Cylinder of 12 wires
CE
GW 1 11 -1 0 -2.8 -1 0 2.8 .001
GR 1 12
GE
EX 0 1 6 0 1 0
EX 0 2 6 0 1 0
EX 0 3 6 0 1 0
EX 0 4 6 0 1 0
EX 0 5 6 0 1 0
EX 0 6 6 0 1 0
EX 0 7 6 0 1 0
EX 0 8 6 0 1 0
EX 0 9 6 0 1 0
EX 0 10 6 0 1 0
EX 0 11 6 0 1 0
EX 0 12 6 0 1 0
FR 0 1 0 0 28.5 1
RP 0 361 1 1000 -90 0 1.00000 1.00000
EN

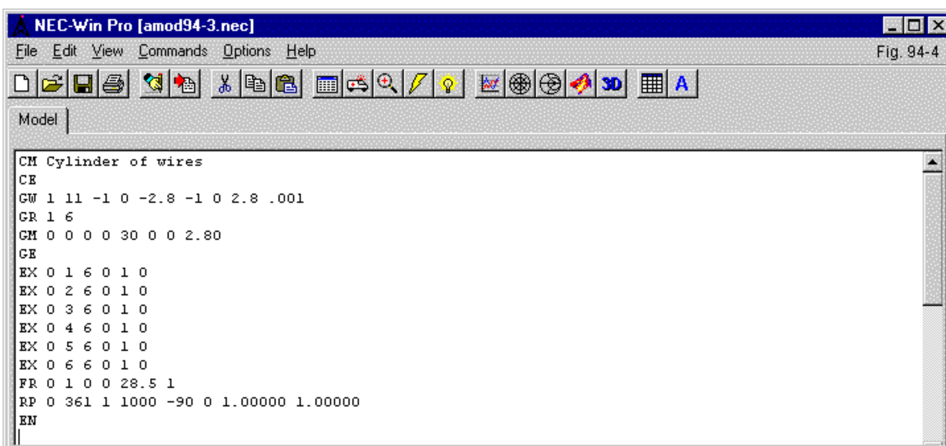
NEC-Win Pro [amod94-3.nec]
File Edit View Commands Options Help
Fig. 94-4
Model
CM Cylinder of wires
CE
GW 1 11 -1 0 -2.8 -1 0 2.8 .001
GR 1 6
GM 0 0 0 0 30 0 0 2.80
GE
EX 0 1 6 0 1 0
EX 0 2 6 0 1 0
EX 0 3 6 0 1 0
EX 0 4 6 0 1 0
EX 0 5 6 0 1 0
EX 0 6 6 0 1 0
FR 0 1 0 0 28.5 1
RP 0 361 1 1000 -90 0 1.00000 1.00000
EN

Examine the model (93-3) in **Fig. 94-4**. This model adds an allowable post-symmetry rotation and movement of the 6-wire structure in the very first model.

Since the GM entry affects the entire structure, it will run on both NEC-2 and NEC-4. The first motion entry in the command rotates the structure 30°. You can see the rotation by referencing the Y-axis line in the inner right-of-center view in **Fig. 94-1**. Compare its orientation to the un-rotated left-most view within the figure. The second maneuver within the GM command elevates the entire cylinder 2.8-m along the Z-axis. Since neither motion disturbs the symmetry of the structure, the moves show up correctly in the segmentation data of the output report. Compare the data–especially the Z-axis values–for this model with the comparable values in the report for the first model. Here is a small sample from each model's segmentation data.

Unmoved Model

SEG. NO.	COORDINATES OF SEG. CENTER X	Y	Z	SEG. LENGTH	ORIENTATION ANGLES ALPHA	BETA	WIRE RADIUS	CONNECTION DATA I-	I	I+	TAG NO.
1	-1.00000	0.00000	-2.54545	0.50909	90.00000	0.00000	0.00100	0	1	2	1
2	-1.00000	0.00000	-2.03636	0.50909	90.00000	0.00000	0.00100	1	2	3	1
3	-1.00000	0.00000	-1.52727	0.50909	90.00000	0.00000	0.00100	2	3	4	1
4	-1.00000	0.00000	-1.01818	0.50909	90.00000	0.00000	0.00100	3	4	5	1
5	-1.00000	0.00000	-0.50909	0.50909	90.00000	0.00000	0.00100	4	5	6	1
6	-1.00000	0.00000	0.00000	0.50909	90.00000	0.00000	0.00100	5	6	7	1
7	-1.00000	0.00000	0.50909	0.50909	90.00000	0.00000	0.00100	6	7	8	1
8	-1.00000	0.00000	1.01818	0.50909	90.00000	0.00000	0.00100	7	8	9	1
9	-1.00000	0.00000	1.52727	0.50909	90.00000	0.00000	0.00100	8	9	10	1
10	-1.00000	0.00000	2.03636	0.50909	90.00000	0.00000	0.00100	9	10	11	1
11	-1.00000	0.00000	2.54545	0.50909	90.00000	0.00000	0.00100	10	11	0	1

Moved Model

SEG. NO.	COORDINATES OF SEG. CENTER X	Y	Z	SEG. LENGTH	ORIENTATION ANGLES ALPHA	BETA	WIRE RADIUS	CONNECTION DATA I-	I	I+	TAG NO.
1	-0.86603	-0.50000	0.25455	0.50909	90.00000	0.00000	0.00100	0	1	2	1
2	-0.86603	-0.50000	0.76364	0.50909	90.00000	0.00000	0.00100	1	2	3	1
3	-0.86603	-0.50000	1.27273	0.50909	90.00000	0.00000	0.00100	2	3	4	1
4	-0.86603	-0.50000	1.78182	0.50909	90.00000	0.00000	0.00100	3	4	5	1
5	-0.86603	-0.50000	2.29091	0.50909	90.00000	0.00000	0.00100	4	5	6	1
6	-0.86603	-0.50000	2.80000	0.50909	90.00000	0.00000	0.00100	5	6	7	1
7	-0.86603	-0.50000	3.30909	0.50909	90.00000	0.00000	0.00100	6	7	8	1
8	-0.86603	-0.50000	3.81818	0.50909	90.00000	0.00000	0.00100	7	8	9	1
9	-0.86603	-0.50000	4.32727	0.50909	90.00000	0.00000	0.00100	8	9	10	1
10	-0.86603	-0.50000	4.83636	0.50909	90.00000	0.00000	0.00100	9	10	11	1
11	-0.86603	-0.50000	5.34545	0.50909	90.00000	0.00000	0.00100	10	11	0	1

The 30° rotation shows up in the X and Y coordinates for the first tag. The elevation become clear from the all-positive Z values for the same tag number.

The right-most view in **Fig. 94-1** shows a 6-wire cylinder that is close top and bottom by circular structures. The NEC-2 model in **Fig. 94-5** shows how we can perform the operation. (Because the structure development involves GM commands that affect individual tags and not the entire structure, there are separate NEC-2 and NEC-4 versions of the model, due to difference in the GM command structure between the cores.)

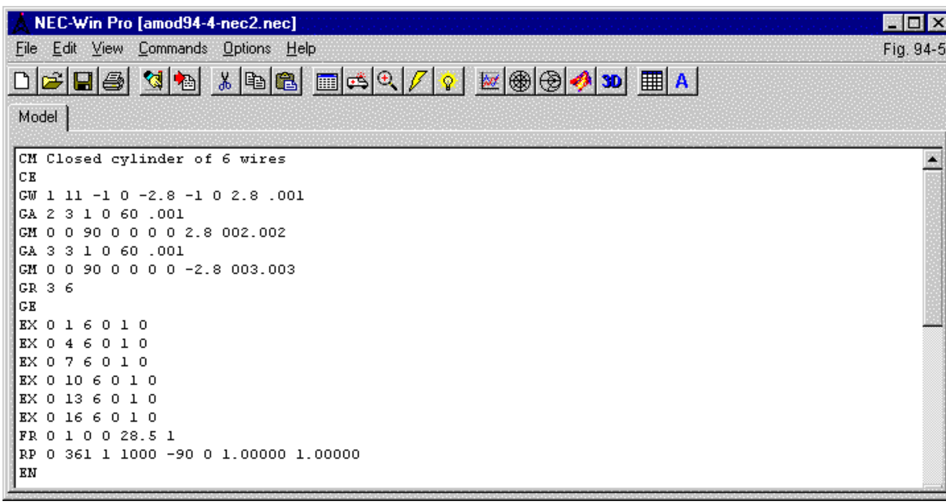

After creating the initial vertical wire, we enter two separate GA commands to create 60° arcs, the angular distance between the wires in the ultimate set. However, GA initially creates each arc vertically, so we must rotate each one by 90°, while moving it to the proper end of the initial wire. We assign to the GA structures a number of segments so that the segment length within that structure is approximately the same as the segment length within the vertical wires but with enough segments to form an adequate arc. The result is an initial structure consisting of a vertical wire with an arced wire attached to each end. The GR command finishes the full cylinder with its closed top and bottom ends.

The following sample lines from the segmentation data show the 3 tags of the initial structure and the same data for the last replication in the overall model. To orient yourself, note the source assignments in **Fig. 94-5** to Tags 1 and 16 and find those tags in the partial table.

SEG. NO.	COORDINATES OF SEG. CENTER X	Y	Z	SEG. LENGTH	ORIENTATION ANGLES ALPHA	BETA	WIRE RADIUS	CONNECTION DATA I-	I	I+	TAG NO.
1	-1.00000	0.00000	-2.54545	0.50909	90.00000	90.00000	0.00100	-66	1	2	1
2	-1.00000	0.00000	-2.03636	0.50909	90.00000	0.00000	0.00100	1	2	3	1
3	-1.00000	0.00000	-1.52727	0.50909	90.00000	0.00000	0.00100	2	3	4	1
4	-1.00000	0.00000	-1.01818	0.50909	90.00000	0.00000	0.00100	3	4	5	1
5	-1.00000	0.00000	-0.50909	0.50909	90.00000	0.00000	0.00100	4	5	6	1
6	-1.00000	0.00000	0.00000	0.50909	90.00000	0.00000	0.00100	5	6	7	1
7	-1.00000	0.00000	0.50909	0.50909	90.00000	0.00000	0.00100	6	7	8	1
8	-1.00000	0.00000	1.01818	0.50909	90.00000	0.00000	0.00100	7	8	9	1
9	-1.00000	0.00000	1.52727	0.50909	90.00000	0.00000	0.00100	8	9	10	1
10	-1.00000	0.00000	2.03636	0.50909	90.00000	0.00000	0.00100	9	10	11	1
11	-1.00000	0.00000	2.54545	0.50909	90.00000	-90.00000	0.00100	10	11	63	1
12	0.96985	-0.17101	2.80000	0.34730	0.00000	-100.00000	0.00100	31	12	13	2
13	0.85287	-0.49240	2.80000	0.34730	0.00000	-120.00000	0.00100	12	13	14	2
14	0.63302	-0.75441	2.80000	0.34730	0.00000	-140.00000	0.00100	13	14	-45	2
15	0.96985	-0.17101	-2.80000	0.34730	0.00000	-100.00000	0.00100	34	15	16	3
16	0.85287	-0.49240	-2.80000	0.34730	0.00000	-120.00000	0.00100	15	16	17	3
17	0.63302	-0.75441	-2.80000	0.34730	0.00000	-140.00000	0.00100	16	17	35	3

86	-0.50000	0.86603	-2.54545	0.50909	90.00000	-150.00000	0.00100	-49	86	87	16
87	-0.50000	0.86603	-2.03636	0.50909	90.00000	0.00000	0.00100	86	87	88	16
88	-0.50000	0.86603	-1.52727	0.50909	90.00000	0.00000	0.00100	87	88	89	16
89	-0.50000	0.86603	-1.01818	0.50909	90.00000	0.00000	0.00100	88	89	90	16
90	-0.50000	0.86603	-0.50909	0.50909	90.00000	0.00000	0.00100	89	90	91	16
91	-0.50000	0.86603	0.00000	0.50909	90.00000	0.00000	0.00100	90	91	92	16
92	-0.50000	0.86603	0.50909	0.50909	90.00000	0.00000	0.00100	91	92	93	16
93	-0.50000	0.86603	1.01818	0.50909	90.00000	0.00000	0.00100	92	93	94	16
94	-0.50000	0.86603	1.52727	0.50909	90.00000	0.00000	0.00100	93	94	95	16
95	-0.50000	0.86603	2.03636	0.50909	90.00000	0.00000	0.00100	94	95	96	16
96	-0.50000	0.86603	2.54545	0.50909	90.00000	30.00000	0.00100	95	96	46	16
97	0.33682	-0.92542	2.80000	0.34730	0.00000	-160.00000	0.00100	14	97	98	17
98	0.00000	-0.98481	2.80000	0.34730	0.00000	-180.00000	0.00100	97	98	99	17
99	-0.33682	-0.92542	2.80000	0.34730	0.00000	160.00000	0.00100	98	99	-28	17
100	0.33682	-0.92542	-2.80000	0.34730	0.00000	-160.00000	0.00100	17	100	101	18
101	0.00000	-0.98481	-2.80000	0.34730	0.00000	-180.00000	0.00100	100	101	102	18
102	-0.33682	-0.92542	-2.80000	0.34730	0.00000	160.00000	0.00100	101	102	18	18

By locating the coordinates of each segment junction in the original wire, you may add arcs at each junction and create a cylinder that is closed at all available intermediate points. Note in the sample model that the 6 EX0 entries now use new tag numbers to reflect the 3-tag initial structure. When creating structures by symmetry, it is useful to keep track of the ways that geometry modifications will affect other parts of the total model. If a scratch pad will not suffice, you may consult the Necvu segment identification feature or the segmentation data to track these affects.

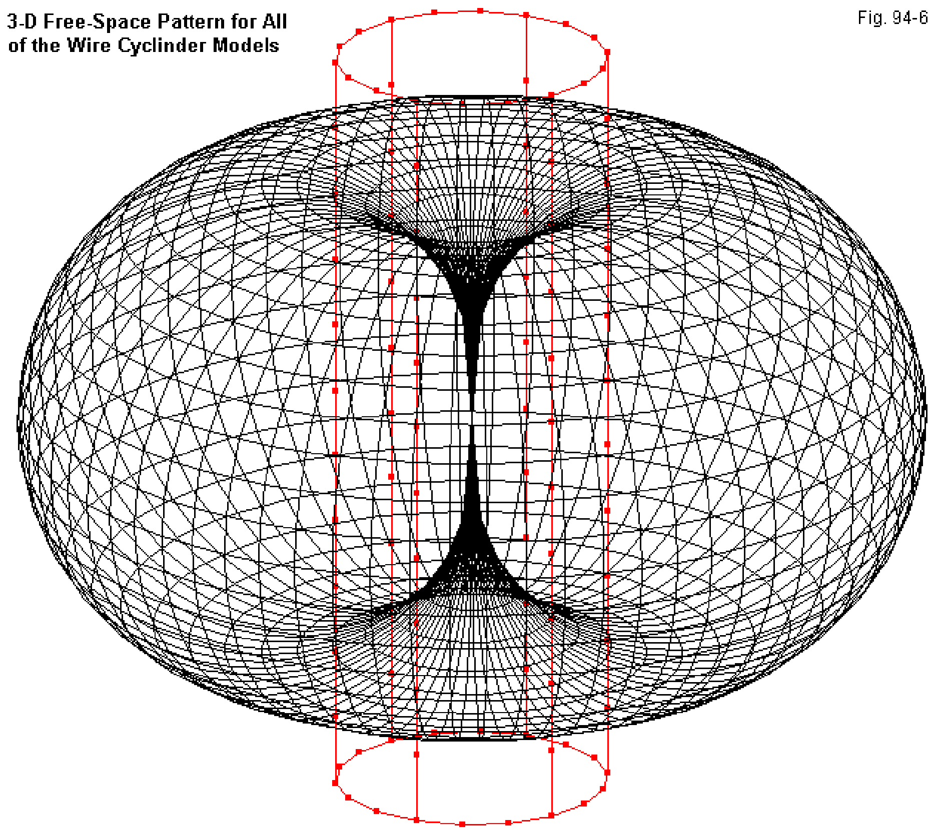

I placed sources at the center of each wire in the structures as a convenience when checking the accuracy of each model. The result is a structure that performs similarly to a simple fat dipole, as shown by the 3-dimensional pattern in **Fig. 94-6**. (The red lines are a conventionalized representation of the capped cylinder oriented at corresponding angles relative to the field lines. Without the end caps, the maximum free-space gain is 2.08 to 2.10 dBi, about the same as that of a dipole. The beamwidth of the E-plane pattern is consistently about 83°.)

Even though these small sample models do not fairly show the core-run time-saving, the largest model (132 segments) required less than twice the time of the smallest (66 segments). Wire cylinders also offer some advantages when modeling large diameter tubular structures, since the radii of the individual wires forming them via GR may have the same size as wire attached to them (so long as those wires do not destroy the symmetry). A disadvantage is that GR-formed cylinders are not suitable for antennas such as slotted cylinders, since there is no way to remove selected wires from the finished product.

For very large models, both GX and GR (but not in the same model) can speed core runs. Although the sample models are small in order to make them clear, symmetry's true home is the model that otherwise would press the core in terms of required matrix space or the time it takes a PC to process the model.

A Special Note on the "Destruction" of Symmetry

A number of modelers have read NEC manual warnings about the conditions in which symmetry is "destroyed." Unfortunately, these warnings appear in unqualified form. As a result, some modelers do not use the GR command when another wire (GW) command must appear afterwards for fear that the structure created by the GR command simply will not appear in the model.

In fact, the structure does appear and becomes just a set of wires specified by the geometry function of the GR command. The symmetry mode of calculation, however, does not function. Hence, if we have a following GW command or another condition that defeats or destroys symmetry, we do not lose the modeled structure created by GR. We only lose the increased speed of the run that symmetry would permit.

To illustrate the correct situation, examine the model (94-5) in **Fig. 94-7**. The model is the same as the very first model in this episode, with one addition. The initial GW command established a wire, and the GR command creates the resulting circle of 6 wires. In this model, GW 11 adds a new wire.

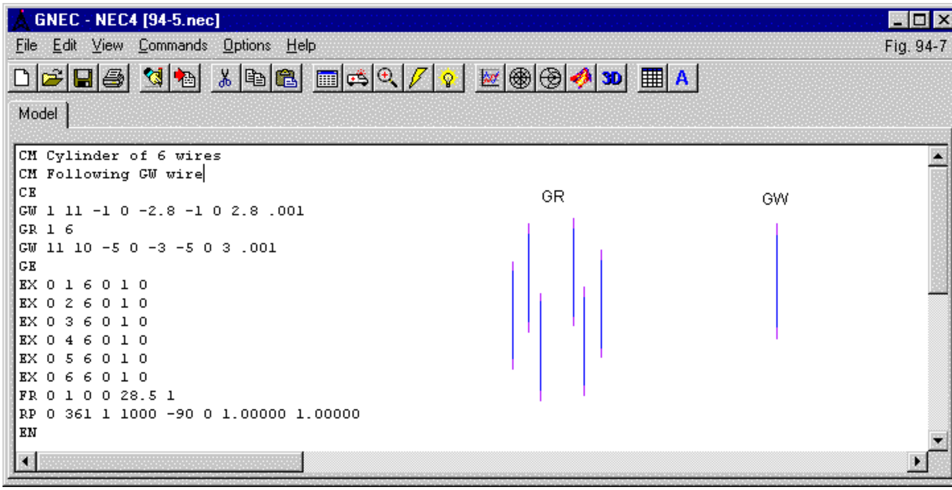

To the right of the model file, I have inserted the Necvu rendering of the model that emerges from the wire specification section of the NEC output report. The 6 wires in the circle emerge from GW 1 and the GR command. To see how NEC handles this case, we may examine the first section of the NEC output report.

```
                          - - - STRUCTURE SPECIFICATION - - -

                               COORDINATES MUST BE INPUT IN
                               METERS OR BE SCALED TO METERS
                               BEFORE STRUCTURE INPUT IS ENDED


 WIRE                                                                        NO. OF    FIRST  LAST     TAG
 NO.       X1        Y1        Z1         X2        Y2        Z2      RADIUS   SEG.     SEG.   SEG.     NO.
   1    -1.00000   0.00000  -2.80000   -1.00000   0.00000   2.80000   0.00100    11        1     11       1
     STRUCTURE ROTATED ABOUT Z-AXIS  6 TIMES.  LABELS INCREMENTED BY    1
   2    -5.00000   0.00000  -3.00000   -5.00000   0.00000   3.00000   0.00100    10       67     76      11

  TOTAL SEGMENTS USED=   76     NO. SEG. IN A SYMMETRIC CELL=   76     SYMMETRY FLAG=  0
```

Note the very last entry that sets the symmetry flag at 0. If symmetry had been in effect, the flag would read -1. Hence, the model will run with all 7 wires in place, but will not use symmetry in the calculation process. Since GR is a highly functional geometry command, even apart from its potential to invoke symmetry, we should keep it in mind for many purposes, for example, when modeling radial systems, cylinders, and numerous other shapes.

Conclusion

Our brief foray into cylindrical rotation does not capture everything that we may do with the GR command. However, I hope that these notes make the command somewhat more accessible than it might otherwise have been.

95. Some Basics of the NT Command

The NT command allows you to implement 2-port networks in a model using non-radiating methods, much like the TL command. In fact, the TL command is a specialized implementation of more general networks. However, use of the TL command presumes a basic mastery of handling short circuit admittance matrix parameters. As a result, the command has little general use among the total body of those using NEC. Short circuit admittance matrix parameters and their calculation from more conventional antenna parameters is a subject well beyond the scope of this series. However, there are a number of applications of NT networks that admit of some approximations and hence some short cuts in the calculation procedure. They will suffice to allow us to illustrate the fundamental uses of the command, as well as its entry structure.

The NT command will let you perform easily some difficult modeling tasks, such as placing a loading element in parallel with a source or creating a parallel connection between segments on different wires within a model. It also allows you to incorporate extremely complex networks into a model so long as you can reduce them to the short circuit admittance parameters required by a 2-port network. In virtually all cases, the command is less troublesome than calculating the values to fit its entry positions. The problem facing the modeler who has not previously used networks is less a matter of understanding the command entries than it is in knowing what entries to make in the floating decimal positions.

The command structure itself is very straightforward. As the sample line below shows, the integer entries specify the specific tag and segment numbers between which we connect the network. In some cases, one of the tags will be a remote wire, and occasionally, it will serve as a "place-holder" to terminate the network. However, there are many applications in which both wires will be active parts of the structure geometry.

CMD	I1	I2	I3	I4	F1	F2	F3	F4	F5	F6
	TAG1	SEG1	TAG2	SEG2	Y11R	Y11I	Y12R	Y12I	Y22R	Y22I
NT	2	1	1	6	5.8e-5	-7.3e-3	-5.8e-5	1.7e-2	5.8e-5	-4.8e-3

The floating decimal entries call for port values according to the standard 2-port labeling. See **Fig. 95-1**.

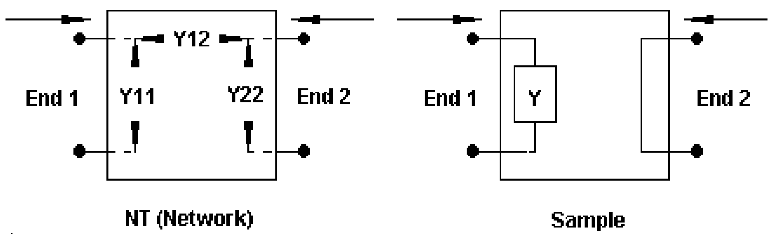

Fig. 95-1

End 1 corresponds to tag 1-seg1, and end 2 to tag 2-seg2. Since the entries that go into the network are usually non-symmetrical, it is important to keep the ends straight. In the sample to the right, we wish the Y element to be in parallel with the assigned tag and segment. Therefore, we must assign its value to the Y11 real and imaginary component positions in the command and be certain the I1 and I2 specify the segment to which the Y element is parallel.

Y11 is the short circuit input admittance, expressed in terms of real and imaginary components. In other contexts, we might call the real component the conductance (G) and the imaginary component susceptance (B). Both use Siemens or mhos as the unit of measure, and they are the inverse of resistance and reactance, respectively. Hence, admittance (Y), also measured in mhos is the reciprocal of impedance (Z). Y22 is the output short circuit reverse-transfer admittance, as indicated by the arrow in the sketch. Since each port has balanced currents, the net current transferred between port 1 and 2 is zero. Hence, Y12 does not represent a physical connection between ports. Rather, it is the short circuit transfer admittance. Since the matrix is symmetric, it is unnecessary to specify Y21, since the forward transfer admittance and the reverse transfer admittance are equal. Y12 and Y22 are also specified in terms of real and imaginary components.

Besides being specific to an assigned frequency, multiple NT entries must be grouped together. You may intermix them with TL commands, but the group must have no other commands separating the members of the group. Intervening commands other than NT or TL will result in the next TL or NT entry destroying previous NT and TL commands. If your NEC core does not employ auto dimensioning, you must set the parameter MAXNET high enough to include the total number of NT and TL commands to be used in the model. For most models, this setting is trivial. However, there may be a large number of driven elements in an array, each with a current source. Since each current source invokes a network, some assemblies may require a very high number of NT commands.

In an earlier episode, we examined a technique for creating parallel sources, but requiring only 1 source assignment. By using a very short transmission line, we effected a virtual short circuit between the specified segments, but with the connections in parallel with the source. The technique proves useful when close space wires might yield inaccuracies if drawn to a single source wire due to very small angles between wires at the junctions. See **Fig. 95-2**.

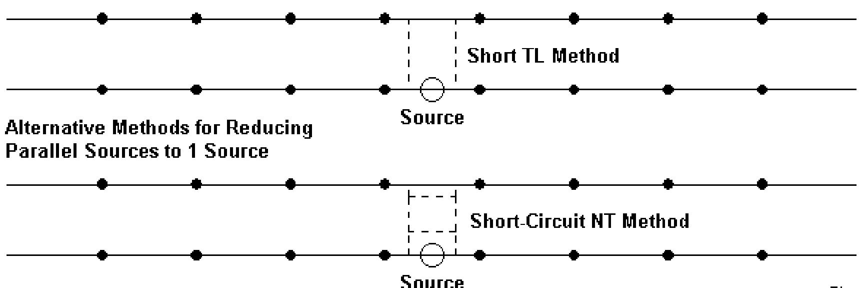

Fig. 95-2

The following lines show the excitation and transmission line commands for the parallel-wire dipole. See model 95-1.

```
CM Parallel-Wire Dipole
CE TL method
GW 1 79 0 -.47 .006 0 .47 .006 .0005
GW 2 79 0 -.47 -.006 0 .47 -.006 .0005
GW 3 1 0 -.47 -.006 0 -.47 .006 .0005
```

```
GW 4 1 0 .47 -.006 0 .47 .006 .0005
GE
FR 0 1 0 0 150 1
EX 0 2 40 00 1 0
TL 1 40 2 40 140 .001
RP 0 1 361 1000 90 0 1.00000 1.00000
EN
```

The reported source impedance of the dipole is 71.427 - j1.873 Ω. For comparative purposes, the impedance report has far more decimal places than practical applications would require. Now let's suppose that we would like to create the virtual short circuit between wires using the NT command. Like TLs, NTs are in parallel with sources and in series with loads on the same segment.

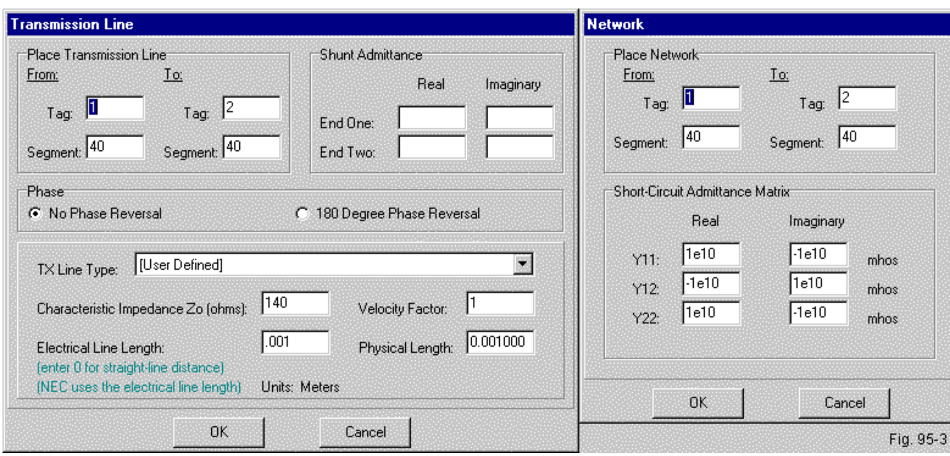

Fig. 95-3

Fig. 95-3 compares the entry assist screens for the required TL and NT entries. The TL entry uses a very short length: 1 mm. By using an electrical length entry as short as 1e-10, the impedance specification would have become wholly arbitrary. Now examine the right side of the figure and the following model (95-1a).

```
CM Parallel-Wire Dipole
CE NT method
GW 1 79 0 -.47 .006 0 .47 .006 .0005
GW 2 79 0 -.47 -.006 0 .47 -.006 .0005
GW 3 1 0 -.47 -.006 0 -.47 .006 .0005
GW 4 1 0 .47 -.006 0 .47 .006 .0005
GE
FR 0 1 0 0 150 1
EX 0 2 40 00 1 0
NT 1 40 2 40 1e10 -1e10 -1e10 1e10 1e10 -1e10
RP 0 1 361 1000 90 0 1.00000 1.00000
EN
```

Creating a virtual short circuit with an NT command is seemingly complex, but once you have the formula, you may copy it as many times as you need it. In fact, there is a pattern to the entries. Let us set the conductance of the connecting wire (G) to 1e10 and the susceptance (B) to the same value. To create a short circuit with these initial values, we need to set the admittance matrix of the NT command as follows.

Parameter	Real		Imaginary	
Y11	+G	1e10	-B	-1e10
Y12	-G	-1e10	+B	1e10
Y22	+G	1e10	-B	-1e10

We shall later see that this entry set views the short circuit as a special form of a PI network translated into admittance matrix entries. For the moment, we may simply memorize the form–of course, after running the model and confirming that it yields the correct source impedance: 71.430 - j1.868 Ω. Both the TL and NT versions of the parallel-wire dipole return free-space gain values of 2.13 dBi. You may also wish to examine the currents on various corresponding segments of the model to establish their virtual identity.

A second relatively simple use of the NT command that we have already encountered appears in an earlier episode: the current source. Examine the following model, a basic dipole with a current source. See model 95-2.

```
CM dipole with current source
CE 0 deg at antenna source
GW 1 11 0 -.2375 0 0 .2375 0 .001
GW 2 1 9999 -.005 9999 9999 .005 9999 .001
GE
FR 0 1 0 0 299.7925 1
EX 0 2 1 00 0.00000 1.00000
NT 2 1 1 6 0 0 0 1 0 0
XQ
EN
```

In this case, we create the required dipole (GW1) and add a second remote 1-segment wire (GW2) located too far away from the key element to have any affect on the pattern data. The remote wire is very short, very thin, and never given a material load. Next, we place a network (NT) between the dipole source segment and the remote wire, using the standard set-up of the NT command for a current source. Using the NT assistance screen in the software, shown on the left in **Fig. 95-4**, will ease the burden of remembering which entry point receives the value of 1 for the Y12 imaginary position. Finally, we add an EX0 command, placing the source on the remote wire and phase shifting the value by 90°.

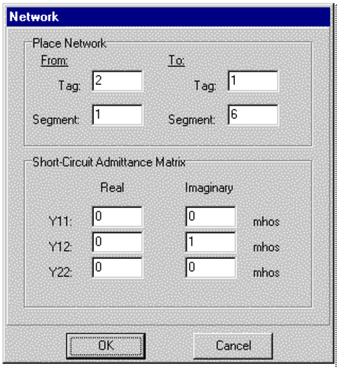

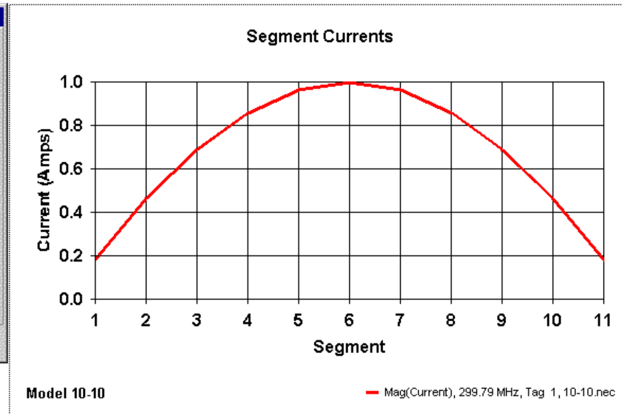

Fig. 95-4

By entering a Y12-imaginary value of 1.0 mho in the network, we obtain a 90° phase shift in the current at the element relative to the phase of the voltage at the source on the other side of the network. As well, whatever value the source shows as its voltage will appear at the other side of the network on the element as the current value. The technique of "forcing" current values is widely used in phased array design, but here, it functions to provide a current source with a known value at the true feedpoint of the antenna. One very significant use of current sources is to allow rectangular plots of the element currents reference to a standard value, such as 1.0. The right side of **Fig. 95-4** shows such a plot for the dipole.

For easy extraction of the required data that applies to the antenna feedpoint (in contrast to the model source on the remote wire), we must learn how to "read" the data. The first key output report entry is the antenna input parameters, shown below for our current-source dipole.

- - - ANTENNA INPUT PARAMETERS - - -

TAG	SEG.	VOLTAGE (VOLTS)		CURRENT (AMPS)		IMPEDANCE (OHMS)		ADMITTANCE (MHOS)		POWER
NO.	NO.	REAL	IMAG.	REAL	IMAG.	REAL	IMAG.	REAL	IMAG.	(WATTS)
2	12	0.00000E+00	1.00000E+00	-1.16117E-01	7.17602E+01	1.39353E-02	-2.25490E-05	7.17602E+01	1.16117E-01	3.58801E+01

1. The phase-shifted voltage value–1.0 v imaginary–is the real current level at the element feedpoint. You may verify this from the current table for segment 6.

```
 SEG.   TAG           - - - CURRENT (AMPS) - - -
 NO.    NO.      REAL        IMAG.       MAG.        PHASE
  6     1      1.0000E+00 -2.2205E-16  1.0000E+00    0.000
```

2. The impedance at the element feedpoint appears as an admittance (and its inverse as an impedance). If you create a standard dipole model using a voltage source, its impedance with a voltage source is 71.76 + j 0.12 Ω, the value that now appears under the admittance entry.

3. The power report is accurate for the current-source model. Hence, by the technique of power adjustment shown in earlier episodes, we would adjust the imaginary voltage value as the square root of the ratio of new power to old to arrive at the correct source for the desired power level. A value of 5.279 volts imaginary will yield a 1000-watt power level.

The NT command also offers use the potential for having one more alternative way to perform a specific task. Consider the following model (95-3), a simple 3-element Yagi designed for 14.175 MHz and using 1" (0.025 m) aluminum elements.

```
CM 3-el Yagi with beta match
CM Pre-match version
CE
GW 1 101 -5.292 0 0 5.292 0 0 0.0125
GW 2 50 -4.947 3.024 0 -0.049 3.024 0 0.0125
GW 3 1 -0.049 3.024 0 0.049 3.024 0 0.0125
GW 4 50 0.049 3.024 0 4.947 3.024 0 0.0125
GW 5 101 -4.786 6.049 0 4.786 6.049 0 0.0125
GS 0 0 1
GE 0
EX 0 3 1 0 1 0
LD 5 0 0 0 2.5E7
FR 0 1 0 0 14.175 1
RP 0 1 360 1000 90 0 1 1
EN
```

The elements employ a high segmentation density, with the driver element (GW2 - GW4) subdivided. The left side of **Fig. 95-5** shows the evolution of the element, along with the first alternative that we shall use in our quest to match the antenna to a 50-Ω feedline. However, run this pre-match version of the antenna to obtain its "natural" source impedance: 23.42 - j24.59 Ω. The reported antenna gain is 7.84 dBi with an AGT value of 0.99977, indicating a very adequate model and accurate output reports (as always, within the limits of the AGT test).

Our matching goal has several options, but we shall choose to add a beta match. The beta match is a version of an L-network with down conversion from the source (50 Ω) to the load. This system requires a series impedance element on the load side of the network, already in place in the form of the capacitive reactance of the source. The other element of the network consists of a shunt reactance of the opposite type (relative to the series reactance) on the source side of the network. To achieve this goal, we need to be able to place a load in parallel with the source. However, LD loads appear in series with the source and thus are not applicable.

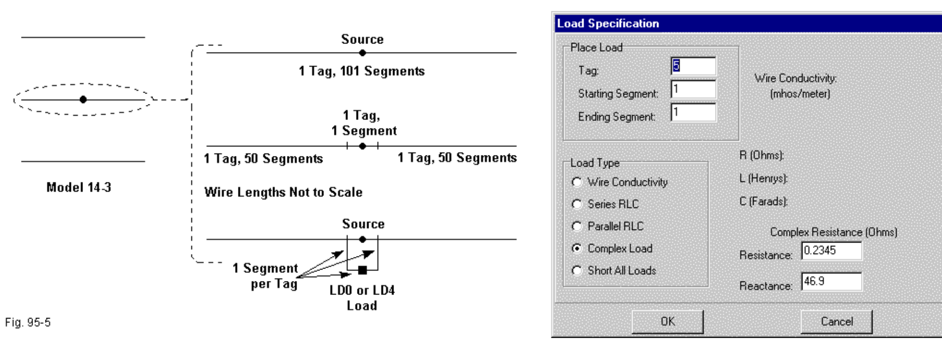

Fig. 95-5

One tactic that we can use is to create a physical structure to give a parallel position for the load. The last part of the sketch in **Fig. 95-5** shows a way to accomplish this feat. By using 1-segment wires around the 1-segment source wire, we create a box. Since the wires are short, they contribute very little to the radiation pattern. However, they provide a place for the desired shunt reactance. Examine the additional wires for the box in the following model (95-3a). Note that they place the box at right angles to the plane of the antenna, although an in-line orientation would work as well. The new wires appear between the original drive entry and the director, which is now GW8. As well, the final end of the driver (GW7) follows the box structure. Excitation remains on GW3.

```
CM 3-el Yagi with beta match
CM vertical placement
CE
GW 1 101 -5.292 0 0 5.292 0 0 0.0125
GW 2 50 -4.947 3.024 0 -0.049 3.024 0 0.0125
GW 3 1 -0.049 3.024 0 0.049 3.024 0 0.0125
GW 4 1 -0.049 3.024 0 -0.049 3.024 0.098 0.0125
GW 5 1 -0.049 3.024 0.098 0.049 3.024 0.098 0.0125
GW 6 1 0.049 3.024 0.098 0.049 3.024 0 0.0125
GW 7 50 0.049 3.024 0 4.947 3.024 0 0.0125
GW 8 101 -4.786 6.049 0 4.786 6.049 0 0.0125
GS 0 0 1
GE 0
EX 0 3 1 0 1 0
LD 4 5 1 1 0.2345 46.9
LD 5 0 0 0 2.5E7
FR 0 1 0 0 14.175 1
RP 0 1 360 1000 90 0 1 1
EN
```

The required value for the shunt element derives from standard L-network equations:

$$\delta = \sqrt{\frac{R_{High}}{R_{Low}} - 1} \qquad X_S = \delta R_{Low} \qquad X_P = \frac{R_{High}}{\delta}$$

The term “delta” (ä) is the loaded Q of the network and derives from the high and low resistance values at the circuit terminals. The required series reactance is delta times the low resistance and appears in series with it. The shunt or parallel reactance is of the opposite type from the series reactance and is the high resistance divided by delta. There are numerous utility programs available for calculating the required values. By using the natural source resistance and the feedline characteristic impedance to determine delta, we discover that the existing series capacitive reactance is almost precisely what the equations calculate. Hence, we need only calculate a corresponding shunt or parallel reactance: j46.9 Ω inductive. Based on experience, we may assign the shunt element a Q of about 200. The final values appear in the LD4 entry for the model.

We might run the model to obtain its performance values: 7.86 dBi gain, 57.58 + j1.51 Ω impedance, 1.008 AGT, 0.036 AGT-dBi, and an adjusted gain of 7.82 dBi. The AGT value shows that the wire box has a small affect on model adequacy, and the adjusted gain value suggests that the box also has a small affect on performance of the driver. The fact that we did not arrive at precisely 50 Ω impedance is a measure of how far off from ideal the series reactance is, as well as the affects of the wire box. Perhaps one of the chief advantages of this system of adding a parallel load is that it allows the simulation of inductors (in contrast to beta hairpin assemblies. By converting the load to a type 0 using the same series resistance, but an inductance of 0.527 µH, the model becomes perfectly frequency nimble, with accurate output values for frequency sweeps across the operating passband.

Although subsequent alternative shunt loads will not require the driver scheme used for the box version, we shall retain it so that the core model remains constant in all of our trials. In the following model, we see a version of the antenna using a technique that we met in previous episodes when exploring the use of transmission lines. This model (95-3b) employs a standard shorted transmission line stub calculated to provide the required reactance. Then, we trimmed the stub to a length that yielded the most satisfactory source impedance.

```
CM 3-el Yagi with beta match
CM TL 600-Ostub
CE
GW 1 101 -5.292 0 0 5.292 0 0 0.0125
GW 2 50 -4.947 3.024 0 -0.049 3.024 0 0.0125
GW 3 1 -0.049 3.024 0 0.049 3.024 0 0.0125
GW 4 50 0.049 3.024 0 4.947 3.024 0 0.0125
GW 5 101 -4.786 6.049 0 4.786 6.049 0 0.0125
GW 6 1 1.001 1.001 1.001 1 1 1 0.000322
GS 0 0 1
GE 0
```

```
EX 0 3 1 0 1 0
LD 5 0 0 0 2.5E7
TL 3 1 6 1 600 0.262584 0 0 1e10 1e10
FR 0 1 0 0 14.175 1
RP 0 1 360 1000 90 0 1 1
EN
```

GW6 provides the remote termination wire for the shorted stub. The TL command specifies a 600-Ω line with a length of 0.263 m, simulating an open or ladder line stub assembly. Run the model to obtain its output reports: 7.84 dBi gain, 49.23 - j0.005 Ω impedance, 0.999 AGT. The near-ideal value of AGT requires no gain report adjustment, and the gain value coincides with the report from the pre-matched model. Although the TL line cannot show losses within it, they should be negligible. Like the use of an LD0 load in the box model, this version of the beta-matched Yagi is also frequency nimble.

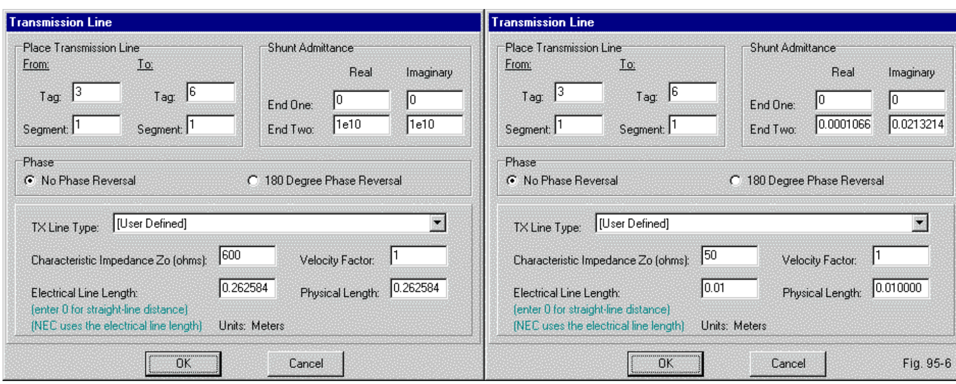

Fig. 95-6

Fig. 95-6 shows the assist screen for the TL stub in the model that we just examined. However, it is not the only way in which we might use the TL command to effect a parallel load on the Yagi source segment. The right side of the figure shows an alternative set of entries. Examine the next model (95-3c). You will note that the geometry remains unchanged from the previous model. However, the TL line reflects the values shown in the figure.

```
CM 3-el Yagi:  14.175 MHz
CM TL + shunt admittance beta match
CE
GW 1 101 -5.292 0 0 5.292 0 0 0.0125
GW 2 50 -4.947 3.024 0 -0.049 3.024 0 0.0125
GW 3 1 -0.049 3.024 0 0.049 3.024 0 0.0125
GW 4 50 0.049 3.024 0 4.947 3.024 0 0.0125
GW 5 101 -4.786 6.049 0 4.786 6.049 0 0.0125
GW 6 1 2000 2000 2000 2000.001 2000.001 2000.001 0.000814
GS 0 0 1
GE 0
EX 0 3 1 0 1 0
LD 5 0 0 0 2.5E7
TL 3 1 6 1 50 0.01 0 0 0.0001066 -0.0213214
FR 0 1 0 0 14.175 1
RP 0 1 360 1000 90 0 1 1
EN
```

As a special form of a network, the TL command allows the use of shunt admittance values at either end of the line for various simulation purposes. In this case, instead of using a stub, we specify a very short line length. The line is so short that no significant transformation of voltage, current, or impedance can occur. On the "far" end of the line, we insert the shunt admittance equivalents of the series values of resistance and reactance that we need for the match. The real component of an admittance (Y) is conductance (G), and the imaginary component is susceptance (B). Since the conversion requires converting a series impedance into a shunt or parallel admittance, we may use these equations:

$$G_P = \frac{R_S}{R_S^2 + X_S^2} \qquad B_P = -\frac{X_S}{R_S^2 + X_S^2}$$

The subscripts "S" and "P" indicate series and parallel values, respectively. Using the original values of the required impedance for a coil with a Q of 200, we convert 0.2345 + j49.6 Ω to 1.066E-4 - j2.132E-2 mhos. These values go on end 2 of the line.

If you run the model, you will obtain the following reports: 7.82 dBi gain, 48.98 - j0.32 Ω impedance, 0.999 AGT. The resistive component of the impedance is slightly low because we did not adjust the coil reactance for a closer approach to 50 Ω before converting the reactance to a susceptance. The limitation of this method of creating a beta match is that it is frequency specific and does not yield highly accurate values in a frequency sweep.

We are not quite done with our beta matched Yagi. We have painlessly slipped into the realm of admittances, and so we might as well create the parallel-matching element using the NT command. Examine the following model (95-3d) and its NT command that replaces the TL commands.

```
CM 3-el Yagi:  14.175 MHz
CM NT + shunt admittance values
CE
GW 1 101 -5.292 0 0 5.292 0 0 0.0125
GW 2 50 -4.947 3.024 0 -0.049 3.024 0 0.0125
GW 3 1 -0.049 3.024 0 0.049 3.024 0 0.0125
GW 4 50 0.049 3.024 0 4.947 3.024 0 0.0125
GW 5 101 -4.786 6.049 0 4.786 6.049 0 0.0125
GW 6 1 2000 2000 2000 2000.001 2000.001 2000.001 0.000814
GS 0 0 1
GE 0
EX 0 3 1 0 1 0
LD 5 0 0 0 2.5E7
NT 3 1 6 1 0.0001066 -0.0213214 0 0 1e10 1e10
FR 0 1 0 0 14.175 1
RP 0 1 360 1000 90 0 1 1
EN
```

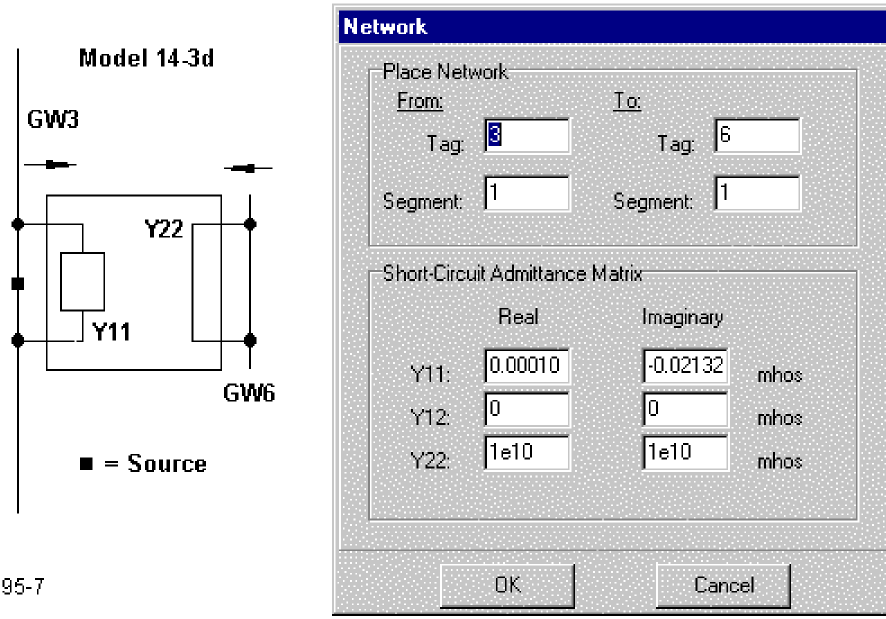

Fig. 95-7

To place a load in parallel with a source on a specific segment, we may use the system shown in model and in **Fig. 7**. We place the shunt admittance values on the end of the network connected to the target segment. These are the Y11 values, which are identical to those used for the short-TL version of the model. Y12 remains blank, as indicated by the zero entries. The other end of the network requires a short circuit, normally created by the use of very high values of real and imaginary admittance for Y22. The network short circuit adds nothing to the structure geometry of a model, and so the short-circuited end of the network may connect to any wire without affecting antenna performance. Since GW6 is left over from the TL models, we used that 1-segment wire as the network terminus.

You may run the model for its reports: 7.82 dBi gain, 48.98 - j0.01 Ω impedance, 0.999 AGT. The reduced reactance results from not having a 0.01-m line between the source segment and the load. Since we are using admittance values (comparable to using impedance values in an LD4 load), the model is frequency specific. Its chief advantage lies in the place it occupies in our progression of beta-matched models. Hopefully, by revealing its relationship to other techniques that we may use to achieve relatively the same goal, the function and nature of NT networks is somewhat clearer.

In this episode, we have looked at some fairly simple applications of the NT command and their relationship to alternative ways of achieving the same goals. Indeed, the more commands that we master, the more ways that we may create modifications to the geometry of a model. The flexibility lets us select the means that best suits the need.

There are further applications of the NT command that more directly involve us in the 2-port-network nature of the command. In the next episode, we shall examine how to add to our antenna models the matching networks that bring the source impedance from its natural value to that ubiquitous 50-Ω value. Along the way, we shall also show some short cuts to the required calculations, although a hand-calculator will still be a necessary adjunct to our modeling efforts.

96. Some Further Applications of the NT Command

In the last episode, we examined the basics of the NT or network command, along with some specialized uses. The command itself is straightforward in its structure.

CMD	I1	I2	I3	I4	F1	F2	F3	F4	F5	F6
	TAG1	SEG1	TAG2	SEG2	Y11R	Y11I	Y12R	Y12I	Y22R	Y22I
NT	2	1	1	6	5.8e-5	-7.3e-3	-5.8e-5	1.7e-2	5.8e-5	-4.8e-3

The integer entries identify the terminal tags and segments for the network, while the 6 floating point positions take the admittance values for the 2-port network. In this episode, we shall probe a bit further into the use of the NT command to simulate complex real networks of components. Note that we shall have to be careful when we use the term "network" with respect to the NT command's contents. The term refers to a 2-port admittance parameter network. At the same time, these handy networks serve to capture the key ingredients of many passive arrays of components that we more traditionally call networks. In theory, the 2-port network can stand in for any component network, no matter how complex.

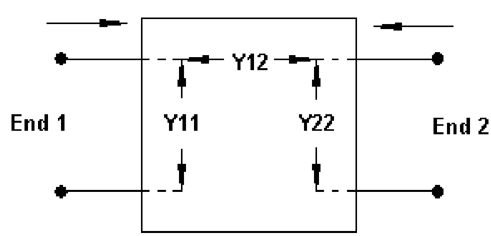

2-Port Admittance Parameter Network

Fig. 96-1

The terms of a 2-port network, shown in **Fig. 96-1**, have names with meanings:

Y11: short circuit input admittance
Y22: short circuit output admittance
Y12: short circuit reverse transfer admittance
Y21: short circuit forward transfer admittance

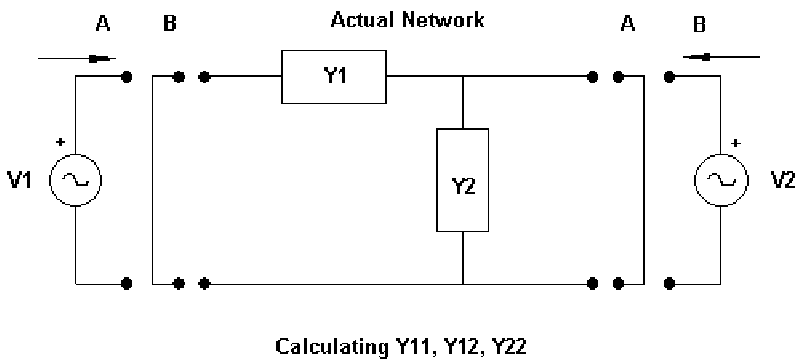

Fig. 96-2

Consider a real component network, such as the central part of **Fig. 96-2**. One form of analysis that we can perform (A) is to short-circuit the output and apply a voltage to the input. Then we can reverse the procedure (B), applying a voltage to the output side with the input side short-circuited. Under these conditions, the following relationships will hold.

$$I_1 = y_{11} V_1 + y_{12} V_2 \qquad I_2 = y_{21} V_1 + y_{22} V_2$$

With the output shorted, we can calculate the values of Y11 and Y21:

$$y_{11} = \frac{I_1}{V_1} \qquad y_{21} = \frac{I_2}{V_1} \qquad If\ V_2 = 0$$

With the input shorted, we can likewise calculate the values of Y22 and Y12:

$$y_{12} = \frac{I_1}{V_2} \qquad y_{22} = \frac{I_2}{V_2} \qquad \mathit{If}\ V_1 = 0$$

Since we have restricted ourselves to passive networks, we need not calculate both Y12 and Y21, because

$$y_{12} = y_{21}$$

Perhaps the only special thing we must do is get used to the fact that NEC nomenclature puts the admittance terms in capital letters, while textbooks shown them in the lower case. Those same textbooks have also replaced–in most cases–the traditional E with a V for voltage, as in the above equations. As well, we shall also have to remember that admittance parameter networks involve calculations based on shunt or parallel admittance, not on series admittance.

Impedance Matching a Folded Dipole to a 50-Ω Source

In order to see some practical cases using the NT command, let's set up a folded dipole at 28.5 MHz, as in the following model (96-1).

```
CM Folded Dipole
CM Pre-match version
CE
GW 1 99 -2.4892 0. 0. 2.4892 0. 0. .0005119
GW 2 1 2.4892 0. 0. 2.4892 0. .0762 .0005119
GW 3 99 2.4892 0. .0762 -2.4892 0. .0762 .0005119
GW 4 1 -2.4892 0. .0762 -2.4892 0. 0. .0005119
GE 0
FR 0 1 0 0 28.5 1
GN -1
EX 0 1 50 00 1 0
XQ
EN
```

The key parameter for our work will be the source impedance: 286.705 + j0.651 Ω. Since we do not need a pattern, the model uses the XQ command rather than an RP command. In episode 73, we reviewed a technique for adding a component network to the model in order to match the folded dipole to a 50-Ω source. See **Fig. 96-3**.

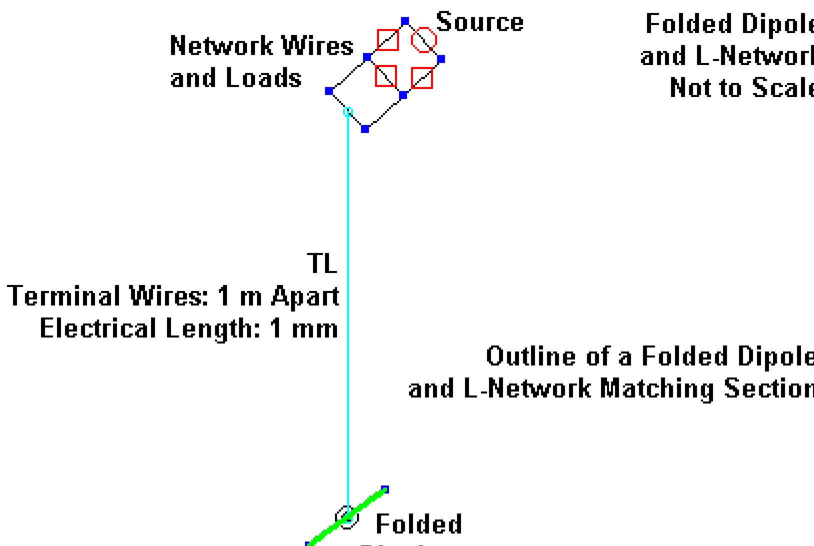

Fig. 96-3

To create this antenna plus matching network (an L circuit), we ended up with a model like the following one (96-2).

```
CM Folded Dipole
CM TL + LD matching network to 50 Ω
CE
```

```
GW 1 99 -2.4892 0. 0. 2.4892 0. 0. .0005119
GW 2 1 2.4892 0. 0. 2.4892 0. .0762 .0005119
GW 3 99 2.4892 0. .0762 -2.4892 0. .0762 .0005119
GW 4 1 -2.4892 0. .0762 -2.4892 0. 0. .0005119
GW 5 1 0. -.0254 1 0. .0254 1 .0005119
GW 6 1 0. .0254 1 .0254 .0254 1 .0005119
GW 7 1 .0254 -.0254 1 0. -.0254 1 .0005119
GW 8 1 .0254 -.0254 1 .0254 .0254 1 .0005119
GW 9 1 .0508 -.0254 1 .0254 -.0254 1 .0005119
GW 10 1 .0254 .0254 1 .0508 .0254 1 .0005119
GW 11 1 .0508 -.0254 1 .0508 .0254 1 .0005119
GE 0
TL 1 50 5 1 290 .001
LD 0 9 1 1 0. 2.6E-07 0.
LD 0 10 1 1 0. 2.6E-07 0.
LD 0 8 1 1 0. 0. 4.19E-11
FR 0 1 0 0 28.5 1
GN -1
EX 0 11 1 00 1 0
RP 0 1 361 1000 90 0 1.00000 1.00000
EN
```

The added lines or GW entries provide a wire framework to hold the components, as indicated by the LD0 entries. A very short transmission line (TL) makes a virtual direct connection to the normal folded dipole feedpoint while the actual wire grid structure is at a considerable distance from the main antenna structure to prevent unwanted interactions between the two groups of wires. The model returns a matched source impedance of 50.231 + j1.412 Ω.

The wire-grid system holds both advantages and disadvantages. On the plus side, it is accurate within general limits and is amenable to frequency sweeps. On the minus side, the extra wires do have an affect on the network and require great care to achieve reasonable results.

In contrast, if we replace the wire grid with the NT command, we vastly simplify the model. At the same time we can achieve considerable accuracy, since the NT network is a non-radiating structure that does not interfere with the structure geometry of the model. However, an NT replacement for the component network has 2 drawbacks: it is frequency specific (like an LD4 load that specifies resistance and reactance), and it requires some external work to arrive at the values for the 6 floating decimal positions in the command.

Those who have little or no experience using 2-port networks usually have two stages of learning curve to endure. The first involves getting used to converting component values into shunt admittance values rather than using the more familiar impedance terms. In isolation, of course, conductance (G) is the inverse of resistance (R), and susceptance (B) is the inverse of reactance (X). Originally, to signify the inverse relationship, the unit of conductance, susceptance, and admittance was the mho, more recently changed to the Siemen (S). G and B occur together, just as do R and X. As well, we tend to think of R and X in series form: R +/- jX Ω. However, admittance normally appears in shunt or parallel form: G +/-jB S. To convert a series-form impedance to a shunt-form admittance requires that we combine the inversion with a series-to-parallel operation, so that the actual conversions look like the following:

$$G_p = \frac{R_s}{R_s^2 + X_s^2} \qquad B_p = -\frac{X_s}{R_s^2 + X_s^2}$$

Note the reversal of sign on the susceptance equation, due to the change of phase angle when changing from a series to a parallel form.

The second stage of the learning curve involves deriving the correct values for Y11, Y12, and Y22 when converting a component network into a 2-port network. Depending on the complexity of the component network, along with our adeptness at working with nodal equations, etc., the work can become tedious. However, for many tasks, there is no way around the work.

For our illustrations, we can simplify the entire operation by setting up a few restrictions. First, capacitors will have an indefinitely high Q, and so we may safely ignore their conductance. This holds true only of good quality capacitors used in the HF region, and so we shall continue to work below 30 MHz. Second, if an inductor has a sufficiently high Q (perhaps 200 or so and up), then under conversion, the low series resistance will not alter the susceptance value of the resulting admittance.

We may then directly calculate capacitor and inductor shunt admittance values from the following equations:

$$B_C = 2\pi FC \qquad B_L = -\frac{1}{2\pi FL} \qquad G = \frac{|B|}{Q}$$

We should recognize the first 2 simplified forms as the negative inverse of forms that we would use to calculate reactance values. The third form is a handy way to arrive at the conductance of the inductor: by dividing its absolute value of susceptance by the coil Q. For uniformity in this exercise, all component network inductors will have a Q of 300.

Under the simplifying assumptions, we may then calculate the real and imaginary components of the 2-port network for L and PI networks using the following simple equations:

Parameter	Real	Imaginary
Y11	Gp1 + Gs	Bp1 + Bs
Y12	-Gs	-Bs
Y22	Gp2 + Gs	Bp2 + Bs

The p1 and p2 subscripts refer to the shunt or parallel components in a real network, while s refers to the series component. Let's apply these procedures to a few matching networks that we might calculate (usually from a utility program) to match our original folded dipole to a 50-Ω source. We may always compare our results to the source impedance obtained from our wire grid model.

Three Networks

Let's begin with an up-converting L circuit using a series inductor and a shunt capacitor on the load side of the L circuit. The arrangement would appear like the left-hand side of **Fig. 96-4**. The component values come from one of my utility programs.

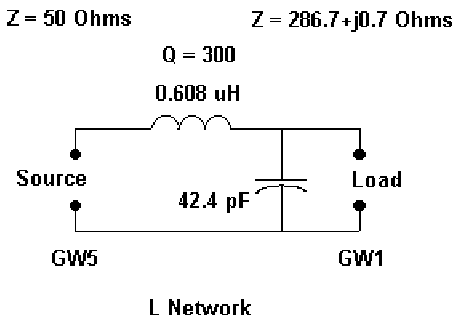

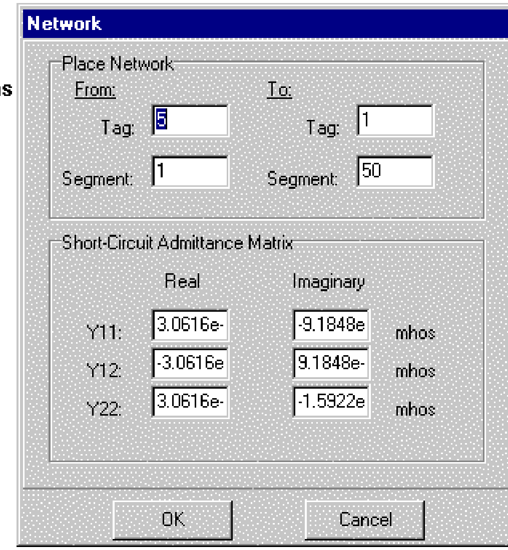

Fig. 96-4

This may be as good a time as any to note some differences among network-calculating utilities. Some programs offer you the choice of both coil and network Q (called "delta" (δ) in Terman's classical work). Other programs calculate the components for the lowest possible value of delta or working Q, which achieves the highest network efficiency. The latter types of programs are best, since you may not know what the lowest feasible value of working Q may be. Hence, you may select a Q that is too high in the sense of resulting in a less efficient network. In any event, always use the highest component (coil) Q and the lowest network Q that you can, while having manageable components. You may wish to calculate the network Q or delta from the following conventional equations for calculating L circuits (about 2.17).

$$\delta = \sqrt{\frac{R_{High}}{R_{Low}} - 1} \qquad X_S = \delta R_{Low} \qquad X_P = \frac{R_{High}}{\delta}$$

The calculated components are a 0.608 µH series coil and a 42.4 pF shunt capacitor. We need to convert these values first into shunt admittance values and then into parameter entries. We shall use basic units throughout.

Component	Value	G (Conductance)	B (Susceptance)
P1	None	0	0
S	0.608E-6	3.0616E-5	-9.1848E-3
P2	42.4E-12	0	7.5926E-3

Parameter	Real		Imaginary	
Y11	Gp1 + Gs	3.0616E-5	Bp1 + Bs	-9.1848E-3
Y12	-Gs	-3.0616E-5	-Bs	9.1848E-3
Y22	Gp2 + Gs	3.0616E-5	Bp2 + Bs	-1.5922E-3

You can recognize the calculated values of Y11-Y22 in **Fig. 96-4** within the NT assistance screen from NEC-Win Pro. The total model (96-3) has the following appearance.

```
CM Folded Dipole
CM Ls-Cp L-network version: NT
CM Ls = 0.608 ìH, Q = 300; Cp = 42.4 pF
CE
GW 1 99 -2.4892 0. 0. 2.4892 0. 0. .0005119
GW 2 1 2.4892 0. 0. 2.4892 0. .0762 .0005119
GW 3 99 2.4892 0. .0762 -2.4892 0. .0762 .0005119
GW 4 1 -2.4892 0. .0762 -2.4892 0. 0. .0005119
GW 5 1 -.001 0 1000 .001 0 1000 .00005
GE 0
FR 0 1 0 0 28.5 1
GN -1
EX 0 5 1 00 1 0
NT 5 1 1 50 3.0616e-5 -9.1848e-3 -3.0616e-5 9.1848e-3 3.0616e-
5 -1.5922e-3
XQ
EN
```

The model requires only 1 wire in addition to the folded-dipole wires. It serves to provide a new source segment for the input end of the 2-port network. The NT entries follow the order shown in the conversion table. Be certain to orient the terminating wires so that the network operates in the correct direction.

If we run the model, it returns a source impedance of 50.410 + j0.042 Ω. Since the network includes a conductance value, the network does show losses. The folded dipole itself uses perfect wire, so that the GW parts of the model have no loss. Hence, the reported efficiency of 99.28% gives us a sense of the relative losses incurred by adding an actual L matching circuit to the antenna.

Why did the circuit not show a perfect 50-Ω resistive impedance? There are 2 factors that are not clearly separable within the model. First, the external L circuit calculator rounds value to a maximum of 3 significant digits. Second, we used a considerable number of simplifying assumptions. Finally, the fact that we carried out the impedance calculation to 3 decimal places is a function of our desire to compare calculations, not to arrive at a practical matching solution. Rounded to "whole" Ω, the result is practically perfect.

We may equally use the same L-circuit with the reactances (or susceptances) reversed, as in the left side of **Fig. 96-5**.

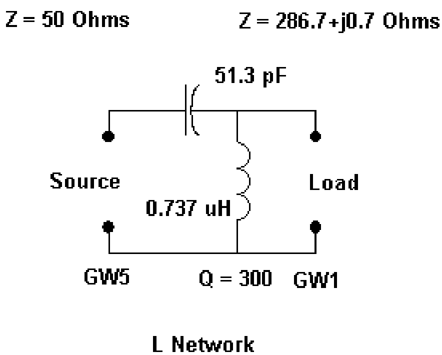

Fig. 96-5

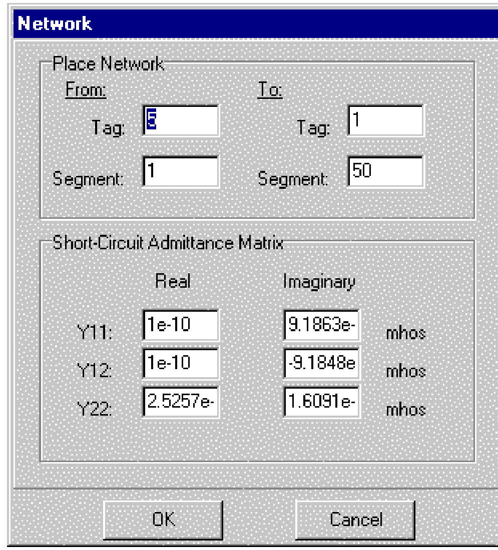

As we work our way through the calculations, the susceptance values will be close to those of the first example. However, their signs will be reversed. Numerical differences result from the reported component values having only 3 significant digits. As well, because we have swapped places for the capacitor (indefinitely high Q) and the coil (Q = 300), the shunt conductance values in the component network (and the resulting 2-port network) will also differ from the first example. The initial calculations call for a 51.3-pF series capacitor and a 0.737 μH shunt inductor.

Component	Value	G (Conductance)	B (Susceptance)
P1	None	0	0
S	51.3E-12	0	9.1863E-3
P2	0.737E-6	2.5257E-5	-7.5772E-3

Parameter	Real		Imaginary	
Y11	Gp1 + Gs	1E-10	Bp1 + Bs	9.1863E-3
Y12	-Gs	1E-10	-Bs	-9.1863E-3
Y22	Gp2 + Gs	2.5257E-5	Bp2 + Bs	1.6091E-3

When working with NEC, unless specifically instructed otherwise, entering zero is not usually wise. Hence, the real components of Y11 and Y12 become exceedingly low numbers (1E-10) that still have calculational value. At this value level, the sign become meaningless. The entries appear in the assistance screen on the right side of **Fig. 96-5** and are evident in the NT entry in the model itself 96-4).

```
CM Folded Dipole
CM Cs-Lp L-network version: NT
CM Cs = 51.3 pF; Lp = 0.737 ìH, Q = 300
CE
GW 1 99 -2.4892 0. 0. 2.4892 0. 0. .0005119
GW 2 1 2.4892 0. 0. 2.4892 0. .0762 .0005119
GW 3 99 2.4892 0. .0762 -2.4892 0. .0762 .0005119
GW 4 1 -2.4892 0. .0762 -2.4892 0. 0. .0005119
GW 5 1 -.001 0 1000 .001 0 1000 .00005
GE 0
FR 0 1 0 0 28.5 1
GN -1
EX 0 5 1 00 1 0
NT 5 1 1 50 1e-10 9.1863e-3 1e-10 -9.1848e-3 2.5257e-5 1.6091e-
3
XQ
EN
```

Note that, except for the NT entry, the model is identical to the one used in the first example. One advantage of using NT networks is that, if you can calculate the Y11 - Y22 entries, you may try many networks with minimal model revision. Running the model yields a source impedance of 50.293 - j0.317 Ω, well within the limits set by our rounded component values and our initial assumptions. The efficiency remains 99.28%, since the delta of our L circuit did not change with the alteration of the components.

There is no reason why we cannot calculate a true 3-legged PI network to serve as our matching circuit. **Fig. 96-6** shows on the left the resulting components that we shall need.

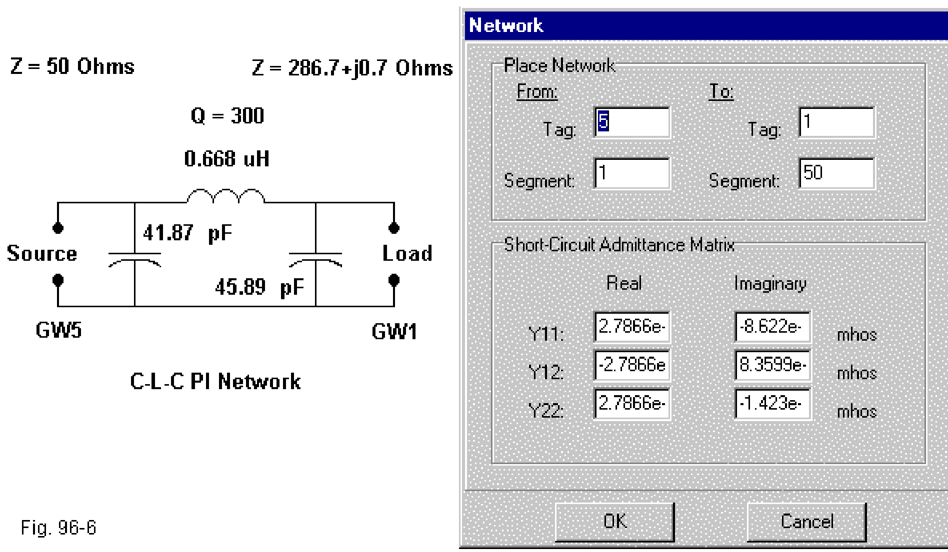

Fig. 96-6

Our calculation scratch pad will have the following appearance.

Component	Value	G (Conductance)	B (Susceptance)
P1	41.87E-12	0	7.4977E-3
S	0.668E-6	2.7866E-5	-8.3599E-3
P2	45.89E-12	0	8.2176E-3

Parameter	Real		Imaginary	
Y11	Gp1 + Gs	2.7866E-5	Bp1 + Bs	-8.622E-4
Y12	-Gs	-2.7866E-5	-Bs	8.3599E-3
Y22	Gp2 + Gs	2.7866E-5	Bp2 + Bs	-1.423E-4

The assistance screen shows the values, as does the following model (96-5) for this situation.

```
CM Folded Dipole
CM C-L-C PI-network version: NT
CM Cp1 = 41.87 pF; Ls = 0.668 ìH, Q = 300; Cp2 = 45.89 pF
CE
GW 1 99 -2.4892 0. 0. 2.4892 0. 0. .0005119
GW 2 1 2.4892 0. 0. 2.4892 0. .0762 .0005119
GW 3 99 2.4892 0. .0762 -2.4892 0. .0762 .0005119
GW 4 1 -2.4892 0. .0762 -2.4892 0. 0. .0005119
GW 5 1 -.001 0 1000 .001 0 1000 .00005
GE 0
FR 0 1 0 0 28.5 1
GN -1
EX 0 5 1 00 1 0
NT 5 1 1 50 2.7866e-5 -8.622e-4 -2.7866e-5 8.3599e-3 2.7866e-
5 -1.423e-4
XQ
EN
```

The 2-port NT version of our matched folded dipole shows a source impedance of 50.340 - j0.301 Ω. The efficiency is down to 99.10%, indicating the inherently higher losses for a 3-component network than for a 2-component network that performs the same impedance transformation.

In general, then, for the class of network applications with which we have been dealing, the simplifying assumptions have created no noticeable problems for the use of the NT command to simulate 2- and 3-component matching networks in the HF region.

A Harder Case: The T

So far, we have worked with the PI network and incomplete forms of it in converting component networks into shunt admittance values and then into Y11 - Y22 entry values for the 2-port network of the NT command. We have not attempted an analysis of another popular matching network, the T. In its most common form, the C-L-C T is a high-pass network as well as an impedance transformer. We can easily calculate values for a fixed-component version to serve our folded dipole, as shown on the left in **Fig. 96-7**.

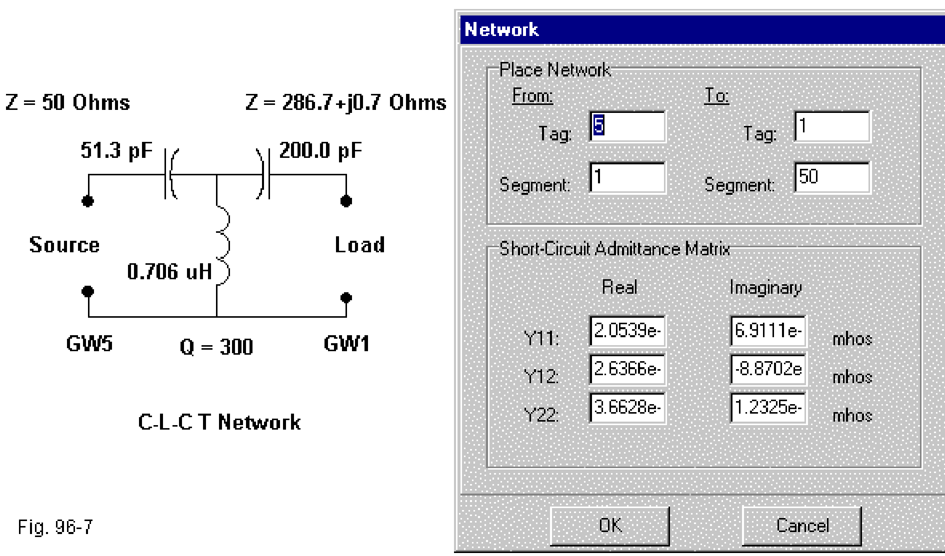

Fig. 96-7

The figure shows the component values, which result in the following initial shunt admittances.

Component		Value	G (Conductance)	B (Susceptance)
Cs1	(Y1)	51.3E-12	0	9.1863E-3
Lp	(Y3)	0.706E-6	2.6366E-5	-7.9099E-3
Cs2	(Y2)	200.0E-12	0	3.5814E-2

We may develop a new set of conversion formulas, or we may convert the admittance-based T network into an equivalent PI network, using standard conversion equations. The crossover labels for the components have conventional designations, as shown in **Fig. 96-8**.

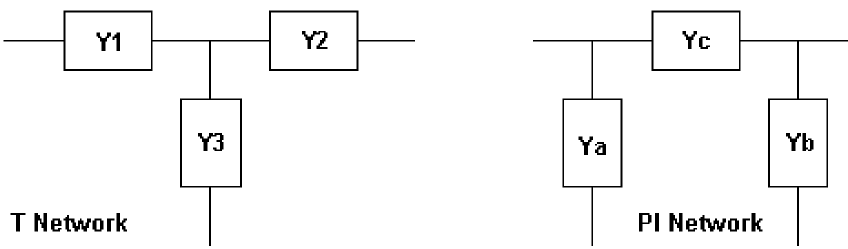

Converting a T to a PI

Fig. 96-8

The conversion equations are very straightforward.

Conversion Formula	Label	Values Based on the Example
Yt = Y1 + Y2 + Y3		3.7090E-2
Yc = Y1 Y2 / Yt	Ls	8.8702E-3
Ya = Y1 Y3 / Yt	Cp1	-1.9591E-3
Yb = Y2 Y3 / Yt	Cp2	-7.6377E-3

Not included in the conversion is the conductance. For a Q of 300, the original inductor conductance is 2.6366E-5. If we divide the conductance into the series component susceptance, we obtain a virtual Q of 336.5. We may use this value with each of the imaginary values in the following table to arrive at an approximation of the appropriate real entry. In general, the 2-port paths all involve the T inductor, but the virtual Q for each of the shunt legs of our conversion PI will likely be higher than the Y12 value. Nevertheless, the error will create little or no harm. With this in mind, we can create the final table of entries for the NT command.

Parameter	Real		Imaginary	
Y11	Gp1 + Gs	2.0539E-5	Bp1 + Bs	6.9111E-3
Y12	-Gs	2.6366E-5	-Bs	-8.8702E-3
Y22	Gp2 + Gs	3.6628E-6	Bp2 + Bs	1.2325E-3

The assistance screen reproduced in **Fig. 96-7** shows these entries, as does the model (96-7) itself.

```
CM Folded Dipole
CM C-L-C T-network version: NT
CM Cs1 = 51.3 pF; Lp = 0.706 ìH, Q = 300; Cs2 = 200.0 pF
CE
GW 1 99 -2.4892 0. 0. 2.4892 0. 0. .0005119
GW 2 1 2.4892 0. 0. 2.4892 0. .0762 .0005119
GW 3 99 2.4892 0. .0762 -2.4892 0. .0762 .0005119
GW 4 1 -2.4892 0. .0762 -2.4892 0. 0. .0005119
GW 5 1 -.001 0 1000 .001 0 1000 .00005
GE 0
FR 0 1 0 0 28.5 1
GN -1
EX 0 5 1 00 1 0
NT 5 1 1 50 2.0539e-5 6.9111e-3 2.6366e-5 -8.8702e-3 3.6628e-
6 1.2325e-3
XQ
EN
```

If we run the listed model, we obtain a source impedance of 49.681 + j0.016 Ω, a value that is as close to perfect as any other the other results in this exercise. As well, the efficiency value is comparable to those for the other NT examples in this set.

These samples provide you with a starting point in expanding your use of the NT command beyond the kinds of special cases that we reviewed on the previous episode of this series. However, beware of extending the simplified calculations beyond the type of non-critical HF situation that we presumed at the start. Full exploration of NT potentials requires some exercises in mastering the techniques of converting a large number of component networks into terms suitable for use with the 2-port admittance parameter network of the NT command.

At the other extreme, for those who do not wish to make any calculations externally to the modeling program, one implementation of NEC-2 may be useful. NEC2GO contains a special matching network module. It begins with the source impedance of an unmatched antenna. Then it gives you the choice of available networks to match the antenna's impedance to a source impedance of your choice. As well, you may choose both the coil and the network Q. Your network choices include applicable L, PI, and T circuits. The program then creates a new source wire and the NT command to implement the network selected. The only caution you need to exercise is to select a working Q that will yield the best combination of efficiency and manageable component values.

97. Integrating Commands: A Case Study

In past episodes, we have examined some of the commands available on more advanced implementations of NEC. In each case, we looked at the command in relative isolation, with only enough of a model to illustrate how we enter and basically use the command. Although such guidance is a necessary step on the road to mastery of the command, it does not reveal the full power of the commands. That power only becomes apparent as we gradually learn how to integrate the commands into a model so as to achieve a goal.

There is no set of examples that will fully illustrate how we may effectively integrate commands for more effective modeling. The number of structure geometry and control commands is simply too large to sample every potential combination that we might effectively use. At most, we can look at a case study to see the thinking process that goes into setting up a model. Then, the rest is up to your own ingenuity in developing the most effective model for the task specifications that oversee the work.

The case study that I shall present involves a relatively recent innovation in AM broadcast antenna design. The antenna is called the Star-H, and has been developed by Kinstar, a joint partnership between the Star-H Corporation and Kintronic Laboratories. For more information, see the July, 2004, issue of *antenneX* or the web sites indicated in that article. The article author, Dave Cuthbert, WX7G, adapted the antenna–at least in model form–to 160 meters and introduced a further space-reduction technique.

The basic star-H divides the vertical portion of the array into 4 parallel vertical wires, on the premise that each wire will have 4 times the impedance of a single vertical, a desirable situation for easier impedance matching and lower power losses in the resistive connections from part-to-part. A second feature of the antenna is converting each vertical leg into an inverted-L configuration. Since each of the 4 folded sections will form a symmetrical horizontal collection with the same current magnitude and phase angle everywhere along each wire, the horizontal fields will cancel, leaving only the radiation from the base-fed vertical wires. The effect is comparable to a 4-spoke top hat arrangement, except that each leg of the array will have its own higher source impedance. **Fig. 97-1** shows the general outline of the array. Since the view is broadside, you will have to visualize the horizontal legs projecting into and out of the page that correspond to the ones going from side to side.

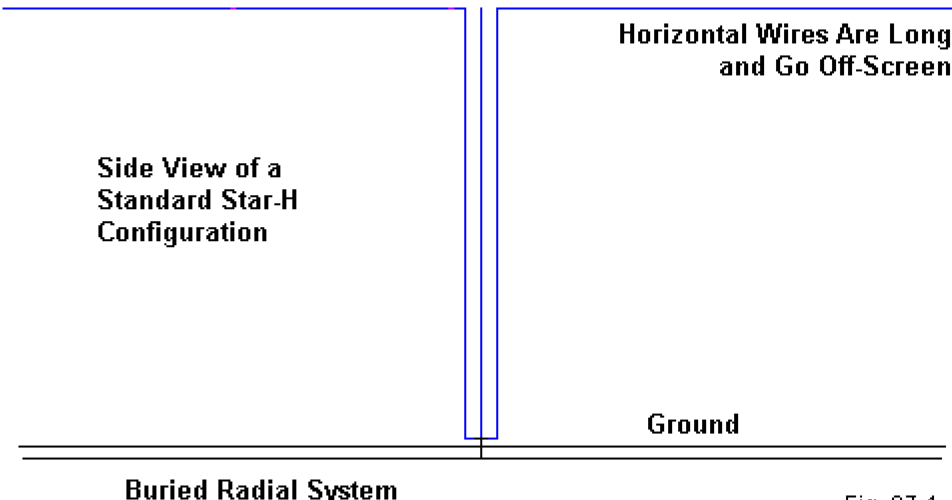

Fig. 97-1

Te object of the design is to reduce the height required by the array to about 1/3 the height of a full size 1/4-λ monopole. Each inverted-L section thus requires a very long horizontal section. Since the center 4 wires and the end of each horizontal wire require support–presumed to be a power pole or similar–the antenna needs considerable real estate. In scaling the antenna to the 160-m amateur band, Cuthbert folds each horizontal end toward but not to an adjacent corner. The result is an array that might fit a reasonable plot of ground without either excessive vertical or horizontal demands.

The resulting model that I created used AWG #12 wire throughout (without loss, since the model is for illustration of some modeling principles). The vertical sections are 50' high, with the initial parts of the horizontal portions being 35' long. Hence, the tip-to-tip distance is a maximum of 70'. The foldovers are about 45' long and approach the tip of the next corner. **Fig. 97-2** shows the Cuthbert design as adapted here.

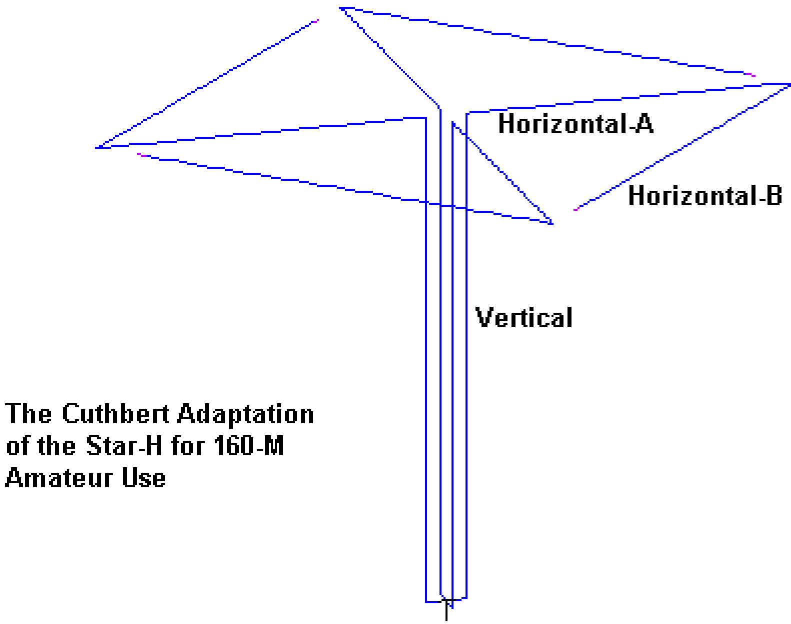

Fig. 97-2

The Star-H developers recommend an industry-standard 120-radial system beneath the antenna and the ground. My interest in the design was to find out its potential when used over such a radial system. In outline, the system has the appearance of **Fig. 97-3**, if we could view it with X-ray vision from overhead.

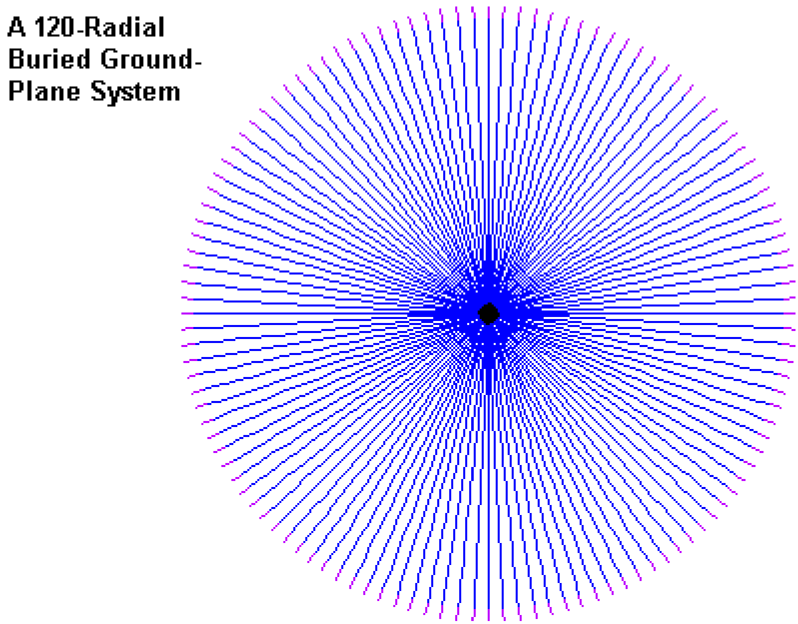

Fig. 97-3

Of course, a buried radial system requires the use of NEC-4 software, so the following modeling exercise uses GNEC. Each radial is 1/4-λ long at 1.8 MHz. A wavelength at that frequency is about 166.6-m or 546.6' long, so the radials are each 136' long. Hence, the entire structure of the antenna itself, including the bent inverted-L legs, will fit well within the limits of the field, which is 272' from tip-to-tip.

In the process of testing various constructs for the field, I confirmed the fact that a truly symmetrical arrangement of wires in a radial pattern does no need to have the same segmentation density of wires that do not result in mutually canceling fields. Hence, while the other portions of the array use a segment length of about 1', the buried ground plane structure uses only 25 segments per radial. I raised the number of segments per radial from 10 to 25 using a test 1/4-λ monopole, and the impedance change was minuscule: Δ R was 0.02 Ω and Δ X was 0.05 Ω. Further increases in the segments per radial seemed unjustified, although you can add a GC command and taper the segment lengths along the radial.

Even with the sparse segment population, a 120-radial field requires 3000 segments to go with 120 wires or GW tag entries. Software having only GW or individual wire entry facilities thus results in very large model files, even before entering the upper portions of the antenna. However, NEC has two commands well worth using on this model:

The WG or "write a numerical Green's function file" command allows us to separate the radial system portion of the model from the upper structure. By including the companion GF or "re-call a numerical Green's function file" in a separate model containing the upper portion of the structure, we can run the radial system once for a given frequency and use its output with any number of antenna structures. When the NEC core runs with the second file, it need not perform the entire set of matrix calculations over again, but calls up the results from the Green's file saved with an .NGF extension and combines them with the added structural elements in the new file. The result is a very great saving in run time, although the actual saving depends on the ratio of added segments to those handled by the initial model that created the Green's function file. In the present case, the radial system will use 3000 segments, but the additions will use no more than 530 more.

A 3000-segment radial system, if composed solely of GW entries, would require considerable run time before it wrote the .NGF file. However, we can shorten that run time to something insignificant by using another available command. The GR or "rotational symmetry" command requires only the establishment of the first wire. Then, we simply specify that we wish a total of 120 structures at 3°- intervals to arrive at a fully symmetrical and complete ground radial system. If nothing disturbs the symmetry, then we end up with a rapid-fire run. In fact, it required less than 10 seconds on a 1.8 GHz PC.

The following lines show the radial portion of the antenna model at 1.8 MHz. See model 97-1.

```
CM 160-m radial system: 1/4 wl long/radial, #12 wire
CE
GW 1 25 0 0 -1 0 136 -1 .00673
```

```
GR 1 120
GS 1 0 0
GE
FR 0 1 0 0 1.8 1
GN 2 0 0 0 13.0000 0.0050
WG radials.ngf
EN
```

The geometry section is a paradigm of simplicity, with only the first radial and the rotational symmetry commands. Since the dimensions are in feet, we need to add a scaling factor, which uses the automated feet-to-meters option available in NEC-4. The “plain” GE command and a more complex entry (GE -1 -1 0) yield the same results. The presence of a ground does not disturb rotational symmetry since the model makes no attempt to rotate the symmetrical structure from its initial orientation.

The actual ground is the usual entry for average soil conditions, with a conductivity of 0.005 S/m and a dielectric constant or permittivity of 13. If you change either the frequency (set at 1.8 MHz) or wish to use a different set of ground conditions, you will have to make a decision. You may alter the entries in the model that writes the .NGF file and re-run an unchanged model with the added structure. Alternatively, you may save the results of changing the frequency or ground conditions under a different file name with the .NGF extension and make similar changes in the model with the antenna structure. Each .NGF file for the 120 radials uses about 1.7 MB of hard drive storage, which is greater than the sum of all other input, output, and temporary files combined for the model with the antenna structure, but still a very small file of its type.

The alternative method of creating the radials would use the GM command. See model 97-2.

```
CM 160-m radial system: 1/4 wl long/radial, #12 wire
CE
GW 1 25 0 0 -1 0 136 -1 .00673
GM 1 119 0 0 3 0 0 0
GS 1 0 0
GE
```

```
FR 0 1 0 0 1.8 1
GN 2 0 0 0 13.0000 0.0050
WG radials.ngf
EN
```

The GM command creates all of the necessary radials. However, it requires 320 seconds (on the same computer) to run and requires an .NGF file storage space of 141 MB. Those numbers represent 32 times the run time and 82 times the storage space of the GR version of the radial system.

The corresponding antenna structure file that recalls the radial system results will have an appearance that depends on the complexity of the superstructure. The following model (97-3) is for a test monopole that is full length, but still uses AWG #12 wire.

```
CM 160-m monopole over radials
CM call radials.ngf
CE
GF radials.ngf
GW 201 1 0 0 -1 0 0 0 .00673
GW 202 1 0 0 0 0 0 1 .00673
GW 203 131 0 0 1 0 0 132 .00673
GS 1 0 0
GE -1 -1 0
EX 0 202 1 0 1 0
RP 0 181 1 1000 -90 90 1.00000 1.00000
EN
```

The first structure entry is a call for the .NGF file contents. Then we add the monopole structure. GW201 is a 1' wire connecting the hub of the radials to the surface (Z = 0). GW202 is a 1' 1-segment wire from the ground up and serves as the source segment (see the EX0 entry). GW 203 handles the rest of the vertical monopole. In this case, the height worked out to exactly 1' per segment. Since the model that wrote the .NGF file uses 120 tag numbers, the antenna structure begins with a higher number. In this case, the number was chosen for easy tracking of more complex antenna structures above ground. Note the use of the more elaborate GE command to ensure that the model records that a ground plane is present, but that the current expansion should undergo no modification, since there are buried wires within the total structure.

The model that calls and uses an .NGF file holds the excitation and radiation pattern requests. However, it contains no ground specification (GN) for frequency setting (FR). Those commands appear in the model that wrote the .NGF file. Since those specifications are necessary to both parts of the model and must be self-consistent, they begin life in the earlier model.

Despite the fact that we have 3133 total segments in the monopole and its radial system, the model required under 1 minute to complete the calculations. This speed proved very useful, since a number of experimental heights were required before the antenna achieve near-resonance. The model showed a gain of 1.30 dBi at a take-off angle of 23° elevation (theta = 67°). The reported impedance for lossless wire was 36.028 - j2.021 Ω. These values become reference marks for models of the Cuthbert version of the Star-H for 160 meters.

Above the 1' above ground level, the new array requires 4 identical structures. For each leg of the array, there is a short (2') wire running horizontally away from center. Then there is a vertical section that I set at 50'. Next, there is another horizontal wire at the 50' level running 35' away from the vertical leg. Finally, we have a 45' wire running from the end of the previous wire toward the corner of the next structure.

In some implementations of NEC, we would have to repeat the 4-wire set for each leg of the modified Star-H. However, implementations using the full command set allow us to simplify the set-up. The following model (97-4)–using a single source of excitation–shows how we can minimize the number of GW entries.

```
CM 160-m star-H over radials
CM call radials.ngf
CE
GF radials.ngf
GW 201 1 0 0 -1 0 0 0 .00673
GW 202 1 0 0 0 0 0 1 .00673
GW 203 2 0 0 1 0 2 1 .00673
```

```
GW 204 50 0 2 1 0 2 50 .00673
GW 205 35 0 2 50 0 35 50 .00673
GW 206 45 0 35 50 32 3 50 .00673
GM 10 3 0 0 90 0 0 0 203 1 206 45
GS 1 0 0
GE -1 -1 0
EX 0 202 1 0 1 0
RP 0 181 1 1000 -90 90 1.00000 1.00000
EN
```

It is possible to use the GR command in the antenna model. We would need to move the first two GW entries to follow the GR command, which applies to the structure as it departs the center line (X = Y = 0). GR will create the wires, but not use symmetry in the calculation. The GR version of the model has the following appearance (97-5).

```
CM 160-m star-H over radials
CM call radials.ngf
CE
GF radials.ngf
GW 203 2 0 0 1 0 2 1 .00673
GW 204 50 0 2 1 0 2 50 .00673
GW 205 35 0 2 50 0 35 50 .00673
GW 206 45 0 35 50 32 3 50 .00673
GR 10 4
GW 201 1 0 0 -1 0 0 0 .00673
GW 202 1 0 0 0 0 0 1 .00673
GS 1 0 0
GE -1 -1 0
EX 0 202 1 0 1 0
RP 0 181 1 1000 -90 90 1.00000 1.00000
EN
```

The use of GR in the upper portion of the antenna does not gain anything significant in terms of run time. Both models require just over 124 seconds to run. Because the bulk of the run time involves loading and processing the results of the 3000-segment .NGF file, the remaining 530 segments of new geometry require only a small part of the run time. To effect a significant saving of run time (apt perhaps to larger models than the present example), we would need to design the upper structure so that the GR command had no following GW lines.

The single-feed version of the Cuthbert-modified Star-H reports a gain of 1.05 dBi (in both the GM and GR versions of the model) with an TO elevation angle of 25° (65° theta). The source impedance report is 13.183 + 0.548 Ω. We may also provide the model with 4 separate feedpoint, using the first segment of GW 204 (and its counterparts, GW 214, GW 224, and GW 234). See model 97-6. We do not change the model otherwise, since the feedpoints appear in series with the structure. Hence, they need completion to ground and use the same routes through GW201 and GW202 on the way to the radial system below ground.

```
CM 160-m star-H over radials
CM call radials.wgf
CE
GF radials.ngf
GW 201 1 0 0 -1 0 0 0 .00673
GW 202 1 0 0 0 0 0 1 .00673
GW 203 2 0 0 1 0 2 1 .00673
GW 204 50 0 2 1 0 2 50 .00673
GW 205 35 0 2 50 0 35 50 .00673
GW 206 45 0 35 50 32 3 50 .00673
GM 10 3 0 0 90 0 0 0 203 1 206 45
GS 1 0 0
GE -1 -1 0
EX 0 204 1 0 1 0
EX 0 214 1 0 1 0
EX 0 224 1 0 1 0
EX 0 234 1 0 1 0
RP 0 181 1 1000 -90 90 1.00000 1.00000
EN
```

The 1.80-MHz performance report includes a gain of 1.10 dBi at a TO elevation angle of 25° (65° theta), and individual source impedances of 52.421 + j2.004 Ω. **Fig. 97-4** provides a comparison of the patterns of the two modified Star-H antennas (solid line) and the reference 1/4-λ monopole.

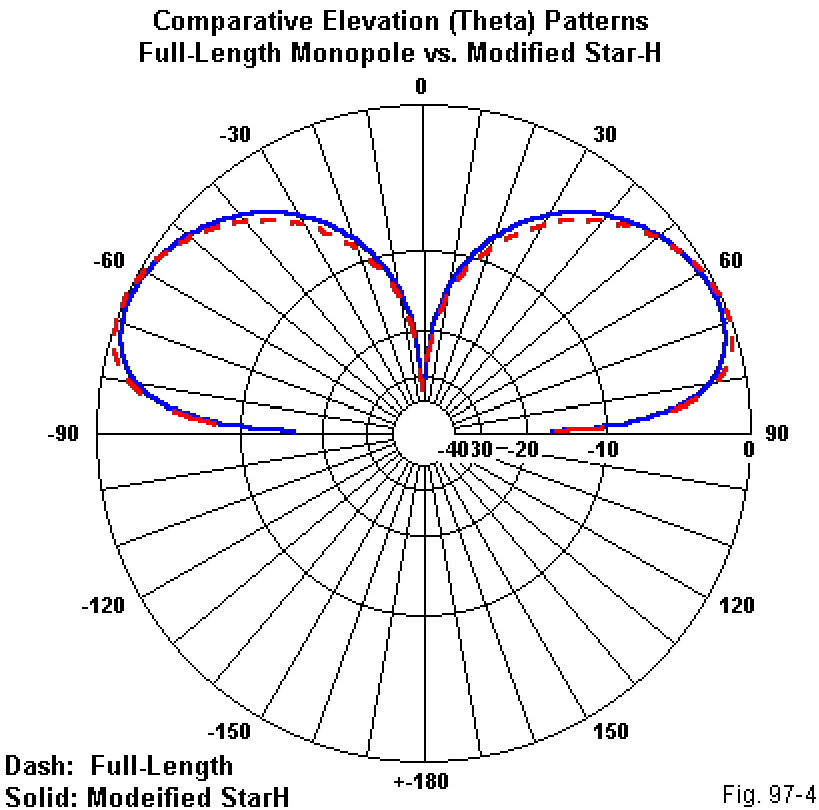

Fig. 97-4

The 2° difference in the TO angle and the 0.2-dB difference in gain is a function of the full-size monopole's greater length and the resulting current distribution. For high power BC application, the basis for the use of 4 feedlines lies not only in the lower losses associated with the higher impedances. As well, the system distributes the total source current among 4 feedlines, further reducing the stress on each cable due to heating. For local stations using power levels up to a few thousand watts, high power coaxial cables would likely serve well and avoid problems of routing and spacing from other objects that parallel feedlines involve. A carefully tuned 4-source system might easily avoid the use of any matching components at the individual sources, simply by "pruning" the 4 wires to achieve matching conditions.

Even in amateur service, a 4-port coaxial system is usable, although amateurs operate across a span of frequencies within each assigned band. One advantage of the 4-source feed system is the simplicity of extending the 2:1 SWR range of the antenna while sustaining the lower losses of the higher impedance. The key is to adjust the height of the array so that the resistive portion of the impedance extends from perhaps 35 Ω to perhaps 80 Ω as we move the frequency above 1.8 MHz. The rate of change of the resistive portion of the impedance is about 8 Ω per 100 kHz in the 50-Ω region. The second part of the balancing act is to use a horizontal length that is slightly long at the lowest frequency. Then the antenna exhibits inductive reactance everywhere within the band. A series capacitor at each feedpoint can compensate for the reactance, leaving only a resistive impedance for the individual cables. The rate of change of the reactance is nearly 80 Ω per 100 kHz and shows a nearly linear curve. Selecting a capacitor with a suitably wide range to match the reactance range to be compensated is both possible and feasible. The only update to this very old technique is that the remote capacitors require careful ganging and equally careful weatherproofing.

At the equipment end of the 4 lines, you may change the impedance of each line to 200 Ω using a 1:4 UNUN. The 4 higher impedances then require only parallel connection to match 50-Ω equipment outputs and inputs. In more critical situations, such as BC service, where the exact pattern shape makes a licensing difference, the system must have means of ensuring that the balance of power is correct at the antenna terminals.

These notes on matching systems are secondary to the main focus of this column: the use the NEC resources to produce the most efficient and effective model. By integrating a number of commands into a model, we produced a 120-radial system and an .NGF file that we can apply to an unlimited number of antennas. To modify the model for other frequencies, we need only make two small maneuvers. First, we would reset the frequency in the FR command. Second, we would change the length of the radial to suit the frequency and whatever other design specifications might be relevant to the project. Since the model invokes the rotational symmetry (GR) command, the radial revision effort requires a change to only a single GW entry. We might make the radial system one step more complex by entering a GC command following the single GW entry. In that command, we might length-taper the radial from the center outward so that the innermost segment has a length to match the depth of the field (1'). We may also change the size of the system simply by altering the angle and total number of structures within the GR command. The result is a model that runs extremely rapidly and requires minimal storage space for the resulting .NGF file.

The antenna structure file that calls upon the radial system .NGF file is also compact. For symmetrical systems, we may create only one of the upper structures and use either the GM and GR command to replicate the initial structure the require number of times. In the present project, if we wished to alter the balance between the vertical and horizontal portions of the upper structure, we would need to enter only a single set of new coordinates. The GM command would replicate the first as many times as might be necessary to finish the task. In addition, the use of the .NGF file for the radial system shortens the run time between design revisions from somewhere in the 6- to 10-minute range down to 2 minutes on the PC used for this exercise. As a result, the entire design perfection procedure takes a matter of hours rather than days.

There are other commands that we might have incorporated into our integrated model. For example, we might design and add a matching network to the single-source version of the model, using NT-command techniques explored in the two most recent columns. We can easily calculate the required components for a down converting L-circuit and from that point find usable entries of Y11, Y21, and Y22 in the 2-port NT command. By estimating the value of the coil Q, we can get a measure of the network losses. Of course, we may add into the final design a material loading value (LD5) for both the radials and the upper antenna structure.

Antenna modeling, then, is not just a matter of learning the terms of each command. It is also a matter of learning to see opportunities for integrating the commands into a model (or, in this case, a pair of models) so as to yield the most effective combination that will minimize unnecessary work (as well as work time) and maximize flexibility. Since these goals tend to be task specific, there is no single general rule that will cover all cases. Rather, there are only case studies–like the present one–that may alert you to the possibilities. At that point, your own ingenuity must take over.

98. Planar Reflectors: Wire Grid vs. SM Patches

In previous episodes of this series, we have by-passed one set of geometry commands: SP, SM, and SC. These commands are not available on the most popular entry level commercial versions of NEC-2 (such as NEC-Win Plus and EZNEC), although other versions of NEC-2 that a beginning or intermediate modeler might use (such as NEC2GO and 4NEC2) do allow access to the complete NEC-2 command set. In general, SP and SM, along with necessary extensions via SC, create surface patches and are found in specific advanced modeling problems tackled by relative advanced modelers using such programs as NEC-Win Pro, GNEC, or custom versions of NEC-2 and NEC-4.

However, a number of applications of SM (and its necessary extension card, SC) have begun to appear. For example, I have recently seen planar reflector and UHF horn models employ the SM command. Therefore, it may be useful to explore the simplest of the surface patch commands in order to grasp some of the requirements, advantages, and limitations of using it.

Surface Patch Basics

We create a surface patch with the SM command by defining its corner coordinates. The more general SP command permits a range of specific regular patch shapes, such as triangular, rectangular, and quadrilateral geometries, as well as a shapeless patch description. Wherever the specification of X, Y, and Z coordinates exceeds the 6 floating decimal places in a NEC-2 command line (unchanged in NEC-4), we must add an SC command to complete the coordinates. In addition, SP allows a succession of SC cards to complete complex structures with relative efficiency.

SM is a simpler command. It creates only a rectangular patch, but that patch consists of a user-specified number of patches defined in terms of the number of patches for both width and height. The SM command allows only the single SC command necessary to complete the coordinate entry. The following sample command lines provide an example of SM/SC structure.

Cmd	I1	I2	F1	F2	F3	F4	F5	F6
	# Patches-Width	# Patches-Height	C1-X	C1-Y	C1-Z	C2-X	C2-Y	C2-Z
SM	12	12	0.	-.6	-.6	0.	.6	-.6

Cmd	I1	I2	F1	F2	F3
	Not Used	Not Used	C3-X	C3-Y	C3-Z
SC	0	0	0.	.6	.6

Defining a rectangular shape requires that we define three consecutive corners of the rectangle. Hence, we must use the SC entry for the third corner (C3), while the coordinates for the first two corners (C1 and C2) appear in the SM command. The integer entries of the SC card are unused and hence receive automatic zeroes. However, the integer entries of the SM command specify how many patches will exist along the width and height of the overall patch. For purposes of modeling, "width" means the line between corners 1 and 2, while height means the line between corners 2 and 3, regardless of the actual orientation of the patch within the Cartesian coordinate system.

We can find the fundamentals of using patches within the NEC-2 and NEC-4 manuals. The patch "formulation uses the Magnetic Field Integral Equation [MFIE], and is restricted to closed surfaces with non-vanishing enclosed volume. It is not applicable to a conducting plate or shell of zero thickness." Essentially, proper use of surface patches requires modeling the entire volume, even of a thin plate. "Theoretically the MFIE can be used for a thin box or cylinder, but the solution may become inaccurate due to the decreasing condition number of the matrix and the simple point matching and pulse current expansion used in the solution in NEC."

"As with wire modeling, patch size measured in wavelengths is very important for accuracy of the results. A minimum of about 25 patches should be used per square wavelength of surface area, with the maximum size for an individual patch about 0.04 square wavelengths." For a square patch, these terms translate into a minimum of about 5 patch widths per wavelength of edge dimension. A higher patch density up to reasonable numbers is usually desirable.

"In general, the use of surface patches is restricted to modeling voluminous bodies. The surface modeled must be closed since the patches only model the side of the surface from which their normals are directed outward." See **Fig. 98-1** for a simplified representation of a surface patch and its outward-directed unit normal vector. The arrow represents the outward-directed normal, the foundation for patch calculations. The complete NEC output file contains in the early geometry section a listing of surface patches created by an SM command. Included in the listing are the “COMPONENTS OF UNIT TANGENT VECTORS.” The patches also have a current distribution table.

The Surface Patch and Its "Outward-Directed, Unit Normal Vector"

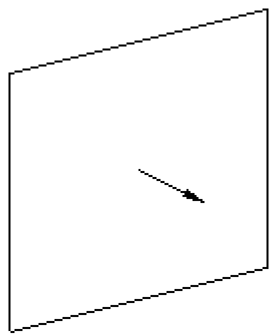

Fig. 98-1

The NEC manual also points out that “if a somewhat thin body, such as a box with one narrow dimension, is modeled with patches, the narrow sides (edges) must be modeled as well as the broad surfaces. Furthermore, the parallel surfaces on opposite sides cannot be too close together or severe numerical error will occur.” The manual also strongly suggests that models employing new shapes be compared to experimental outcomes in order to establish the validity of the patch modeling.

Since we shall not use the SP command itself or attempt to attach a wire directly to a patch structure, we may use these extracts from the manual notes as a basis for our next steps into the use of SM commands.

Planar Reflectors: Wire-Grid or SM Patches

Let’s begin our efforts with a single dipole that uses a planar reflector to provide directivity, that is, gain and a usable front-to-back ratio. The general outline–shown only in a facing view–appears in **Fig. 98-2**. The dipole is resonant at 300 MHz and the reflector dimensions are 1.2 by 1.2 meters (or wavelengths).

Planar Reflector Composed of a 12 by 12 Square
of Either Wire-Grid Squares or Surface Patches

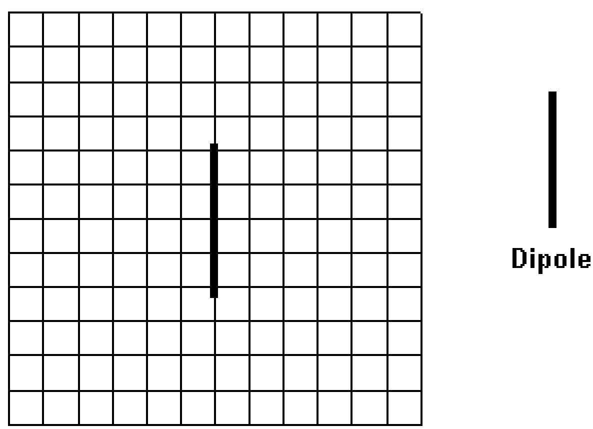

Fig. 98-2

The reflector consists of 12 units both horizontally and vertically. Ordinarily, we would construct the reflector with a wire-grid structure. The maximum length of each wire segment in the grid is 0.1-λ, and the wire diameter is the cell-wire length divided by PI. The radius is half this value, 0.0159 meter (or wavelength). The following model (98-1) captures these elements.

```
CM Dipole .175 m from planar reflector
CM Planar Reflector 299.7925 MHz (WL=1 m)
CM Y = 1.2 m;  Z = 1.2 m
CM standard wire-grid: Seg L=0.1 m; radius=L/PI=0.0159 m
CE
GW 1 12 0 -.6 0 0 .6 0 .0159
GM 1 6 0 0 0 0 0 -.1 1 1 1 12
GM 1 6 0 0 0 0 0 .1 1 1 1 12
GW 12 12 0 0 -.6 0 0 .6 .0159
GM 1 6 0 0 0 0 -.1 0 12 1 12 12
GM 1 6 0 0 0 0 .1 0 12 1 12 12
GW 24 11 .175 0 -.218 .175 0 .218 .004
GE 0 -1 0
FR 0 1 0 0 299.7925 1
GN -1
EX 0 24 6 0 1 0
RP 0 361 1 1000 -90 0 1.00000 1.00000
RP 0 1 361 1000 90 0 1.00000 1.00000
EN
```

The geometry entries up to but not including GW 24 define the planar reflector. You can simplify the structure, but the present model is one of a system of planar reflector models having a uniform horizontal and vertical centerline set. Hence, the necessary wire replications occur on each side of these center wires.

The technique being applied to patch versions of the planar reflector is interesting because it directly violates the manual recommendation that requires the modeling of the reflector as a closed geometrical shape with volume. The operative theory behind the use of patch-based reflectors is that the surface is a perfect tangential reflecting surface. Hence, on this account, we need not be concerned with the remaining 5 surfaces of the reflector, but may deal only with the surface facing the driver element (or elements, in more complex planar reflector arrays).

If we accept this account, then we may replace the wire-grid structure with a simpler array of patches. The corresponding surface-patch or SM version of the model (98-2) has the following appearance.

```
CM Dipole .175 m from planar reflector
CM Planar Reflector 299.7925 MHz (WL=1 m)
CM Y = 1.2 m;  Z = 1.2 m
CM SM patch: 10 patches/meter
CE
SM 12 12 0. -.6 -.6 0. .6 -.6
SC 0 0 0. .6 .6
GW 24 11 .175 0 -.218 .175 0 .218 .004
GE 0 -1 0
FR 0 1 0 0 299.7925 1
GN -1
EX 0 24 6 0 1 0
RP 0 361 1 1000 -90 0 1.00000 1.00000
RP 0 1 361 1000 90 0 1.00000 1.00000
EN
```

We may enter the patch lines manually or use such help screens as may be available. The sample help screen from GNEC in **Fig. 98-3** allows entry of all of the 3 corner coordinate sets on one screen and it then creates both the SM and SC lines necessary for the NEC input file. The sample entries apply to a model that we shall examine a little further on in this discussion.

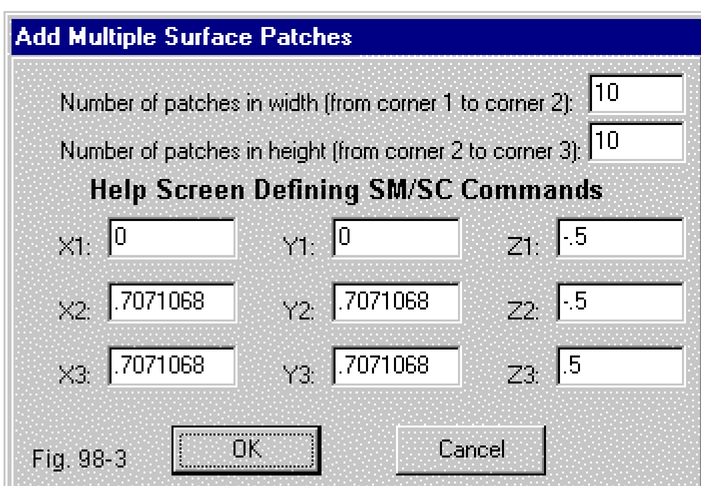

Fig. 98-3

Our fundamental question is how well the wire-grid and SM reflectors track each other. The answer to this question depends on how accurate the SM assumption is, namely, that the only relevant outward-directed normal vector for a planar reflector is from the surface directly facing the driving element(s). One way to approach that question is to overlay the resulting E-plane (theta) and H-plane (phi) patterns for the array, as in **Fig. 98-4**. Note in the models that the driver dimensions and the driver spacing from the reflector do not change between models.

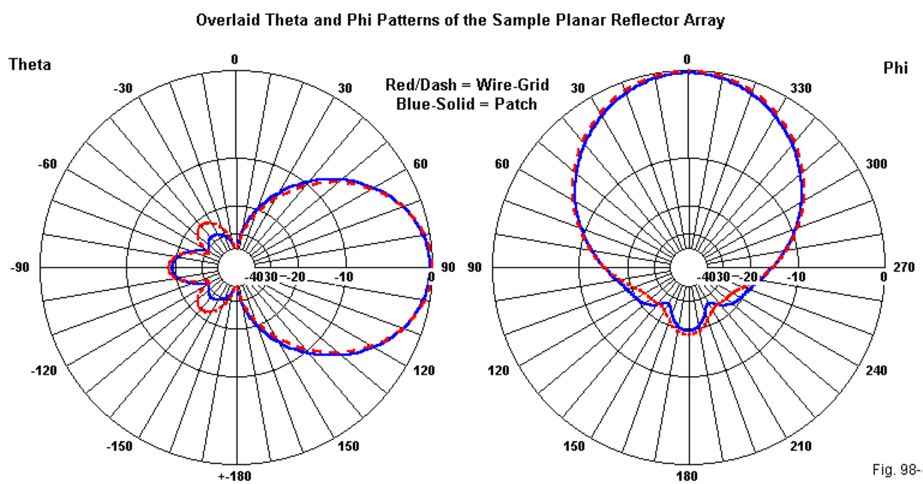

Fig. 98-4

In the forward direction, there is no major difference, although the dashed lines for the wire-grid model show a slightly higher gain. The key differences lie in the rearward structure. In the theta pattern especially, the patch reflector does not show the full development of the quartering rearward sidelobes and may give an erroneous impression of the worst-case front-to-back ratio.

Nevertheless, the simple models used here suggest that the two types of reflectors are viable alternatives for at least preliminary modeling. I ran both models through a small range of reflector sizes, varying the width from 1.0 m to 1.4 m and then the height through the same range. The wire grid model shows a distinct peak using the 1.2 by 1.2 meter reflector. The following table compares the results for both the wire-grid and the patch reflectors. In the model designations, H means the horizontal reflector length at right angles to the dipole, while V means the vertical reflector length parallel to the dipole.

Comparison of Wire Grid and SM Patch Reflectors					300 MHz	
Single dipole 0.175 m (wl) ahead of reflector						
Wire Grid Reflector						
Model	R	X	Gain	F-B	E BW	H BW
H1.0-V1.0	49.85	-0.24	8.86	17.31	58	82
H1.0-V1.2	49.62	-1.1	9.22	17.83	54	82
H1.0-V1.4	49.05	-0.94	9.14	20.7	56	84
H1.2-V1.0	49.82	-0.42	8.97	18.3	58	82
H1.2-V1.2	49.44	-1.25	9.31	18.33	54	80
H1.2-V1.4	48.93	-1.06	9.19	20.23	56	84
H1.4-V1.0	49.75	-0.46	8.95	19.59	58	84
H1.4-V1.2	49.29	-1.18	9.27	19.19	54	82
H1.4-V1.4	48.86	-1.01	9.12	20.32	56	88
SM Patch Reflector						
Model	R	X	Gain	F-B	E BW	H BW
H1.0-V1.0	50.48	0.13	8.89	17.1	58	80
H1.0-V1.2	50.95	-0.28	9.02	18.17	56	82
H1.0-V1.4	50.85	-0.65	9.03	19.55	56	82
H1.2-V1.0	49.63	-1.34	9.11	18.63	60	78
H1.2-V1.2	50	-1.68	9.24	19.16	58	78
H1.2-V1.4	49.89	-1.97	9.22	20	58	80
H1.4-V1.0	48.46	1.24	9.13	20.5	60	78
H1.4-V1.2	48.84	-1.48	9.23	20.42	58	80
H1.4-V1.4	48.78	-1.72	9.18	20.64	58	82

The gain for the SM-patch 1.2 by 1.2 reflector is also the highest value among the set. However, the gain change from one reflector vertical width to the next, for a given horizontal length, is not as great as with the wire-grid models. The shallowness of the patch curves shows up clearly in **Fig. 98-5**.

The gain values used in the table are corrected for the average gain test (AGT). For the patch models, the AGT values ranged from 0.974 up to 0.989. In contrast, the wire-grid models had AGT values of about 0.998 or better (where 1.0 is perfect, since the test was run with free-space models with no resistive losses). The AGT scores, plus an understanding of the ways in which using the SM-patch reflector violates the prescribed handling of patch constructs, strongly suggests that the SM-patch reflector models are secondary in precision to the wire-grid variety.

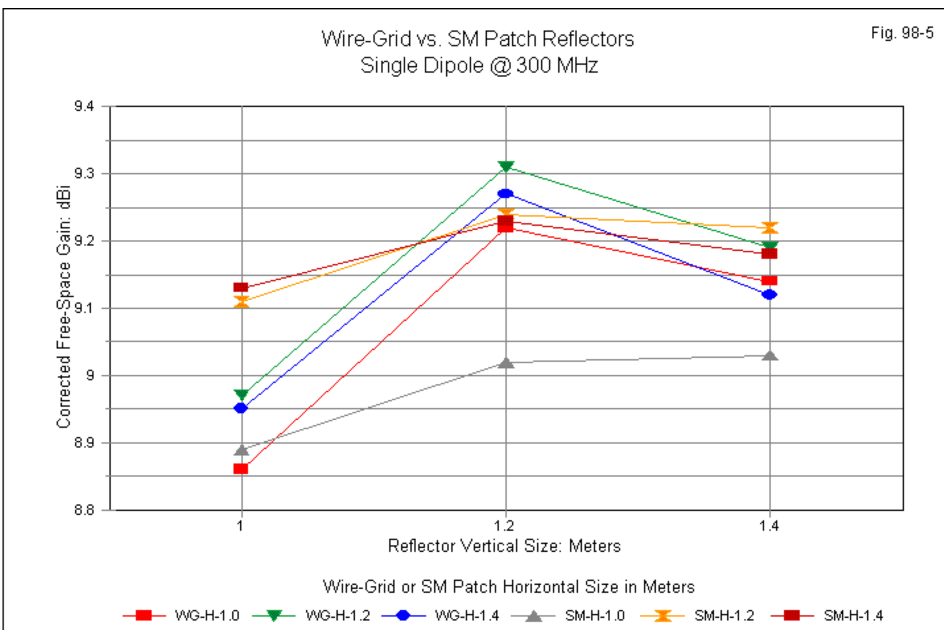

Nevertheless, the SM-patch models do afford reasonable first approximations of planar reflector results from wire-grid reflectors. They run about 4 times faster than wire-grid reflectors, and the input files are somewhat simpler.

Patch density within the SM/SC command lines does make some difference in the output reports. To check this aspect of the patch reflector, I varied the patch density of the basic 1.2 by 1.2-meter (wavelength) reflector from 10 patches/meter up to 15 patches/meter (with added check values of 6 and 20 patches/meter). The following table summarizes the reported values.

Variations in Performance Reports Due to Variations in Patch Density
Reflector: 1.2 by 1.2 Meters (Wavelengths)

Patches/ 1.2 Meter	Reported Gain dBi	Front-to-Back Ratio dB	Impedance R+/-jX Ohms	AGT	AGT-dBi
6	9.12	18.98	50.85 - j1.65	0.966	-0.14
10	9.14	19.11	50.03 - j1.72	0.975	-0.11
11	9.14	19.13	50.00 - j1.70	0.976	-0.10
12	9.13	19.16	50.00 - j1.70	0.976	-0.11
13	9.13	19.17	50.00 - j1.67	0.976	-0.10
14	9.13	19.18	49.99 - j1.66	0.976	-0.10
15	9.13	19.19	49.99 - j1.65	0.976	-0.10
20	9.12	19.22	49.98 - j1.63	0.976	-0.10

The significance of these variations depends on the uses to which we try to put the SM patch reflector models. The patch density of 10 per dimension is about 3 times the recommended minimum per unit area as measured in wavelengths. As a result, changes from one step to the next are small. As we increase the patch density above 10/dimension, gain decreases very slowly, while the front-to-back ratio increases at an equally slow rate. Increasing patch density has very little effect on the AGT value for the model.

While these facts are significant to the understanding of how SM-patch reflector models tend to respond to changes in the reflector geometry commands, they do not yield results that would impact a design or analysis situation. Given that SM-patch planar reflector models are at best first approximations of more accurate but more complex wire-grid models, we may consider the models fully converged at a patch density of 10 patches per linear wavelength.

Corner Reflectors: Wire-Grid or SM Patches

The SM-patch planar reflector illustrates the use of a single patch structure that simulates a single physical (conductive) plane structure. The SM/SC command set has also been used to simulate more complex structures, such as horns. Hence, the structure requires the use of multiple SM/SC command pairs to include all planes of the structure. In each case, the operating presumption (assuming that the modeler has appreciated the restrictions on the use of patches) is that the single outward-normal unit vector of the incomplete volume provides an adequate basis for the modeling effort.

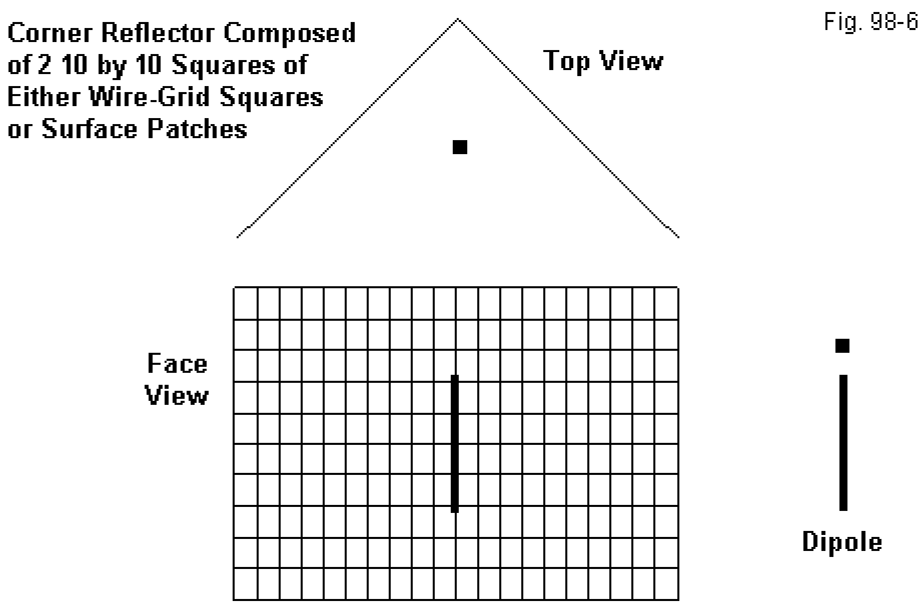

We may test a multiple-SM structure using one-sided techniques with a model far simpler than a horn. A corner reflector of conventional design consists of 2 identical planes joined along one edge, usually called the apex. The angle between the planes is conventionally 90°, although other angles are both feasible and desirable if we wish to optimize the gain potential of the array. **Fig. 98-6** outlines the basic construction of the corner array using a single dipole driver, regardless of whether we employ a wire-grid or an SM-patch model for the reflector surfaces.

Our purposes involve only comparing one form of modeling with another, so we may select smaller reflector planes as illustrative models. In fact, each of the two reflector planes will consist of 1.0 by 1.0 meter wire or patch grids. Since the test frequency remains 300 MHz, the use of 10 units per linear dimension of the planes will yield 10 segments or 10 patches per wavelength. The wire-grid version of the model (98-3) has the following appearance.

```
CM Dipole .324 m from corner reflector
CM Basic Corner Reflector: 299.7925 MHz; 1 m = 1 wl
CM T1 = center line, T2, T3 = verticals + GM
CM T4, T5 = horizontal centers + GM
CM Density = 0.1 m x 0.1 m
CM Size = 1.0 m x 2.0 m
CE
GW 1 10 0 0 -.5 0 0 .5 .0159
GW 2 10 0 -.1 -.5 0 -.1 .5 .0159
GM 0 9 0 0 0 0 -.1 0 2 1 2 10
GW 3 10 0 0 0 0 -1 0 .0159
GM 0 5 0 0 0 0 0 -.1 3 1 3 10
GM 0 5 0 0 0 0 0 .1 3 1 3 10
GM 0 0 0 0 45 0 0 0 2 1 0 0
GW 4 10 0 .1 -.5 0 .1 .5 .0159
GM 0 9 0 0 0 0 .1 0 4 1 4 10
GW 5 10 0 0 0 0 1 0 .0159
GM 0 5 0 0 0 0 0 -.1 5 1 5 10
GM 0 5 0 0 0 0 0 .1 5 1 5 10
GM 0 0 0 0 -45 0 0 0 4 1 0 0
GW 101 11 .324 0 -.2119 .324 0 .2119 .004
GE 0 -1 0
```

```
FR 0 1 0 0 299.7925 1
GN -1
EX 0 101 6 0 1 0
RP 0 361 1 1000 -90 0 1.00000 1.00000
RP 0 1 361 1000 90 0 1.00000 1.00000
EN
```

The CM lines show some of the particulars of the structure, including the dipole distance from the apex of the corner reflector. This value will not change when we arrive at the SM/SC version of the model. As with the planar wire-grid reflector, the reflector plane modeling uses a horizontal center wire line in order to be able to change with ease the vertical height of the reflector, adding the same amount to the top and bottom. The vertical wires begin with an apex wire and an initial wire on each side of the apex. Then the initial side wires are replicated the proper number of times to arrive at the horizontal dimension for each plane. Of course, we rotate each plane 45° to yield the 90° final angle. From the dipole (GW 101) onward, the model is straightforward. Note that the comment on reflector size gives the total size of the pair of reflector planes as if they were laid out in a single plane.

The SM/SC version of the corner reflector is deceptively simple. See model 98-4.

```
CM Dipole .324 m from corner reflector
CM Basic Corner Reflector: 299.7925 MHz; 1 m = 1 wl
CM SM panels
CM Density = 0.1 m x 0.1 m
CM Size = 1.0 m x 2.0 m
CE
GW 1 11 .324 0 -.2119 .324 0 .2119 .004
SM 10 10 0 0 -.5 .7071068 .7071068 -.5
SC 0 0 .7071068 .7071068 .5
SM 10 10 .7071068 -.7071068 -.5 0 0 -.5
SC 0 0 0 0 .5
GE 0 -1 0
FR 0 1 0 0 299.7925 1
GN -1
EX 0 1 6 0 1 0
```

```
RP 0 361 1 1000 -90 0 1.00000 1.00000
RP 0 1 361 1000 90 0 1.00000 1.00000
EN
```

As we might expect, the same corner reflector requires only 2 SM/SC entry pairs to form the reflector planes. Of course, we must do some initial calculations to establish the corner points for each of the two planes so that each one is 45° each side of the X-axis for this model. The only change to the dipole is to give it a tag number of 1, since there are no other wires in this version of the corner reflector.

However, the SM/SC entries deserve a bit closer attention. From the perspective of model symmetry, they do not use the same set of corners. However, from the perspective of patch construction, they do. **Fig. 98-7** illustrates the "right-hand rule" according to which we need to construct joining patches.

Fig. 98-7

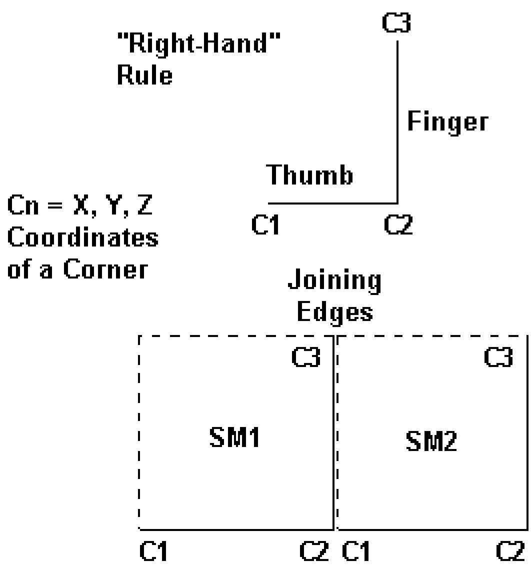

If we do not adhere to the right-hand rule, the resulting patterns yielded by the overall model will lead us to conclude that we cannot construct single-surface SM/SC corner reflectors at all. When properly constructed, the SM/SC model will produce comparable but not identical results relative to the wire-grid version of the array. **Fig. 98-8** provides an overlay of the theta (E-plane) and phi (H-plane) patterns for the subject structure.

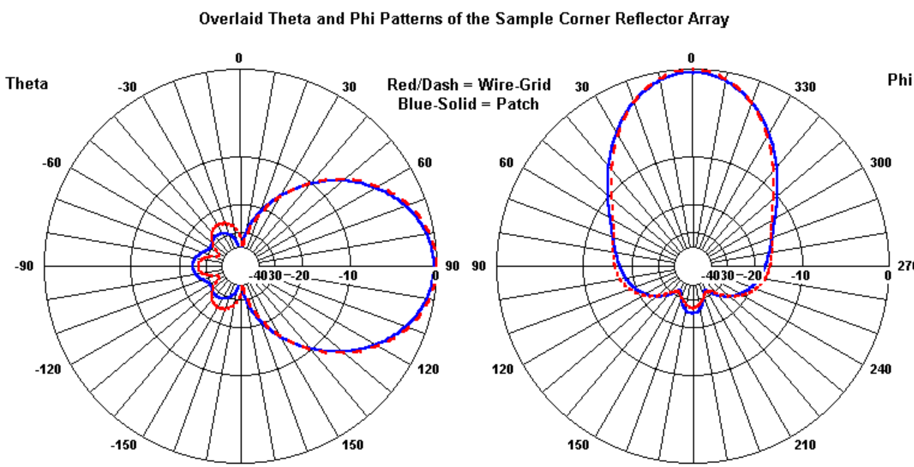

Fig. 98-8

As with the single planar reflector, the SM/SC corner reflector does not show very significant differences in the forward gain. Rather, the key difference is that the SM/SC construct does not show the full development of the rearward lobes. Due to the operation of the corner array, there are also differences in the reported beamwidth, especially in the phi (H-plane) pattern. The following table shows the differences in numerical terms.

Variations in Performance Reports of Wire-Grid and Patch-Based Corner Reflectors
Each Reflector Plane: 1.0 by 1.0 Meters (Wavelengths)

Version	Reported Gain dBi	Front-to-Back Ratio dB	E-plane Beamwidth	H-plane Beamwidth	Impedance R+/-jX Ohms	AGT	AGT-dBi
Wire-Grid	10.98	26.57	56 deg.	48 deg.	49.94 + j0.14	0.999	-0.01
SM-Patch	10.75	24.15	56	52	47.37 - j1.65	0.970	-0.13

As was the case with the single plane reflector, the corner reflector shows a significantly lower AGT value than we obtain for the wire-grid model. If we correct the gain value, it climbs to 10.88 dBi, somewhat closer to the wire-grid model value. However, using the AGT to correct the resistive portion of the source impedance results in 45.95 Ω, a value that is further distant from the wire-grid value. Increasing the source resistance would require increasing the distance of the dipole from the reflector apex, which might correspond roughly to the radius of the wires in the wire-grid reflector.

Nevertheless, due to the fact that single-sided SM-SC planes can only partially simulate the operation of a physical structure, we must treat the SM-patch version of the corner reflector as a first approximation. It has the advantage of faster run times and simpler input models, but it does show lower AGT values and deficiencies in the development of certain parts of the array pattern, relative to wire-grid models.

Because the SM-patch reflector model is based on the assumption that only a single plane surface is relevant to array performance, the SM/SC model of plane reflective surfaces will always have limitations. First, it cannot apply at all to any array in which the assumption is not close to being correct. Second, as we have seen, even where the assumption is close to being correct, it is rarely if ever precisely correct.

However, as a speedy method of constructing first approximations of arrays and arriving at reasonable performance values, one-sided SM/SC planar surfaces have a useful role to play in some modeling enterprises. They can play that role well so long as we remember that the world of multiple surface patches is right-handed.

99. S-N, RCA, and MININEC Grounds

We have in past episodes discussed the ground calculation systems associated with the most common antenna modeling cores, MININEC and NEC. A development in one of the commercial MININEC packages (Antenna Model) brings those ground calculation systems back into focus.

The Basic or Native Ground Calculation Systems

The MININEC ground calculation system is perhaps the most rudimentary, since its development paralleled the original intent of MININEC: to offer reasonably accurate round-wire antenna modeling in a Basic package that would run on early PCs with very limited RAM and disk storage. Over the years, the latest public domain version of MININEC (3.13) has undergone various degrees of modification to achieve two major goals. One aim of redevelopment was to extend the 128-segment and later 256-segment limit for models. Conversion of the package to a Windows format and a compatible programming code system has yielded MININEC versions with almost unlimited segments, although almost all such packages make their core runs more slowly than the compiled FORTRAN that is common to most NEC packages. The second goal was to correct some of the modeling weaknesses that included an error that increased with frequency, problems with very close-spaced wires, and potential errors associated with angular structures. Various software packages have addressed individual limitations, but Antenna Model has achieved the most thorough set of correctives.

Perhaps the one enduring feature of MININEC that resisted alteration for the longest period is the ground calculation system. As far back as 1991, Roy Lewallen, W7EL (author of ELNEC and EZNEC programs) provided careful warnings about the use of the MININEC ground calculation systems with horizontal wires closer to ground than about 0.2 λ. (See "MININEC: The Other Edge of the Sword," *QST*, Feb., 1991.) Since then, warnings have emerged concerning errors ranging from small to large with sloping wire constructs where one end is at ground or close to ground. These constructs have a horizontal component and to that degree suffer the MININEC ground calculation limitation. Vertical wires do not have the same limitation as horizontal wires. When a vertical wire touches the ground, it will return a plausible antenna pattern and gain report. However, the source impedance does not change with changes in the assigned ground quality. Rather, MININEC always returns the source impedance over perfect ground. Hence, it is not possible to track variations of source impedance due to ground losses with the MININEC native ground calculation system. If the modeler constructs radials, then all wires must be above ground, and the radials are subject to the horizontal-wire limitation that we have already noted.

NEC (both -2 and -4) offers two real-ground calculation systems. The use of 2 separate systems results again from the early days of slower computers. The Reflection Coefficient Approximation (RCA) system produces faster core run times, but it suffers from a minimum height restriction for horizontal wires. Various sources give different values for the recommended minimum height above ground, ranging from 0.1 to 0.2 λ. The error introduced into horizontal wires below the recommended limit does not follow the same trends as MININEC ground calculation errors under the same circumstances. Vertical wires touching the ground also produce errors. However, NEC's RCA system does have a mode of operation that simulates ground radial systems using the number of radials and radial length specified by the user. It is available only in packages that make the full set of NEC commands available. Like the MININEC ground calculation system, the RCA system in the radial mode produces plausible patterns and gain reports. However, it responds to differences in the ground quality and the number and length of radials. Still, in this mode of operation, the RCA system returns source impedance reports based on perfect-ground or image calculations.

The second NEC ground calculation system is usually called the Sommerfeld-Norton (S-N) system. It runs more slowly than the RCA system, but that factor has largely become a superfluous concern with the speed of modern PCs. With respect to horizontal wires, the S-N ground calculation system provides accurate gain and source impedance reports with wires very close to ground. If h is the height above ground in wavelengths and a is the wire diameter in wavelengths, then the closest approach to ground for a wire (in wavelengths) should be as follows:

$$(h^2 + a^2)^{1/2} > 10^{-6}\lambda$$

If a is very small relative to h, then we may use the recommended closest approach for the height alone.

With respect to vertical wires, the S-N ground calculation system suffers the same limitation as the RCA system. Vertical wires touching the ground will yield erroneous results. As a result, models dealing with vertical monopoles and arrays based upon them must construct radial systems in accord with other limitations of their NEC core. For NEC-2, all wires must be above ground, although with the S-N ground calculation system, the vertical and radial wires may approach the ground in accord with the recommended equation. In NEC-4, we may model buried radials. Radials may converge below ground or may have sloping sections that converge above ground. In either case, a wire that passes Z=0 may do so only at a segment or a wire junction.

Packaged Ground Calculation Systems

Most antenna modeling packages provide the user with the ground calculation systems native to the core used in the package. MININEC packages provide the user with the MININEC ground. NEC-2 and NEC-4 packages make the S-N and RCA ground calculation systems available. However, there are 2 known exceptions to this general trend.

EZNEC (in all its version-4 forms: regular, Plus, and Pro) gives the user a choice between the S-N and the MININEC ground systems with either the NEC-2 or NEC-4 cores. The premises behind this set of options are straightforward. First, modern PCs do not need the speed advantage that was once a main reason for using the RCA system. The time saved between ground calculation systems at the original PC CPU speed of 2 MHz was significant, but almost undetectable with current 2 GHz CPUs. S-N system calculations can still be saved to a file to free the RAM in successive runs for mutual impedance and currents calculations, but current RAM capabilities have largely obviated the need for this step. Therefore, for all antenna models with horizontal components, the S-N ground calculation system's greater accuracy dictates its use.

Second, there are still a number of modeling applications in which the user will wish to connect a vertical wire directly to ground without employing a radial system. Preliminary performance comparisons of various sorts become highly efficient using this technique. However, neither the S-N nor the RCA systems return plausible results in NEC using this technique, especially with respect to the source impedance. Although less than perfect relative to models using buried radial systems in NEC-4 plus the S-N system, a MININEC ground provides quite reasonable values for initial comparisons, along with the source impedance that applies to the use of a perfect ground.

There is a qualification that we must note on this account. The RCA system, when set up for buried radials, would offer the advantages for initial comparisons with a MININEC ground, with the added advantage of showing some sensitivity to the conditions of the radial field. However, the set-up for this option involves a somewhat interesting relationship between the ground specifications command and the pattern request command. The ground specification command is divided between 2 possible commands, GN and GD.

If the GN command's I2 (NRADL) entry is greater than zero, then you must use the GD command to enter a second medium. If NRADL is 1 or more, then the meanings of F3 through F6 change from a more basic set-up of the command. Let's see what happens to the GN command under these conditions.

Cmd	I1	I2	I3	I4	F1	F2	F3	F4	F5	F6
	IPERF	NRADL	0	0	EPSR	SIG	RADS	RADW	-	-
GN	0	8	0	0	13	.005	.237	.001		

I2 shows a request for 8 radials. The single-medium ground quality values go into F1 and F2 as always. However, F3 and F4 have new meanings. RADS is the radius of the screen, or the length of the individual radials in the screen. RADW indicates the radius of the individual wires composing the set of radials. Both values are in meters.

In NEC-2, the RP command must have an I1 assignment of 4 for a simple set of radials. If there are GN and GD commands requesting both a screen and a second medium, then the NEC-2 RP command must let I1 = 5 for a screen and a linear cliff or let I1 = 6 for a screen and a circular cliff. NEC-4 uses I1 = 0 in the RP command for all these cases, since the type of cliff will be set in the GD command. NEC-4 will read a NEC-2 model with only a screen request by treating the RP4 request as RP0.

The radial screen option in the GN command applies only to the RCA real ground type (I1 = 0) and is not allowable with a request for an SN ground (I1 = 2). The calculations are based upon a modified reflection coefficient, and the resulting source impedance report will be the same as for a perfectly conducting ground (I1 = 1). Despite this limitation, the system is more versatile than simpler ground systems (such as those used with MININEC cores), since it will show differences in far-field patterns due to changes in the ground quality and changes in the number of radials.

As currently implemented, EZNEC has no provision for setting the RP pattern request command to the values required by the RCA ground radial set-up. Hence, the facility that the program makes available for verticals without modeled wires for a radial system is the MININEC ground. Packages that make the complete set of NEC-2 or NEC-4 commands available to the user may substitute the RCA ground radial set-up for the MININEC ground calculation system for initial comparisons of vertical antennas and arrays.

Special Note: As with all comments on the current capabilities of an existing program, the notes are believed to be accurate as of the time of writing. However, software developers tend to continuously upgrade and modify their offerings. Hence, what is true at the time of writing may prove to be outdated by the time of publication.

The second package to provide the user with non-standard ground calculating systems is a version of MININEC: Antenna Model. We have noted on more than one occasion that this package provides the most thorough set of correctives to the shortcomings of the raw MININEC version 3.13. As noted in previous columns, for comparable models, Antenna Model's MININEC core tracks very well with NEC-4. As well, MININEC offers the added advantage of showing no limitations wherever we have junctions (angular or linear) of wires having different diameters. However, like other MININEC offerings, Antenna Model lacks some features that are standard in NEC, such as the TL transmission-line and the NT network facilities.

Antenna Model shared one limitation with all versions of MININEC: the use of the MININEC ground calculation system. However, the software developers found a way the graft both the RCA and the S-N ground calculation systems to their MININEC package. Hence, with two qualifications, Antenna Model offers the same ground calculation advantages as NEC. The first qualification is that MININEC is like NEC-2 in that all wires must be above ground level. Second, MININEC offers no provision for setting up the complex interaction of commands that allows the RCA ground calculating system to add radials. Hence, the chief benefit of the addition of NEC ground calculating systems to the Antenna Model MININEC package lies in the realm of an improved ability to handle horizontal or slanted wires close to the ground. For example, Antenna Model is the only MININEC offering that is capable of producing accurate models of NVIS antennas that ordinarily have one or more wires within 0.2-λ of the ground.

Some Comparisons

Whenever we encounter a new modeling program feature, we should make a set of test runs in order to establish whether or not the claimed specifications of the feature are as accurate as we need for our work. The exact dividing line between acceptable and unacceptable will, of course, vary with the specifications for the modeling work that we do.

Since the addition of the NEC ground calculating systems to MININEC in Antenna Model benefit low-lying horizontal wires the most, I set up a series of small tests, of which the following one is an example. I created a simple dipole for 29.97925 MHz, where a wavelength is exactly 10 meters. I used 31 segments for a NEC-4 model and 30 segments for the corresponding MININEC model. The dipole used a perfect or lossless wire with a diameter of 1 mm. With a length of 0.485-λ (4.85 meters), the model produced resonant dipoles in free space on both NEC-4 and MININEC. Resonance here means a remnant reactance of under +/-j 1.0 Ω. The source impedance in NEC-4 was 71.99 - j0.43 Ω, while in Antenna Model's MININEC, the source impedance was 71.84 -j0.56 Ω. The differences fall well within what we would expect with a simple 1-segment change in segment density. The change, of course, reflects the difference in the position of the source relative to the segments themselves (MININEC at a junction, NEC within a segment). In both cases, the free-space gain was 2.14 dBi.

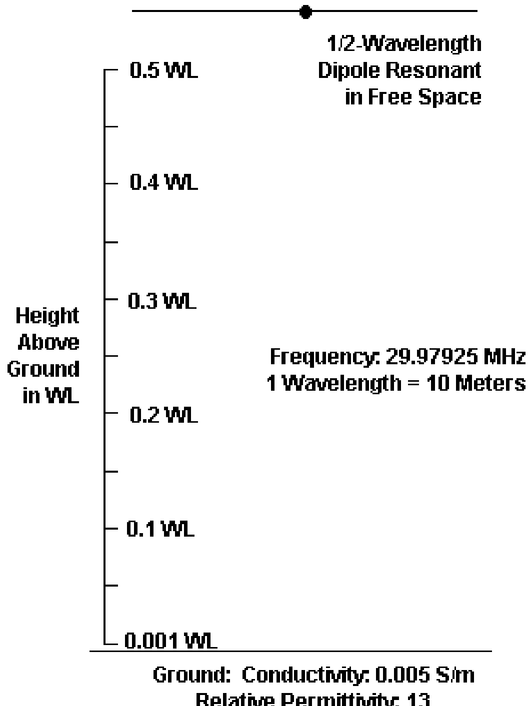

Fig. 99-1

With this model, I then created all of the ground calculation system variation that I might compare, using the so-called "standard" or "average" ground quality: conductivity: 0.005 S/m, relative permittivity: 13. I then set the dipole at a series of heights, beginning at 0.5-λ above ground. Each successive step brought the antenna 0.05-λ closer to ground down to a height of 0.05-λ. To simulate the closest approach to ground permissible, I set the final step at 0.001-λ above ground. The values for this height appear in the tables, but not in the graphs, since the increment is not linear and since some of the values would have obscured variations among the other steps in the sequence. **Fig. 99-1** outlines the test set-up.

The first test directly compared the Antenna Model MININEC use of the S-N system against the NEC-4 version of the antenna. The NEC-4 test employed EZNEC Pro/4, but there is no detectable difference among the core outputs of NEC-4 offerings. Indeed, running the same NEC-4 compiled Fortran core on different CPUs and operating systems generally shows a wider variation in results than running two different NEC-4 cores on the same CPU and operating system.

1.0-mm Perfect Dipole Resonant in Free Space					29.97925 MHz		1 wl = 10 m			**Table 1**
NEC-4 (EZNEC) S-N Ground						MININEC (AM) S-N Ground				
Height wl	Gain dBi	TO Angle	Source R	Source X		Height wl	Gain dBi	TO Angle	Source R	Source X
0.5	7.23	28	68.53	-9.74		0.5	7.29	28	67.47	-9.8
0.45	6.75	31	74.64	-10.95		0.45	6.75	31	74.43	-11.04
0.4	6.28	35	80.94	-8.36		0.4	6.28	35	80.71	-8.49
0.35	5.92	40	85.16	-2.18		0.35	5.92	41	84.95	-2.35
0.3	5.74	48	85.36	6.12		0.3	5.74	49	85.18	5.92
0.25	5.75	61	80.56	13.95		0.25	5.75	63	80.43	13.76
0.2	5.86	90	71.51	18.31		0.2	5.86	90	71.43	18.12
0.15	5.36	90	61.11	16.8		0.15	5.35	90	61.06	16.64
0.1	3.53	90	55.06	9.5		0.1	3.52	90	55.1	9.38
0.05	-0.93	90	65.1	5.86		0.05	-0.94	90	65.2	5.84
0.001	-7.78	90	184.6	285.8		0.001	-7.81	90	202.51	330.57

Table 99-1 shows the results of the test. From 0.5-λ down to 0.05-λ, the correlation of results is as exact as we may expect from models with slightly different segmentation densities. The only variant result is the source impedance at a height of 0.001-λ (1 cm). Antenna Model certifies its results only to 0.01-λ, although the variance in source impedance is only about 7% at 1/10 the minimum recommended height of use. For all practical cases, Antenna Model's MININEC with the S-N ground is the equal of NEC's results with the S-N ground calculating system.

1.0-mm Perfect Dipole Resonant in Free Space					29.97925 MHz		1 wl = 10 m			**Table 2**
NEC-4 (GNEC) RCA Ground						MININEC (AM) RCA Ground				
Height wl	Gain dBi	TO Angle	Source R	Source X		Height wl	Gain dBi	TO Angle	Source R	Source X
0.5	7.24	28	68.5	-9.97		0.5	7.23	28	68.31	-10.01
0.45	6.74	31	74.58	-11.23		0.45	6.74	31	74.53	-11.3
0.4	6.26	35	81.26	-8.58		0.4	6.26	35	81.01	-8.72
0.35	5.9	41	85.71	-2.17		0.35	5.89	41	85.5	-2.38
0.3	5.71	49	86.01	6.61		0.3	5.71	49	85.9	6.33
0.25	5.74	64	80.95	15.23		0.25	5.72	63	81.05	14.92
0.2	5.91	90	70.78	20.55		0.2	5.87	90	71.27	20.39
0.15	5.64	90	57.48	19.67		0.15	5.54	90	58.67	20.18
0.1	4.47	90	44.4	10.36		0.1	4.22	90	47.18	13.91
0.05	1.45	90	37.3	-10.86		0.05	0.82	90	44.05	14.63
0.001	-7.24	90	110.06	-99.5		0.001	-22.08	90	769.51	-7828.65

Since Antenna Model also implements the NEC RCA ground calculation system, we might as well perform the same set of modeling steps using it. However, we cannot find our NEC-4 counterpart models in EZNEC. So this set of models uses NSI's GNEC. See **Table 99-2**. Note that the correlations between both the gain and the impedance reports are quite tight down to a height of about 0.2-λ. Then we see a drifting apart of values that becomes more extreme from 0.1-λ down to the minimum height. For reasons that we shall see shortly, it is unlikely that we would uses this ground below 0.2-λ for horizontal wires, so the divergence of reported values between the NEC-4 and the MININEC cores is more artifactual than significant.

1.0-mm Perfect Dipole Resonant in Free Space					29.97925 MHz		1 wl = 10 m			**Table 3**
NEC-4 (EZNEC) MININEC Ground						MININEC (AM) Native Ground				
Height wl	Gain dBi	TO Angle	Source R	Source X		Height wl	Gain dBi	TO Angle	Source R	Source X
0.5	7.3	28	66.98	-17.48		0.5	7.3	28	66.79	-17.48
0.45	6.53	31	78.01	-18.94		0.45	6.52	31	77.76	-19.03
0.4	5.84	35	89.1	-13.7		0.4	5.84	35	88.83	-13.86
0.35	5.39	41	96.35	-2.07		0.35	5.39	41	96.11	-2.3
0.3	5.25	49	96.2	13.46		0.3	5.25	49	96.04	13.2
0.25	5.5	63	86.61	28.43		0.25	5.5	63	86.55	28.21
0.2	6.14	90	68.16	37.39		0.2	6.14	90	68.15	37.24
0.15	6.8	90	44.57	35.6		0.15	6.8	90	44.55	35.51
0.1	7.61	90	21.74	21		0.1	7.61	90	21.7	20.93
0.05	9.67	90	5.63	-5		0.05	9.67	90	5.6	-4.54
0.001	38.73	90	0.002	-20.6		0.001	39.82	90	0.002	-19.26

We can find the MININEC ground calculation system both in the MININEC-based Antenna Model and in the NEC-4-based EZNEC Pro/4. Therefore, we might as well complete the picture by comparing the reports for the same set of models using what most experts consider to be the least adequate system for horizontal wires. In fact, as shown in **Table 99-3**, the two cores yield as close to identical results as we can expect from the models involved, given the slight difference in segment density. The numerical differences between the MININEC ground results and the RCA ground results suggest that, while both use reflection coefficient approximations, they do not operate in exactly the same manner. The fact that the MININEC ground yields the same results whether attached to NEC-4 or to MININEC, while the RCA ground does not, is another indicator of differences between the two fast-running ground calculation systems.

There are alternative ways of viewing the same data. For example, we can compare in NEC-4 the gain values for both the S-N and RCA ground calculation systems. **Fig. 99-2** connects the dots, omitting the values for 0.001-λ.

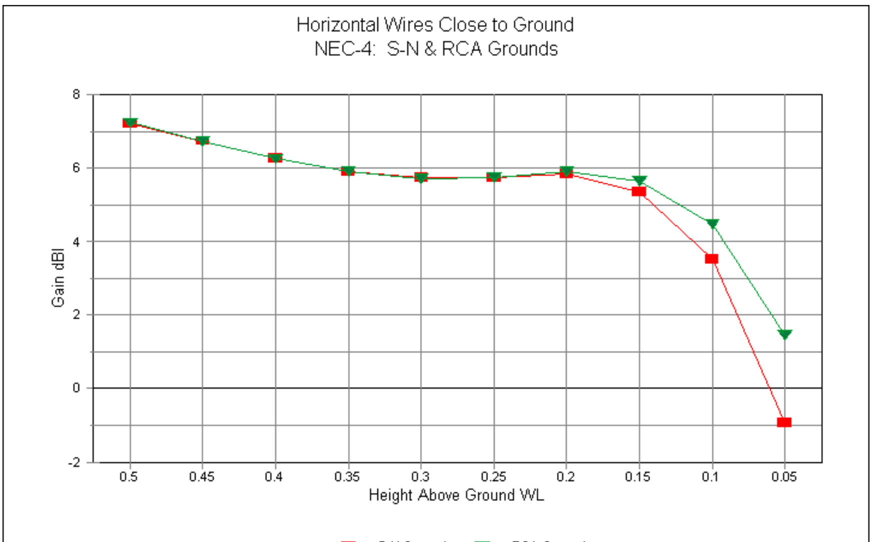

Fig. 99-2

The chart shows that below 0.2-λ, the RCA system supplies gradually inflated gain values for the horizontal wire gain values. This is the same height at which we found some divergence between the NEC-4 and MININEC reported gain values and represents a rough limit for the reliability of the RCA system. **Fig. 99-3** shows the corresponding source resistance information over the same range of wire heights.

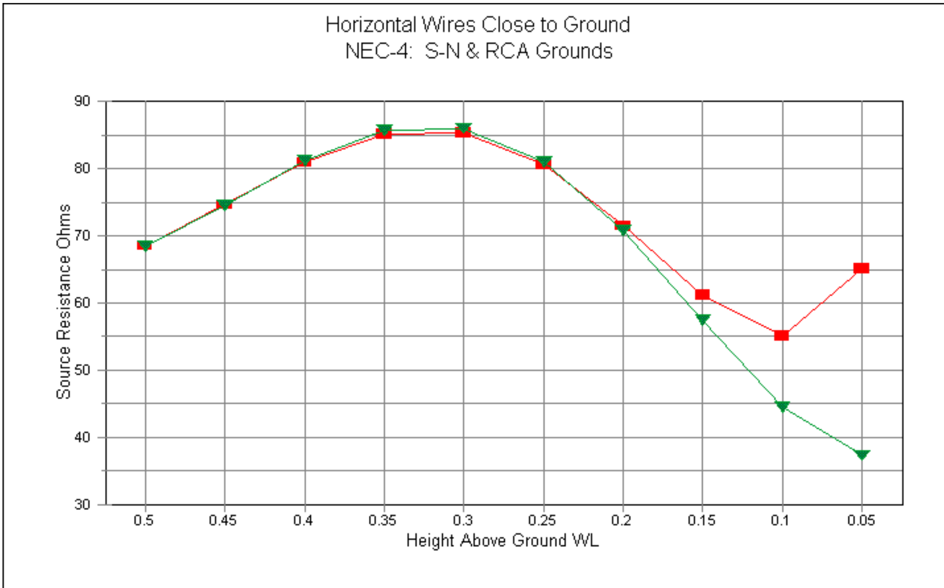

Fig. 99-3

At 0.2-λ wire height, we find the same divergence of S-N and RCA values. However, there is a fair tracking down to 0.1-λ. At that point, the RCA source impedance reports continue downward, while the S-N values turn upward. This divergence has caused some users to consider 0.1-λ to be the minimum usable height for RCA ground calculation system results. However, if you examine **Table 99-1** and **Table 99-2**, you will see that the NEC-4 reports for the lowest height show a lower source resistance for the RCA system than for the S-N system. The indication is that the turn upward in source resistance occurs at a lower height in the RCA system than in the S-N system. The net result is that the safest position at which to limit the use of the RCA system with horizontal wires is about 0.2-λ above ground.

Since 2 out of the 3 ground systems available in the Antenna Model implementation of MININEC are "imports," we might as well include all three systems in graphing the gain and source resistance reports. **Fig. 99-4** compares the three reported values drawn from the right-hand columns of the 3 tables. Once more, I have omitted the lowest height, since it is not a linear increment and because its values would obscure changes in other values in the graph.

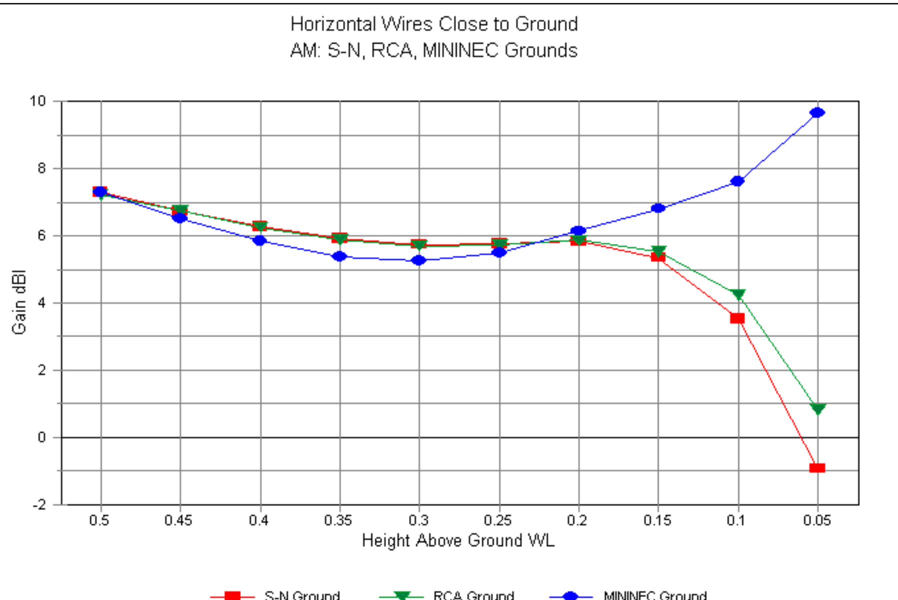

Fig. 99-4

The S-N and RCA lines track well down to a height of 0.2-λ. The RCA terminal value at 0.05-λ is lower than for its counterpart using NEC-4, as shown in **Table 99-2**. However, the split from the S-N reported value sets 0.2-λ as a practical limit for using the RCA value. The major surprise may lie in the comparison of the S-N and RCA curves on the one hand and the MININEC ground curve on the other–throughout the complete range of values. Except for a coincidence of gain report at 0.5-λ, the MININEC ground curve diverges from the two other curves all along the range of heights, describing a shallow parabola. The coincidence of values near 0.2-λ is mostly coincidental, since the upward progression at heights below that level is a simple continuation of the questionable curve across its entire range from 0.5-λ downward.

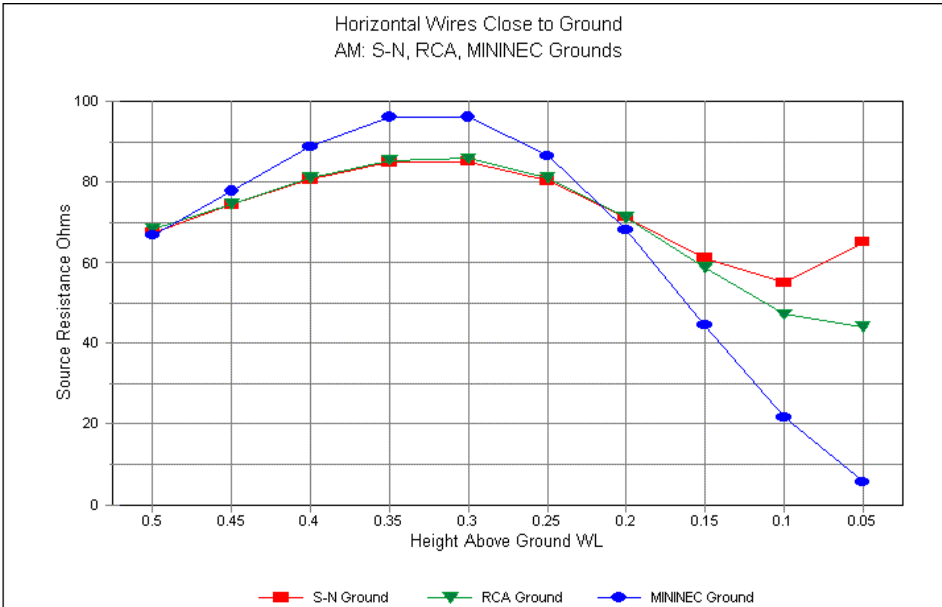

Fig. 99-5

The graph of source resistance values in **Fig. 99-5** shows a similar curve, but reversed. The inflation or deflation of source resistance values, relative to the S-N and RCA curves, is inversely proportional to the gain divergence. Hence, the MININEC ground system reports the highest gain values with the lowest source resistance values. In the end, for horizontal wires below 0.5-λ, the MININEC curves suggest that the formulation of the ground calculation was likely crude, over-simplified, or hasty, if not some combination of all three. That Antenna Model has grafted the S-N and RCA systems to its implementation of MININEC (especially when combined with its extensive correctives for most of the other MININEC weaknesses) provides the user with more assured results for any antenna structure having horizontal wires below 0.5-λ. The only redeeming function of the MININEC ground system is its ability to handle vertical antennas and arrays without demanding a radial system for at least initial comparisons. However, implementing the RCA radial command would allow the removal of the MININEC system altogether. This last remark, of course, is made with total ignorance of the programming difficulties that might be involved.

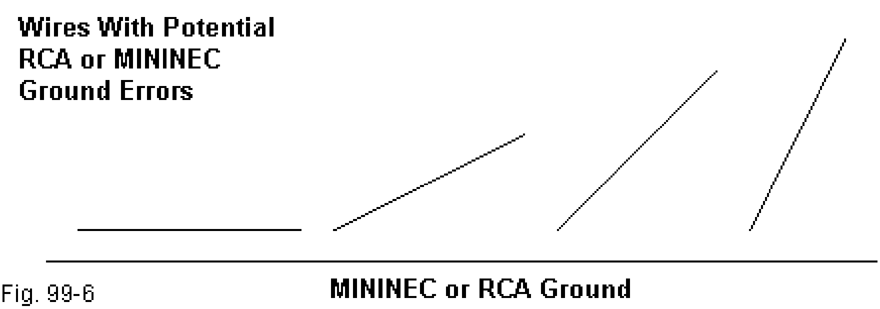

Fig. 99-6

As a final reminder, we might also attend to **Fig. 99-6**. Each of the sloping wires has a horizontal as well as a vertical component. Hence, using either the MININEC or the RCA ground calculation systems, we shall encounter errors in both the gain and source impedance reports when part or all of the structure is below 0.2-λ. The error will be proportional to a. the amount of the wire that is below 0.2-λ and b. the relative preponderance of the horizontal component relative to the vertical component. Modelers of complex vertical arrays that may use sloping (guy) wires as active elements, whether directly or parasitically excited often ignore this factor. Ignoring this situation imperils accuracy of the results.

MININEC is still widely used by numerous antenna modelers, especially since very cheap or free software using the core is readily available. However, not all public-domain MININEC implementations are equal. Indeed, the extensive modifications of the core–and now the ground calculating system–within Antenna Model almost remove it from the realm of MININECs except as a record of its genetic heritage.

Of course, Antenna Model is limited in the same manner as NEC-2: all wires must be above ground. For the most accurate round-wire modeling of arrays using buried radials, NEC-4 remains the core of choice. Nevertheless, the addition of the S-N and RCA ground systems within Antenna Model has given us a good occasion on which to compare low horizontal wire results for all of the extant ground calculation systems. Those comparisons are the main focus of these notes.

100. The Dipole and the Coax

The most usual way to feed a resonant dipole uses a simple coaxial cable. Most basic handbooks and texts recommend that the system builder insert a common-mode choke at the feedpoint–between the dipole feedpoint terminals and the coaxial cable. Readily available forms of common-mode choke include a transmission line transformer with a 1:1 impedance ratio and a ferrite-bead collection following the designs proposed initially by Walt Maxwell (W2DU). In either case, the device establishes compatibility between the balanced feedpoint of the dipole and the seemingly single-ended construction of the coaxial cable.

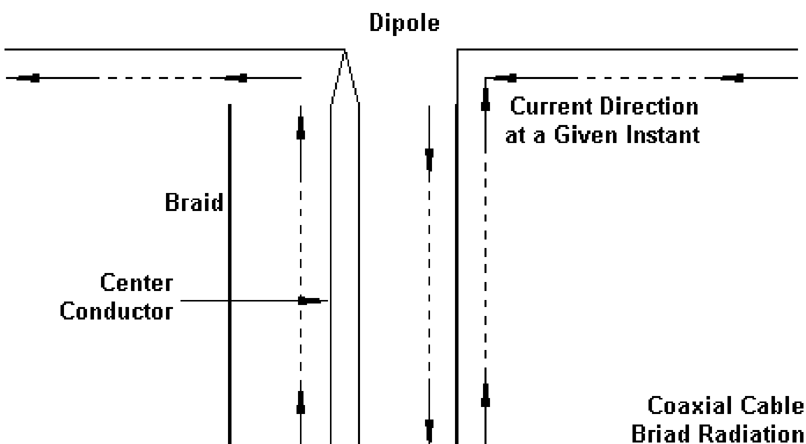

Fig. 100-1

Fig. 100-1 presents one traditional way to portray the situation at the dipole feedpoint. Its general purpose is to show why the insertion of a balun is important as a precautionary measure in dipole construction. By extension, the situation applies to any split element fed by coaxial cable. The dipole is merely the most fundamental case.

At any given instant, the currents between the coaxial cable center conductor and the inner side of the shield or braid are equal and opposite. However, according to the graphic, once the cable terminates at the dipole feedpoint, the current has multiple paths of travel. The diagram suggests that the center conductor has only a single path: the left leg of the dipole within the figure. However, the current from the braid has 2 paths: the right leg of the dipole in the figure and the outer side of the coaxial cable braid. The function of the choke is then to attenuate so far as possible the current that would appear on the coaxial cable braid outer side. It performs this function largely by introducing a large inductive impedance to such currents. The function is similar to that of an RF choke within an amplifier circuit. However, the arrangement must have a form that does not disturb the currents between the center conductor and the inner side of the cable braid.

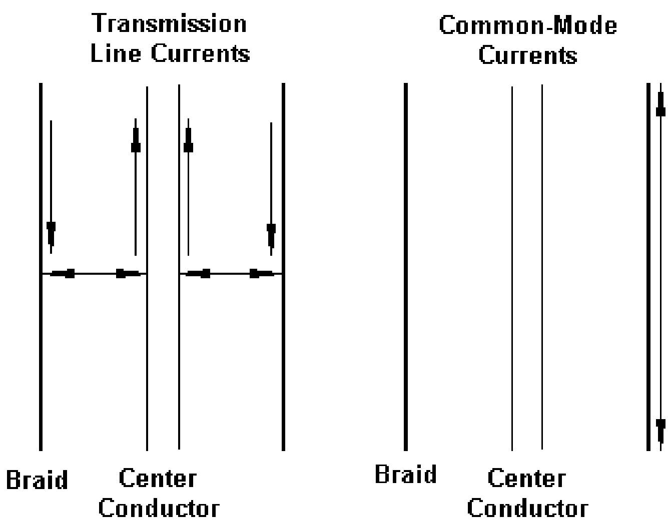

Transmission Line and Common-Mode Currents in Coaxial Cables

Fig. 100-2

As suggested by **Fig. 100-2**, we then have 2 sets of currents to consider. The left portion not only portrays the current as directional, but also indicates the field between the center conductor and the inner side of the braid, so that we have at any point of measurement currents of equal magnitude but opposite polarity or phase angle. These are transmission-line currents in the conventional sense. If we replace the resonant antenna with a resistor of vanishingly small dimension (but still capable of converting the RF energy into heat without self-destruction), we should measure only transmission line currents at any measurement point. If we place a complex load of similarly small lumped components at the cable end, we shall obtain the same results, although the lack of a match between the cable characteristic impedance and the load will alter the pattern of current values along the line.

On the right in **Fig. 100-2**, we have the common-mode currents that appear on the surface side of the coaxial cable braid. Common-mode currents in theory may derive from either conductor, but always appear on the coaxial cable outer side due to skin effect. Therefore, in theory, the current on the braid outside side is the sum of currents other than transmission line currents on the entire coaxial cable structure. Since the transmission-line currents are equal in magnitude but opposite in phase angle, they cancel. The common mode currents are the remainder, whatever their source. Because common mode currents appear on the braid outer side, they are capable of radiation, just as the current on the antenna legs proper. Because those currents may appear all along the coaxial cable length, they may also be found at the transmitting equipment, where the cases form an irregular extension of the coaxial cable outer side. (Note: many writers would simply refer to the coaxial cable braid outer surface. However, at any frequency, there is always some depth to the current-conducting portion of the braid. Hence, I have used the term "outer side" instead. The depth of penetration, of course, is a function of frequency.)

The feedpoint of a dipole element represents a small gap in the antenna. Between the terminals of the gap, the feedline provides a series source of energy for the antenna, thus completing the path between those terminals. This very basic fact is important, because it drives the conventional method of trying to model the effects of common mode currents within both NEC and MININEC antenna modeling software. Neither software core is capable of physically modeling conventional coaxial cables. The transmission line function within NEC creates lossless non-radiating mathematical models of lines and hence cannot capture common mode radiation. Therefore, the method used to show common mode radiation is to place a third leg into the dipole. Its feedpoint end connects as closely as possible to one side of the feedpoint segment or pulse, depending upon the software used.

In these notes, we shall not question the appropriateness of the model as a means for effectively modeling common-mode currents on a coaxial cable feedline. That discussion belongs to another context. Within the prescribed modeling effort, there are some modeling issues that deserve review.

Modeling the "Coax" Wire With a Dipole

Therefore, let's begin with a simple dipole that is resonant at 29.97925 MHz, where 1 wavelength = 10 meters. If we use 1-mm diameter wire and make the dipole 0.485-λ (4.85 meters), the antenna will show a free-space resonant impedance in both NEC and MININEC. The MININEC model will use 30 segments so that the center feedpoint falls on a pulse. The corresponding NEC model uses 31 segments so that its center feedpoint falls at the center of a segment (model 100-1). Both models show a free-space gain of 2.14 dBi. The reported MININEC source impedance is 71.84 - j0.56 Ω, while the reported NEC-4 source impedance is 71.99 - j0.43 Ω. The two values are close enough to qualify the models as the same for the purposes of the exercise to follow. The MININEC software used here is Antenna Model, while the NEC-4 software is EZNEC Pro/4.

We shall try to model the coaxial cable using a 6.35-mm (1/4") diameter wire connected as close to the model source as possible. The conductor size corresponds roughly to the outer diameter of the braid in such cables as RG-58 and RG-8X. For the exercise, we shall use a third-wire length of 0.25-λ (2.5 meters). For the purposes of the exercise, the wire will run from its connection point straight downward, relative to a horizontal dipole. In modeling terms, we construct the dipole proper in the X-Y plane, with the third wire representing the coaxial cable modeled along the Z-axis. **Fig. 100-3** shows–for the MININEC model–the difference between the simple dipole and the dipole plus its "coax" wire. The outline of the NEC model would be similar.

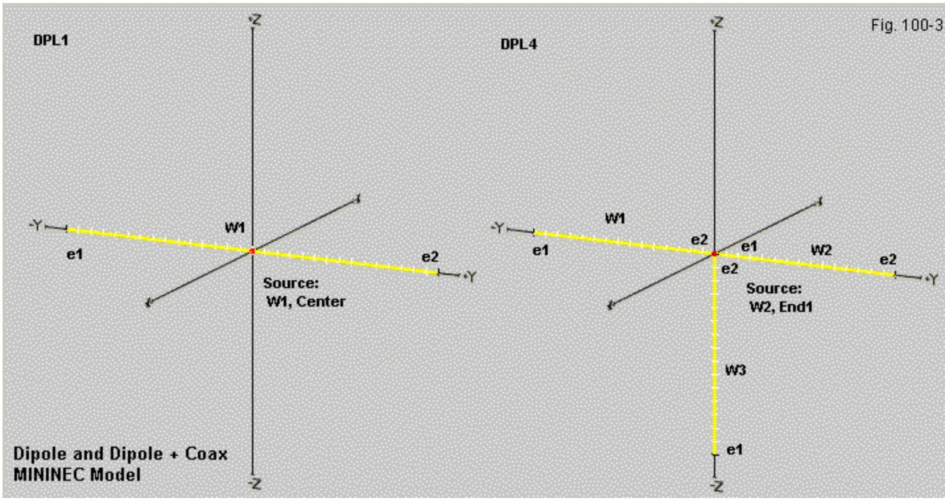

The diagram does list the ends of each wire. That aspect of the figure will change as we move from one model to another. **Fig. 100-4** shows why, at least in part.

The MININEC model places a source on a pulse, which occurs at the junction of two segments or wires. Since a junction of segments or wires contains an ambiguity relative to which of the segments has the pulse, the convention is to place the pulse on the higher-number segment (using an absolute segment count). Hence, the source pulse appears in the MINNEC model in the middle of Fig. 4 on the second or right-leg wire of the dipole. In order to calculate current correctly, we must bring both wire 1 (the left dipole leg) and wire 3 (the coax wire) together so that both wires have end 2 at the junction of wire 2, end 1.

Fig. 100-4

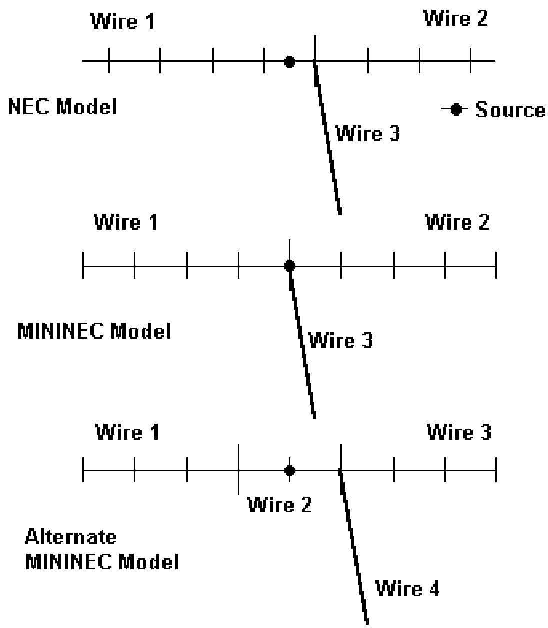

Models Used to Test Modeling Properties of the "Coax" Wire Situation Within NEC and MININEC

The model that we have just described brings the coax wire as close to the source as is possible. Presumably, this procedure adheres most closely to reality, as earlier described. The alternative modeling procedure in the lower part of **Fig. 100-4** creates a 2-segment center wire for the dipole itself. The coax wire connects to one side of the center wire. We shall use this model only briefly to make a comparison near the end of these notes.

In a NEC model, we cannot connect a coax wire directly to the source point. As the upper part of **Fig. 100-4** shows, the source occupies a segment, and by convention, we mark this fact by placing the source indicator in the center of the segment. At best, we must connect the coax wire to the segment or the wire junction occurring at one or the other end of the source segment. Since every segment has a definite length, the coax wire junction will be offset from the true center of the dipole. Part of the exercise will be to explore the effects of that offset. In this case, the source appears on the last segment of wire 1, which extends past the dipole center so that the source segment is centered within the overall dipole length.

NEC is sensitive to having the source segment be equal in length to the adjacent segments. The closer we can come to meeting this condition, the more accurate will be the reported source impedance. Hence, for both MININEC and NEC models, the goal was to use segment lengths as close to equal as feasible within the overall 30/31-segment structure of the 4.85-meter dipole.

Some MININEC Results

The MININEC model, as suggested by **Fig. 100-4**, uses 3 wires. The 1-mm diameter dipole wires are equal in length, and each has 15 segments. The length of the individual segments is 161.667 mm. The 6.35-mm-diameter coax wire in "Dipole Plus" is 2.5 m long and also uses 15 segments. Hence, the individual segments are 166.667 mm long, about 5 mm longer than those in the dipole.

The following table summarizes the reported characteristics of both the dipole alone (reference to "dpl1" on graphics) and the dipole with its coax wire added (reference to "dpl4" on graphics). AGT refers to the average gain test value.

MININEC Models:
Standard Dipole vs. Dipole Plus Coax Wire: Free Space

Model	Maximum Free-Space Gain dBi	Source Impedance R+/-jX Ω	AGT
Dipole	2.14	71.84 - j 0.56	0.9999
Dipole Plus	2.04	45.68 - j12.85	0.9994

The currents on each side of the source segment of the standard dipole are, of course, exactly equal for the symmetrical element. However, for the dipole + coax wire model, we find the following values. W1e2 means wire 1, end 2, etc. W2e1 is the source pulse for the antenna.

Relative Current Levels at the Dipole+Coax Wire Feedpoint: MININEC

Angle	Current Components		Current Magnitude/Phase	
Wire/End	Ireal	Iimag	Imag	Iphase
W2e1 (SO)	1.00000E+00	0.00000E+00	1.00000E+00	0.000
W1e2	3.01968E-01	-3.47609E-01	4.60453E-01	-49.019
W3e2	6.98032E-01	3.47609E-01	7.79795E-01	26.473

The real and imaginary components of the non-source wire ends add up to equal the current value of the source-wire end. The model, then, carries with it the presumption that the current on one side of the source pulse divides between the two existing wires on the other side. The wires are all lossless in the models. The higher current on the coax wire is a function of its greater diameter, its greater length, and the non-linearity of its direction relative to the dipole. MININEC does not have the NEC limitation relative to junction of wires having different diameters, as indicated by the AGT score of the dipole + coax wire model. Hence, the model's reported values require no correctives.

Fig. 100-5 presents the 3-D patterns in free space for both the simple dipole and the dipole + coax wire models. The simple dipole "donut" pattern is useful for reference in gauging the differences that are part of the dipole + coax wire pattern. To what degree the pattern bulges appear in the pattern of the antenna over a real ground requires that we revise the model. So I moved the dipole to place it 1 λ (10 meters) above average ground (conductivity 0.005 S/m; relative permittivity 13). The open end of the coax wire is now 7.5 m above ground. The table that follows **Fig. 100-5** summarizes the performance data for the simple dipole vs. the dipole + coax wire.

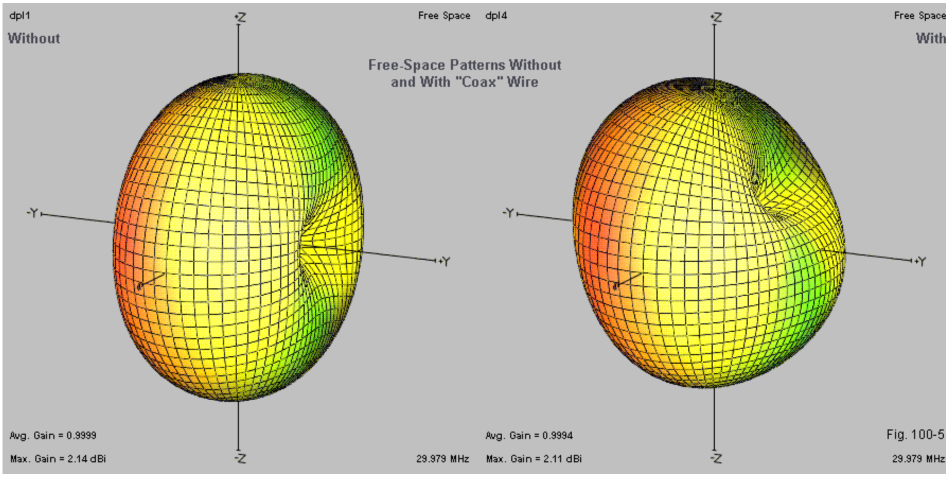

Fig. 100-5

MININEC Models: Standard Dipole vs. Dipole Plus Coax Wire
1 WL Above Average Ground

Model	Maximum Gain dBi	TO Angle degrees	Source Impedance R+/-jX Ω
Dipole	7.65	14	70.29 - j 5.62
Dipole Plus	6.68	14	45.11 - j14.75

Fig. 100-6 presents azimuth and elevation patterns for both antennas. In order to gather a feel for the maximum gain reduction associated with the dipole + coax wire model, focus on the pattern places marked "Note." In the azimuth pattern, note the shallower nulls off the dipole ends, with the side toward the coax wire being shallower than the opposite side of the pattern. As well, in the elevation pattern, note the shallower null between elevation lobes. Energy that creates these shallower nulls is not available in the main bi-directional lobes that determine the maximum gain of the antenna.

Fig. 100-6

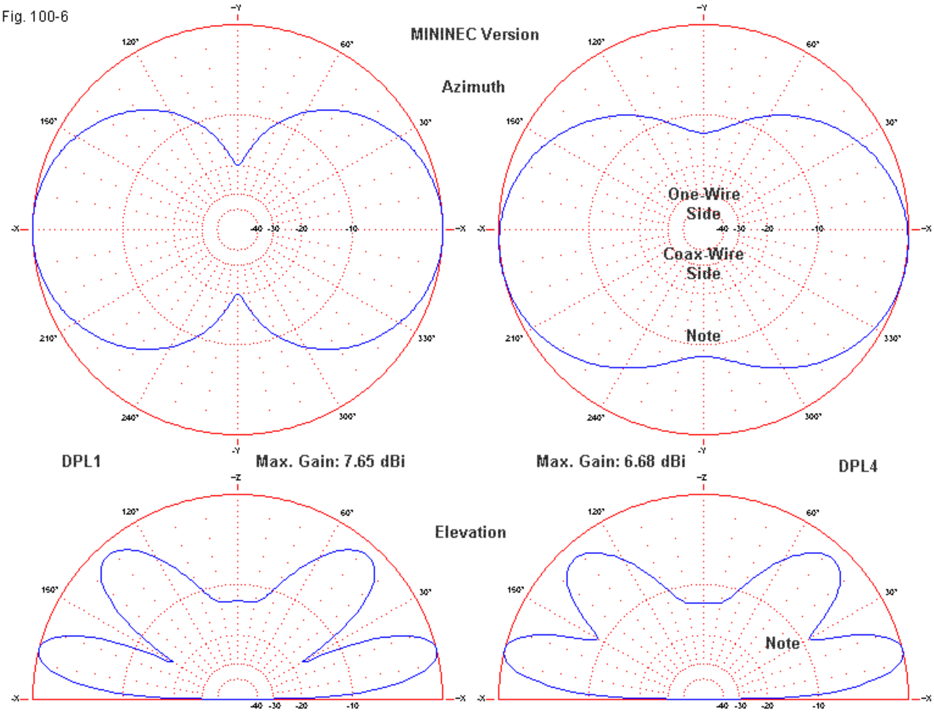

Modeled Dipole Patterns at 10 Meters Above Average Ground Without and With "Coax" Wire

Some NEC Results

As shown at the top of **Fig. 100-4**, the NEC model must have a slightly different structure relative to the MININEC model. The standard dipole uses 31 segments, each 156.452 mm long. The source is on segment 16 at the exact center of the dipole. When we add a coax wire, it must be at a junction of wires or segments. For simplicity within EZNEC, I cut the dipole wire into two pieces. Wire 1 is 2.503226 m long and has 16 segments. The source is on the last segment of this wire. Wire 2 is

2.346774 m long and has 15 segments. As a result of this division, the segment length remains unchanged and is the same on both wires. See model 100-2. The coax wire, wire 3, begins at the junction of wires 2 and 3 and runs downward for 2.5 m. It uses 16 segments, each of which is 156.25 mm long, very close to the length of the segments in the dipole wires. See model 100-3.

The dipole + coax wire model contains two problematical features. First, the junction of the coax wire and the dipole wire is displaced from the exact dipole center by half the length of a model segment. Second, the coax wire, with a diameter of 6.35 mm, differs from the 1-mm diameter of the dipole wires, creating an angular junction of wires with dissimilar diameters. NEC has a known limitation in such cases, and the error is greater in NEC-2 than NEC-4. The following table summarizes the free-space performance reports of the 2 cores for both the simple dipole and the dipole + coax wire models. There is no significant difference between NEC-2 and NEC-4 with respect to the simple dipole.

NEC Models: Standard Dipole vs. Dipole Plus Coax Wire: Free Space

Model	Maximum Free-Space Gain dBi	Source Impedance R+/-jXÙ	AGT	AGT-dB	Corrected Gain dBi
Dipole	2.14	71.99 - j 0.43	1.000	+/-0.0	2.14
Dipole Plus					
NEC-4	1.72	44.95 + j16.99	0.958	-0.19	1.91
NEC-2	1.66	45.70 + j17.33	0.943	-0.25	1.91

The source resistance of the models is close to the value for the corresponding MININEC value. However, the reactive component of the source impedance is about 30 Ω distant from the MININEC value. Therefore, I created the alternative MININEC model shown in **Fig. 100-4**. In this model, the junction of the coax wire is 1 pulse/segment away from the source. All of the segments in the dipole portion of the model have the same length. Placing the junction another half-segment-length away from the source has interesting consequences. First, the free space gain of the model is 1.92 dBi, virtually the same as the corrected gain values for the NEC-2 and NEC-4 models. Second, the source impedance report is 45.99 + j32.94 Ω. The resistive component has not changed by much, but the reactive component is considerably more inductive than the NEC reports. The junction position of the coax wire with the dipole wire, relative to the source, appears to make a consistent and systematic difference to the reported reactance at the source.

The current reports for the NEC model also differ from those emerging from MININEC. NEC currents refer to specific segments, with the segment center taken as the virtual read-out position. The source segment current by assignment was 1 A RMS (the convention used within EZNEC software). Since the NEC core uses peak values, the NEC output report shows a corresponding value of 1.4142E0 as the peak value. The comparison of values must use the segment current on each side of the source segment. Hence, the perfect addition that we experienced with the MININEC model is not likely to appear. The question is to what degree we find the current division holding to the MININEC model standard. The following table tells us some of the story. The source is located on wire 1, segment 16. Wire 1, segment 15 is the adjacent segment on the dipole side without the coax wire. Wire 2, segment 1 is the first segment of the remainder of the dipole that meets with wire 3, segment 1, the first segment of the coax wire. The values are for NEC-4

Relative Current Levels at the Dipole + Coax Wire Feedpoint: NEC-4

	Current Components		Current Magnitude/Phase Angle	
Wire/Segment	Ireal	Iimag	Imag	Iphase
W1s16 (SO)	1.4142E+00	-3.4217E-16	1.4142E+00	0.000
W1s15	1.4047E+00	-7.9009E-03	1.4047E+00	-0.322
W2s1	3.0643E-01	-3.9072E-02	3.0891E-01	-7.226
W3s1	1.1108E+00	3.0984E-02	1.1112E+00	1.598

The sum of the coax-side real current components is 1.4172E+00, which is only slightly higher than the real current on W1S15. The sum of the imaginary components is -8.088E-03, very close to the imaginary component on W1S15. Within the limits of the model adequacy, as indicated by the less-than-perfect AGT score, the currents add up correctly to indicate a current division on the coax-wire side of the dipole. However, relative to the MININEC model, we find two anomalies. First, the ratio of coax wire current to dipole wire current in the NEC-4 model is about 3.62:1, whereas in the MININEC model, the ratio is about 2.31:1. This difference is likely due to a combination of the position of the wire junction relative to the source position and the error introduced by the junction of wires with differing diameters.

The second anomaly between the cores is less easily explained. The MININEC model showed widely divergent phase angles between the currents on the dipole and coax wires: -49° and +26.5°, respectively. The NEC-4 model shows only a small divergence of the same current phase angles: -7.2° and +1.6°, respectively. It is likely that the lack of coincidence between the wire junction and the source forms the ultimate reason for the small difference in phase angles within the NEC-4 models. The lack of coincidence of the phase angles would require careful measurement of an actual antenna situation in order to tell us decisively which modeling core provides the more realistic report.

Over real ground, using the same conditions as in the MININEC model, we obtain similar results, as shown by the following table. The dipole + coax wire model uses NEC-4 data. See model 100-4.

NEC Models: Standard Dipole vs. Dipole Plus Coax Wire
1 WL Above Average Ground

Model	Maximum Gain dBi	TO Angle degrees	Source Impedance R+/-jX Ω
Dipole	7.64	14	70.68 - j 5.64
Dipole Plus	6.08	14	45.28 + j14.69

Fig. 100-7 provides comparative simple dipole and dipole + coax wire azimuth and elevation patterns. The simple dipole patterns–as well as the tabular data–are virtually identical to those for the corresponding MININEC model. The gain data for the NEC model of the dipole + coax wire is 0.6-dB lower than in the MININEC model, a value that exceeds the free-space AGT correction factor. However, the pattern elements that reduce maximum gain relative to the simple dipole are evident in the figure. Of course, due to the position of the source relative to the wire junction, the azimuth pattern shows a reversal between the deeper and shallower nulls off the dipole ends. The patterns also show the relative strengths of the vertical and horizontal components of the total far field.

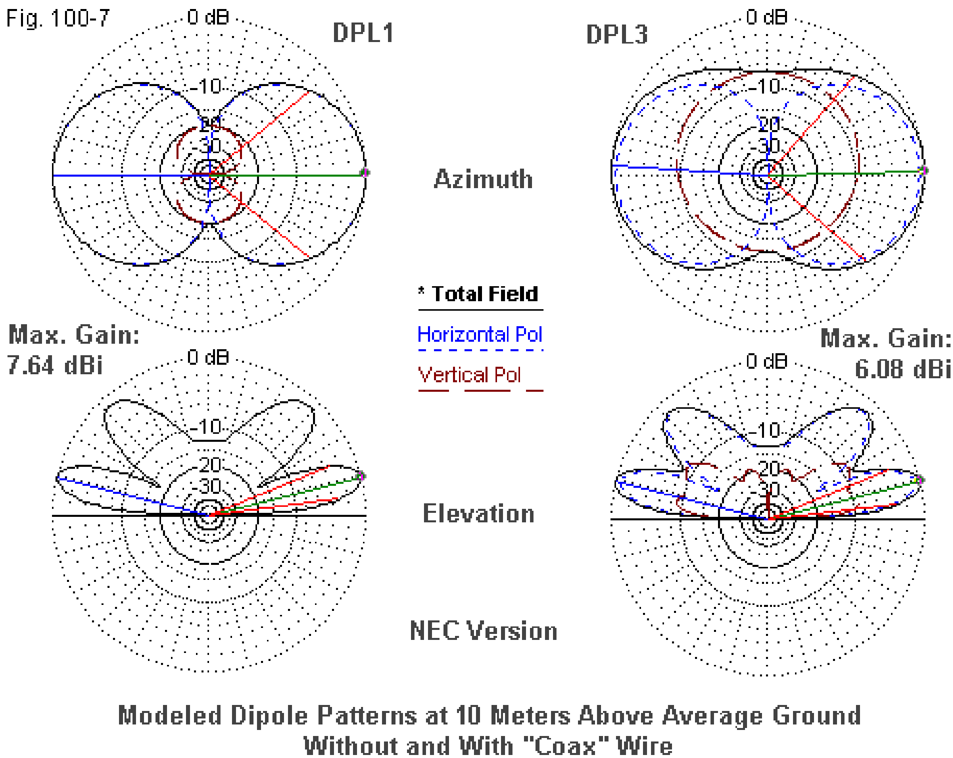

Some Tentative Conclusions

The test models use an artificial situation to allow some detailed comparisons between MININEC and NEC models of a dipole + coax wire. The MININEC version of the model, using the highly corrected Antenna Model implementation of the core, still requires careful construction in order to model effectively the coax wire as an alternative path for currents right at the feedpoint of the dipole. NEC has several limitations that prevent such exacting models, including the source placement within a segment rather than at its junction and its weakness in handling angular junctions of wires having dissimilar diameters.

The results show both areas of correspondence and divergence. The resistive component of the source impedance shows a good correlation between models, although the reactive component is apparently sensitive to the position of the wire junction relative to the source. Gain and pattern values are comparable, if we allow for the imperfect AGT scores of the NEC models. Perhaps the greatest divergence appears in the reported current phase angles on the joining coax and dipole wires, along with the reported ratio of currents in each wire.

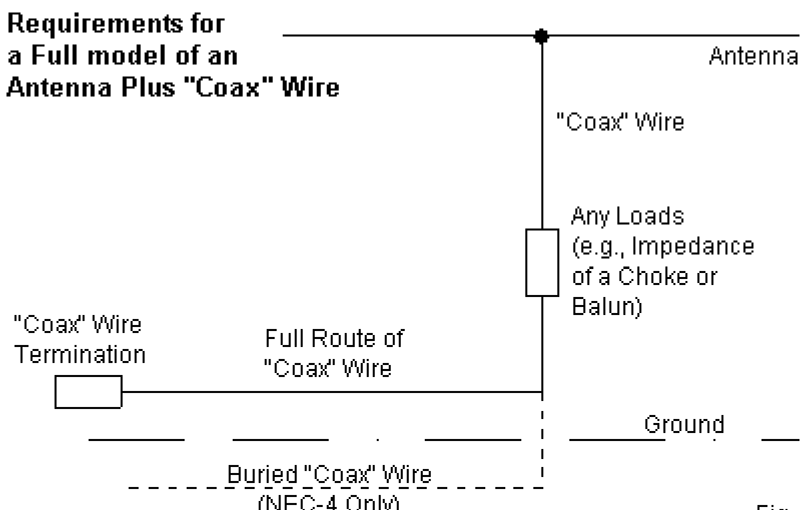

Fig. 100-8

The exercise has aimed to compare NEC and MININEC models attempting to capture the coax braid as an alternative path for antenna currents. As such, it sets up an artificial and simplified situation. Any complete model of the situation must include all of the factors shown in **Fig. 100-8**. Indeed, the list of factors is incomplete, but suggests that modeling the coax wire is not a simple task. Any results that presume an open-ended wire termination will be suspect with respect to reality. Even a high-impedance choke or balun added to a line at the end of a 1/4-λ coax run will not necessarily terminate the common-mode currents, since the antenna element impedance is also very high at that point. Nothing short of a complete model will do for modeling an actual situation.

Throughout, I have referred to the currents on the outer side of the coax braid as common mode currents. It is not wholly clear that the usage is correct, if we conceive of such currents as an alternative path for the current on the inner side of the braid at the junction with the antenna feedpoint. However, since common-mode currents will appear only on the outer side of coax braid, they are in some respects indistinguishable from what we might otherwise call "alternate-path" currents.

Whether the alternate-route portrayal of these currents is complete in itself may rest on the measured feedpoint impedance of the dipole with the coax attached. (For a related set of experiments measuring dipole element and coax braid currents, see Roy Lewallen, W7EL, "Baluns: What They Do and How They Do It," *The ARRL Antenna Compendium*, Vol. 1, pp. 157-164.) In the test situation, we find a very large difference in the resistive components between the simple dipole and the dipole + coax wire models, regardless of the modeling software used. Confirmation of the simple alternate path scenario is as simple as measuring the impedance in the coaxial cable at the termination of the 0.25-λ line (without introducing any paths to ground or other disruptive conditions) and then back calculating to the actual feedpoint impedance at the dipole feedpoint.

The situation does demonstrate that modeling is not an end in itself. In many situations, the results of modeling require experimental confirmation, if only to show that a model either is or is not a model of the situation under analysis. Unlike the present model set–with the definite difference between the source resistance of a simple dipole and of the dipole + coax–not all proposed models present clear cut cases for deciding whether or not the model captures a given electrical situation.

Appendix: Antenna Models

This volume—the fourth of the projected volumes—of antenna modeling notes comes with 100 antenna models, almost all of which have text references (Model xx-x). I have included most of the models in 3 different formats: .EZ for users of EZNEC, .NWP for NEC-Win Plus users, and .NEC for NEC-Win Pro, GNEC, and generic NEC-2 core users. The folder (directory) structure simply follows this scheme.

N:\models\ez	for EZNEC format files
N:\models\nec	for generic ASCII NEC files
N:\models\nwp	for NEC-Win Plus format files

I recommend that you copy the most relevant set of files into your hard drive for use. NEC-Win Plus, for example, will store its output files in the same directory as the basic model file, and that requires a space to which the computer can write. Each file name follows the text by starting with the column number, followed by the model number within the chapter. So Model 74-3 is the third model used in conjunction with column #74.

The files are not likely to add to your collection of models in the sense of providing new or interesting antenna designs. For that purpose, I have assembled collections of interesting models from my own storehouse. These collections are available from *antenneX*. The files that go with this volume of antenna modeling notes are those referenced in the text. As such, they are illustrations of the principles discussed in the text. Hence, you may read along with your own modeling software active and investigate further the model under discussion.

You will find some discrepancy between many of the model outputs and the performance figures cited in the text. This situations has a number of sources, all related to the fact that I began the series in the last century (the late 1990s). In some cases, I simply could not find the file used for a column, and so I had to reconstruct as best I could the model under discussion. Sometimes, the text did not provide complete modeling data, so I approximated the text model as closely as possible. Although the exact figures may not jive between text and model, the trends certainly do.

In other cases, software developments are the source of slight numerical deviance between the model as used when I wrote and the same model when you run it on your current software. When I began the series of columns, EZNEC was a DOS program, and now uses Windows. NEC-Win Plus did not yet exist. In the course of time and software development, the NEC cores have undergone customizing and enhancement for speed—with special reference to the latest Fortran compilers. In the process, there have been changes in the order of operations and rounding conventions, enough to create slight output differences. With respect to guiding construction, showing performance trends, or yielding reliable analysis, the changes make no noticeable difference relative to older outputs. However, in order to show trends as sensitively as possible, many parts of the output data cited in the text will be overly precise. That fact will create an illusion of difference where no operationally significant difference exists.

Models for columns that deal with advanced commands—such as GC, GH, GM, GX, and WGF—require the use of a raw core or a program that includes the complete command set. Hence, they appear only in .NEC format.

I regret that I cannot include in this collection samples of MININEC files. I have and use several MININEC programs, including ELNEC, AO, MMANA, NEC4WIN, and the most recent and able version, Antenna Model. Each version uses a different file format, and there are few means of converting a MININEC file from one format to another except by writing the model from scratch. In contrast, I was able to convert files from one to another of the NEC formats. Conversion is not perfect, and so some EZNEC files given in English measures will appear in metric form in the generic NEC and NEC-Win Plus formats.

With these limitations in mind, I hope that the attached files enhance your safari through the topical jungle within this volume of antenna modeling notes.

Other Publications

We hope you've enjoyed this 4th in a series of volumes of the **Antenna Modeling Notes.** Together with volumes 1, 2 and 3, you'll find many other very fine books and publications by the author L.B. Cebik, W4RNL in the ***antenneX Online Magazine BookShelf*** at the web site shown below.

A Publication by
antenneX Online Magazine
http://www.antennex.com/
POB 271229
Corpus Christi, Texas 78427-1229
USA

ISBN: 1-877992-78-X